EMEP Status Report 2/2020

July 2020

Assessment of transboundary pollution by toxic substances: Heavy metals and POPs

METEOROLOGICAL SYNTHESIZING CENTRE - EAST

Oleg Travnikov, Nadezhda Batrakova, Aleksey Gusev, Ilia Ilyin, Mikhail Kleimenov, Olga Rozovskaya, Victor Shatalov, Irina Strijkina

CHEMICAL CO-ORDINATING CENTRE

Wenche Aas, Knut Breivik, Pernilla Bohlin Nizzetto, Katrine Aspmo Pfaffhuber

CEIP/Umweltbundesamt Austria

Katarina Mareckova, Stephan Poupa, Robert Wankmueller, Katrin Seussall

MCS-E

Meteorological Synthesizing Centre - East

2nd Roshchinsky proezd, 8/5
115419 Moscow
Russia
Phone.: +7 926 906 91 78
Fax: +7 495 956 19 44
E-mail: msce@msceast.org
Internet: www.msceast.org

CCC

Norwegian Institute for Air Research (NILU)

P.O. Box 100NO-2027 Kjeller
Norway
Phone: +47 63 89 80 00
Fax: +47 63 89 80 50
E-mail: kjetil.torseth@nilu.no
Internet: www.nilu.no

CEIP

Umweltbundesamt GmbH

Spittelauer Lände 5
1090 Vienna
Austria
Phone:+43-(0)1-313 04
Fax: +43-(0)1-313 04/5400
E-mail: emep.emissions@umweltbundesamt.at
www.umweltbundesamt.at

EXECUTIVE SUMMARY

Heavy metals and persistent organic pollutants (POPs) are toxic substances that adversely affect human health and ecosystems. The problem of the environmental pollution by these contaminants is targeted by various international bodies including the UNECE Convention on Long-range Transboundary Air Pollution (hereafter, CLRTAP or the Convention). The priority heavy metals and POPs addressed by the Convention include lead (Pb), cadmium (Cd), mercury (Hg), polychlorinated biphenyls (PCBs), polychlorinated dibenzo(p)dioxins and dibenzofurans (PCDD/Fs), hexachlorobenzene (HCB), and polyaromatic hydrocarbons (PAHs). The priority PAHs are benzo(a)pyrene (B(a)P), benzo(b)fluoranthene (B(b)F), benzo(k)fluoranthene (B(k)F), and indeno(1,2,3-cd)pyrene (IP). Scientific support of implementation of the Protocols on Heavy Metals and POPs under the Convention is provided by the Co-operative Programme for Monitoring and Evaluation of Long-range Transmission of Air Pollutants in Europe (EMEP, www.emep.int). Research and operational assessment of heavy metal and POP pollution are carried out by relevant EMEP Centres – the Centre on Emission Inventories and Projections (CEIP), the Chemical Coordinating Centre (CCC), the Meteorological Synthesizing Centre – East (MSC-E).

This Status report presents an overview of activities of the EMEP Centres focused on research and assessment of heavy metal and POPs pollution in 2018 carried out in accordance with the bi-annual workplan of the Convention for 2020-2021 [ECE_EB.AIR_144_Add.2]. The report includes information on emissions, monitoring, and model assessment of heavy metal and POP pollution in 2018; research activities and co-operation with subsidiary bodies to the Convention and international organizations. Detailed technical information aimed to support the Status Report is available in the Supplementary Data Reports on heavy metals [*Ilyin et al.,* 2020] and POPs [*Gusev et al.,* 2020] as well as at the MSC-E website (www.msceast.org).

Emissions

Completeness and consistency of reported data on heavy metal emissions have improved significantly. Forty three countries reported data on the priority heavy metal emissions, and 42 countries - on POP emissions in 2020. The quality of submitted data differs quite significantly among countries. Uncertainty of reported data (national totals and sectoral data) is considered relatively high and affects long-term trends of the emissions in the EMEP domain. Heavy metal emissions in the western part of the EMEP domain show smooth downtrend. Emission trends of heavy metals in the eastern part of the EMEP domain as well as POP trends in the both EMEP parts exhibit strong fluctuations because of incomplete or inconsistent reporting by particular countries. In order to improve reported emission data, re-calculations of national emissions are performed regularly. Due to the re-calculations the emissions data of 25 countries changed by more than 15% for one or several pollutants, and the changes were minor (< 1%) for 8 countries.

The main emission sectors for heavy metals and PCB are ‘Industry’ and ‘Public electricity and heat production’. The most of PAHs are emitted by the sector ‘Other stationary combustion’. This sector and ‘Industry’ are almost equally important for emissions of PCDD/Fs and HCB. Sectoral gridded emissions of heavy metals and POPs in the new resolution were reported by 31 countries. Final

emissions maps for modelling were generated by MSC-E based on the reported emissions data collected and gap-filled by CEIP and supplemented by additional information on vertical distribution, seasonal variation and chemical speciation emissions. Global emission maps were also prepared based on data derived from research projects and expert estimates.

Monitoring

Measurements of heavy metal and POP pollution levels are performed in the EMEP monitoring network under methodological guidance of CCC. Measurements of Pb and Cd concentrations in air or in precipitation were carried out in 2019 at 64 stations. Measurements of Hg were performed at 25 stations, and 15 of them were co-located. The highest concentrations of Pb and Cd in air in 2018 were observed at stations in Hungary, Slovakia, the Benelux countries. The highest concentrations in precipitation of Pb were noted for Spain and Slovakia, and for Cd – in Estonia and Spain. The highest concentrations of total gaseous and elemental Hg were measured in Germany, whereas the highest Hg concentrations in precipitation – in the Czech Republic. Besides, concentrations of Pb, Cd and Hg in precipitation were much higher in 2018 compared to the previous year because of extremely dry summer.

In total 32 sites reported data on POPs, whereof 26 sites reported measurements in both air and precipitation. The highest PAH and PCB levels took place at sites located in the central part of Europe, whereas the highest HCB levels are noted for the Arctic stations (Spitsbergen, Greenland). The regional distribution of PAHs for the different seasons clearly shows higher concentrations during winter in Eastern Europe, where the emissions from residential heating are highest. The analysis of intra-annual changes of PAH concentrations shows strong seasonal variability with higher air concentrations in winter for all considered PAHs that can be attributed to a combination of both elevated emissions during winter and/or reduced half-lives during summer. Besides, based on the EMEP measurement data for the selected PAHs, it is suggested that sampling strategies based on filters only (PM10) may represent a poor measure of total concentrations in air for low-molecular PAHs.

Transition to finer spatial resolution makes possible more thorough analysis of heavy metal and POP levels in highly populated and urbanized areas. In order to facilitate evaluation of the model performance MSC-E utilized monitoring data from AIRBASE database collected and processed by European Environmental Agency (EEA). In particular, information on the observed air concentrations of B(a)P in 2018 from more than 700 national monitoring sites was involved into the analysis of pollution levels. Besides, measurement data from about 120 national sites were used in the country-scale study of heavy metal pollution in Germany.

Status of heavy metal and POP pollution in 2018

Assessment of heavy metal and POP pollution of the EMEP region is performed using both modelling results and measurement data and includes evaluation of spatial patterns of pollution levels as well as transboundary transport in 2018. The assessment is based on the gridded emissions data for the previous 2017 year. Besides, changes in pollution levels due to inter-annual meteorological variability

are evaluated. Update of the modelling results based on the new emission data for 2018 is available In Annex A.

The performed analysis shows that the highest levels of Pb, Cd, and Hg deposition took place in 2018 in Central Europe (Poland, Germany, the Czech Republic, Slovakia) and Southern Europe (Italy, Bulgaria, the Balkan countries). Considerable deposition of Cd also occurs in the European part of Russia. Elevated Hg deposition fluxes are predicted in the high Arctic as a result of intensive Hg oxidation during springtime. The lowest deposition fluxes are in Northern Europe as well as in the Caucasus and Central Asia.

High levels of PAH air concentrations in 2018 occurred in countries of Central, Eastern, and Southern Europe. Countries of Central and Southern Europe are also characterized by elevated concentrations of PCDD/Fs, whereas relatively high concentrations of PCB-153 are predicted in Western Europe. Model estimates indicate substantial spatial gradients of PCDD/Fs and PCB-153 concentrations in the EMEP region, whereas spatial distribution of HCB concentrations is more homogeneous that can be conditioned by its relatively high persistence in the atmosphere.

The assessment of pollution changes due to the inter-annual meteorological variability indicate considerable increase of Pb (13-17%) and Cd (17-20%) deposition in 2018 compared to the previous year in Western and Southern Europe. Eastern Europe as well as Caucasus and Central Asia were characterized by the largest decline of Pb and Cd deposition (7-14%). Mercury deposition flux increased in Southern Europe (18%) and Western Europe (7%) but decreased in Central Europe (8%). The most significant increase of PAH air concentrations (16 %) took place in Northern Europe followed by Southern and Central Europe. At the same time, decreasing air concentrations were estimated for Western and Eastern Europe. It should be noted that concentration and deposition changes can be larger in particular countries (up to ±50%).

Modelled air concentrations and wet deposition of heavy metals generally agree with the levels observed at the EMEP monitoring network. The mean relative bias between the annual average modelled and observed air concentrations does not exceed -10% and -5% for Pb and Cd, respectively. Deviation between the modelled and observed Hg^0 air concentrations does not exceed ±10%. Simulated wet deposition fluxes of all heavy metals demonstrate satisfactory agreement with measurements with deviations being mostly within a factor of two. However, the model tends to underestimate (by 20-25%) observed wet deposition of Pb and Cd and overestimate Hg wet deposition.

The modelling results on the sum of 4 PAHs agree with EMEP measurements with the mean relative bias about -9% and high spatial correlation (0.8). Validation of individual PAH compounds indicates some underprediction of observed B(a)P and B(k)F air concentrations by the model, and over-prediction of observed B(b)F and IP concentrations. Similarly, the model tends to underpredict AIRBASE measurements of B(a)P at rural and suburban monitoring stations. Modelled air concentrations of PCB-153 and HCB reasonably well agree with measurements with average relative biases -2% and -27%, respectively, and significant spatial correlation (0.6-0.75). Monitoring of PCDD/F air concentration was carried out in 2018 only at two EMEP stations (SE0014R and SE0022R)

for the period of four months. Comparison of measured and modelled air concentrations shows systematic underestimation of observed values at both stations by a factor of 2.

Atmospheric deposition of Pb and Cd in the EMEP countries is largely formed by anthropogenic emissions and secondary sources (wind re-suspension). Anthropogenic sources make up the largest contribution in Central Europe (66% for Pb and 80% for Cd), whereas the effect of secondary sources is the most significant in Caucasus and Central Asia. Contribution of non-EMEP sources is relatively small except for the countries located close to the borders of the EMEP region. Regional anthropogenic emissions sources contribute 25% of Hg deposition in the EMEP countries, whereas contribution of intercontinental transport exceeds 75%. However, this large estimate contains implicit contribution of EMEP emissions that flew out through the boundaries and returned back to the region. The contribution of transboundary transport exceeds deposition form national sources in 38, 41 and 38 of 51 EMEP countries for Pb, Cd and Hg, respectively.

Anthropogenic emission sources made up the most significant contribution to PAH pollution levels. Contrary to this, for PCDD/Fs, PCB-153, and HCB significant contribution (about 50-70%) is estimated for secondary emission sources. Model assessment of POP long-range transport indicates considerable role of transboundary transport between the EMEP countries. In particular, contribution of transboundary transport to PAH deposition exceeds 50% of total deposition in 27 of 51 EMEP countries. The prevalence of transboundary pollution of domestic sources is also characteristics of 20, 30, and 39 countries for PCDD/Fs, PCB-153, and HCB, respectively.

Marine environment is protected on national and international levels by a number of regional conventions such as HELCOM, OSPAR, Barcelona Convention, Bucharest Convention, and Tehran Convention. Information on heavy metal and POP atmospheric input to the marginal seas surrounding the EMEP region is prepared by MSC-E. These are the Baltic, North, Mediterranean, Black, and Caspian Seas. Deposition fluxes of heavy metals and POPs to different marginal seas vary significantly depending on location of anthropogenic and secondary sources, and meteorological conditions. Deposition fluxes of Pb and Cd are higher for the Mediterranean, Caspian and Black seas and are lower the Baltic and North Seas. The highest deposition fluxes of Hg take place to the North Sea. The most significant deposition of most POPs is estimated for the Baltic or Black Sea, whereas the lowest is for the Caspian Sea.

Information of pollution of the Arctic by heavy metals and POPs in 2018 is prepared by MSC-E. The information on the Arctic pollution includes spatial distribution and sources apportionment of heavy metal and POP deposition. Due to remoteness of Arctic from main emission sources of Europe, Asia or North America deposition fluxes of heavy metals and POPs in the Arctic are typically lower compared to those in temperate latitudes. Russian Federation makes up the largest contribution to the Arctic anthropogenic pollution by all considered heavy metals and POPs. The reason for that is location of significant of the country within the Arctic region. Some other EMEP countries also considerably contribute to pollution of the region (e.g. Sweden, Norway, Finland, Kazakhstan, France, Germany).

Contamination of the EMEP countries by heavy metals and POPs is affected by long-range transport of the pollutants from emission sources located in other regions or continents. It is particular

relevant for Hg and some POPs (HCB, PCDD/Fs), which are characterized by long residence time in the atmosphere. Therefore, model assessment of pollution levels in the EMEP domain is supported by global scale simulations. It should be noted that the global scale modelling of heavy metal and POP pollution requires reliable and up-to-date global emission inventories. However, no data on contemporary emissions is available for Pb, Cd, HCB and PCDD/Fs. Thus, improvement of the global scale assessment requires additional efforts for development of global emissions inventories for heavy metals and POPs in co-operation with other international bodies (UN Environment, Stockholm Convention, Minamata Convention).

Information for exposure assessment

The ultimate aim of pollution assessment is evaluation of risks for human health and ecosystems associated with adverse effects of the pollution. Therefore, MSC-E continues providing the effect community with information that can be useful for the exposure assessment. In particular, information of ecosystem-specific deposition of heavy metals and POPs is provided for evaluation of the critical loads exceedances. Besides, exceedances of the PAH air quality standards are analyzed along with discussion about heavy metal and POP content in composition of particular matter that can lead to additional toxicity of atmospheric aerosol.

Information on calculated deposition fluxes of heavy metals and POPs is used for evaluation of the effects of the pollutants on human health and biota. In order to support this activity of the Working Group on Effects, MSC-E regularly calculates deposition fluxes to various types of land cover (forests, shrubs, grasslands, crops, water bodies, etc.) within the EMEP domain. Data on the modelled Pb, Cd and Hg deposition to 17 land-cover types is available at the MSC-E website. However, the most recent estimates of the adverse effects of heavy metals on human health and biota relate to 2010 and can hardly reflect present status of pollution. More efforts of the effects community in the field of evaluation of heavy metal and POP pollution adverse impacts are needed.

Results of model simulations for 2018 and measurements from national monitoring stations, collected in the AIRBASE, indicate high level of annual mean B(a)P air concentrations, exceeding the EU target value, in number of EMEP countries (Poland, Spain, Italy, Germany, the Czech Republic, Portugal, Hungary, Serbia, and Bulgaria). Areas of high concentrations (above the EU target value) are also noted in some of the EECCA countries. Considerable part of total population of the EMEP countries lived on territories, where the air quality guidelines for B(a)P air concentrations were exceeded (5% for the EU target level and 60% for the WHO reference level). Along with B(a)P, modelling results on 4 PAHs were also used to estimate population exposure to mixture of toxic PAHs in the form of B(a)P equivalent air concentrations.

Particular attention is paid to the chemical composition of atmospheric aerosol (PM_{10} and $PM_{2.5}$), which may contain toxic substances such as heavy metals, PAHs and other organic pollutants (e.g. PCB and PCDD/Fs). Current assessments of air pollution by particulate matter (PM) are largely focused on the mass concentration analysis. However, impact of PM on human health may be more significant due to the presence of hazard constituents. For instance, aerosol particles from solid fuels combustion can be enriched with toxic PAH compounds. In some cases, PAH concentration in PM can exceed the established EU and WHO target levels even if the guideline levels for PM are not

exceeded. Besides, PAHs can be contained in condensable PM, which is generated from hot gaseous phase during contact with cooler ambient air. Thus, simultaneous measurements of PM and its components may be useful for more precise risk assessment. The influence of chemical composition of on the PM toxicity is the subject of future research.

Research activities

The main directions of the research included evaluation of PAH pollution and population exposure in the EMEP countries, downscaling of heavy metal pollution assessment for Germany, further study of Hg oxidation and reduction in the atmosphere, update of model parameterizations of gas-particle partitioning, degradation and air-surface exchange of POPs.

High levels and lack of decrease of PAH air concentrations in the EMEP countries during two recent decades have been indicated as an important issue in the Long-term Strategy of the Convention. Specific attention in this respect is paid to the emissions from residential combustion and biomass burning as prevailing source categories of PAHs. In order to contribute to these activities, MSC-E collects and analyses information on physical-chemical properties of toxic PAHs, reported national inventories and expert estimates of PAH emissions as well as approaches to assess population exposure to PAH pollution. Besides, trends in observed and modelled PAH concentrations in air are analyzed and exceedances of air quality guidelines are estimated. Along with this, importance of consideration of wider list of toxic PAHs is emphasized and experimental model simulations are carried out to estimate population exposure to mixture of 16 toxic PAHs. Particular attention is also given to the interaction of PAHs and PM in the atmosphere, and contribution of toxic PAHs to the adverse effects of aerosol particles.

A country-scale study of heavy metal pollution in Germany was performed jointly by EMEP/MSC-E and the German Environment Agency (UBA). The main objective of the study was generation of detailed information on levels and spatial distribution of air concentration and atmospheric deposition of three heavy metals (Pb, Cd, and Hg) for the period 2014-2016. The fine resolution modelling on a country scale provides detailed patterns of heavy metal pollution in the country. Refined national emissions inventory for heavy metals and updates of other input information favour general improvement of the model assessment in comparison with previous EMEP operational modelling. Simulated spatial patterns well agree with background measurements at the EMEP stations. Measurement data from national monitoring networks significantly expand the scope of the analysis. However, more detailed information on the methodology, physical conditions and pollution from local sources in the surrounding of the monitoring stations is needed. Evaluation of the modelling results against national monitoring data reveals discrepancies in some locations or provinces of Germany. Performed analysis showed that the differences between the modelled and measured data can be caused by a number of factors related to uncertainties of emissions data, measurements and modelling approaches. Further in depth analysis of the revealed discrepancies requires assessment on a local scale involving national expertise, collection of more detailed information on emissions and measurements as well as local scale modelling.

Atmospheric chemistry is critical for Hg dispersion in the atmosphere from emission sources and pollution of terrestrial and aquatic ecosystems. It determines the overall Hg residence time in the

atmosphere and deposition to the ground. Despite significant improvements in measurements and modelling of Hg cycling in the environment, current knowledge on Hg chemistry in the atmosphere remains incomplete. The GLEMOS model was used for evaluation of the newest suggested mechanisms of Hg oxidation initiated by the reactions with Br and OH as well as photo-reduction of oxidized Hg in the atmosphere. It was shown that inclusion of the mechanisms to the model allows partly reproducing observations but demonstrates insufficient Hg oxidation in the free troposphere. Further analytical studies of Hg redox mechanisms are needed along with the model evaluation to improve model assessment of Hg pollution on both global and regional scales.

The work on the refinement of parameterizations of particle-bound B(a)P degradation and gas-particle partitioning processes in the GLEMOS model was continued. A new parameterization of B(a)P sorption to various components of aerosol particles (water soluble, organic, and inorganic sub-fractions) based on the poly-parameter linear free energy relationships (pp-LFER) was tested. Besides, inclusion of additional species, namely, NO_3 and ozone, into parameterization of gaseous phase B(a)P degradation and alternative degradation constants for particulate phase B(a)P degradation in the atmosphere were considered. Evaluation of currently used and updated parameterizations showed comparable results with somewhat better agreement of modelling results with measurements in case of new pp-LFER approach. Therefore, analysis and testing of this approach will be continued with the aim to include it to the operational model simulations.

Gaseous exchange of POPs between the atmosphere and vegetation is an important process that affects their distribution in the environment. To improve description of the air-vegetation process in the GLEMOS model, an overview of model parameterizations available in the literature was performed. An alternative approach, considering the vegetation and soil as parts of a single compartment (ecosystem) was selected to be implemented in the GLEMOS model after additional testing to describe the cycling of POPs between the environmental compartments (air, vegetation, and soil).

Modelling of atmospheric transport of POPs and Hg requires data on concentrations of various chemical reagents and constituents of aerosol particles. Datasets of the reagents generated by two chemistry transport models (MOZART-4 and GEOS-Chem) were compared and tested with the GLEMOS model for simulation B(a)P. The test simulations showed generally better agreement of the modelling results with measurements in case use of the data from GEOS-Chem. Therefore, the GEOS-Chem model is planned to be preferably used as a chemical preprocessor of reactants concentrations for the GLEMOS model in future.

Cooperation with subsidiary bodies of the Convention and other international bodies

Scientific co-operation is an important part of MSC-E activities aimed at support and improvement of heavy metal and POP pollution assessment within EMEP as well as dissemination of the assessment results to wider international audience. Co-operation with the Working Group on Effects (WGE) included join analysis and interpretation of moss measurement data together with experts from ICP-Vegetation. Results of current research activities and future plans of MSC-E were discussed at the recent meeting of the Task Force on Measurements and Modelling (TFMM). The work on the model retrospective analysis of long-term changes of Hg and POP levels is initialized by the Centre in

collaboration with the Task Force on Hemispheric Transport of Air Pollution (TF HTAP). The Centre also contributes to the work of the Task Force on Techno-Economical Issues (TF TEI) aimed at further reduction of PAH pollution levels in the EMEP countries. In co-operation with the Arctic Monitoring and Assessment Programme (AMAP) the Centre takes part in the new AMAP Assessments on the Arctic pollution by Hg. Besides, regular evaluation of airborne pollution load of heavy metals and POPs to the Baltic Sea is carried out in the framework of cooperation with the Helsinki Commission (HELCOM). Finally, MSC-E continues collaboration and data exchange with the Stockholm and Minamata Conventions.

Main challenges and directions of future research

Future directions of the EMEP centre's activities will be aimed at improvement of heavy metal and POP pollution assessment in the EMEP region. Detailed assessment of PAH concentrations trends, contributions of the key emission sources, and evaluation of exceedances of the EU and WHO target levels will be further performed to support activities of WGE, TF Health and TFTEI. Besides, quality of B(a)P modelling will be improved in the framework of the EMEP EuroDelta-Carb intercomparison exercise (TFMM) and a country-scale assessment of PAH pollution in Poland. The newly descovered mechanisms of Hg oxidation and photo-reduction in the atmosphere will be further studied and evaluated along with Hg exchange processes between the atmosphere and other environmental media (water bodies, vegetation etc.). A retrospective analysis of long-term changes of Hg and POP pollution will be performed in co-operation with TF HTAP to identify the key drives of the pollution changes. The emissions, monitoring and modelling issues revealed in the recent country-scale study for Germany will be further examined in co-operation with national experts in order to improve assessment of heavy metal pollution on both national and regional scales. Particular attention of research and development activities will be paid to particle-related processes occurred with heavy metals and POPs in the atmosphere. Finally, MSC-E will continue long-term co-operation with WGE focusing on joint analysis of heavy metal measurements in moss, preparation of information on Hg deposition to various ecosystems, and estimates of B(a)P exceedances of air quality guidelines.

ACKNOWLEDGEMENTS

The operational and research activities described in this repoort have been funded by the EMEP Trust Fund. Besides, the country-scale case study of heavy metal pollution in Germany was partly funded by the German Environment Agency (UBA).

CONTENTS

INTRODUCTION

Heavy metals and persistent organic pollutants (POPs) are toxic substances that adversely affect human health and ecosystems. The problem of the environmental pollution by these contaminants is targeted by various international bodies including the UNECE Convention on Long-range Transboundary Air Pollution (hereafter, CLRTAP or the Convention). In particular, the Long-term Strategy of the Convention states that despite decrease of these pollutants emissions for the recent decades, current pollution levels still pose risks to human health and the environment [ECE/EB.AIR/142/Add.2]. The priority heavy metals and POPs addressed by the Convention include lead (Pb), cadmium (Cd), mercury (Hg), polychlorinated biphenyls (PCBs), polychlorinated dibenzo(p)dioxins and dibenzofurans (PCDD/Fs), hexachlorobenzene (HCB), and polyaromatic hydrocarbons (PAHs). The priority PAHs are benzo(a)pyrene (B(a)P), benzo(b)fluoranthene (B(b)F), benzo(k)fluoranthene (B(k)F), and indeno(1,2,3-cd)pyrene (IP).

Scientific support of implementation of the Protocols on Heavy Metals and POPs under CLRTAP is performed by the Co-operative Programme for Monitoring and Evaluation of Long-range Transmission of Air Pollutants in Europe (EMEP, www.emep.int), which provides information on emission inventories, monitoring, and modelling of transboundary pollution. Research and operational assessment of heavy metal and POP pollution are carried out by relevant EMEP Centres – the Centre on Emission Inventories and Projections (CEIP), the Chemical Coordinating Centre (CCC), the Meteorological Synthesizing Centre – East (MSC-E).

This Status report presents an overview of activities of the EMEP Centres focused on research and assessment of heavy metal and POPs pollution in 2018 carried out in accordance with the bi-annual workplan of the Convention for 2020-2021 [ECE/EB.AIR/144/Add.2]. The report consists of six chapters. Chapter 1 presents the status of heavy metal and POP emissions reporting by the EMEP countries and preparation of emissions data for modelling. In Chapter 2, observations of these contaminants in the EMEP monitoring network are described along with measurements available from other monitoring networks. Results of the assessment of heavy metal and POP pollution levels in 2018 are presented in Chapter 3. The assessment is based on emissions data reported for the previous year 2017. Besides, changes in pollution levels due to inter-annual meteorological variability were evaluated. Update of the modelling results based on the new emission data for 2018 is available In Annex A. Recent research and the model development activities are discussed in Chapter 4. Cooperation of MSC-E with subsidiary bodies of the Convention, international organizations and national experts is discussed in Chapter 5. Main challenges and plans for future activities are formulated in Chapter 6.

Detailed technical information aimed at supporting the Status Report is available in the Supplementary Data Reports on heavy metals [*Ilyin et al*., 2020] and POPs [*Gusev et al*., 2020] and Technical Report [*Gusev et al*., 2020]. Besides, description of the current stable version of the Global EMEP Multi-media Modelling System (GLEMOS) as well as information on heavy metal and POP pollution in the EMEP region and in individual EMEP countries is presented at the MSC-E website (www.msceast.org).

Chapter 1. EMISSIONS OF HEAVY METALS AND POPs

1.1. Official emission data for 2018

The EMEP Reporting guidelines [*UNECE*, 2014] request all Parties to the *LRTAP Convention* to report annually emissions and activity data of air pollutants (SO_x, NO_x, NMVOCs, NH_3, CO, heavy metals[1], POPs[2], PM (and voluntary BC)). Furthermore, Parties have to report every four years projection data, gridded data and information on large point sources (LPS) to the EMEP Centre on Emission Inventories and Projections (CEIP).

1.1.1. Reporting of emission inventories in 2020

Completeness and consistency of submitted data have improved significantly since EMEP has been collecting information on emissions. Forty three Parties (84%) submitted data to CEIP in 2020[3], compared to 47 Parties (92%) in 2019 (Fig. .1.1). Eight Parties[4] did not submit any data in 2020. Forty three Parties reported priority heavy metals (Cd, Hg, Pb), from which 40 Parties provided time series, 3 Parties reported only 2018 data, 38 Parties reported data on five additional heavy metals (Arsenic (As), chromium (Cr), copper (Cu), nickel (Ni), selenium (Se), zinc (Zn) and their compounds) (Fig. 1.2). Forty two Parties reported data on POPs (total PAHs, PCDD/Fs, HCB, PCBs), out of which 41 also reported data on additional PAHs (B(a)P, B(b)F, B(k)F, IP).

The quality of submitted data across countries differs quite significantly. When compiling the inventories, countries have to use the newest available version of the EMEP/EEA *air pollutant emission inventory guidebook*, which is the version of 2016 [*EMEP/EEA Guidebook*, 2016]. However, many countries still use the Guidebook 2013 [*EMEP/EEA Guidebook*, 2013] or older versions. Uncertainty of reported data (national totals, sectoral data) is considered relatively high. The completeness of reported data is not satisfactory for all pollutants and sectors neither. Detailed information on recalculations, completeness and key categories, plus additional review findings, can be found in the annual EEA & CEIP technical inventory review reports and their Annexes[5].

---

1 *Heavy metals (Cd- Cadmium, Hg- Mercury, Pb-Lead) and its compounds*

2 *Persistent Organic Pollutants (Total PAHs, PCDD/Fs, HCB, PCBs)*

(j) Polycyclic aromatic hydrocarbons (PAHs). For the purposes of emission inventories, the following four indicator compounds shall be used: benzo(a)pyrene, benzo(b)fluoranthene, benzo(k)fluoranthene, and indeno(1,2,3_cd)pyrene;

(k) "Dioxins and furans" (PCDD/F), which are polychlorinated dibenzo p dioxins (PCDD) and polychlorinated dibenzofurans (PCDF), tricyclic, aromatic compounds formed by two benzene rings, connected by two oxygen atoms in PCDD and by one oxygen atom in PCDF, and the hydrogen atoms of which may be replaced by up to eight chlorine atoms;

(l) "Polychlorinated biphenyls" (PCBs), which means aromatic compounds formed in such a manner that the hydrogen atoms on the biphenyl molecule (two benzene rings bonded together by a single carbon-carbon bond) may be replaced by up to 10 chlorine atoms;

3 *The original submissions from the Parties can be accessed via the CEIP homepage on* https://www.ceip.at/ms/ceip_home1/ceip_home/status_reporting/2020_submissions/index.html

4 *Albania, Azerbaijan, Bosnia and Herzegovina, Georgia, Liechtenstein, Monaco, Russian Federation and USA.*

5 https://www.ceip.at/ms/ceip_home1/ceip_home/review_process/review_reports/index.html

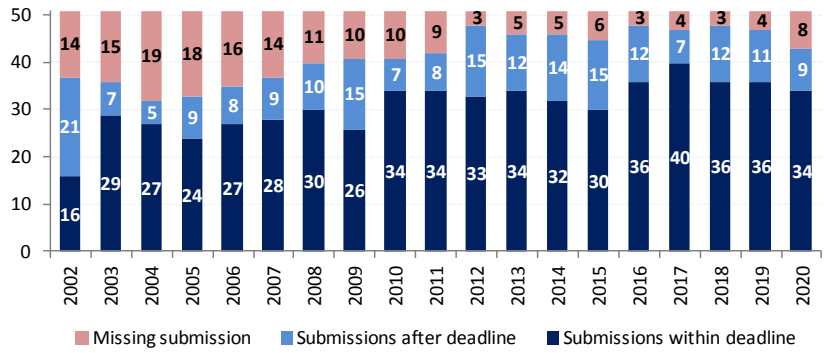

Fig. 1.1. *Parties reporting emission data to EMEP since 2002, as of 1 June 2020.*

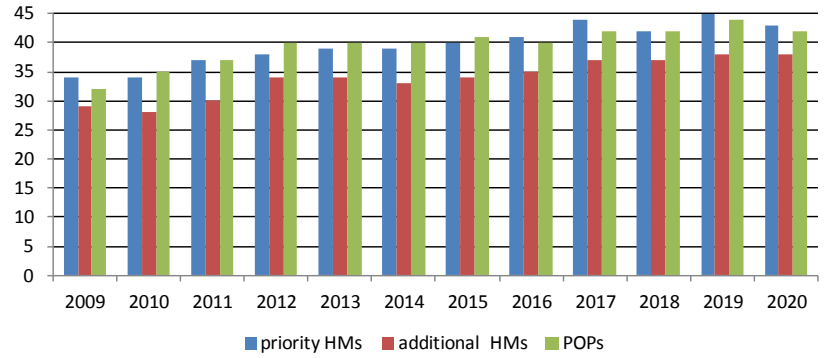

Fig. 1.2. *Parties reporting of HMs and POPs to EMEP since 2009, as of 1 June 2020.*

1.1.2. Emission trends in the EMEP area – reported data

For priority heavy metals and POPs the emission trends and completeness of reported data show different pictures for the EMEP-East and EMEP-West regions. The EMEP-West region includes the EU28 countries, Monaco, Albania, Bosnia & Herzegovina, North Macedonia, Montenegro, Serbia, Iceland, Liechtenstein, Norway and Switzerland. The EECCA countries and Turkey are summarized in the EMEP-East region[6].

EMEP West area – POPs

The strong fluctuations in emission trends of POPs for the EMEP-West region (Fig. 1.3) are mostly due to the reporting of single countries. The high reductions of HCB from 2001 to 2002 are due to the strong drop of emissions reported by Germany, and the peak in 2009 is mainly due the reporting of Albania. The significant increase from 2000 to 2006 of PAHs and B(a)P, the strong drop in 2007 and the drop in 2018 are mainly due to the reporting of Bulgaria. The peak in 2013 B(k)F emissions is mainly due to the reporting of Spain. It has to be mentioned that Austria reports total PAH emissions, but does not report the four PAH compounds B(a)P, B(b)F, B(k)F and IP. Albania did not report any POPs, and Liechtenstein did not report PCB.

[6] https://www.ceip.at/ms/ceip_home1/ceip_home/review_process/review_process_general/index.html

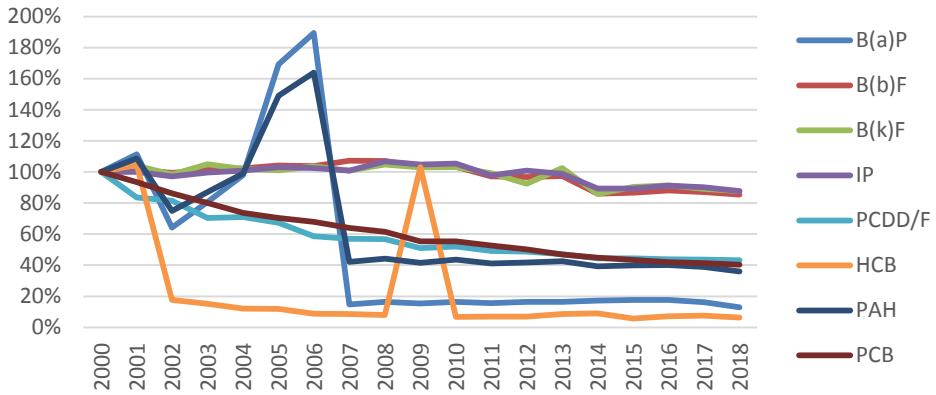

Fig. 1.3. *Emission trends of POPs 2000-2018 in the EMEP West area (reported data).*

EMEP East area – POPs

Reporting of POPs in the EMEP East region is quite incomplete and shows high peaks and inconsistent time series. The Russian Federation reported some POPs for the year 2000 only, and Turkey did not report any POPs at all. Belarus did not report data for the year 2000 and incomplete data for 2001. Ukraine reported very high levels of POPs for 2010 to 2013 (constant values) and data for 2017 and 2018 only. Figure 1.4 shows POPs emissions from 2002 to 2018 for EMEP East without emissions of Ukraine.

The increase of HCB emissions in 2009 is mainly due to the reporting of Azerbaijan and Kazakhstan. The increase in PCDD/F emissions in 2009 and the drop in 2015 are also mainly due to the reporting of Azerbaijan.

The drop in POPs emissions in 2018 is mainly due to missing data of Azerbaijan, Georgia, Kyrgyzstan and Moldova and, for most of the pollutants, a strong drop in emissions reported by Kazakhstan for that year. The peak in 2016 PAH emissions is mainly due to reporting of Kyrgyzstan, which reported values for 2016 and 2017 only.

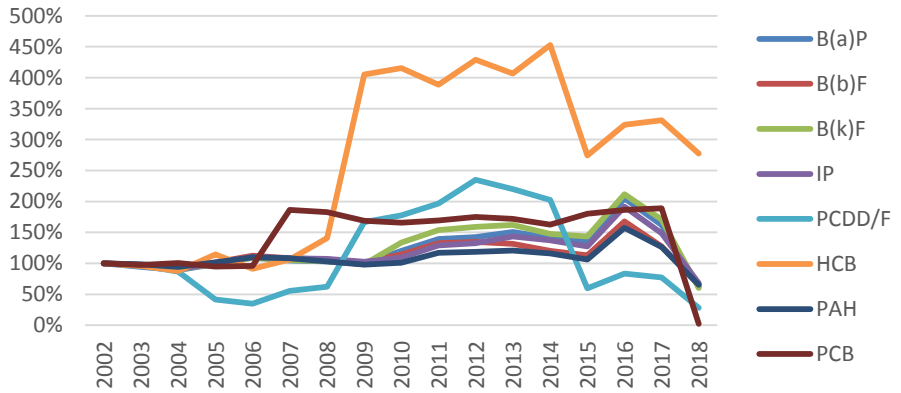

Fig. 1.4. *Emission trends of POPs 2002-2017 in the EMEP East area (reported data) without Ukraine.*

EMEP West area – priority heavy metals

Priority heavy metals of the EMEP West area show a rather smooth downtrend and a dip in the year 2009, which reflects the economic recession leading to lower industrial production in that year (Fig. 1.5). The strong decrease of Pb emissions from 2000 to 2002 is mainly due to lower emissions in the transport sector in Italy and Spain.

The continuous decrease of Hg emissions since the year 2010 is mainly due to decreases reported by France, Germany, Italy and the United Kingdom.

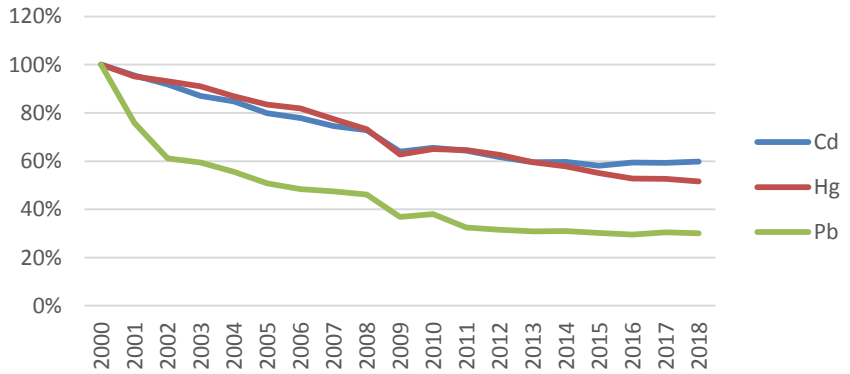

Fig. 1.5. *Emission trends of priority heavy metals 2000-2018 in the EMEP West area (reported data).*

EMEP East area – priority heavy metals

Unlike EMEP West, *priority heavy metals of the EMEP East area show an unstable trend from 2000 to 2007*, which is mainly due to incomplete reporting (Fig. 1.6). The dip in 2001 Pb and Cd emissions is mainly due to a gap in reporting of the Russian Federation, which reported for 2000, 2002-2006 and 2009 (jump in Cd emissions) only. Ukraine and Belarus did not report data for 2000. Azerbaijan, Georgia, Kyrgyzstan and Moldova did not report data for 2018. Kazakhstan and Turkey are the only countries, which reported complete time series for all three heavy metals since the year 2000.

The strong jump of Hg emissions in 2018 is due to a high value reported by Armenia for the GNFR sector "E_Solvents" (the value is about 1000 times higher than for 2017).

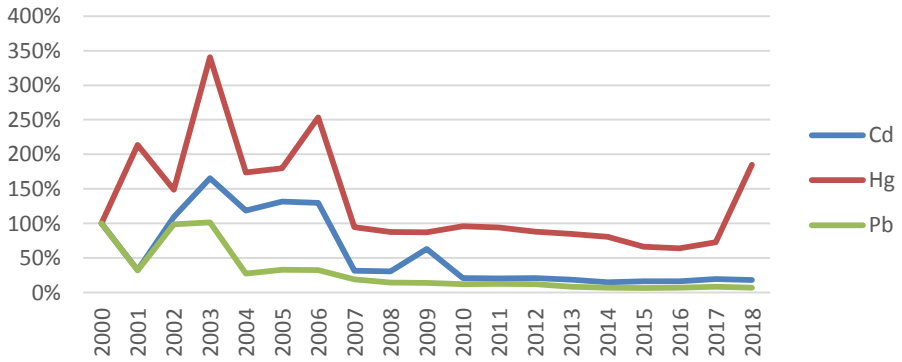

Fig. 1.6. *Emission trends of priority heavy metals 2000-2018 in the EMEP East area (reported data).*

1.1.3. Comparison of 2017 data reported in 2019 and in 2020

Reported data of 2017 emissions (reported in 2020) were compared with 2017 emissions (reported in 2019). For 25 countries, data changed by more than 15 % for one or several pollutants (see Fig. 1.7 and Annex B2). For eight countries, 2017 data is unchanged or nearly unchanged (< 1 %).

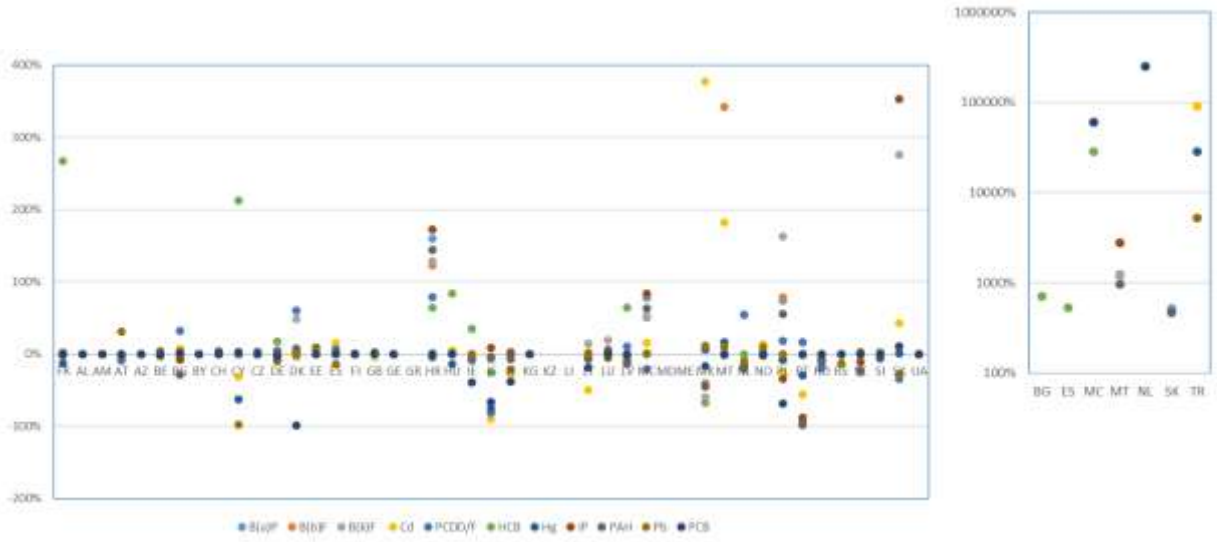

Fig. 1.7. *Recalculations between the 2020 and 2019 submission for 2017 values (reported data). The separate chart at the right side shows countries and pollutants with recalculations > 400% in logarithmic scale.*

Greece (GR), Kazakhstan (KZ), Liechtenstein (LI), Moldova (MD) and Montenegro (ME) reported data in 2020 but did not submit data in the year 2019.

Several countries reported significant recalculations for some of the pollutants (see right part of Fig. 1.7, which is displayed in logarithmic scale). Analysis shows that the 2017 values reported in the 2019 submissions where extremely low (e.g. Netherlands: PCB; Turkey: Cd, Hg, Pb; North Macedonia: HCB, PCB).

Both for PAHs and its compounds and for HCB, the recalculations submitted by Portugal (-97% for PAHs and -97% for HCB) contributed most to overall recalculations in the EMEP area.

1.1.4. Data sets for modellers in 2020

Data used by CEIP were reported by the Parties to the LRTAP Convention as sectoral emissions (NFR14) and National Total emissions according to the UNECE guidelines for reporting emissions and projections data under the LRTAP Convention, Annex I [*UNECE,* 2014].

Reported (NFR[7]) sector data were aggregated to 13 GNFR sectors. In several cases, no data were submitted by the countries, or the reporting is not complete or contains errors. Before modellers can

[7] *NFR – Nomenclature for Reporting*

use such emission data, missing or erroneous information has to be filled in or replaced by expert estimates. To gap-fill missing/erroneous data, CEIP typically applies different methods. The gap-filling procedure is fully documented every year in the technical reports which can be downloaded from the CEIP website[8]. After the gap-filling, sector emissions are used for spatial distribution (mapping) to the EMEP grids.

The Parties for which reported data were (partly) replaced in 2020 are Bulgaria, Germany, Finland, Greece, Italy, North Macedonia, Poland, Portugal, Romania, Serbia, Slovakia, Turkey and Ukraine (see Annex B3).

Contribution of individual sectors to total EMEP heavy metals and POPs emissions

Figure 1.8 shows the *contribution of each GNFR sector to the total emissions of individual air pollutants* (Cd, Hg, Pb, B(a)P, B(b)F, B(k)F, IP, PAHs, PCDD/F, HCB, PCB). To provide as complete a picture as possible of the share of the individual sectors in total EMEP emissions, data as used for EMEP models (i.e. gap-filled data) were used for the calculations. The analysis does not include sea regions.

It is evident that the combustion of fossil fuels and processing of raw materials is responsible for a significant part of heavy metals and POPs emissions.

Industry production emits about 35 % of Cd emissions, followed by 24% from public power and heat plants.

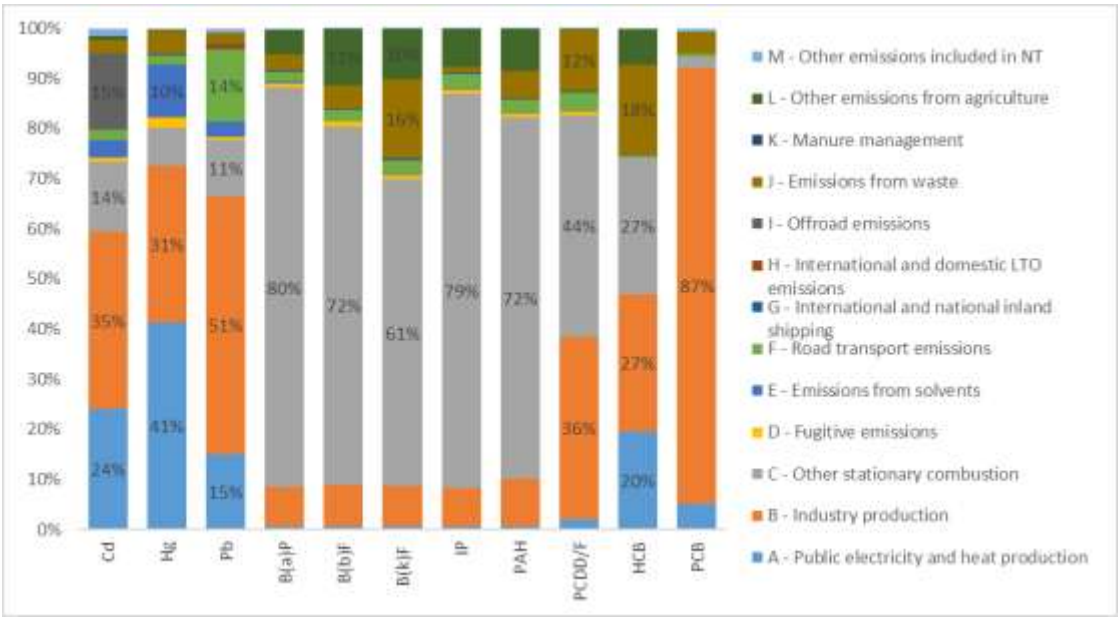

Fig. 1.8. *GNFR sector contribution to national total emissions in 2018, EMEP extended area without sea regions (only percentages above 10% are labelled).*

[8] https://www.ceip.at/ms/ceip_home1/ceip_home/ceip_reports/index.html *(2020 in progress)*

Energy industries emit about 41% of total Hg emissions, mainly from coal power plants, followed by the industry production sector, which released 31% of total emissions.

About 51% of Pb emissions are released by the industry production sector, while each of the other sectors contributes to a maximum of about 15%. Road transport (leaded gasoline) only contributes 14%.

The largest source of PAHs and its compounds (B(a)P, B(b)F, B(k)F, IP) is the 'other stationary combustion' sector, which contributes 72% of total emissions. The main source of PAH emissions are coal and wood stoves/boilers in households. 9% of PAH emissions are related to the industry production sector and 8% of PAH emissions are released by the agriculture sector, mainly from field burning of agriculture residues.

With 44% of total emissions, the 'other stationary combustion' sector contributes most to PCDD/Fs emissions. The main source of PCDD/F emissions are coal and wood stoves/boilers in households. Industry production plants (metal industries) contribute 36% of total PCDD/F emissions and the waste sector (mainly waste incineration) contributes about 12%.

With 27% of total emissions, the 'other stationary combustion' sector has a large share on HCB emissions, which is equal to the share of industry production with also 27%. The energy sector contributes 20% of total HCB emissions.

The dominating sector for PCB emissions is the industrial sector, which contributes 87% to total emissions.

Figure 1.9 illustrates the sector contribution for the EMEP West region and the EMEP East region. North Africa is included in the EMEP East region. The comparison of both graphs highlights some significant differences between West and East.

The continuous revision of inventory data for many countries shows that POPs emissions have the highest uncertainties of all pollutant groups. In addition, data for EMEP East is subject to incomplete reporting or delays in reporting. Especially for POPs, one should therefore draw conclusions carefully when comparing the shares between EMEP East and EMEP West.

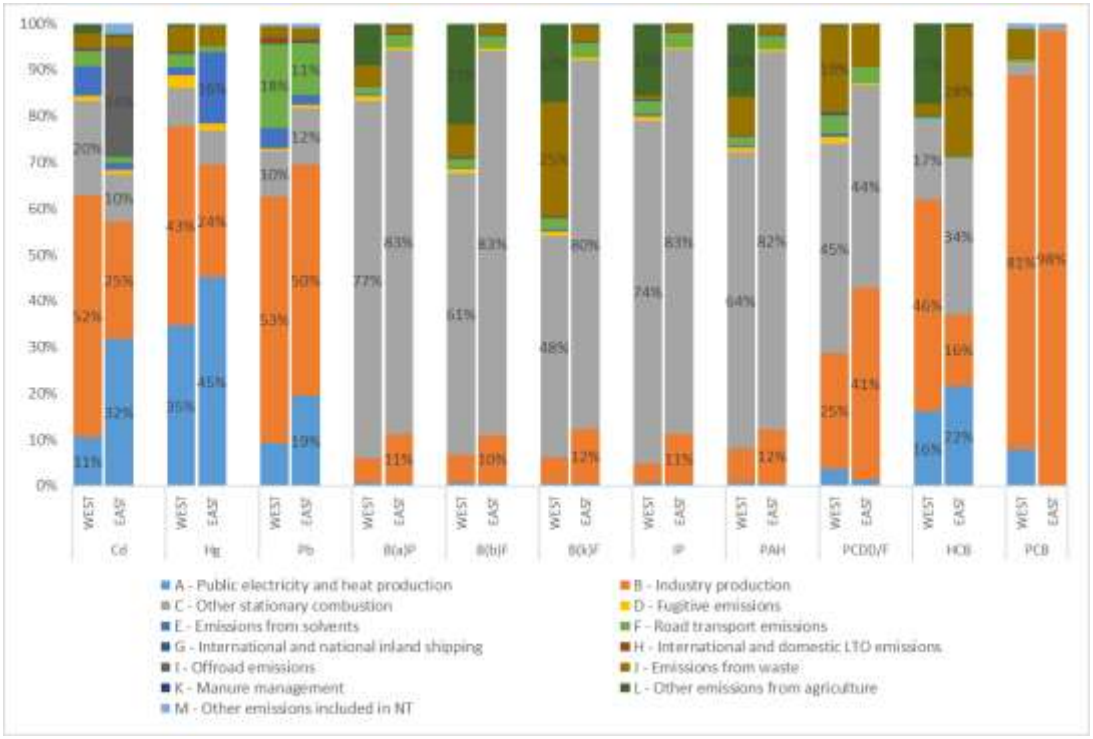

Fig. 1.9*. GNFR sector contribution to national total emissions in 2018 for the EMEP West and EMEP East areas (Only percentages above 10% are labelled. 'Remaining Asian Areas' are included in the EMEP East region and North Africa is included in the EMEP West region.*

Reporting of gridded data

2017 was the first year with a reporting obligation of gridded emissions in the grid resolution of 0.1°x0.1° (long/lat). 31 of the 48 countries which are considered part of the extended EMEP area reported sectoral gridded heavy metal and POP emissions in the new resolution until June 2020. *The majority of gridded sectoral emissions in 0.1°x0.1° (long/lat) resolution have been reported for the year 2015 (30 countries).* For the year 2016, gridded sectoral emissions have been reported by five countries, for the year 2017 by three countries and for the year 2018 by four countries.

Thirteen countries additionally reported gridded emissions for previous years (one country for the whole time series from 1980 to 2018; one country for the whole time series from 1990 to 2018; four countries for the years 1990, 1995, 2000, 2005 and 2010; one country for the years 1990, 2000, 2005 and 2010; one country for the years 2005 and 2010; one country for the year 2005; one country for the year 2010; three countries for the year 2014).

Reported gridded sectoral data in 0.1°x0.1° (long/lat) resolution, which can be used for the preparation of gridded emissions for modellers, covers less than 20 % of the cells within the geographic EMEP area. For the remaining areas missing emissions are gap-filled and spatially distributed by expert estimates. Reported grid data can be downloaded from the CEIP website[9]. An overview of gridded data reported until 2017 and until 2020 is provided in Table 1.1.

[9] https://www.ceip.at/status_reporting/2020_submissionss

Table 1.1. *Gridded emissions reported until 2017 and 2020*

Country	2017	2020	Comments
	Gridded data available for the years.	Gridded data available for the years	
Austria	2015	2015	
Belgium	2015	2015	
Bulgaria	2015	2015	
Croatia	1990, 1995, 2000, 2005, 2010, 2015	1990, 1995, 2000, 2005, 2010, 2015	
Czechia	2015	2015	
Denmark	2015	2015	
Estonia		1990, 1995, 2000, 2005, 2010, 2015	
Finland	2014, 2015	2014, 2015, 2016, 2017, 2018[(a)]	[(a)]Gridded data for 2014, 2015 and 2018 could not be used for the preparation of spatial distributed emission data.
France		2015	
North Macedonia		2015	
Georgia		2015	
Greece		2015	
Hungary	2015	2015	
Ireland	2015	2015	
Italy		2015	Reported gridded data were replaced by CAMS and EDGAR proxies.
Latvia	2015	2015	
Lithuania	2015[(b)]	2015	[(b)]Reported gridded emissions only on national total level, which could not be used for the gridding, which is done on sectoral level
Luxembourg	2005, 2010, 2015	2005, 2010, 2015	
Malta		2016	Grid reporting not in the defined 0.1°x0.1° coordinates
Monaco	2014, 2015	2014, 2015, 2016	
Netherlands		1990, 1995, 2000, 2005, 2010, 2015	
Norway	1990, 1995, 2000, 2005, 2010, 2015	1990, 1995, 2000, 2005, 2010, 2015	
Poland	2014, 2015	2014, 2015, 2018	
Portugal	2015	2015[(c)]	[(c)]The spatial disaggregation of sector 'F – Road Transport' was replaced by CAMS proxies.
Romania	2005	2005, 2015	
Slovakia	2015	2015	
Slovenia	2015	2015	
Spain	1990-2015	1990-2018	
Sweden		1990, 2000, 2005, 2010, 2015	
Switzerland	1980-2015	1980-2018	
United Kingdom	2010, 2015	2010, 2015	

Gridded data of 2018 in resolution 0.1° x 0.1° (long/lat)

For this year, it was agreed with the modellers to perform gap-filling and gridding for the year 2018 in 0.1° x 0.1° longitude/latitude resolution on GNFR sector level.

The 0.1° x 0.1° GNFR grids of heavy metals (Cd, Hg, Pb) and POPs (B(a)P, B(b)F, B(k)F, IP, PCDD/Fs, HCB) were spatially distributed based on the gridding system developed by CEIP. A map of Cd total emissions in 2018 is shown in Fig. 1.10 as an example. The system is module based and uses as a first step reported gridded emission data for each country and sector where it is available and usable. If no reported gridded data in the 0.1° x 0.1° (long/lat) resolution is available, reported gridded PM data is used as a proxy for spatial disaggregation. If reported PM data is not available either, PM data from the Copernicus Atmospheric Monitoring Service (CAMS-81, CAMS-REG-AP-v2.2) and the Emission Database for Global Atmospheric Research (EDGAR) is used as a proxy.

Reported gridded data in 0.1° x 0.1° (long/lat) resolution was used from Austria, Belgium, Bulgaria, Croatia, Czechia, Denmark, Finland, France, Georgia, Greece, Hungary, Ireland, Latvia, Luxembourg, Malta, Monaco, Netherlands, North Macedonia, Norway, Poland, Portugal, Romania, Slovakia, Slovenia, Spain, Sweden, Switzerland and United Kingdom.

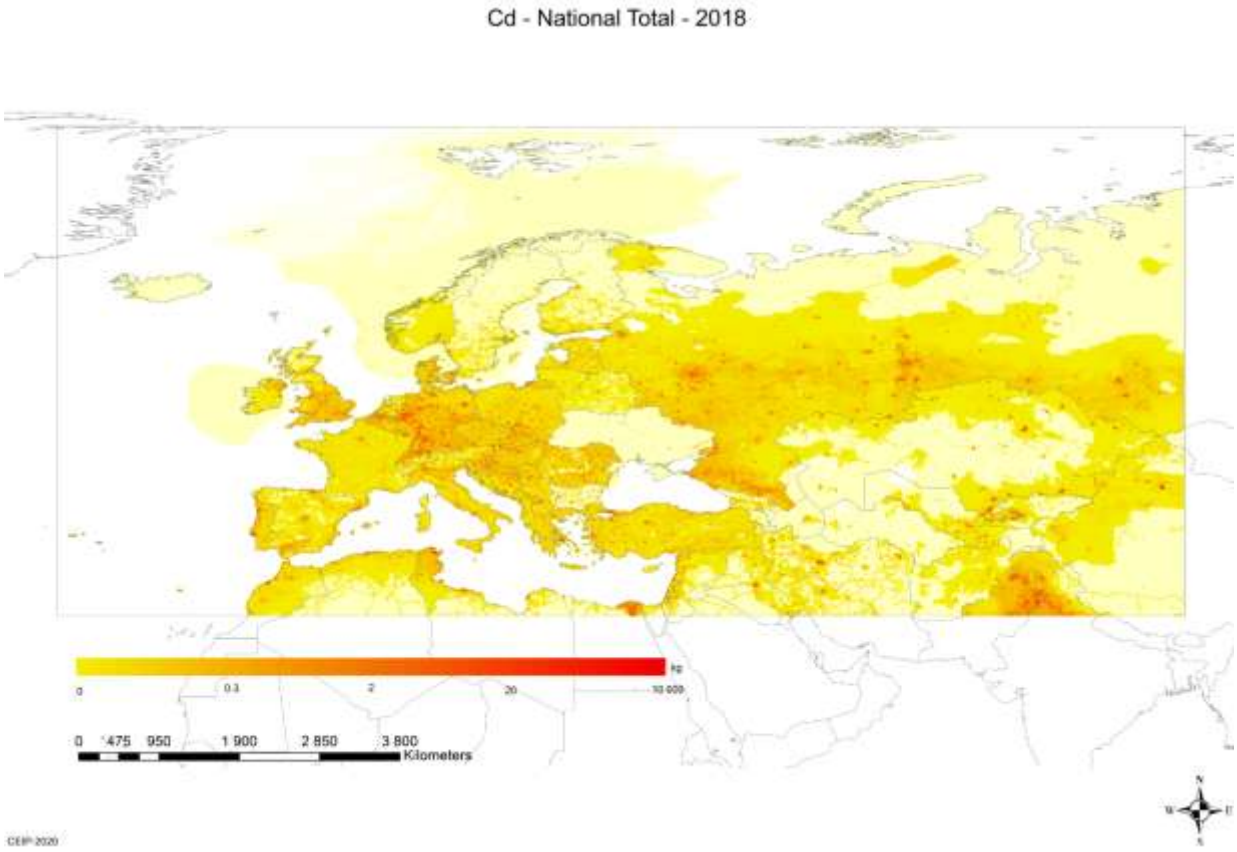

Fig. 1.10. *Visualized gap-filled and gridded Cd emissions in 0.1°x0.1° long-lat resolution.*

1.2. Emission data for modelling

Regional emissions

Model assessment of heavy metals and POPs pollution in the EMEP domain was made on the basis of gridded emission data with spatial resolution 0.1°x0.1° provided by CEIP (*http://www.ceip.at*). Pollution levels of heavy metals and POPs in 2018 were evaluated on the basis of emissions reported for the previous year 2017. Update of the modelling results based on the new emission data for 2018 is available at the MSC-E web site: www.msceast.org. Detailed description of estimated heavy metal and POP emissions in the EMEP countries, gap-filling methods, and expert estimates used for preparation of the emission inventory, can be found in the Technical reports of CEIP [*Tista et al.,* 2019a; 2019b].

Gridded emission data for PCB modelling were based on the available expert estimates and officially reported data of the EMEP countries. Model assessment of PCB pollution levels (total and congener specific) requires definition of emissions of particular PCB congeners. However, currently reported national inventories of PCB emissions provide total releases of PCBs without distribution by particular congeners. Therefore, to evaluate transport and fate of individual PCB congeners, congener specific emission inventory of *K.Breivik et al*. [2007] was used for modelling. The indicator congener PCB-153 was selected to characterize transboundary transport and pollution by PCBs. Spatial distribution of PCB-153 emissions was constructed on the base of gridded PCB emissions officially provided by 24 EMEP countries (namely, Austria, Belgium, Bulgaria, Croatia, the Czech Republic, Finland, France, Georgia, Greece, Hungary, Ireland, Latvia, Lithuania, Luxembourg, North Macedonia, Monaco, Norway, Poland, Portugal, Romania, Slovakia, Slovenia, Spain, and the UK). For other EMEP countries, which did not report gridded emission data, gridded population density was used for allocation of emissions.

Estimates of PCDD/F emissions officially reported by the EMEP countries are most likely subject to considerable uncertainties due to underestimation of releases from some source categories (e.g. 'Residential combustion' and 'Open burning of wastes') and incomplete coverage of all potential sources [*Breivik et al.*, 2004; *Fiedler*, 2007; *Pulles et al.*, 2005; *Pulles et al.*, 2006]. For this reason, emission scenario, representing maximum level of PCDD/F releases to the atmosphere was used in the model simulations. The maximum emission scenario was prepared on the basis of the uncertainty range reported by 12 EMEP countries in their inventory information reports (namely, Belarus, Belgium, Croatia, Cyprus, Denmark, Estonia, Finland, France, Latvia, Poland, Sweden, and the UK). Difference between the maximum and average estimates of PCDD/F emissions in these countries varied from a factor of 1.3 for Latvia up to a factor of 4.3 for Denmark. For other EMEP countries, which did not report uncertainty range in their inventories, the maximum level of national PCDD/F emissions was assumed to be 3-fold higher compared to the officially reported emissions in accordance with the expert estimates [*Pulles et al.*, 2006; *Bogdal et al.*, 2014]. Thus, total PCDD/F emission in the EMEP countries according to the maximum emission scenario exceeded reported data in the inventories by a factor of 3.5 on average. This approach has already been applied in the model assessment for previous year [*Gusev et al*., 2018].

Maps illustrating spatial distributions of the pollutants, namely, Pb, Cd, Hg, B(a)P, sum of 4 PAHs, PCDD/Fs, HCB and PCB-153 emission fluxes from anthropogenic sources in the EMEP region, used in the model simulations for 2018, are presented in Fig. 1.11.

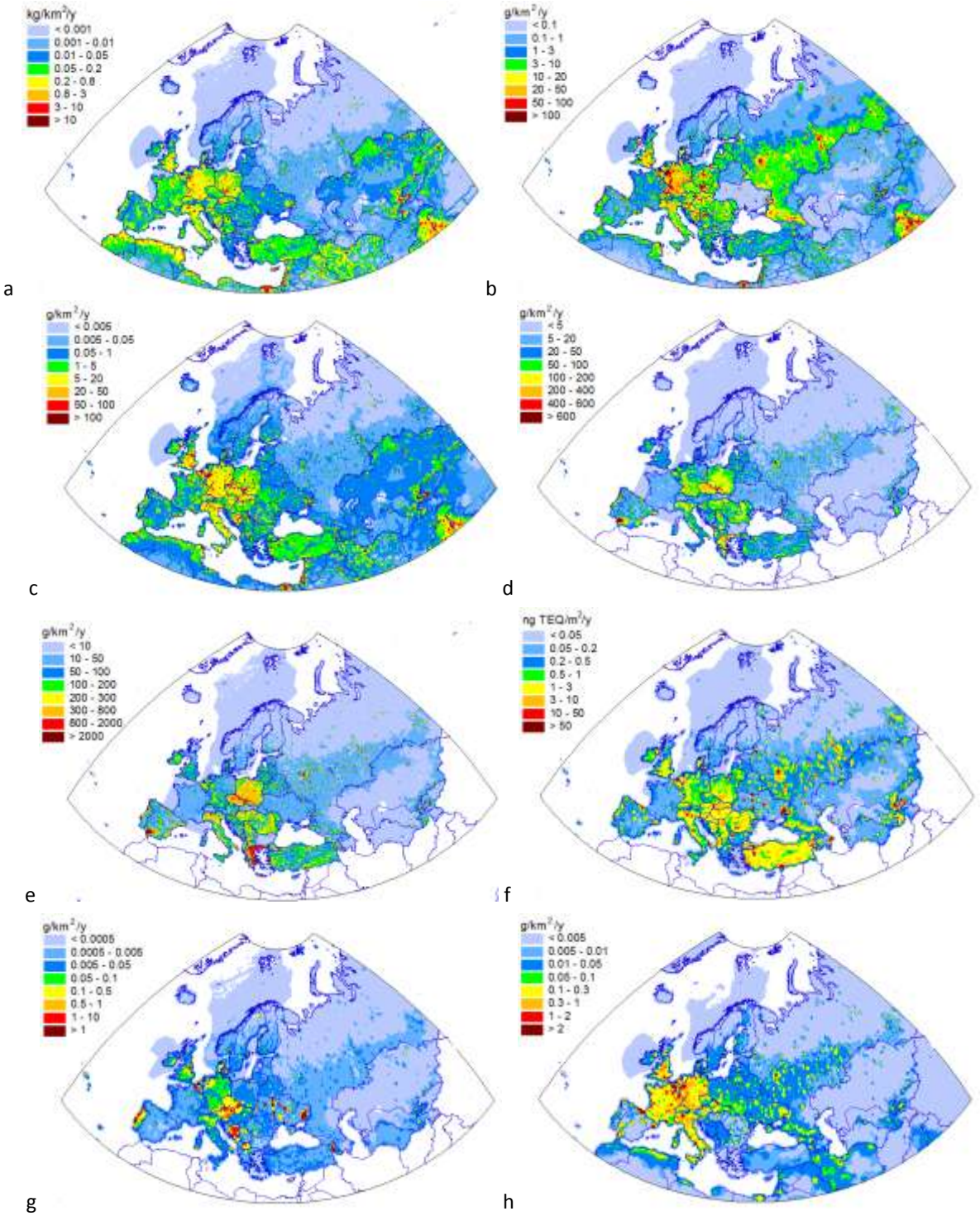

Fig. 1.11. *Spatial distribution of Pb (a), Cd (b), Hg (c), B(a)P (d), sum of 4 PAHs (e), PCDD/Fs (f), HCB (g) and PCB-153 (h) emissions in the EMEP region used in model simulations for 2018*

Along with gridded emission data the GLEMOS modelling system requires additional information on heavy metal and POP emissions, namely, intra-annual variations, distribution of emissions with height and chemical speciation of Hg emissions. Necessary vertical and temporal disaggregation of the emissions was generated using the emission pre-processing tool, developed in MSC-E for the GLEMOS modelling system. More detailed information on the emission pre-processing procedure is presented in the heavy metal Status Report [*Ilyin et al*., 2018].

Global emissions

A number of pollutants, such as mercury and some POPs, are known for their ability to disperse in the atmosphere over the global scale. In order to take into account contribution of intercontinental transport to pollution levels in the EMEP countries and to evaluate boundary and initial conditions required for the regional EMEP modelling, global-scale model simulations are carried out.

Global-scale modelling of Hg is based on gridded emission data produced in the framework of the UNEP Global Mercury Assessment 2013 [*AMAP/UNEP*, 2013] and related to 2010. Intercontinental transport of PAHs is simulated based on emissions, produced by the research group of Peking University [*Shen et al*., 2013]. Global PAH emission inventories with 0.1°x0.1° spatial resolution were developed using a bottom-up approach for the period from 1960 to 2014. For the evaluation of global-scale transport and fate of PCDD/Fs, HCB, and PCBs expert estimates of global emissions were utilized. In particular, global gridded emissions of PCDD/Fs to the atmosphere and soil were prepared using the national emission inventories reported by countries to the Stockholm Convention [*Gusev et al.*, 2014; *Shatalov et al.*, 2014]. Model simulations of HCB global-scale transport were carried out on the basis of experimental emission scenario of historical HCB releases during the period covering several recent decades [*Shatalov et al.*, 2010]. For PCB-153 modelling, data on global emissions were derived from the inventory of *Breivik et al.* [2007]. Spatial distributions of Hg and PCB-153 emissions, used in the global-scale model simulations for 2018, are shown in Fig. 1.12.

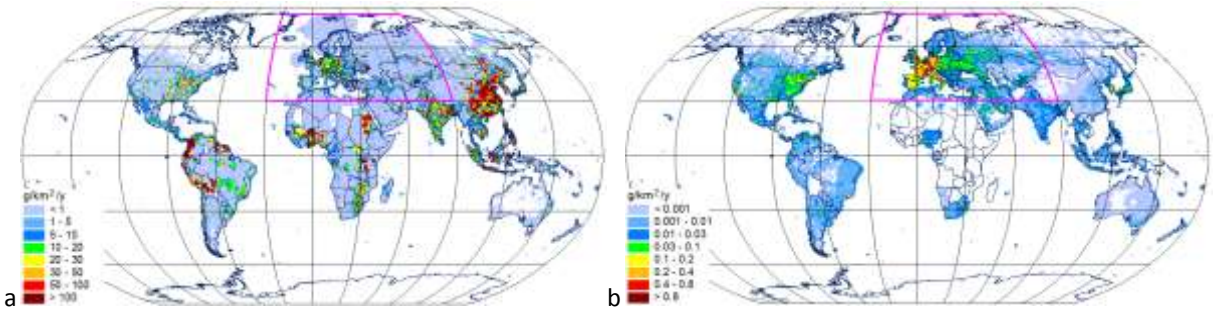

Fig. 1.12. *Spatial distribution of global annual emissions of Hg (a) and PCB-153 (b) with spatial resolution 1°x1°, used in the model simulations for 2018*

Chapter 2. MEASUREMENTS OF HEAVY METALS AND POPs

2.1. Monitoring of POPs and heavy metals in 2018

Heavy metals and persistent organic pollutants (POPs) were included in EMEP's monitoring program in 1999. However, earlier data have been reported and are available. The EMEP database, especially for heavy metals, thus also includes older data, even back to 1976 for a few sites. A number of countries have been reporting heavy metals and POPs within the EMEP area in connection with different national and international programmes such as HELCOM, AMAP and OSPARCOM.

The EMEP monitoring strategy [*UNECE*, 2019] defines the monitoring obligations for the Parties. For POPs, PAHs, PCBs, HCB, chlordanes (CHLs), lindane/γ-hexachlorohexane (γ-HCH), α-HCH, and DDT/DDE are part of the compulsory monitoring programme, while for heavy metals, Hg, Cd and Pb are the 1st priority elements, and Cu, Zn, As, Cr, Ni are the 2nd priority. In addition to these compounds, several Parties report other POPs and trace elements. In addition to regulated POPs, it is recommended to increase the attention on organic contaminants of emerging concern (CECs).The monitoring of CECs provides important knowledge to better understand the CECs' potential for long-range transport and to help authorities in determining adequate policy measures and if necessary, make national or international regulations come into place. Initial monitoring of CECs in background air have shown that many CECs are present in concentrations exceeding the concentrations of the legacy POPs with up to 1000 times.

All the data are available from the EBAS database (http://ebas.nilu.no/), and more detailed information about the sites and the measurement methods, these are found in EMEP/CCC's data report on heavy metals and POPs [*Aas et al*., 2020].

2.1.1. Monitoring of POPs in 2018

The spatial coverage of POP monitoring in Europe is dependent on the components in question. In total there are 32 sites reporting 2018 data on POPs whereof 26 sites report measurements in both air and precipitation. Data are available from 15 Parties. In addition to these, there are measurements also in France which has not been reported to CCC in time to be included in this report. One should further notice that several of the Parties only measure PAHs (i.e. 9 Parties and 21 sites). Excluding these sites there are 11 sites with POP measurements whereof 9 with measurements in both air and precipitation, from 6 Parties. For precipitation measurements, it is a challenge to compare the observations since the measurements are done using several different methods. There are four different matrixes defined for precipitation, i.e. total deposition (precip+dry_dep: 16 sites), concentration in precipitation (precip: 6 sites); concentration in precipitation + POPs deposited in the funnel (precip_tot: 5 sites) and wet deposition (wet dep: 2 sites).

Most POPs are semi-volatile substances, e.g. they may occur in both gaseous and particulate states in the atmosphere. Their gas-particle partitioning is strongly temperature-dependent, and hence partitioning may vary both temporally (diurnal, seasonal) and spatially (e.g. by altitude, latitude).

Several POPs furthermore have a significant potential for reversible atmospheric deposition. POP exchange between the atmosphere and various surface media is strongly temperature-dependent as well. Hence, measured concentrations of POPs in air may in part be a result of volatilization from environmental surfaces contaminated in the past, i.e. secondary emissions. Primary diffusive emissions of intentionally produced semi-volatile POPs (industrial chemicals, organochlorine pesticides) is often temperature-dependent as well. Thus, concentrations of POPs tend to be elevated in air during summer because of elevated primary and/or secondary emissions. To complicate matters, any correlation between air temperature and elevated concentrations of POPs in air at northern background sites may also be a reflection of long-range atmospheric transport (LRAT) from warmer regions with higher emissions. In this year's report, the main focus is on seasonal variability of selected POPs in air in an attempt to (i) highlight the importance of continued long-term seasonally resolved monitoring within EMEP and (ii) identify and discuss some issues which may merit further attention in terms of sources, processes and control strategies.

Seasonal variability of selected PAHs in air during 2018

As PAHs are by-products of combustion, several emission sources are seasonally variable [*Zhang and Tao*, 2009]. Examples include PAHs emitted as a result of domestic burning of wood and coal during winter. A strong seasonal variability in PAH air concentrations have been demonstrated in several studies [e.g. *Miura et al.* 2019], which is also seen in the EMEP monitoring data. Furthermore, concentrations of PAHs in urban air may be orders of magnitude higher than in remote areas as the Arctic, which has been attributed to a profound influence from primary emissions sources in controlling atmospheric burdens [*Prevedouros et al.*, 2004]. Hence, PAHs typically show a strong seasonal and spatial variability.

But unlike most halogenated legacy POPs, several PAHs have a relatively short half-life in air [*Brubaker and Hites*, 1998]. As the reaction rate in air is faster during summer because of higher temperatures and concentration of OH-radicals, their long-range atmospheric potential is predicted be much shorter during summer than winter [*Beyer et al.*, 2003]. Hence, some of the seasonal variability observed in background air is likely affected by interannual variability in the efficiency of atmospheric removal via degradation. Furthermore, a modelling study has suggested that degradation of PAHs in the gas-phase is anticipated to be faster than in the particulate phase [*Lammel et al.*, 2009].

PAHs contain two fused rings or more, and individual substances within the group of PAHs are highly diverse in terms of physical-chemical properties. This has implications fate processes which affect their potential for atmospheric removal via atmospheric deposition. For example, the equilibrium partitioning coefficients between air and water (K_{AW}) span about 3 orders of magnitude for the selected PAHs. High-molecular weight PAHs are therefore anticipated to be more prone to wet deposition than lighter PAHs.

Table 2.2. *Physical-chemical properties and reaction half-lives in air for selected PAHs, along with the number of sites reporting data for air in 2018.*

Abbreviation	Abbr.	Number of rings	Molecular weight (g/mol)	log K_{OA} [a]	log K_{AW} [a]	$t_{1/2}$ air (hours)[b]	Number of sites (2018)
Naphthalene	NAP	2	128.2	5.19	-1.73	12	7
Anthracene	ANT	3	178.2	7.63	-2.69	1.5	20
Phenanthrene	PHE	3	178.2	7.64	-2.76	11	20
Fluoranthene	FLT	4	202.3	8.81	-3.27	26	16
Pyrene	PYR	4	202.3	8.86	-3.27		21
Benzo[a]anthracene	BaA	4	228.3	10.28	-3.59		30
Chrysene	CHR	4	228.3	10.30	-3.82		20
Benzo[a]pyrene	B(a)P	5	252.3	11.48	-4.51		31
Indeno[1,2,3-cd]pyrene	IPY	6	276.3	12.43	-4.70		29
Benzo[g,h,i]perylene	BPE	6	276.3	12.55	-4.77		25

[a] - *Ma et al.* [2010] [b] - *Brubaker and Hites*, 1998

Variability in relevant physical-chemical properties among the PAHs also has implications for air monitoring strategies aiming to determine total concentrations in air. From simple theoretical considerations, PAHs include substances which could be present as gases, sorbed to particles or both. In general terms, low-molecular weight PAHs with a low K_{OA} are anticipated to be mainly present in the gaseous state, whereas high-molecular weight PAHs with a high K_{OA} are anticipated to sorb more strongly to atmospheric particles [*Finizio et al.*, 1997; *Lohmann and Lammel*, 2004]. As exemplified in Table 2.1, log K_{OA}'s for selected PAHs included in Table 2.1 span a wide range from about ~5 to ~12. For this reason, measurements of PAHs with a low K_{OA} PAHs on filters only, may not be representative for total concentrations in air. At the same time, PAHs with a high K_{OA} may be largely present in sorbed state on atmospheric particles and therefore require determination in the particulate phase using filters. For PAHs with an intermediate log K_{OA}, measurements of concentrations in both sorbed and gaseous state might be required to determine total concentrations in air for PAHs [*Meyer et al.*, 2005].

In Figure 2.1, we have used monthly mean concentrations in air as reported to EMEP in 2018 to assess possible impacts of sampling strategies on atmospheric burdens for selected PAHs with divergent physical-chemical properties [ANT, FLT, B(a)P and BPE]. More specifically, we compare data sampled either based on (i) gas + particles combined [air+PM_{10} or air+aerosols] or (ii) PM_{10} only. We caution that this simple analysis is based on mean monthly

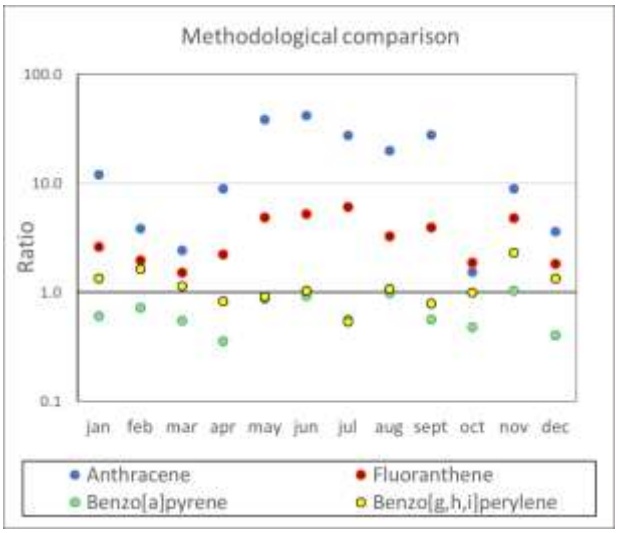

Fig. 2.1. *Methodological comparison based on monthly mean concentrations of selected PAHs in air (air+particles), divided by monthly mean concentrations (PM_{10}) across EMEP sites.*

concentrations across sites and not for one site only. Nevertheless, we see that both B(a)P and BPE which have log K_{OA}'s higher than 11 tend to have a ratio close to 1. This suggests that either methods are anticipated to yield relatively similar results, considering that these represent measurements in air across several sites. For ANT and FLT, which both have a log K_{OA} of less than 9, there is a marked difference not seen for B(a)P and BPE. This shows that ANT and FLT are mainly present in the gaseous state. Interestingly, the difference in this ratio across months appears particularly strong during summer, which potentially might be due to a temperature effect, further enhancing their volatility at warmer temperatures (i.e. presence in gaseous state).

To further explore the issue of seasonal variability, we have plotted the ratio between monthly mean concentration of selected PAHs in air, divided by the annual mean in 2018 for individual sites in Fig. 2.2. We see that there is a strong seasonal variability with higher concentrations in air during winter for all four PAHs. This can be attributed to a combination of both elevated emissions during winter (and/or reduced half-lives during summer). For FLT, which has comparable log K_{OA}'s yet divergent atmospheric half-lives (Table 2.1), it appears as if the seasonal variability is less pronounced for the bulk measurements than the measurements based on PM_{10}. This pattern is the opposite for the less volatile PAHs whereby seasonal variability is less pronounced for measurements derived on the basis of bulk sampling. Again, the latter could be an effect of enhanced volatility during summer whereby an increasing fraction of lower-volatility PAHs are present in the gaseous state.

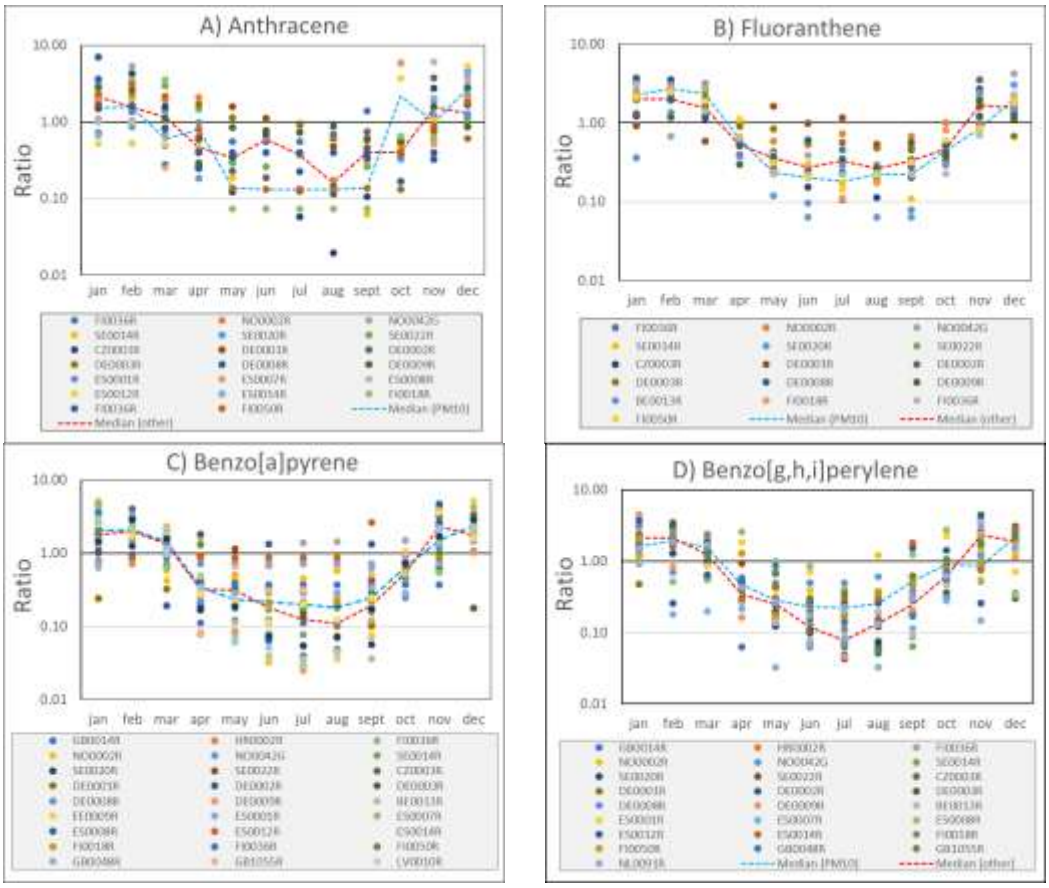

Fig. 2.2. *Ratio between monthly mean concentration of selected PAHs in air, divided by the annual mean in 2018, for selected PAHs at individual sites (dots). We have also included the median ratio across sites which are based on either sampling strategies (stipulated lines).*

The regional distribution of PAHs for the different seasons are shown in Fig. 2.3. It clearly shows the higher concentrations during winter in eastern Europe where the emissions from residential heating are highest.

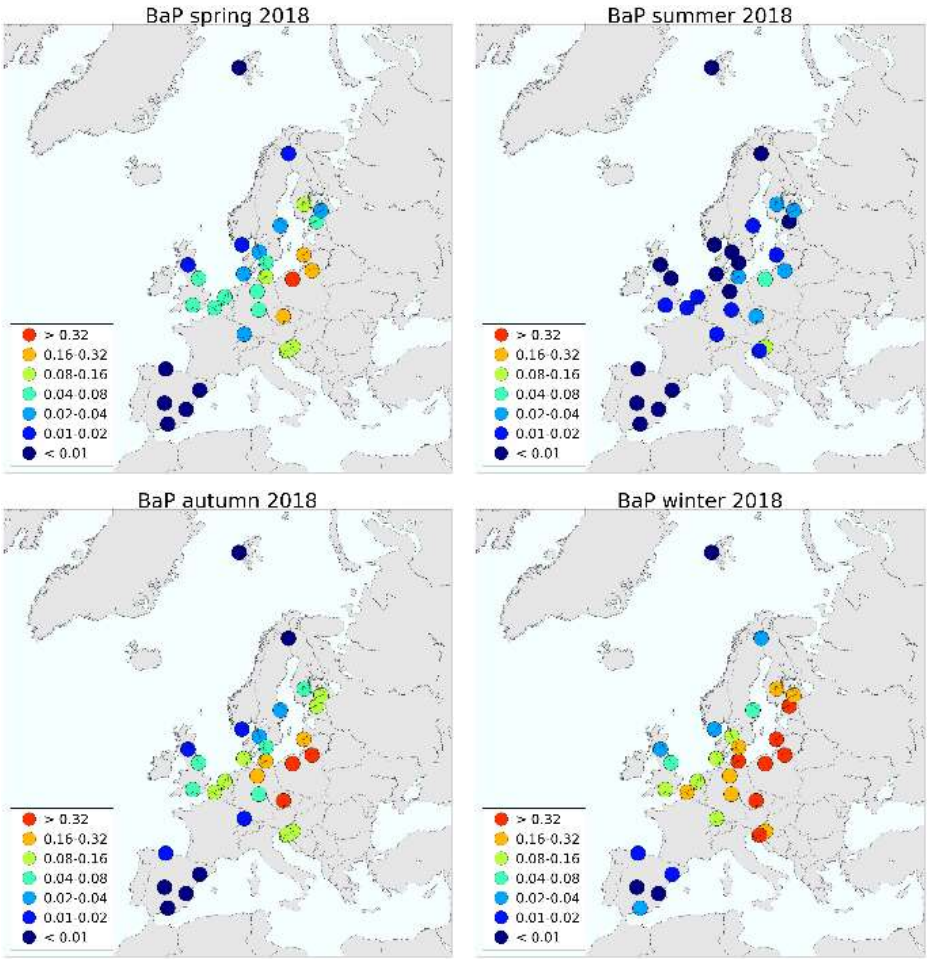

Fig. 2.3. *Spatial coverage of Benzo(a)pyrene at different seasons in 2018, ng/m^3.*

On the basis of EMEP measurement data for the selected PAHs, we suggest that sampling strategies based on filters only (PM_{10}) may represent a poor measure of total concentrations in air for low-molecular (high K_{OA}) PAHs. At the same time, those measurements are nevertheless invaluable for the purpose of model evaluations, i.e. predictions of concentrations in the particulate phase which are not captured by EMEP data representing bulk concentrations.

Long-term trend analyses of benzo(a)pyrene in air

PAHs have been monitored for 10 years or more at 18 EMEP sites. The long-term data series allows for trend analysis using the Digital Filtration (DF) technique that also been adapted on sites within AMAP [*Hung et al.*, 2016; *Yong et al.*, 2019]. The DF technique fits seasonal cycles and inter-annual trends or time series with statistical techniques. An apparent first order half-life, t1/2, is calculated by dividing ln2 with the negative value of the linear regression slope of the trend between the

natural log of air concentrations, ln C (pg/m^3), and time (year). Long-term time trends for individual POPs are expressed as apparent first order half-lives (t1/2, y). It should be noted that the compounds do not necessarily decline/increase linearly or consistently in the first order manner throughout the entire monitoring period. The obtained half-lives don't give precise information but can be used to compare the relative rates of decline or increase of concentrations between the compounds, e.g. a smaller positive number means that the decrease has been sharper than a larger positive number. In contrast, negative values indicate increasing trends. The absolute values of these half-lives or doubling times should be used with caution. When the r2-value for the trend analysis is too low there is no significant trend for the time period (NST in Fig 2.4).

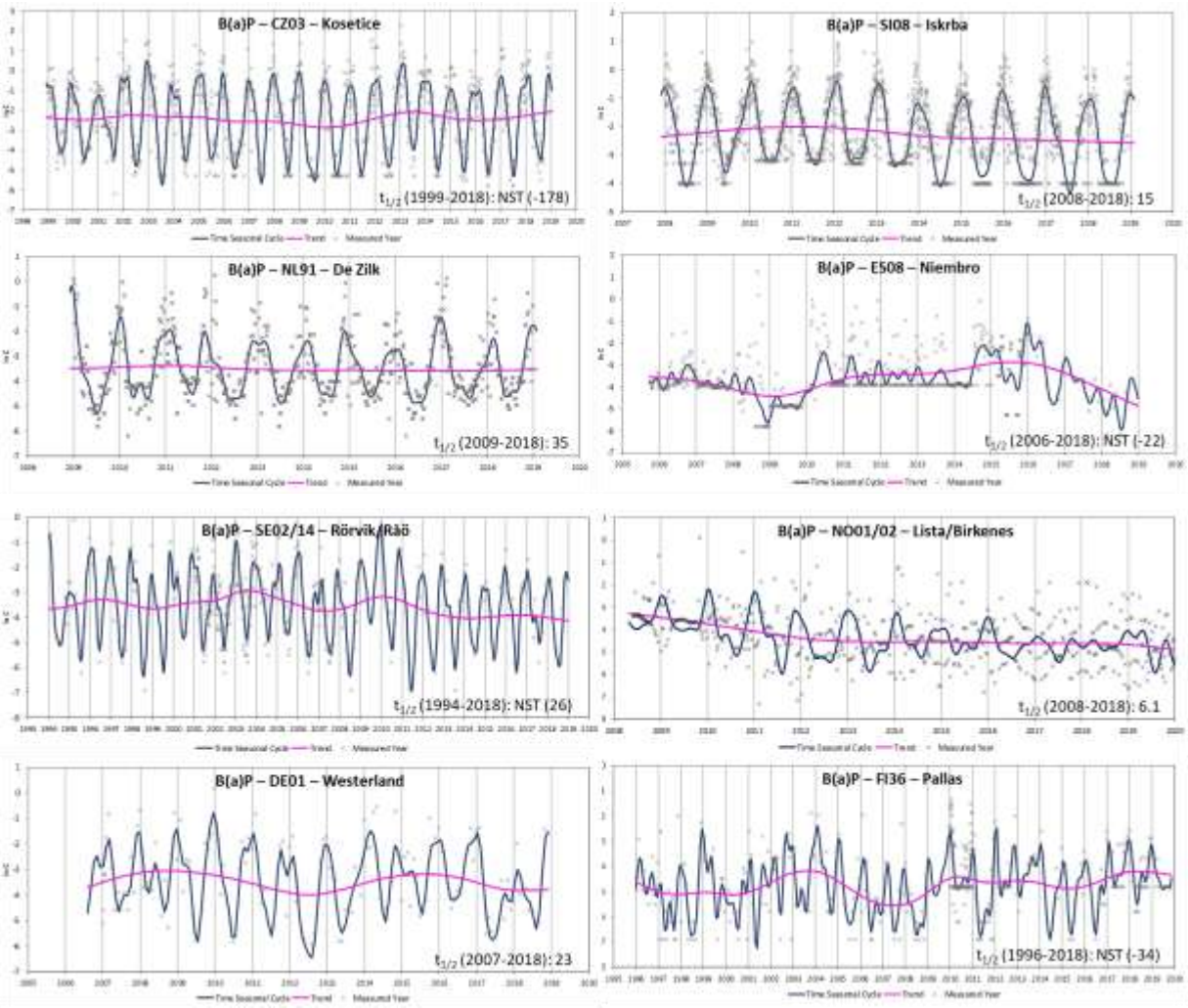

Fig. 2.4. *Temporal-trends of benzo(a)pyrene in air at a selection of EMEP sites. The air concentrations are presented in natural log of concentrations (ln C)*

The results within EMEP are generally in line with the results within AMAP [*Yu et al.*, 2019]. No significant decrease in concentrations of B(a)P is observed at the EMEP sites. Instead stable concentrations are observed over time. Only at one site, Birkenes (NO002) in southern Norway, a small decrease is observed with a half-life of 6.1.

2.1.2. Monitoring of heavy metals in 2018

In 2019, there were 40 sites measuring heavy metals (cadmium or lead) in both aerosols and precipitation, and altogether there were 64 measurement sites. 25 sites were measuring mercury in either air and precipitation, 15 of these with co-current measurements in air and precipitation. In total, 20 Parties to the Convention reports heavy metal data to EMEP. In addition to these, there are measurements also in France and Ireland, which has not been reported to CCC in time to be included in this report.

Annual averages of Pb, Cd and Hg concentrations in precipitation and in air in 2018 are presented in Figure 2.5 to Figure 2.7. For lead, the highest concentration in aerosols is observed in Hungary and Slovakia, flowed by the Benelux countries. In precipitation, the highest volume weighted annual mean is observed in Spain and Slovakia followed by sites in Hungary, Denmark. For cadmium, the highest concentration in aerosols in observed in Poland followed by sites in Belgium, Hungary and Slovakia while in precipitation, the highest level is seen in Estonia and Spain followed by sites in Sweden and Denmark. For total gaseous and elemental mercury, the highest concentration is seen in Germany, while in precipitation, the highest levels are seen in The Czech Republic and surprisingly in Sweden and Finland. The concentrations of mercury, as well as for cadmium and lead, in precipitation observed in Sweden and Finland are considerably higher compared to previous years. The summer of 2018 was special in Scandinavia with drought and many forest fires that may have released and resuspended mercury containing particles to air. The concentrations of aluminum and iron which are typically tracers from mineral dust is also considerably higher in Finland in 2018 than 2017. The precipitation amount was much lower in Sweden and Finland in 2018 compared to a normal year, thus the wet deposition of trace elements are not so different in 2018 compared to 2017. Poland on the other hand recorded suspiciously low concentrations of mercury in precipitation in 2018, half of what was seen in 2017. For mercury in air, the observed concentrations in Spain is extremely low (0.36 ng/m^3) indicating problems with the measurements. This is also the case in Slovenia, but the data coverage is low and therefore not included in the map.

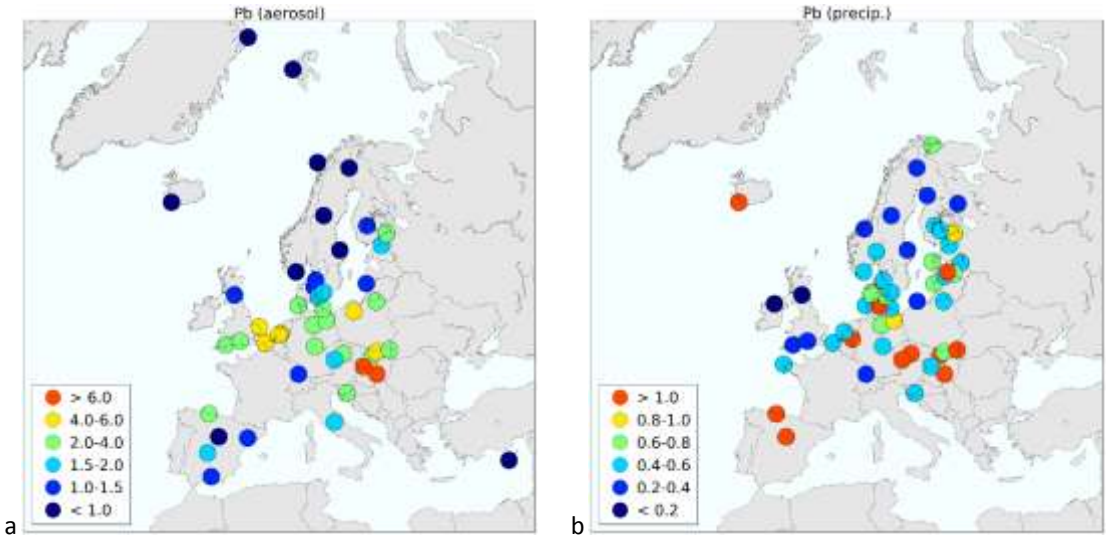

a b

Fig. 2.5. *Annual mean concentrations of lead and in aerosols (a), ng/m^3 and precipitation (b), µg/L in 2018.*

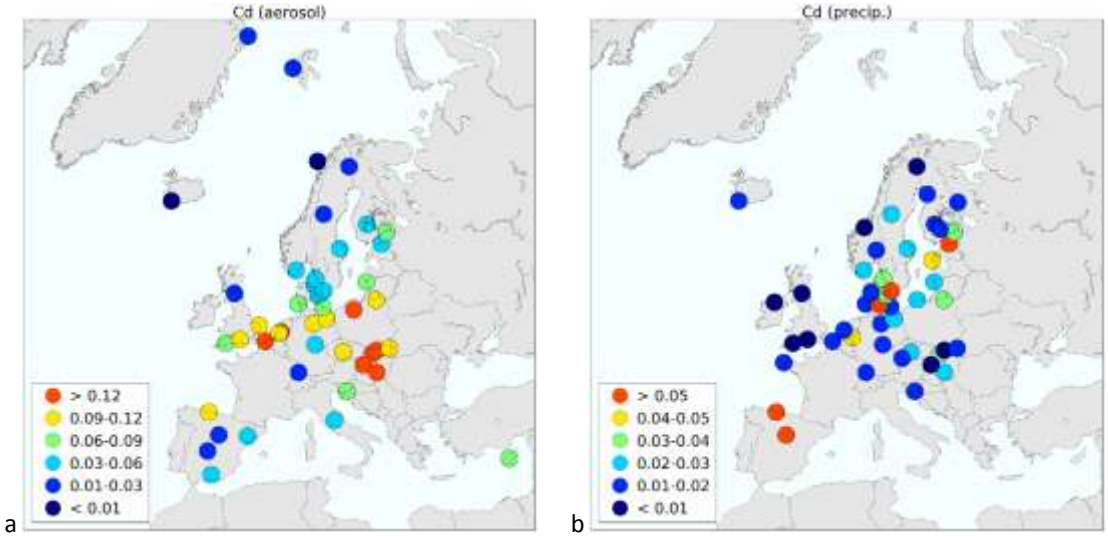

Fig. 2.6. *Annual mean concentrations of cadmium in aerosols (a), ng/m^3 and precipitation (b), μg/L in 2018.*

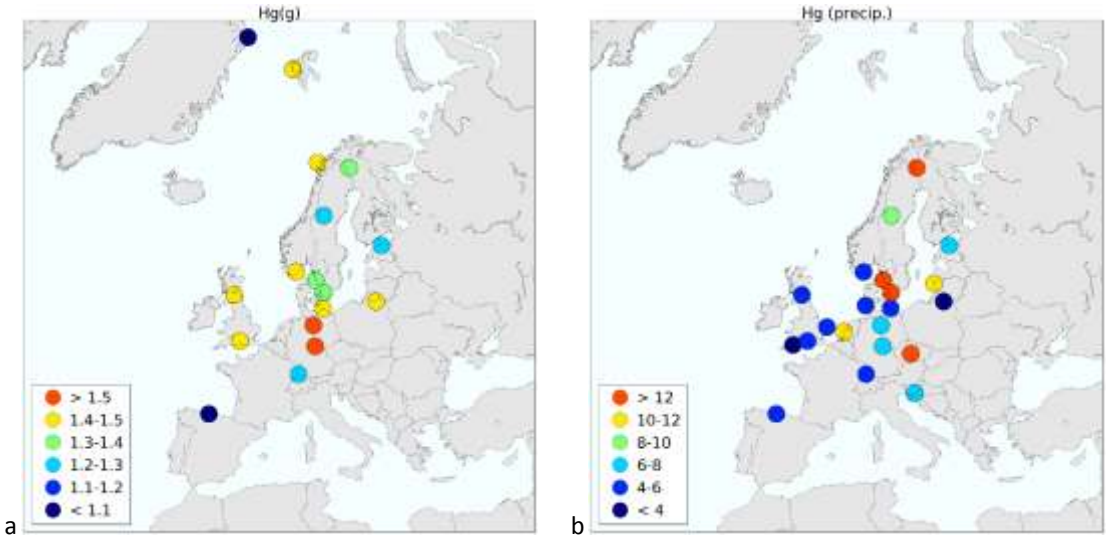

Fig. 2.7. *Annual mean concentrations of mercury in air (a), ng/m^3 and precipitation (b), ng/L in 2018.*

2.2. Supplementary measurements

Measurements at EMEP stations are mostly restricted by remote areas to avoid the influence of nearby located anthropogenic emission sources. To analyze pollution levels in the EMEP region and evaluate modelling results against measurements, EMEP monitoring data can be complemented with the measurements from other monitoring networks and specific monitoring campaigns. In particular, observational data of national monitoring networks in the EU countries are regularly reported to the European Environmental Agency (EEA) [*AIRBASE*, 2020]. The EEA database provides the monitoring data on various pollutants including heavy metals (Pb, Cd, Hg as well as second priority metals) and selected POPs (e.g. PAHs).

The EU national monitoring networks are designed to characterize pollution levels for different types of areas, including rural, suburban, urban, industrial, and traffic areas. In spite of difference in methodology comparing to the EMEP monitoring, AIRBASE measurements, along with fine resolution

modelling results, can be used to better reproduce concentrations and deposition fluxes of heavy metals and POPs in more polluted and densely populated regions.

In accordance with the developed classification [*Larssen et al*., 1999], national monitoring stations in the EU countries are subdivided by the type of area, where stations are located, and from the viewpoint of predominant emission sources affecting the stations. Area types include urban (almost or completely built-up area), suburban (built-up area mixed with agricultural lands, woods etc.) and rural. Rural stations are in addition subdivided into the following categories:

- Rural-Near city (area within 10 km from the border of an urban or suburban area),
- Rural-Regional (10-50 km from major sources/source areas),
- Rural-Remote (50 km from major sources/source areas).

Subdivision of stations regarding to predominant emission sources includes the following types:

- Traffic (located in close proximity to a road and strongly influenced by traffic emissions),
- Industrial (located near single industrial sources or industrial areas),
- Background (not dominated by single emission source; representative of a wider area of at least several square kilometers).

In this report available AIRBASE data on measured B(a)P air concentrations in 2018 were used for the analysis of pollution levels. In 2018 information on measured concentrations of B(a)P in air was reported by about 770 stations (Fig. 2.8). It can be seen that these data provide substantially denser spatial coverage than the EMEP measurements (e.g. in Germany, Poland, Italy, France, and Spain). Besides, AIRBASE data are reported for regions where measurements of EMEP are scare or not available (e.g., Romania, Bulgaria, Ireland, Hungary, Slovakia, Lithuania, Switzerland, Greece, and Denmark). Besides, the data on Pb and Cd air concentrations for 2014-2016 were used in the country-scale study on assessment of heavy metal pollution levels in Germany (See section 4.2).

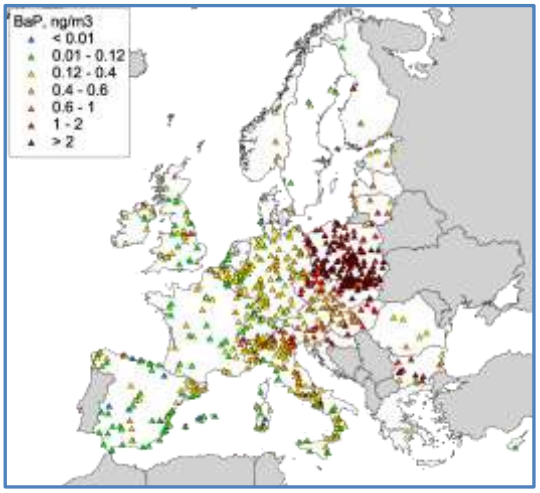

Fig. 2.8. *Concentrations of B(a)P in air observed in 2018 (a) in the EMEP region from AIRBASE database.*

Chaptre 3. STATUS OF HEAVY METALS AND POP POLLUTION IN 2018

The chapter contains results of the assessment of heavy metal and POP pollution levels in the EMEP region in 2018 performed in accordance with the mandate of EMEP [ECE/EB.AIR/2019/8] and bi-annual work-plan [ECE_EB.AIR_144_Add.2]. Spatial patterns of air concentration, deposition and transboundary transport of the pollutants are discussed along with additional information for assessment of human and ecosystem exposure by toxic substances, and estimates of atmospheric pollution of marginal seas and the Arctic. In addition, results of heavy metal and POP pollution assessment on a global scale are described.

3.1. Meteorological conditions of 2018

Information on meteorological conditions is highly important for modelling of heavy metal and POP pollution levels. Atmospheric flows, stability and vertical exchange determine long-range transport of the pollutants. Wet scavenging and deposition are affected by atmospheric precipitation. Rates of chemical reactions resulting in Hg and POP transformations depend on air temperature. Flux of dust re-suspension is controlled by soil moisture and wind velocity.

Meteorological conditions change from one year to another. It occurs due to relatively short-term inter-annual variability and because of long-term climatic changes. Therefore, meteorological parameters of 2018 are analyzed via comparison with climatic norm. Climatic norm is assumed as average for the period from 1981 to 2010 [*Blunden and Arndt*, 2019]. Anomalies of meteorological parameters of current (2018) year relative to climatic mean values are considered. Positive anomaly means that the value in 2018 is higher than the climatic norm and vice versa. Besides, meteorological conditions of 2018 are compared with the conditions of previous year because it is helpful for explaining differences in modelling results of 2017 and 2018.

Mean temperature anomaly averaged over European region in 2018 is 1.1°C. This year is the second warmest since 1950 [Blunden and Arndt, 2019]. Over most part of Europe the anomaly is positive ranging from 0-1°C in Spain, the United Kingdom and European part of Russia to 2-3°C in some regions of the Czech Republic, Romania, Poland and Georgia (Fig. 3.1a). Besides, high anomalies (1-3°C) take place in the Arctic. In winter 2017/2018 the highest anomalies (4-5°C) are recorded for the Arctic, the northern part of Russia, Caucasus and Turkey. Over Scandinavia and the south-western part of Europe small negative anomalies (about -1°C) are observed. In summer temperature anomalies take place over most of Europe. In particular, in Scandinavia and Central Europe the air temperature anomalies in summer are 2-3°C on average, reaching 4-6°C at particular synoptic stations [*WMO*, 2019]. In Eastern and Southern Europe the anomalies in summer are about 1-2°C.

Over the central and northern parts of Europe dry conditions predominate in 2018 with annual precipitation reaching 60-80% of climatic norm (Fig. 3.1b). In Latvia, Estonia and the eastern part of Kazakhstan annual precipitation sums reach 40% of the norm. The opposite situation occurs in southern Europe and Middle East where excess of precipitation makes up 25% reaching almost 70%

in some parts of Spain, Italy and the Balkan region. In winter of 2017/2018 France, north of Spain, the Balkan region and the eastern part of Europe experienced excess of precipitation. In spring, summer and autumn of 2018 deficit of precipitation was recorded over most part of central and northern Europe. In particular, in the Scandinavian region the precipitation in the period from March to November constitutes 40-60% of the norm. In some countries, e.g., Germany, Poland, Latvia and Estonia, the deficit was observed throughout the whole 2018.

Analysis of circulation indices demonstrates that large-scale features of atmospheric circulation in the middle troposphere are close to the norm. Somewhat weaker zonal transport is observed in summer and autumn [*HMC*, 2020]. More intensive transport, compared to the norm, is noted for March. Meridional transport was close to the norm in most part of the year, with exception of May and November when more intensive transport took place in high latitudes.

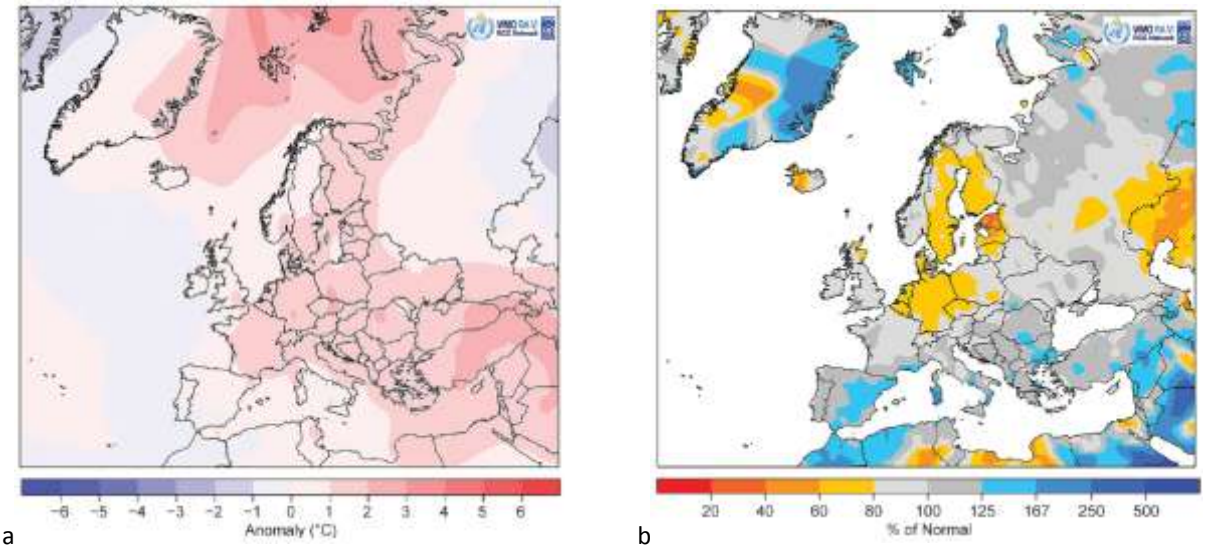

a b

Fig. 3.1. *Anomaly mean annual air temperature (a) and annual precipitation sum (b) in 2018 [Blunden and Arndt, 2019].*

In 2018 annual precipitation sums over the EMEP domain varied from around 200 mm in the Central Asia to 1500 – 2000 mm over windward areas of the British Iles and Scandinavian Peninsula (Fig. 3.2a). In mountainous regions (e.g., the Alps, western Scandinavia, Caucasus, and ridges of Central Asia) the precipitation often exceeds 2000 mm due to orographic effects. Over major part of eastern Europe, Scandinavia and Russia the precipitation range from 500 to 700 mm. Over western and southern Europe they vary from 700 to 1000 mm. Difference between precipitation sums in 2018 and 2017 is expressed in percent relative to 2017. Positive values of the difference mean increase of the precipitation in 2018 compared to 2017, and vice versa. Considerable increase (> 50%) of the precipitation takes place in south-western part of the EMEP domain, e.g., Spain, Portugal, Italy, southern France (Fig. 3.2b). Smaller but still substantial increase (15-50%) occur over most part of France, the Balkan region (Serbia, Albania, Romania), eastern part of Ukraine, south-eastern and central parts of Russia, northern Kazakhstan. The area of the precipitation decline spreads from central Europe (e.g., Germany) through Baltic region, Belarus and Scandinavia to the western part of Russia.

Mean air temperature in the EMEP domain follows zonal distribution varying from 20°C in the south to -5°C in the high latitudes (Fig. 3.3a). Compared to 2017, in 2018 air temperature moderately (0 – 1°C) rose over vast area spreading from France on the west to Belarus in the east, and from Scandinavia in the north to North Africa (Fig. 3.3b). In the central part of Europe (Germany, the Czech Republic, Slovakia, Poland), north of Scandinavia and Russia, and Turkey the increase made up 1 – 1.5°C. Substantial (-1 - -1.5°C) decline of air temperature is noted in Iberian Peninsula, central part of Russia and northern Kazakhstan (Fig. 3.3b).

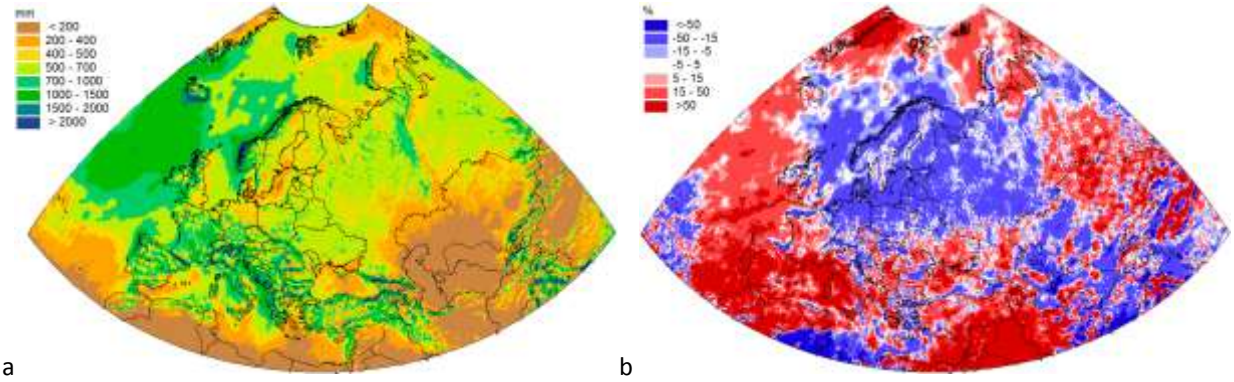

a b

Fig. 3.2. *Annual precipitation sums in 2018 (a) and relative difference between precipitation in 2018 and 2017 (b). Positive values mean increase and negative – decrease of precipitation in 2018 relative to 2017.*

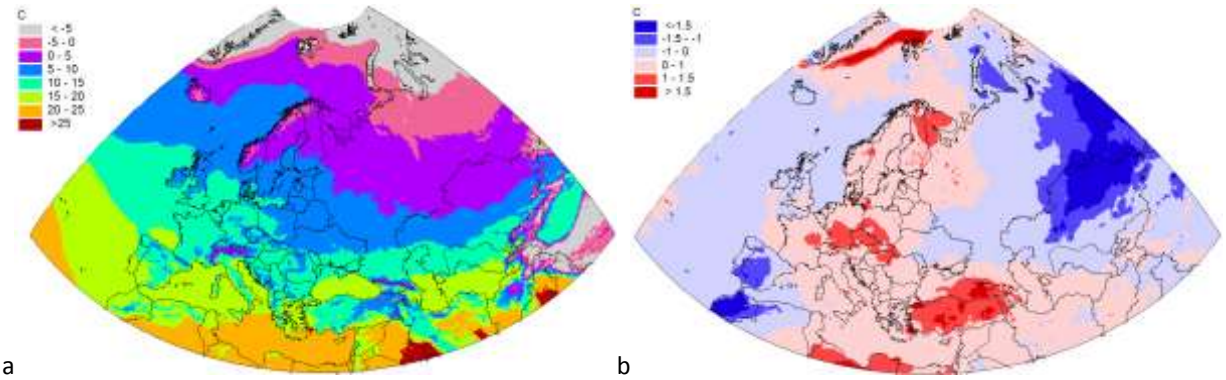

a b

Fig. 3.3. *Annual mean air temperature averaged over atmospheric boundary layer (~1 km) in 2018 (a) and difference between the temperatures in 2018 and 2017 (b)*

3.2. Model setup

The operational model assessment of heavy metal and POP pollution in 2018 has been performed using the GLEMOS model, version v2.0. Description of the current stable version of the model is available at the MSC-E website (http://en.msceast.org/index.php/j-stuff/glemos). New research directions aimed at improvement of the model parameterizations, which will be included to the next versions of the model, are discussed in Chapter 4 of the report.

Modelling of pollution levels in the EMEP countries as well as the transboundary transport between them (source-receptor relationships) have been carried out within the new EMEP domain (https://www.ceip.at/ms/ceip_home1/ceip_home/new_emep-grid/). Anthropogenic emission data for modelling of all pollutants have been prepared based on the gridded emissions fields provided by CEIP (Section 1.1) and complemented by additional emission parameters required for model runs (Section 1.2). Data on wind re-suspension of particle-bound heavy metals (Pb and Cd) from soil and seawater has been generated using the dust pre-processor [*Gusev et al.*, 2006; 2007].

Meteorological information for the model simulations has been generated from the operational analysis data of the European Centre for Medium Range Weather Forecasts [*ECMWF*, 2020] using the meteorological pre-processor based on the Weather Research and Forecast modelling system (WRF) [*Skamarock et al*., 2008]. Atmospheric concentrations of chemical reactants (O_3, OH, SO_2, and Br) and particulate matter (PM2.5), which are required for description of Hg and POP chemistry, were imported from the MOZART and p-TOMCAT models [*Emmons et al*., 2010; *Yang et al*., 2005; 2010].

Boundary conditions for the regional scale simulations of all considered pollutants have been obtained from the GLEMOS model runs on a global scale (Section 3.7). Initial conditions for the evaluation of pollution levels of long-living POPs (e.g. PCBs, HCB, and PCDD/Fs) in the EMEP region were prepared from a long-term global model spin-up based on expert estimates of historical emissions.

3.3. Levels of Heavy Metal and POP pollution

3.3.1. Pollution summary

Assessment of heavy metal and POP pollution of the EMEP region is performed using both modelling results and measurement data and includes evaluation of spatial patterns of pollution levels as well as transboundary transport in 2018. The assessment is based on the gridded emissions data for the previous year 2017. Update of the modelling results based on the new emission data for 2018 is available in Annex A. This section contains introduction and a short summary of the assessment. More detailed analysis of the pollution is given in other sections below for each particular contaminant.

Spatial variation of the pollution levels over the EMEP domain is determined by a number of factors including spatial distribution of anthropogenic and secondary emissions, properties of the pollutant, atmospheric dispersion pathways, meteorological conditions (precipitation intensity etc.) Therefore, spatial patterns of high and low pollution levels of different pollutants have both similarities and distinctions.

Comparison of deposition fluxes of various pollutants averaged over a number of sub-regions of the EMEP region is shown in Fig. 3.5. The deposition fluxes are normalized for the aim of comparison by average deposition of a pollutant over the EMEP domain. Definition of the sub-regions is shown in Fig. 3.4. The same sub-regions are used in the analysis of individual pollutants further in the chapter.

As seen from Figure 3.5a the sub-regions with the highest deposition fluxes of most the pollutants are Central and Southern Europe. It is determined by large emission density and significant precipitation sum in these areas. Exceptions are PCB and HCB, which deposition maximizes in Western Europe and Eastern Europe, respectively, due to significant emission sources located in these sub-regions. The lowest deposition fluxes are in Northern Europe as well as in the Caucasus and Central Asia.

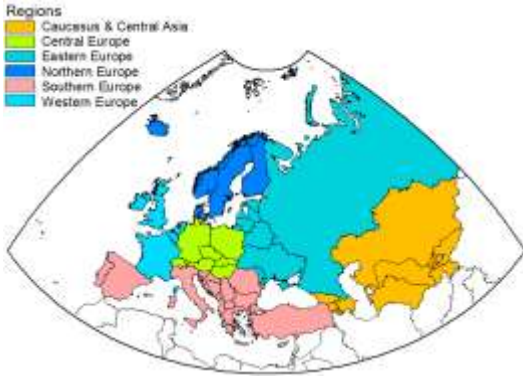

Fig. 3.4. *Definition of sub-regions of the EMEP region used in the report.*

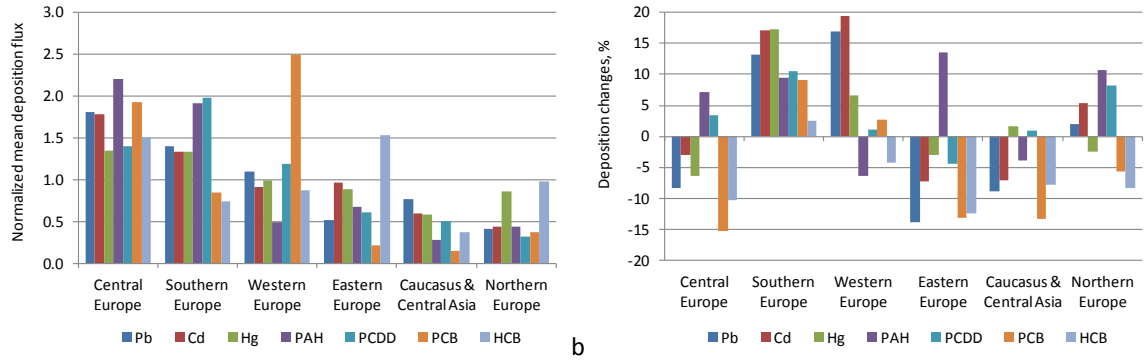

a b

Fig. 3.5. *Normalized mean deposition flux (a) and relative changes of heavy metals and POP deposition between 2018 and 2017 (b) in sub-regions of the EMEP region.*

To evaluate changes in pollution levels due to inter-annual meteorological variability the assessment results are compared with previous estimates for 2017 obtained using the same emissions data. Relative pollution changes between the current 2018 and 2017 years are calculated and analyzed for each contaminant further in the chapter using the following formula:

$$\Delta = \frac{(X_{2018} - X_{2017})}{X_{2017}} \cdot 100\%$$

The relative changes of heavy metal and POP deposition in various sub-regions of the EMEP region are shown in Fig. 3.5b. Deposition of all the pollutants increased in Southern Europe by 2-17% due to increase of annual precipitation sum. Deposition changes in other areas differ among the pollutants. Deposition of heavy metals also considerably increased in Western Europe but somewhat decreased in Central and Eastern Europe. Deposition of PAH increased Eastern and Northern Europe, whereas PCB and HCB decreased in Central, Eastern and Northern Europe as well as in the Caucasus and Central Asia. Explanation of these changes can be found in sections below devoted to particular contaminants.

More detailed information on evaluation of modelling results against measurements, transboundary pollution, deposition-specific deposition is available the Supplementary Data Reports for heavy metals [*Ilyin et al*., 2020] and POPs [*Gusev et al*., 2020].

3.3.2. Lead

Atmospheric lead belongs to particulate species, i.e., it exists in the atmosphere as a part of aerosol composition. Hence, processes of dispersion of Pb in the atmosphere and its scavenging from the atmosphere are determined by properties of the particles-bearers. Chemical forms of Pb (oxides, salts, etc.) in the particles do not affect properties of the particles.

Air concentrations

The highest concentrations of Pb in 2018 are noted for Central Europe (southern Poland, west of Germany), as well as Belgium, the Netherlands and north of Italy (Fig.3.6a). Another area of relatively high Pb concentrations is situated in the Central Asian region (the northern and south-western parts of Kazakhstan, Uzbekistan and Turkmenistan). The lowest levels take place over Scandinavia and the northern part of Russia. Difference between spatially mean concentrations between most and least polluted sub-regions (Central Europe and Northern Europe, respectively) makes up about 10 times (Fig.3.6b). The spatial distribution of modelled concentrations in general agrees with observed Pb levels in the central, northern and southern parts of Europe. Mean relative bias between modelled and observed air concentrations is about -10%. For about 75% of stations the difference between modelled and observed levels stays within a factor of two. More detailed information on agreement between modelled and observed concentrations is given in Supplementary Data Report [*Ilyin et al*., 2020].

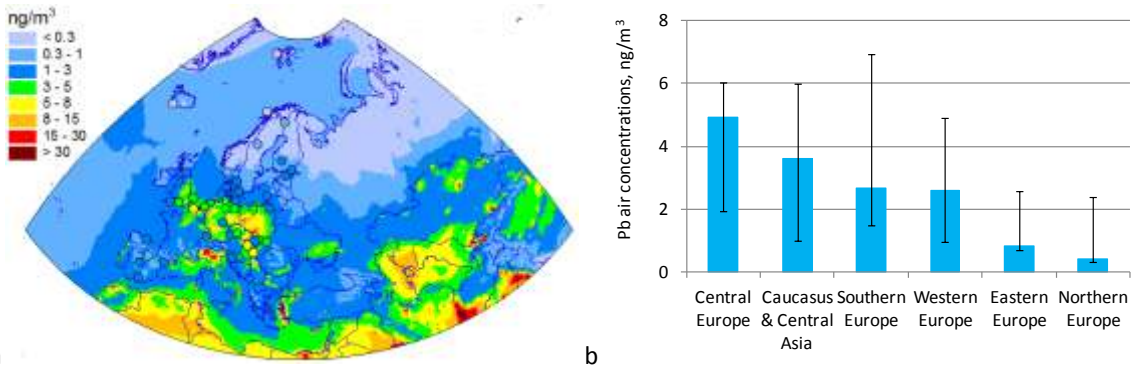

a b

Fig. 3.6. *Annual mean air concentrations of Pb (circles on the map show observed values in the same colour scale) (a) and average air concentrations of Pb to EMEP sub-regions (b) in 2018. Whiskers show the range of concentrations in particular countries of the subregion.*

Changes of air concentrations in 2018 compared to previous (2017) year are distributed unevenly over the EMEP domain. On average, the most significant changes take place in Northern Europe (12% increase) and Eastern Europe (13% decline) (Fig. 3.7b). In other sub-regions the mean changes lie within ±5%. In particular countries the range of the changes is higher lying with ±30% (Fig. 3.7a). For example, the 30% increase is noted for regions in the southern part of Sweden and Norway and in the central part of France.

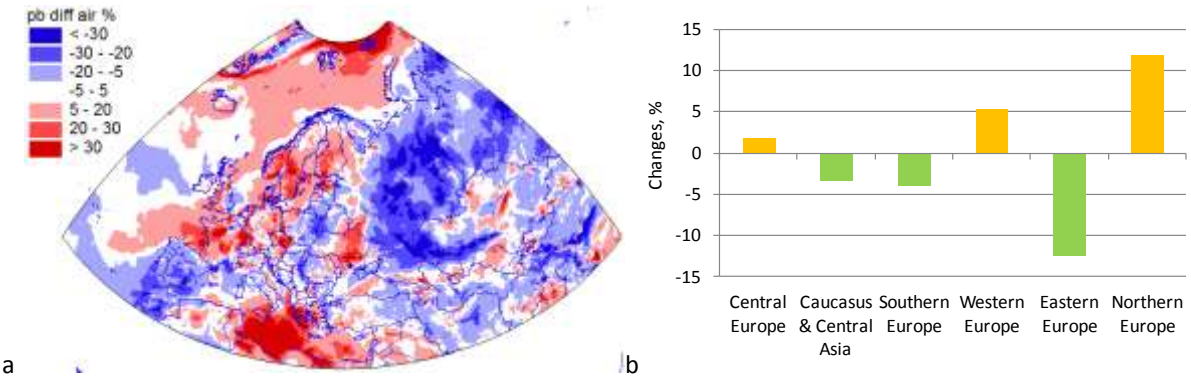

Fig. 3.7. *Relative changes of Pb air concentrations between 2018 and 2017 over the EMEP domain (a) and in various sub-regions (b).*

Deposition fluxes

Spatial pattern of total deposition of Pb in 2018 is shown in Fig. 3.8a. Areas of the highest deposition fluxes, as a rule, coincide with areas of substantial anthropogenic emissions or wind re-suspension. Compared to air concentrations, deposition fluxes over major part of Central Asia are relatively low. Total deposition consists of wet and dry components. Average contribution of wet deposition for the EMEP countries is about 80%, but in the Central Asian region this contribution is much lower due to climatic conditions (arid climate, low precipitation). Similar to concentrations in air, the highest spatially mean deposition flux is noted for Central Europe, and the lowest – for Northern Europe (Fig. 3.8b).

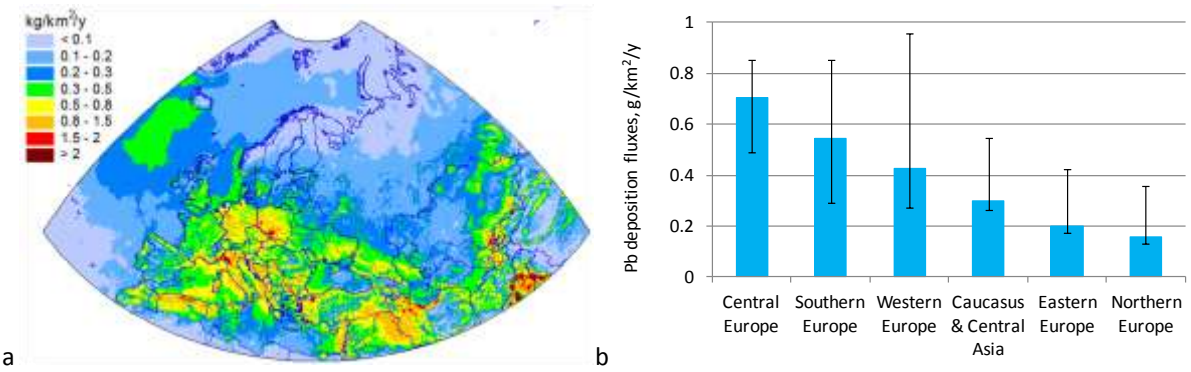

Fig. 3.8. *Annual total deposition flux of Pb (a) and average total deposition flux of Pb to EMEP sub-regions (b) in 2018. Whiskers show the range of concentrations in particular countries of the subregion.*

EMEP monitoring network reports data on measured wet deposition fluxes. The model performance of wet deposition fluxes in 2018 differs markedly among countries and particular stations. Some underestimation (around 20%) of the observed wet deposition fluxes by the model is noted. For 70% of stations modelled and observed annual mean fluxes agree within a factor of two. At some stations the model underestimates the observed fluxes by more than 3-fold. This factor is much higher than estimated intrinsic model uncertainty or reported analytical error of measurements [*CCC*, 2020]. Therefore, these stations require special analysis and are removed from the common statistics. However, comparison of their annual levels and time series with the model is available in the

Supplementary Data Report [*Ilyin et al*., 2020]. More detailed comparison between modelled and observed levels is available in Supplementary Data Report [*Ilyin et al*., 2020].

Total deposition is a sum of contribution of three groups of emission sources. These are EMEP anthropogenic emissions, wind re-suspension of dust particles containing heavy metals, and emissions from sources located outside the EMEP region (non-EMEP sources).

Spatial distribution of deposition from anthropogenic sources is generally reflects the distribution of emissions (Fig. 3.9a). However, compared to distribution of emissions, spatial pattern of deposition fluxes is more dispersed due to meteorological factors (winds, turbulence, wet scavenging etc.). The highest contribution expressed both in relative (about 60%) and absolute (about 0.4 kg/km^2/y) terms of the EMEP anthropogenic sources to total deposition is noted for Central Europe (Fig. 3.9d). The lowest contribution of the EMEP anthropogenic sources takes place for Caucasus and Central Asia (about 35%).

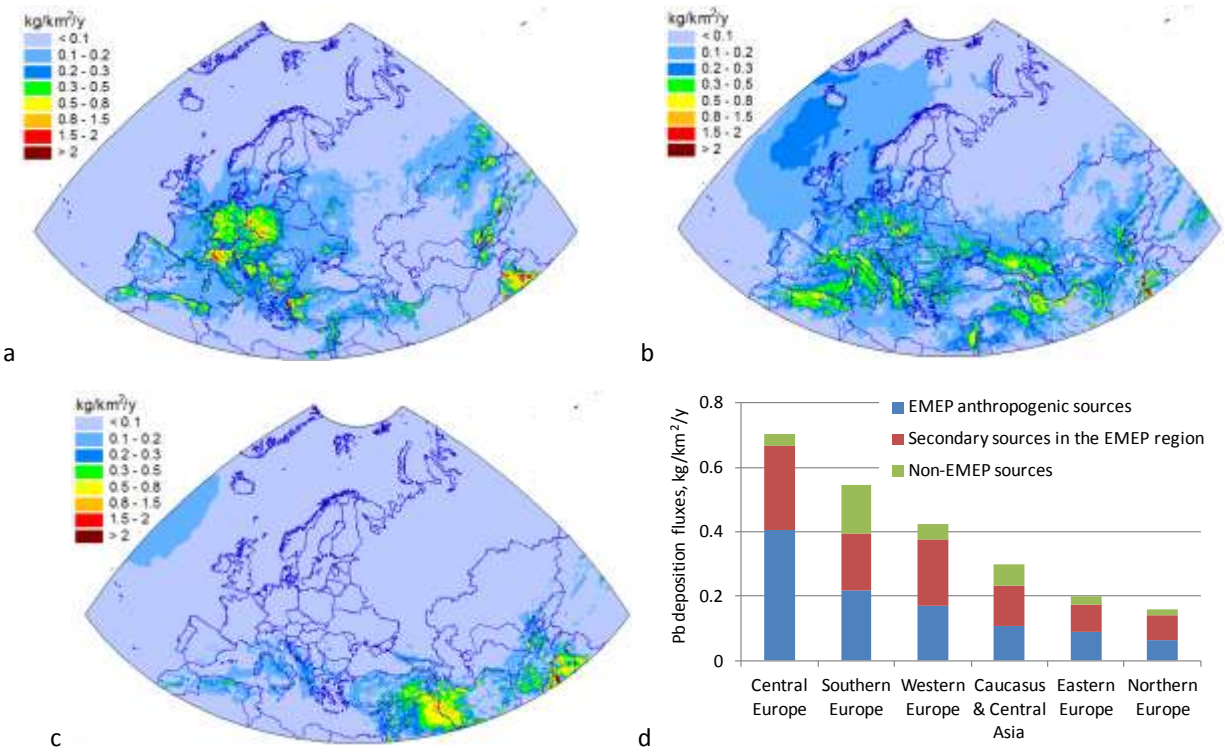

Fig. 3.9. *Annual deposition of Pb in 2018 from EMEP anthropogenic sources (a), secondary sources (wind re-suspension) (b) and non-EMEP anthropogenic sources (c), and mean deposition fluxes from these sources to the EMEP sub-regions (d).*

Spatial distribution of Pb deposition from re-suspension depends on a number of factors, such as concentrations in soils, soil wetness, wind stress etc. Relatively high deposition flux from re-suspension takes place in a number of countries such as Germany, Poland, Italy and southern France (Fig. 3.9b). The reason for this is concentrations in soils with elevated Pb levels due to natural processes or enriched for the long-term accumulation of previously deposited Pb. High deposition from re-suspension over the western part of the Mediterranean Sea, southern part of Russia and the

Caspian Sea are explained by relatively high dust suspension from deserts of the North Africa or Central Asia. On average, around 30% of deposition to South Europe and about 40% of deposition to Eastern Europe, Central Asia and Caucasus come from re-suspension (Fig. 3.9d). In Northern Europe impact from anthropogenic sources is low, therefore relative contribution of wind re-suspension is comparable with that of anthropogenic emissions.

Contribution of non-EMEP sources is the highest near the southern border of the EMEP domain. It is explained by transport from Asian anthropogenic sources of Iran, Iraq, India, etc. (Fig. 3.9c). Sub-region mean contribution of non-EMEP sources varies from 5% in Central Europe to almost 30% in Southern Europe (Fig. 3.9d). More detailed information on contributions of these three groups of sources to deposition in the EMEP countries can be found in Supplementary Data Report [*Ilyin et al.,* 2020].

Changes of total deposition fluxes in 2018 vary within ±50% over most of the EMEP domain (Fig. 3.10a). Mean sub-region changes of the fluxes range from -14% in Eastern Europe to 17% in Western Europe (Fig. 3.10b). In particular countries the increase was most significant in France and Italy (20-50%). The highest decline (> 50%) is noted for the central and northern parts of Russia.

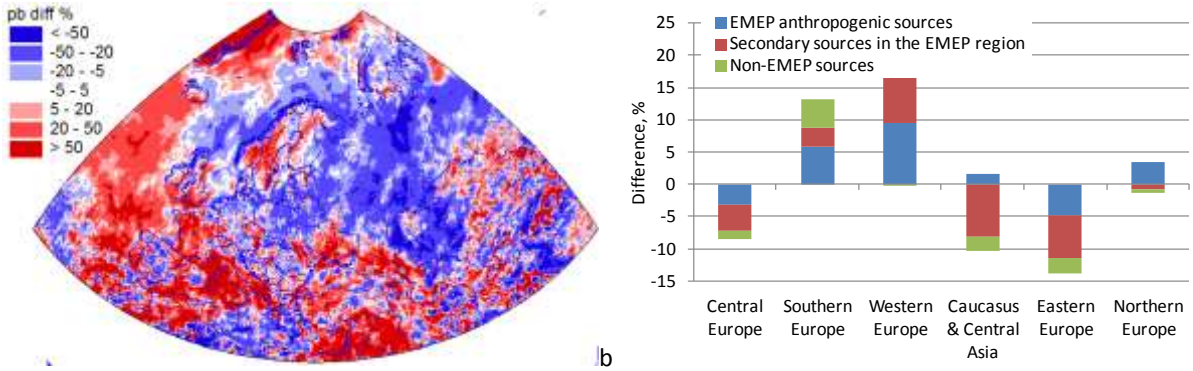

Fig. 3.10. *Relative changes of Pb deposition between 2018 and 2017 over the EMEP domain (a) and in various sub-regions (b).*

Reasons of the pollution level changes in 2018

Changes of pollution levels in 2018 in comparison with 2017 could be explained by variability of meteorological conditions and, in particular, by annual precipitation amount. Rise of air concentrations (Fig. 3.7b) and decline of total deposition in Central Europe (Fig. 3.10b) is explained by decline of atmospheric precipitation in this sub-region. The opposite situation takes place for Southern Europe. In Western and Northern Europe, the increase of deposition is agreed with the rise of atmospheric precipitation. However, air concentrations in Western and Northern Europe also increased. The reason for the increase of air concentrations is atmospheric long-range transport from Central Europe. Due to substantial decline of atmospheric precipitation more mass of Pb remained in the atmosphere. This “extra” mass is transported by the atmospheric flows to neighbouring sub-

regions (namely, Western and Northern Europe) thus favouring increase of air concentrations. It is particularly true for Northern Europe: change in the non-EMEP and re-suspension components of deposition is negative, while anthropogenic component to total deposition increased in spite of the decline of precipitation. Decline of deposition in Caucasus and Central Asia and in Eastern Europe is explained mainly by changes of atmospheric precipitation. Another factor responsible for the corresponding decline of air concentrations is linked with changes in atmospheric circulation.

Transboundary transport

Pollution levels in a country are produced by emission sources located both within the country (national sources) and due to transboundary transport from other countries (foreign sources). Contribution of foreign sources to total anthropogenic deposition of Pb in the EMEP countries ranges from about 15**%** to almost 99**%**, while the remaining part is caused by national emission sources. The contribution of transboundary transport to Pb deposition exceeds 50**%** in 38 countries, and exceeds 75**%** - in 24 countries. For example, only 11% of anthropogenic deposition of Pb to Norway is caused by national sources, while 89% have transboundary origin, mainly from sources of Germany, Poland and the United Kingdom (Fig. 3.11a). In contrast, most (70%) of anthropogenic deposition in Spain is caused by national sources (Fig. 3.11b).

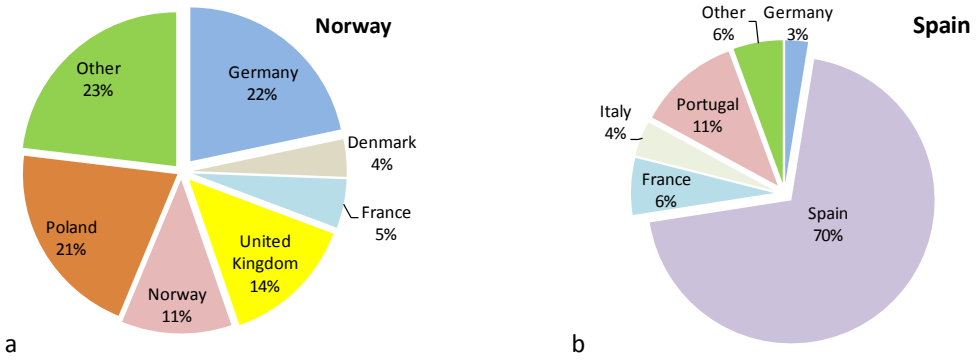

Fig. 3.11. *Contribution of the transboundary transport and national source to anthropogenic Pb deposition in Norway and Spain.*

Changes of deposition from particular countries-sources to a country-receptor can be derived from source-receptor matrices for 2017 and 2018 [*Ilyin et al*., 2019, *Ilyin et al*., 2020]. Example for France is presented in Fig. 3.12. Compared to the previous (2017) year, the total anthropogenic Pb deposition in France increased by 26 t/y and amounted to 96 t/y in 2018. Deposition from national sources increased by 6 t/y, the increase of deposition from other countries was 20 t/y. In particular, contribution of Germany increased by almost 10 t/y (around 3-fold), and Italy – by 4 t/y (1.7-fold). This example demonstrates that ***variability of meteorological parameters can markedly change transboundary fluxes of heavy metals between the EMEP countries.***

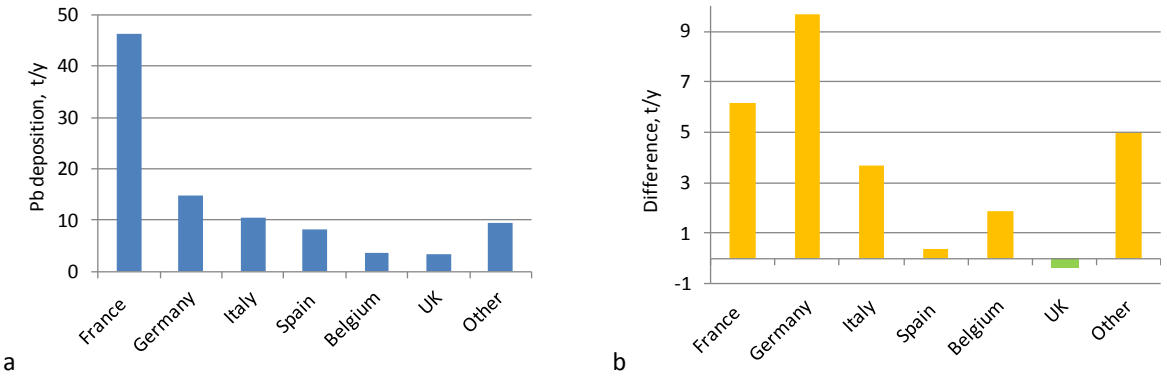

Fig. 3.12. *Major contributors of Pb anthropogenic deposition in France in 2018 (a) and absolute difference of Pb deposition between 2018 and 2017 (b).*

Each EMEP country is considered as a receptor and as a source of transboundary pollution. Magnitude of total deposition from national sources of the EMEP countries to other countries varies markedly depending on the country emission, size and geographical location. Lead emitted by country's sources deposit to own territory of a country and to territories of other EMEP countries. The highest Pb total deposition to territories of other EMEP countries are noted for Kazakhstan (about 240 t/y), followed by Poland (about 140 t/y) and Germany (about 85 t/y), while the deposition to own territory of these countries amounted to 240, 115 and 95 t/y, respectively. For example, in Germany, deposition to own territory accounts for half of the total deposition (Fig. 3.13a).

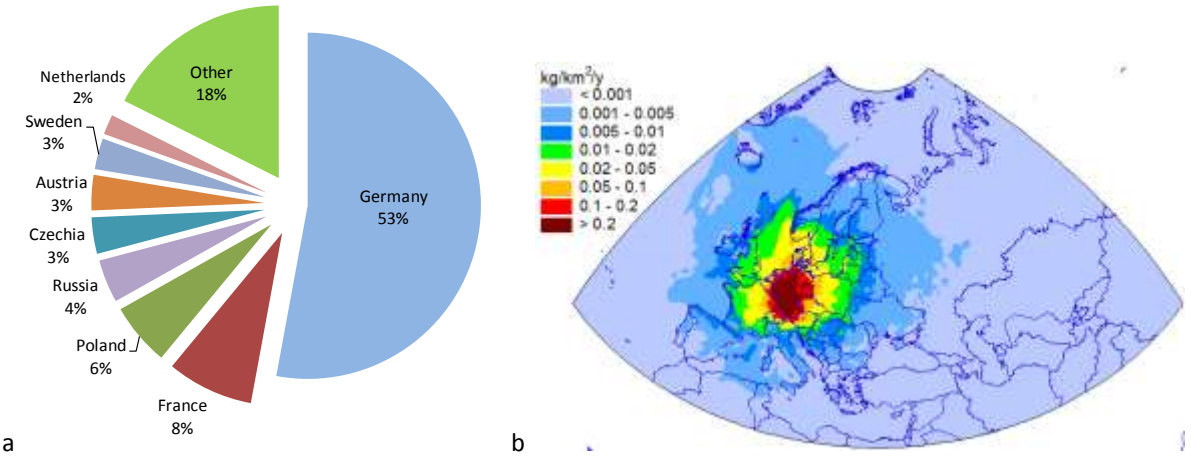

Fig. 3.13. *Contribution of Pb deposition from German anthropogenic sources to own territory and other countries in 2018 (a) and spatial distribution of deposition from the German sources in the EMEP region (b).*

Changes of deposition from a country to territories of other countries are exemplified by Italy (Fig. 3.14). In 2018 the deposition to own territory in Italy is 95 t/y, while the remaining EMEP countries account for 70 t/y (Fig. 3.14a). Compared to the previous year, Pb deposition from Italian sources to national territory increased by 20 t/y and to France by 4 t/y. Deposition to territories of Russia, Austria and Croatia reduced by 4, 2 and 1.5 t/y, respectively (Fig. 3.14b).

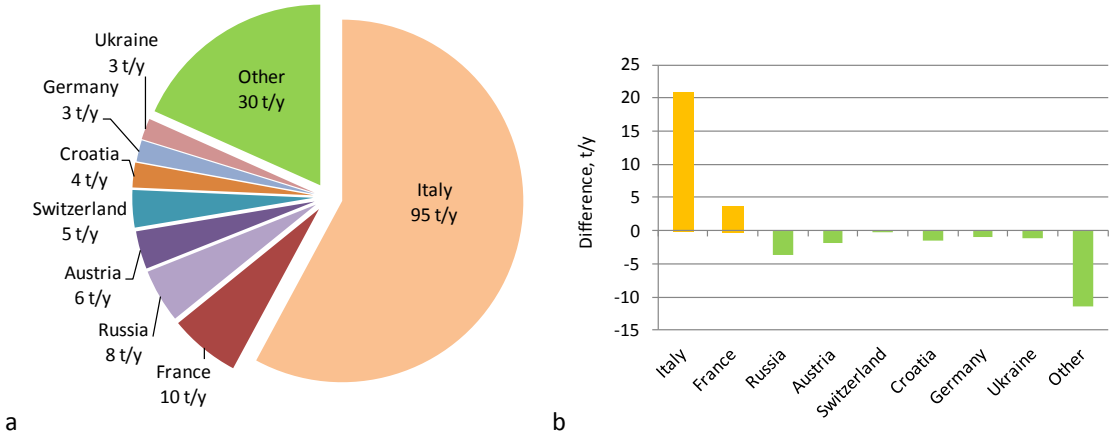

Fig. 3.14. *Contribution of Pb deposition from Italian anthropogenic sources to own territory and other countries in 2018, (a) and changes of Pb deposition between 2018 and 2017 (b).*

3.3.3. Cadmium

Cadmium in the atmosphere presents being bound to the aerosol particles. Therefore, atmospheric transport, dry deposition and wet scavenging of this heavy metal are determined by properties of the particles containing Cd. Chemical forms of Cd (oxides, salts, etc.) in the particles do not affect properties of the particles.

Air concentrations

The highest concentrations (> 0.4 ng/m^3) of Cd in the EMEP domain in 2018 are noted for a number of countries in Central and Eastern Europe (e.g., Germany, Poland, or Russia) (Fig. 3.15a). The lowest levels take place in the northern part of Europe. Central Europe is characterized by the highest sub-region mean air concentrations (Fig. 3.15). Mean concentrations in the Northern Europe are about 10-fold lower than the concentrations in Central Europe. Regional mean levels of Cd in other sun-regions are similar in (Fig. 3.15b). Spatial distribution of the modelled concentrations in the central, northern and southern parts of Europe agrees with that derived from measured levels at the EMEP monitoring network. Mean relative bias between modelled and observed annual mean concentrations is around -5%. For about 75% of stations the modelled levels match the observed ones within a factor of two. More detailed information on agreement between modelled and observed concentrations is given in Supplementary Data Report [*Ilyin et al*., 2020].

Compared to previous (2017) year, the highest increase of air concentrations in 2018 occurs in Northern Europe and parts of Eastern Europe (e.g., the western part of Russia) (Fig. 3.16a). Mean air concentrations in Northern Europe increased by 15% (Fig. 3.16b). However, mean increase in Eastern Europe is negligible because of vast areas with the decline of air concentrations in the central part of Russia and the western part of Kazakhstan. More moderate increase takes place in the western European countries (France, the United Kingdom), reaching 8% on average. Some countries of the Balkan region and Caucasus and Central Asia are also characterized by the increase of air concentrations. However, the mean changes in the corresponding sub-regions are within ±2%.

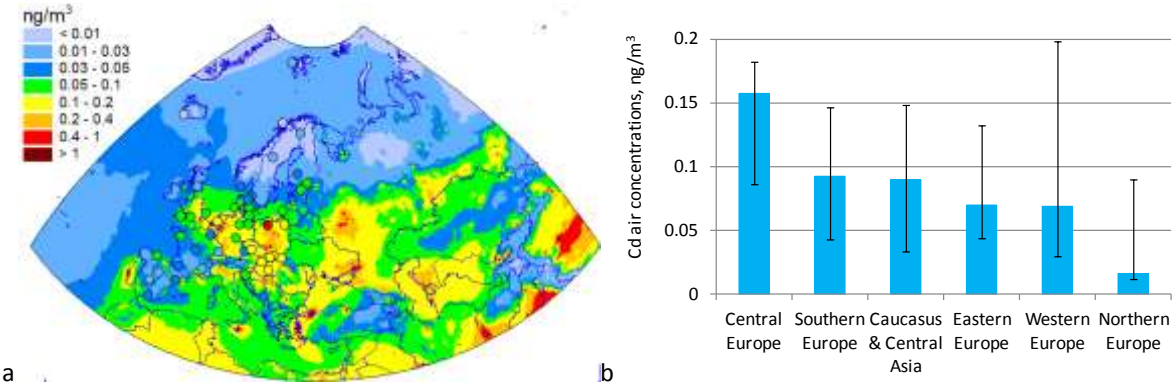

Fig. 3.15. *Annual mean air concentrations of Cd (circles on the map show observed values in the same colour scale) (a) and average air concentrations of Cd to EMEP sub-regions (b) in 2018. Whiskers show the range of concentrations in particular countries of the subregion.*

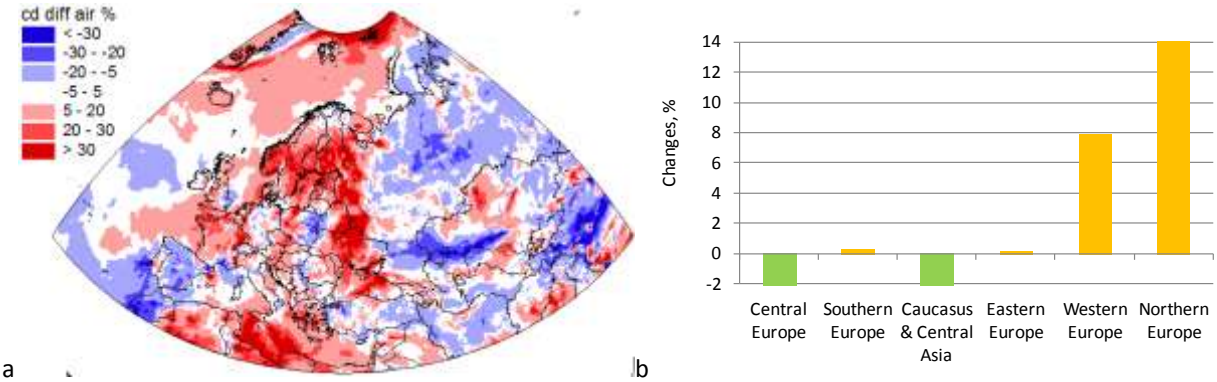

Fig. 3.16. *Relative changes of Cd air concentrations between 2018 and 2017 over the EMEP domain (a) and in various sub-regions (b).*

Deposition fluxes

Spatial distribution of Cd deposition in the EMEP domain is governed by a number of factors such as location of emission sources, wind re-suspension, distribution of atmospheric precipitation and land-cover. In general, areas with higher deposition are the same as areas with higher concentration on air (Fig. 3.17a). The highest sub-region mean deposition takes place in Central Europe, followed by Southern Europe (Fig. 3.17b). The lowest deposition takes place in the northern part of the EMEP domain due to low emissions and in Central Asia because of low atmospheric precipitation (Fig. 3.17a,b).

Total deposition of Cd consists of wet and dry components. Wet deposition of Cd constitutes about 80% of total deposition for the EMEP region as a whole. The agreement between modelled and observed wet deposition fluxes differ significantly among particular stations. Mean relative bias between modelled and observed wet deposition fluxes is about -25% indicating some underestimation of the observed wet deposition. For almost 80% of stations modelled and observed annual mean fluxes agree within a factor of two. For some stations the difference between modelled and observed fluxes in 2018 exceeds a factor of 3. This large difference can hardly be explained by

the model intrinsic uncertainty. Reported analytical uncertainty of measured concentrations in precipitation is also much lower [*CCC*, 2020]. Therefore, these stations require special consideration and are not involved in the statistical analysis. Nevertheless, mean monthly and annual values of Cd deposition at these stations are presented in the Supplementary Data Report [*Ilyin et al*., 2020]. More detailed comparison between modelled and observed levels is available in Supplementary Data Report [*Ilyin et al*., 2020].

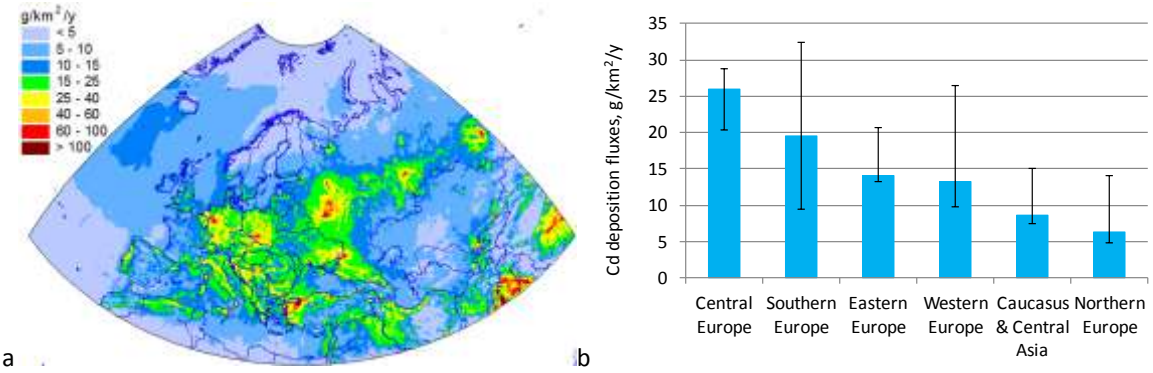

Fig. 3.17. *Annual total deposition flux of Cd (a) and average total deposition flux of Cd to EMEP sub-regions (b) in 2018. Whiskers show the range of concentrations in particular countries of the subregion.*

Sources of Cd are divided in three groups. They are EMEP anthropogenic emissions, wind re-suspension, and emissions from sources located outside the EMEP region (non-EMEP sources). Spatial distribution of Cd deposition from anthropogenic sources is mainly determined by the distribution of anthropogenic emissions (Fig. 3.18a). Compared to map of the anthropogenic emissions, spatial spread of deposition fluxes is wider because of meteorological factors responsible for pollution transport and removal. The highest contribution of anthropogenic sources in sub-regions of the EMEP domain takes place in Central Europe (Fig. 3.18d), amounting to 20 g/km^2/y or 80% of total.

Contribution of wind re-suspension is much lower than that of anthropogenic sources (Fig. 3.18b). Its sub-region mean contribution ranges from 15% in Central Europe to 40% in Caucasus and Central Asia (Fig. 3.18d). Caucasus and Central Asia is the only sub-region where the average contribution of re-suspension to total deposition exceeds that of anthropogenic sources.

Similar to Pb, the highest deposition from non-EMEP sources takes place near the southern border of the EMEP domain (Fig. 3.18c). The reason for this is atmospheric transport through the EMEP domain border from Asian countries (Iran, Iraq, India, etc.). Elevated deposition from non-EMEP sources in the southern Europe are explained by transport of airborne dust from northern Africa. Mean contribution of non-EMEP sources in the sub-regions varies from 6% in Central Europe to about 25% in the Southern Europe (Fig. 3.18d).

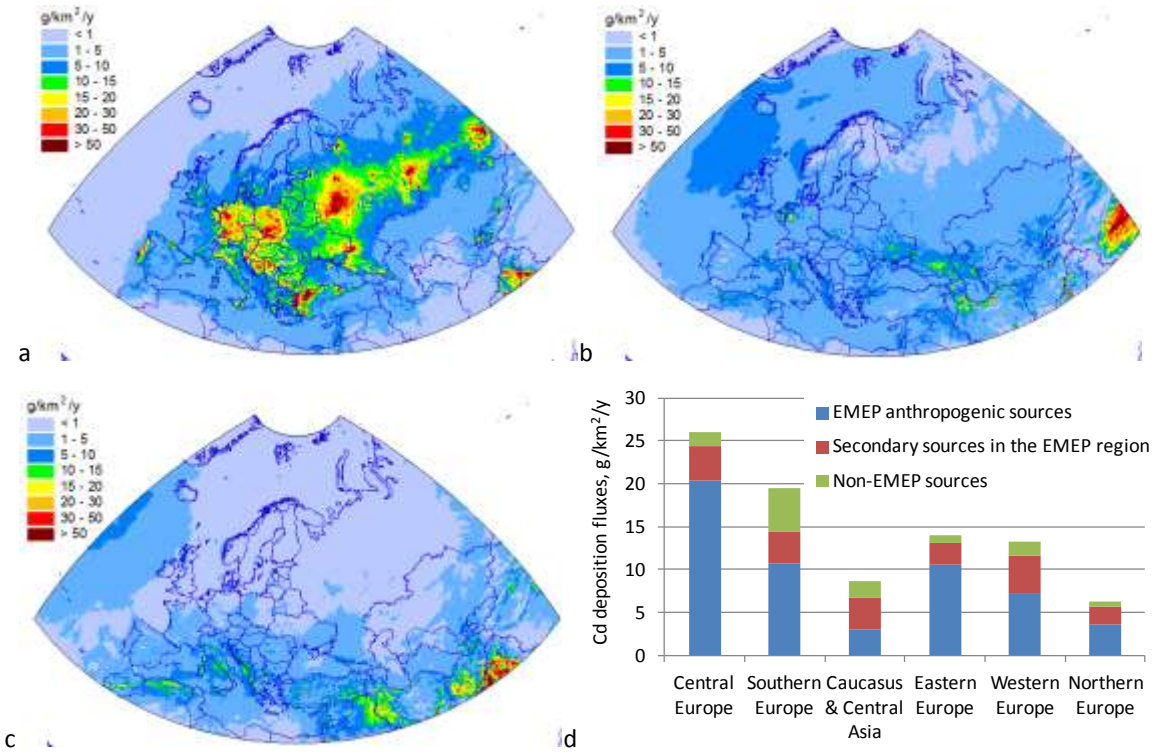

Fig. 3.18. *Annual deposition of Cd in 2018 from EMEP anthropogenic sources (a), secondary sources (wind re-suspension) (b) and non-EMEP anthropogenic sources (c) and mean deposition fluxes from these sources to the EMEP sub-regions (d).*

The change of deposition flux in the EMEP countries in 2018 varies from -50 to 50% (Fig. 3.19a). Most significant increase takes place in France, Italy, Sweden, the Balkan region. The lowest decline takes place in the eastern part of Kazakhstan. In the sub-regions the most substantial mean increase of total deposition occurs in Western and Southern Europe (20% and 17%, respectively) (Fig. 3.19b). Central Europe, Eastern Europe and Caucasus and Central Asia are characterized by 3-7% mean decline of Cd deposition.

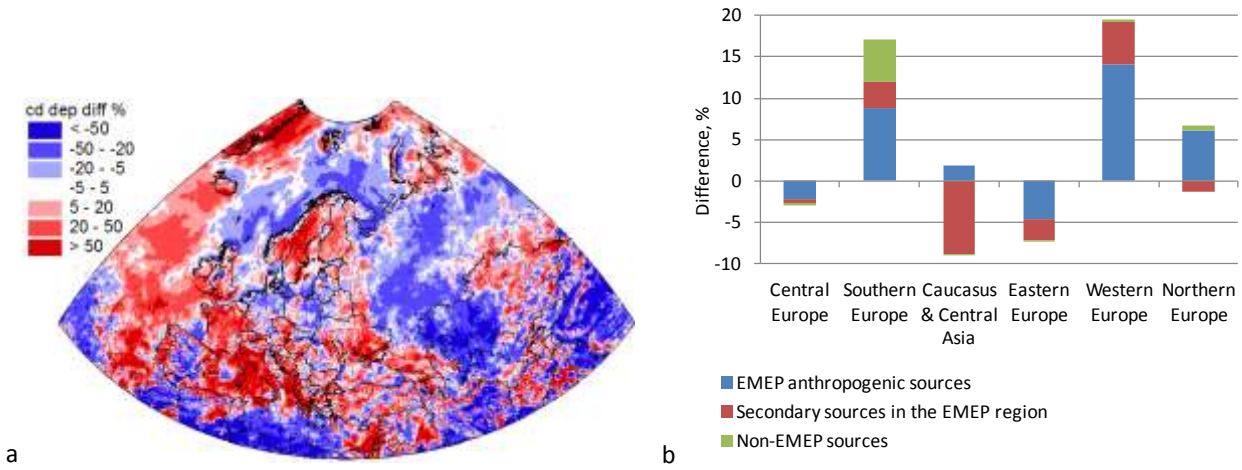

Fig. 3.19. *Deposition fluxes of Cd in 2018 from EMEP anthropogenic sources, secondary sources (wind re-suspension) and non-EMEP anthropogenic sources for EMEP regions (a) and difference between 2017 and 2018 (b).*

Reasons of the pollution level changes in 2018

Decline of precipitation in 2018 resulted to some decrease of Cd total deposition in Central Europe (Fig. 3.19b). In contrast, the increase of annual precipitation favoured increase of Cd deposition in Southern and Western Europe. In spite of growth of precipitation, concentrations of Cd in Western Europe also increased by almost 8% (Fig. 3.16b). The reason for this is increased atmospheric transport from the central European sub-region, as it follows from the analysis of source-receptor matrices for the current (2018) and previous (2017) year. The same idea is applied to explain an increase of deposition in Northern Europe in spite of marked decline of precipitation amounts. Decline of precipitation in neighbouring Central and Eastern Europe resulted to increase of atmospheric transport to Northern Europe and consequent increase of deposition. In particular, deposition to Northern Europe from sources of Central Europe increased by 22%, and from Eastern Europe – by 28% [*Ilyin et al.*, 2020].

Transboundary transport

Deposition from anthropogenic sources in countries comes from national sources and transboundary transport from other EMEP countries (foreign sources). Contribution of foreign sources to Cd deposition in 2018 varies from 7% to about 99%. The contribution of transboundary transport to Cd deposition exceeds 50**%** in 41 countries, and exceeds 75**%** - in 23 countries. For example, in Sweden only 12% of anthropogenic deposition is formed by national sources while the remaining 88% are originated from other countries, e.g., Poland, Germany, Russia etc. (Fig. 3.20a). In contrast to Sweden, in the United Kingdom most of anthropogenic deposition comes from national sources (Fig. 3.20b).

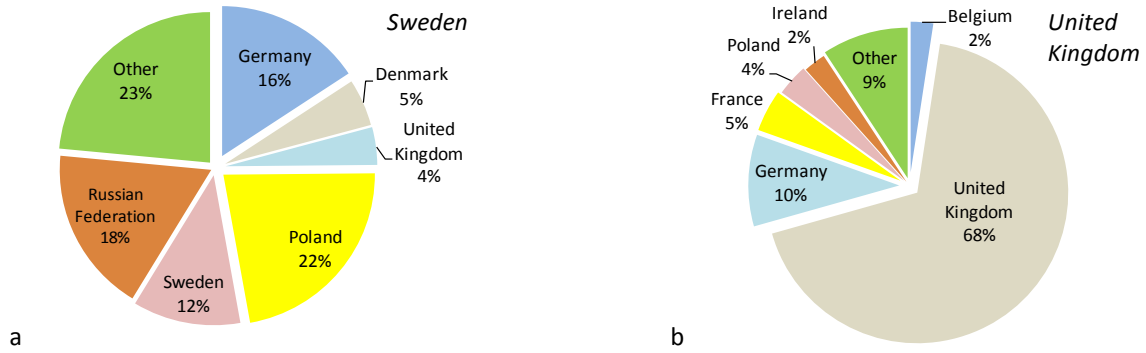

Fig. 3.20. *Contribution of the transboundary transport and national source to anthropogenic Cd deposition in Sweden and United Kingdom.*

Comparison of source-receptor matrices for 2017 and 2018 allows identifying the changes in transboundary transport between countries. Example for Belgium is demonstrated in Fig. 3.21b. The main transboundary contributor of Cd deposition in Belgium is Germany. In 2018 its input makes up about 156 kg/y. It is about 70 kg/y (2-fold) higher compared to 2017 (Fig. 3.21b). Some increase of transboundary transport is also noted from the Netherlands, Poland and other countries. At the same time, about 2-fold decline of contribution from French sources is obtained. This example demonstrates the influence of variability of meteorological conditions on changes of transboundary fluxes between EMEP countries.

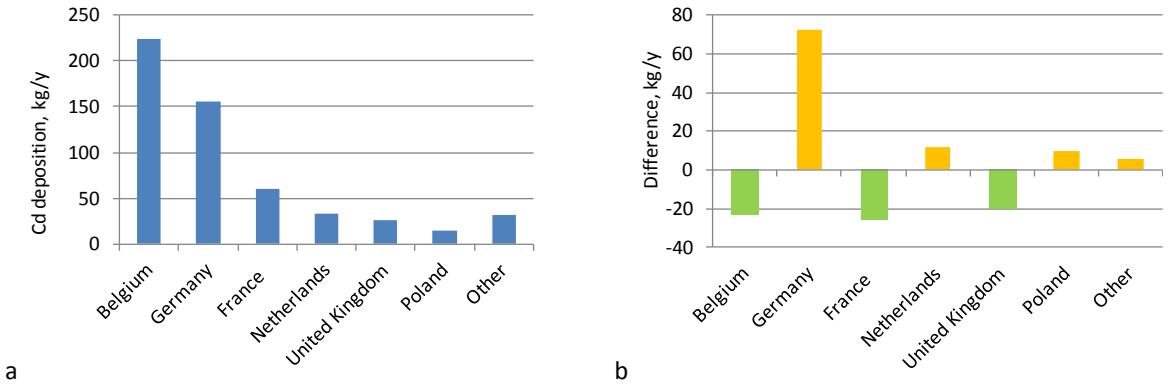

Fig. 3.21. *Cadmium deposition in Belgium from main countries-contributors in 2018 (a) and absolute difference of Cd deposition between 2018 and 2017 (b).*

Each EMEP country can be considered as a source of transboundary pollution in neighbouring countries. The largest Cd deposition to neighbouring countries is made by sources of Russia (14 t/y), Poland and Germany (about 5 t/y each). For example, about a half of deposition from Polish sources falls on its own territory (Fig. 3.22a). Main foreign countries-receptors are Russia, Ukraine, Germany and the Czech Republic.

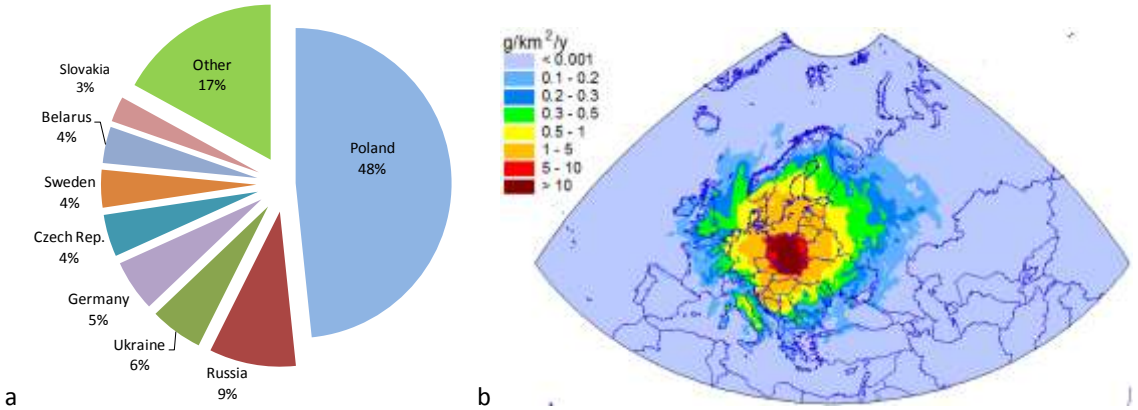

Fig. 3.22. *Contribution of Cd deposition from Polish anthropogenic sources to own territory and other countries in 2018 (a) and spatial distribution of deposition from the Polish sources in the EMEP region (b).*

Changes of deposition from a country's sources to territories of other countries can be analyzed via comparison of the source-receptor matrices for 2017 and 2018. Example of the changes is demonstrated in Fig. 3.23 for Serbia. In 2018 deposition from of Cd form national sources to own territory is 825 kg/y, and to territories of other EMEP countries – 1450 kg/y. Contribution of Serbian sources to deposition in Romania declined by 74 kg/y, and to Russia – by 54 kg/y. At the same time, deposition to Bosnia and Herzegovina and to Croatia increased by about 60 and 40 kg/y, respectively.

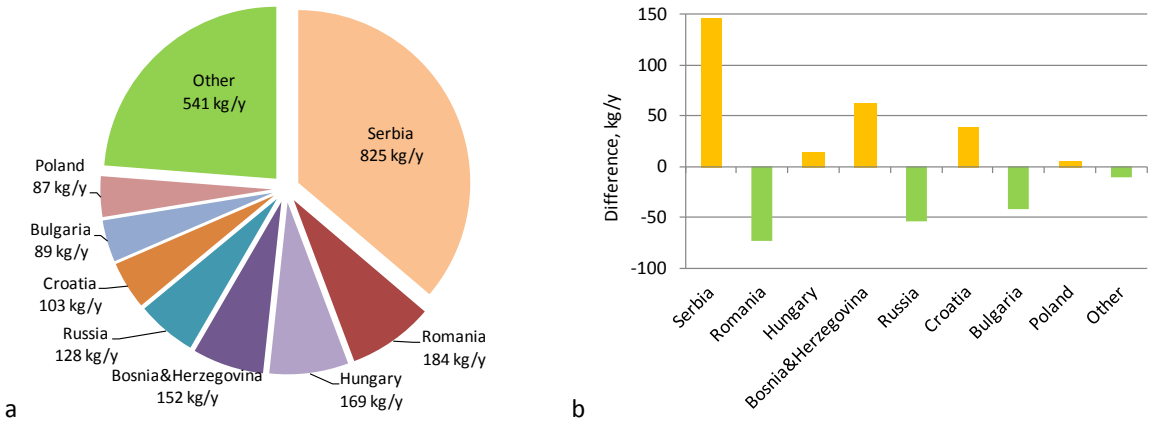

Fig. 3.23. *Contribution of Cd deposition from Serbian anthropogenic sources to own territory and other countries in 2018 (a) and changes of Cd deposition between 2018 and 2017 (b).*

3.3.4. Mercury

Mercury differs from other heavy metals (Pb and Cd) by higher saturation pressure at normal conditions that leads to its presence in the atmosphere predominantly in elemental gaseous form (Hg^0). Besides, it undergoes chemical transformations resulting in formation of various oxidized Hg compounds with diverse physical and chemical properties, which occur in both gaseous and particulate forms. The complex chemical cycling of Hg compounds determines the character of its dispersion in the atmosphere and deposition to the ground.

Spatial patterns of pollution levels in 2018

Air concentration of gaseous elemental Hg, the bulk Hg species in the atmosphere, is evenly distributed over the EMEP region due to its long residence time. The concentration varies from 1.4 ng/m^3 in remote regions (e.g. the Arctic, Northern Russia, the Himalayas etc.) up to 1.8 ng/m^3 in Italy and the Balkan countries (Fig. 3.24a). Elevated Hg^0 concentrations over Southern and Central Europe are caused by higher anthropogenic emissions as well as emissions from natural and secondary sources in these regions (Fig. 3.24b). Lower concentrations are in Northern Europe, Caucasus and Central Asia. The model generally well reproduces measured background Hg^0 concentrations with significant spatial correlation (0.58) and relative bias mostly within ±10%. More detailed information on agreement between modelled and observed concentrations is given in Supplementary Data Report [*Ilyin et al.*, 2020].

Air concentration of Hg^0 slightly (3-5%) increased in Southern Europe (Spain, Italy, Balkan countries) and Western Europe (France, Belgium) in 2018 compared to the previous year due to lower Hg^0 oxidation in the near-ground air that led to higher contribution of regional anthropogenic and natural/secondary sources (Fig. 3.25). At the same time, contribution of non-EMEP sources somewhat decreased in Western and Central Europe, which caused slight decrease of Hg^0 in some countries (Poland and Germany). Decrease of Hg^0 from anthropogenic and secondary sources in Eastern Europe was compensated by increase of contribution of non-EMEP sources but led to some decline of Hg^0 concentration over the European part of Russia.

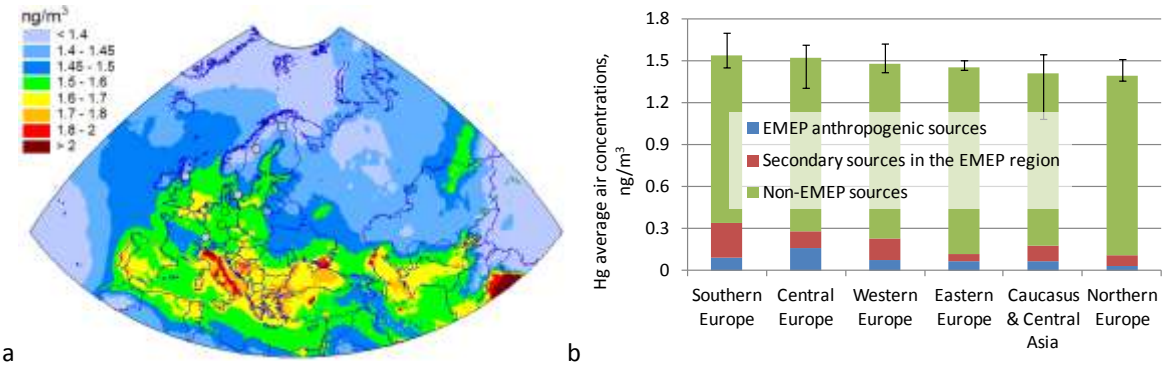

Fig. 3.24. *Spatial distribution of annual mean Hg^0 air concentration over the EMEP domain (a) and average Hg^0 concentration in various sub-regions (b) in 2018. Circles on the map show observed values in the same colour scale. Whiskers show the range of concentrations in particular countries of the subregion.*

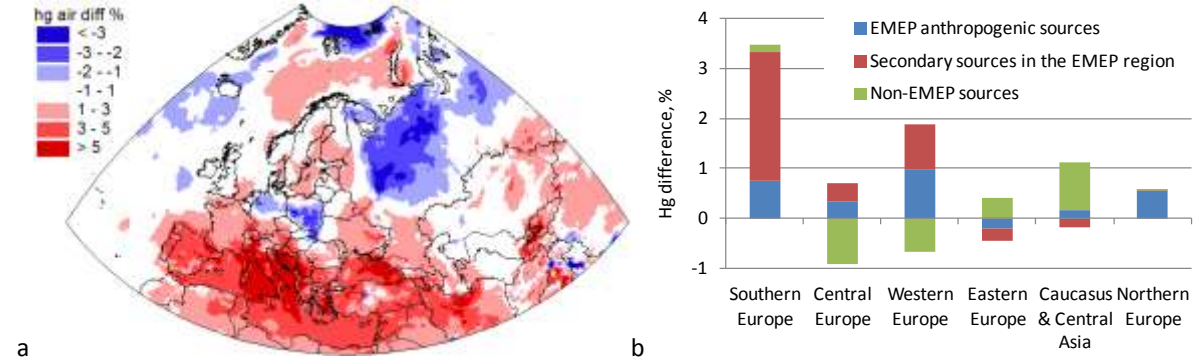

Fig. 3.25. *Relative changes of Hg^0 air concentrations between 2018 and 2017 over the EMEP domain (a) in various sub-regions (b).*

Mercury deposition is largely determined by oxidised Hg forms both emitted and produced chemically in the atmosphere. Therefore, the spatial pattern of Hg deposition is much more variable and reflects the effect of various factors including spatial distribution of emissions, areas of intensive atmospheric oxidation and precipitation pattern. Spatial pattern of Hg deposition generally follows distribution of air concentration (Fig. 3.26a). High deposition fluxes (above 15 g/km^2/y) are predicted in Southern Europe and Central Europe. Countries with the highest average deposition fluxes include Bosnia and Herzegovina, Montenegro, Albania, the Czech Republic, Liechtenstein, Italy and Slovakia (for more information see Supplementary Data Report [*Ilyin et al.*, 2020]). Elevated Hg deposition (10-15 g/km^2/y) also occurs over some territories of Scandinavia and Central Russia due to considerable annual precipitation. Besides, relatively high levels of Hg deposition are also predicted in the high Arctic as a result of intensive Hg oxidation in springtime during the Atmospheric Mercury Depletion Events (AMDEs). However, it should be taken into account that significant amount of Hg deposited to snowpack is re-emitted to the atmosphere.

Relative contribution of regional anthropogenic sources to Hg deposition is largest (up to 50%) in countries of Central Europe (Fig. 3.26b). Contribution of Hg secondary and natural sources is insignificant and does not exceed a few percent. Emissions from these sources being in the Hg^0 form mostly contribute to the Hg global pool. In contrast, contribution of the global pool (non-EMEP sources) is large (50-97% in individual countries). However, it should be noted that the contribution of these sources includes also some fraction of Hg from the EMEP sources (both anthropogenic and secondary/natural), which flew out through the boundaries, mixed up with other sources and returned back to the region.

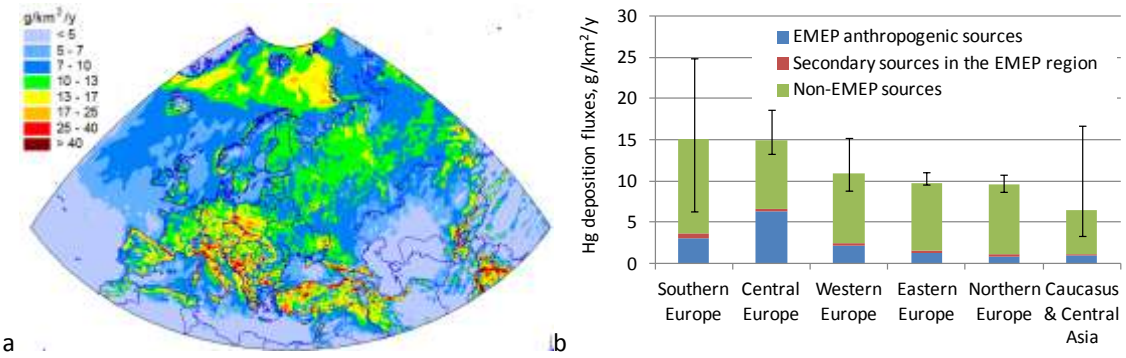

Fig. 3.26. *Spatial distribution of annual Hg deposition flux over the EMEP domain (a) and average Hg deposition in various sub-regions (b) in 2018. Whiskers show the range of concentrations in particular countries of the subregion.*

Mercury deposition from different source types in the EMEP domain is illustrated in more details in Fig. 3.27. As seen spatial patterns of Hg deposition from regional anthropogenic (Fig. 3.27a) and natural/secondary (Fig. 3.27b) emissions generally follow distribution of appropriate emission sources. Deposition of Hg emitted by anthropogenic sources is most significant in industrial regions of Central and Southern Europe as well as in some locations of Eastern Europe. Direct deposition of Hg from regional natural/secondary emissions is much lower and only noticeable in Southern Europe. In contrast, the spatial distribution of Hg deposition from non-EMEP sources largely reflects effect of atmospheric chemistry and the precipitation pattern. Thus, the highest deposition fluxes are in the high Arctic and the Mediterranean region (Fig. 3.27c).

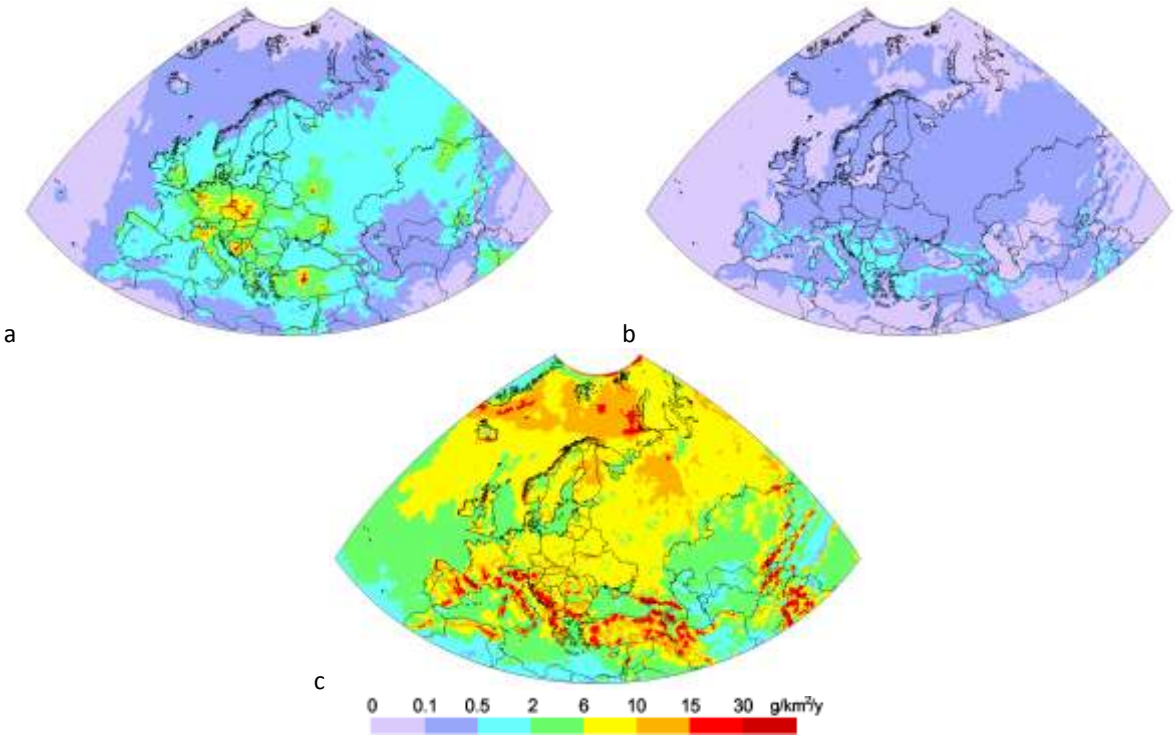

Fig. 3.27. *Annual deposition of Hg in 2018 from EMEP anthropogenic sources (a) natural/secondary sources (b) and non-EMEP sources (c).*

Figure 3.28 illustrates changes of Hg deposition pattern between 2017 and 2018 due to variability of meteorological parameters. Mercury deposition flux increased in Southern Europe and the Mediterranean region (Spain, Italy, the Balkan countries), Western Europe (France, the United Kingdom), southern Scandinavia, the Northern Atlantic, Middle East and, partly, Central Asia. Deposition decreased in Central Europe (Germany, Poland, Slovakia), Eastern Europe (the Baltic countries, Belarus, Northern Russia), over the Northern sea. These changes are largely caused by changes in the precipitation pattern (Section 3.1). In particular, precipitation considerably increased in Southern and Western Europe but decreased in Central and Northern Europe. Inter-annual variation of precipitation governs changes of Hg wet deposition. In Scandinavia, decrease of annual precipitation is accompanied by increase of Hg deposition due to larger contribution of Hg dry deposition from regional anthropogenic emissions.

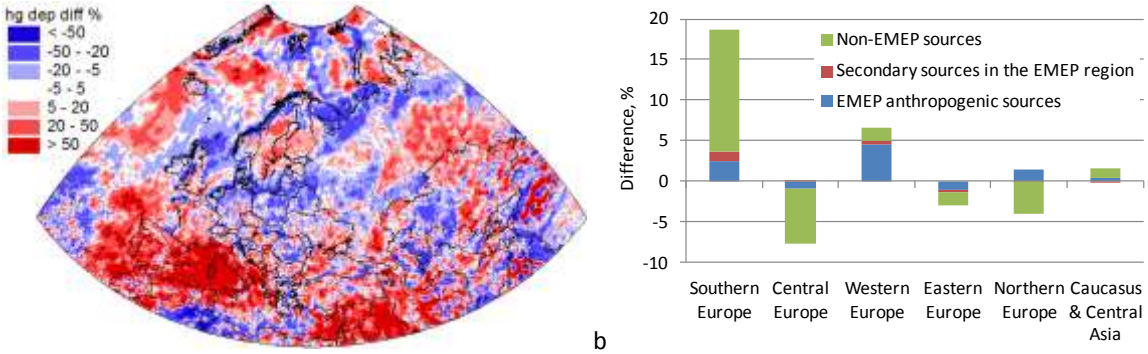

Fig. 3.28. *Relative changes of Hg deposition between 2018 and 2017 over the EMEP domain (a) and in various sub-regions (b).*

The model performance in simulation of Hg deposition can be partly evaluated via comparison of modelled and observed wet deposition fluxes. The model evaluation against EMEP measurements demonstrates satisfactory agreement of modelled and observed values with significant spatial correlation (0.53) and deviations being mostly within a factor of two (Supplementary Data Report [*Ilyin et al*., 2020]). However, the model tends to overestimate the observed values on average by 48%. This inconsistency is presumably connected with uncertainties of speciation of Hg anthropogenic emissions and incomplete knowledge on chemical transformations of Hg in the atmosphere. It should be noted that speciation of Hg emissions is not among the obligatory parameters included to the annual reporting by countries. Therefore, simplified expert estimates are used to prepare emission data for modelling (Section 1.2). Atmospheric chemistry of Hg is still actively investigated by the scientific community including identification of the major oxidation and reduction mechanisms, reaction kinetics and products (Section 4.3).

Transboundary transport

The effect of Hg transboundary transport on country pollution is characterised by relative contribution of national and foreign anthropogenic sources to Hg deposition in the country. The proportion of foreign sources varies from 15-20% for Turkey, Portugal and Italy to more than 95% for Belarus, Monaco and Liechtenstein. Mercury deposition from foreign sources exceeds deposition form national sources in 38 of 51 EMEP countries. An example of two countries with different

contributions of transboundary transport is shown in Fig. 3.29. Mercury anthropogenic deposition in Poland is largely determined by own emissions (71%). Considerable proportion of deposition (21%) is also made by neighbouring countries (Germany, the Czech Republic, Slovakia, the Russian Federation, Ukraine). Contribution of other countries is insignificant (8%). In contrast, transboundary transport makes up almost 90% of total anthropogenic Hg deposition in Croatia. The largest contributors are Bosnia and Herzegovina (25%), Italy (13%), Serbia (12%), Hungary (8%) and Poland (7%). More detailed information on transboundary pollution for each EMEP country is available in Supplementary Data Report [*Ilyin et al.*, 2020].

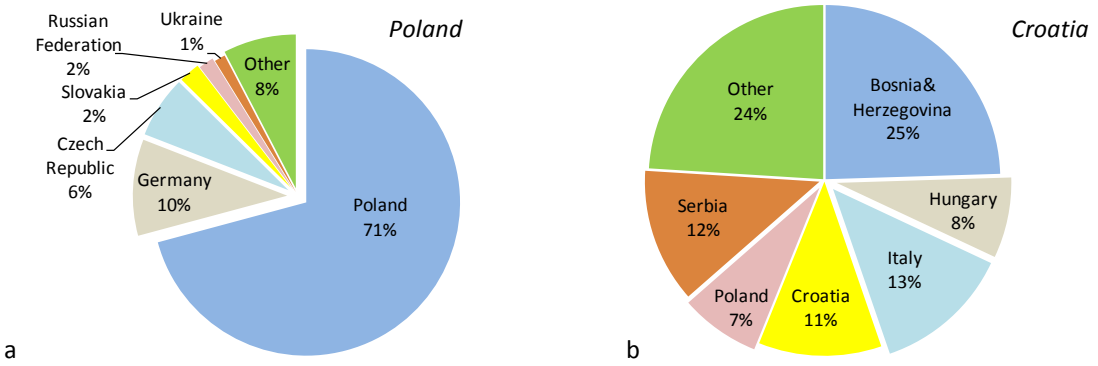

Fig. 3.29. *Contribution of the transboundary transport and national source to anthropogenic Hg deposition in Poland and Croatia*

Patterns of transboundary transport can differ from year to year due to variation of atmospheric circulation and other meteorological conditions. Figure 3.30 presents an example of changes in Hg transboundary pollution in the Czech Republic between 2017 and 2018. National emission sources contributed 44% (325 kg/y) to Hg deposition in this country in 2018. The main foreign contributors include Poland, Germany, Slovakia, Hungary and Austria. Contribution of Poland to Hg deposition in the Czech Republic increased from 110 to 190 kg/y between 2017 and 2018. On the contrary, contribution of Germany decreased from 130 to 105 kg/y due to changes in the atmospheric transport.

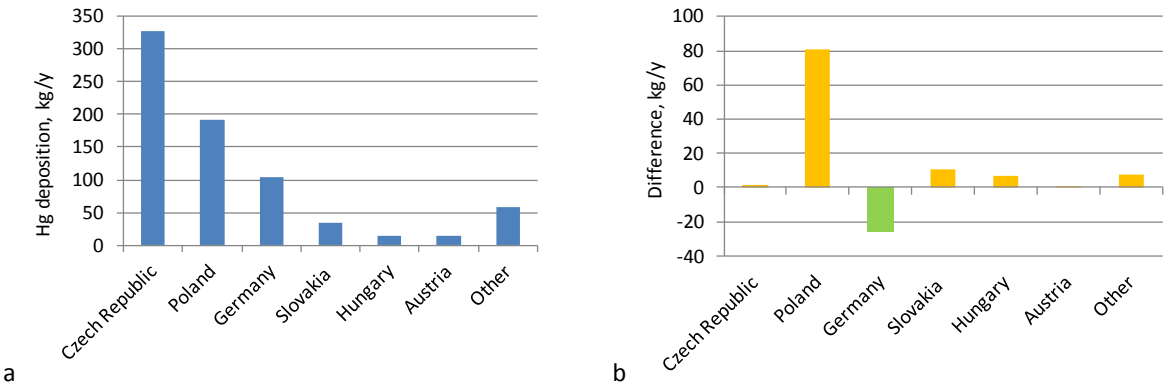

Fig. 3.30. *Major contributors of Hg anthropogenic deposition in the Czech Republic in 2018 (a) and absolute difference of Hg deposition between 2018 and 2017 (b)*

Mercury emitted by national sources partly deposits within a country's territory and partly contributes to transboundary pollution of other countries and regions. Contribution of a country to transboundary pollution depends on amount of national emissions, size and location of the country's territory. About 70% of Hg deposition in the EMEP countries is determined by major source countries – Russia, Kazakhstan, Turkey, Poland, Germany, Italy and Ukraine. For most of these countries Hg deposition almost equally shares between deposition to own territory and territories of other countries. Exceptions are Russia and Turkey, for which deposition to own territory exceeds contribution to transboundary transport by a factor of 4 and 2.5, respectively. Atmospheric transport of national emissions and deposition to other countries also changes because of inter-annual meteorological variability. For instance, export of Hg pollution from Austria decreased between 2017 and 2018 and partly changed of atmospheric dispersion directions that led to increase of Hg deposition from Austrian sources to Germany, the Czech Republic and Italy, as well as to decrease of deposition to the Russian Federation, Hungary and Poland (Fig. 3.31).

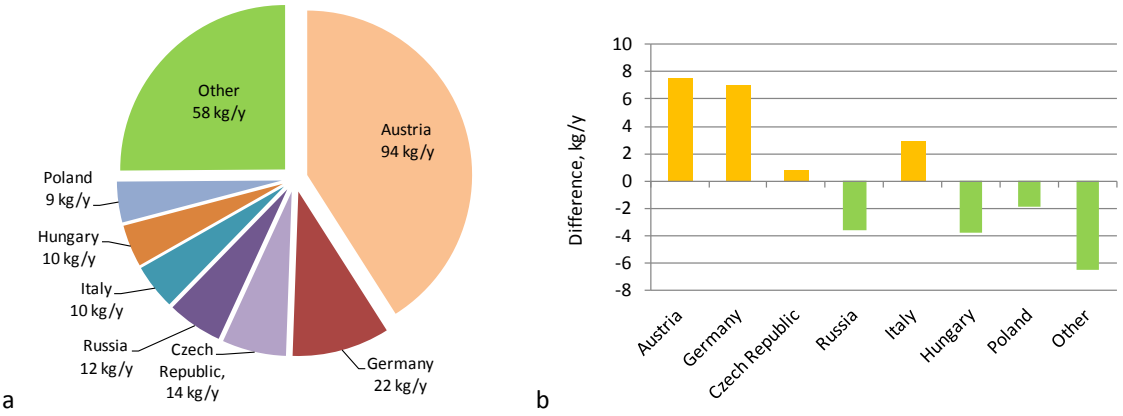

Fig. 3.31. *Contribution of Hg deposition from Austrian anthropogenic sources to own territory and other countries in 2018, (a) and changes of Hg deposition from Austria between 2018 and 2017 (b)*

Thus, transboundary transport significantly contributes to Hg pollution of the EMEP countries and varies in time not only due to changes of national anthropogenic emissions but also because of inter-annual meteorological variability.

3.3.5. PAHs

Polycyclic Aromatic Hydrocarbons (PAHs) comprise a large group of semi-volatile contaminants that naturally occur in the environment in coal, crude oil, and gasoline and can be released to the atmosphere during incomplete combustion of fossil fuels and biomass burning. PAHs are considered as substances posing serious risk for the human health and ecosystems. In order to evaluate PAH pollution levels and exceedances of target values of concentrations, monitoring of air concentrations and model assessment of transboundary transport is carried out. In this section a summary of information on the pollution levels of selected PAHs, namely, Benzo(a)pyrene, Benzo(b)fluoranthene, Benzo(k)fluoranthene, and Indeno(1,2,3-cd)pyrene, in the EMEP region for 2018 is presented. More detailed information on the pollution levels of individual PAHs is given in Supplementary materials [*Gusev at al*., 2020].

Spatial patterns of PAH pollution levels in 2018

Spatial distributions of annual mean modelled and observed air concentrations of sum of the above 4 PAHs in 2018 are presented in Fig. 3.32. Both model estimates and measurements of EMEP monitoring stations demonstrate high concentrations of 4 PAHs in the countries of Central, Eastern, and Southern Europe, e.g. in Poland, the Czech Republic, Hungary, and Greece. Areas of high concentrations can also be noted for northern Italy, Serbia, Spain, Romania, Macedonia, Bulgaria, and Russia. Analysis of exceedances of air quality limits for PAH air concentrations can be found in the Section 3.4. Lowest levels of PAH pollution in 2018 are estimated for countries in Northern Europe as well as in Caucasus and Central Asia.

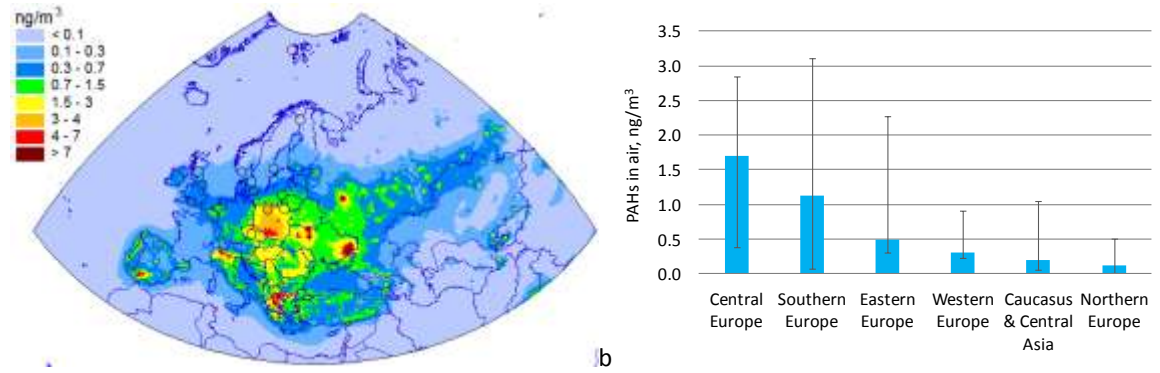

a b

Fig. 3.32. *Spatial distribution of modelled and observed annual mean air concentrations of sum of 4 PAHs in the EMEP domain for 2018 (a) and air concentrations of 4 PAHs in 2018 averaged over different sub-regions of the EMEP domain (b). Whiskers show the range of concentrations in particular countries of the subregion.*

Comparison of modelling results with the data of EMEP measurements shows in general reasonable agreement between modelled and observed concentrations (Fig. 3.32a). Measurements of 4 PAHs in 2018 were performed at 13 monitoring sites in 7 EMEP countries. The model under-predicted annual mean air concentrations of the sum of 4 PAHs with mean relative bias about -9% and spatial correlation about 0.8. For most of selected monitoring sites the difference between the model estimates and measurements is within a factor of 2. More significant discrepancy (under-prediction) was obtained for the Norwegian monitoring site NO0042R in the Arctic (about factor of 3).

Verification of modelling results for individual PAH compounds against the EMEP measurements indicates the under-prediction of observed B(a)P and B(k)F air concentrations, and over-prediction of observed B(b)F and IP concentrations. In particular, the largest mean bias is obtained for B(a)P (about -35%), followed by B(k)F (about -30%), while for B(b)F and IP discrepancies are below 20%. Differences in the model performance for individual PAH compounds may be explained by several reasons including uncertainties in the emission factors applied in national emission inventories for particular PAHs that might not match the distribution of PAHs in actual emissions, as well as the uncertainties in physical-chemical properties used in the model parameterization for these compounds. The model captures the spatial distribution of observed air concentrations of B(b)F and IP with correlation coefficient about 0.8 - 0.9. At the same time spatial correlation between the model predictions and measurements for B(a)P and B(k)F is lower (about 0.6).

Model predictions of PAH pollution in 2018 were also compared with the measurements of AIRBASE on the example of B(a)P. In 2018 monitoring of B(a)P air concentrations were performed at about 700 national stations in 28 European countries. Modelling results tend to under-predict annual mean observed B(a)P air concentrations, especially for the industrial, background urban and suburban monitoring sites. The most significant under-prediction is found for the monitoring sites in Poland, Bulgaria, Austria, and France. The modelling results reproduce the spatial distribution of observed B(a)P concentrations with correlation coefficient about 0.6. In particular, the modelled concentrations reasonably well correlate with the observed pollution levels in Belgium, the Czech Republic, Poland, Bulgaria, and Lithuania (with correlation coefficients about 0.5-0.8). At the same time, poor spatial correlation is found for Italy, Spain, France, the United Kingdom, and Austria. Different performance of the model with respect to bias and spatial correlation with observed concentrations for particular EMEP countries is most likely caused by several reasons. They include the uncertainties in the reported anthropogenic PAH emissions and their spatial distribution as well as possible uncertainties in model parameterizations used in the model simulations for PAHs. More detailed evaluation of modelling results against the monitoring data of EMEP and AIRBASE is given in Supplementary Data Report [*Gusev et al*., 2019].

Spatial distribution of 4 PAH total deposition fluxes calculated for 2018 is shown in Fig. 3.33. Similar to the air concentrations, the highest annual mean deposition fluxes are noted for Central and Southern Europe.

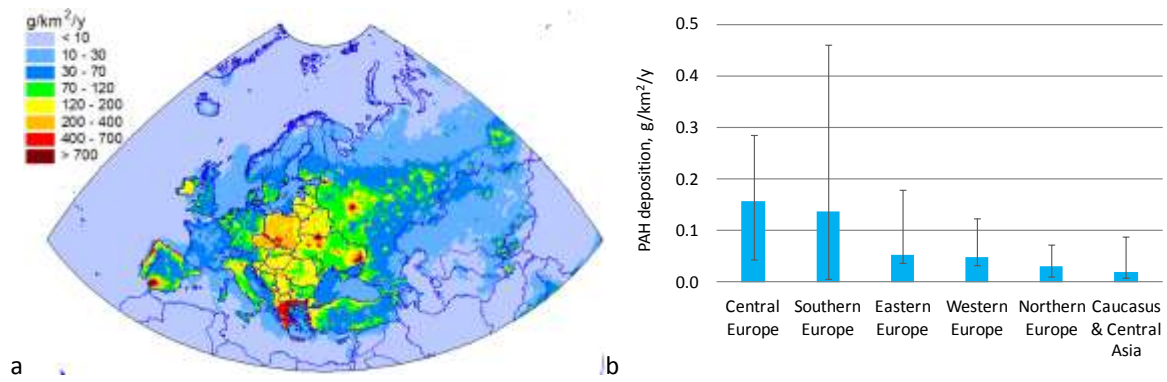

Fig. 3.33. *Spatial distribution of modelled total deposition fluxes of sum of 4 PAHs in the EMEP domain for 2018 (a) and averaged total deposition fluxes of 4 PAHs over different sub-regions of the EMEP domain (b). Whiskers show the range of deposition fluxes in particular countries of the subregion.*

To characterize the effect of inter-annual variability of meteorological conditions on PAH pollution levels modelling results for 2018 were compared with the results for 2017. Model simulations for 2017 and 2018 were carried out using the same set of emission data for 2017. Changes of PAH annual mean air concentrations from 2017 to 2018 are illustrated in Fig. 3.34. The largest increase of concentrations (~16%) is indicated for Northern Europe followed by Southern and Central Europe (~3-4%) as well as in Caucasus and Central Asia (~2%). At the same time decreasing concentrations can be noted for some of the countries in Western and Eastern Europe, 3% and 1%, respectively.

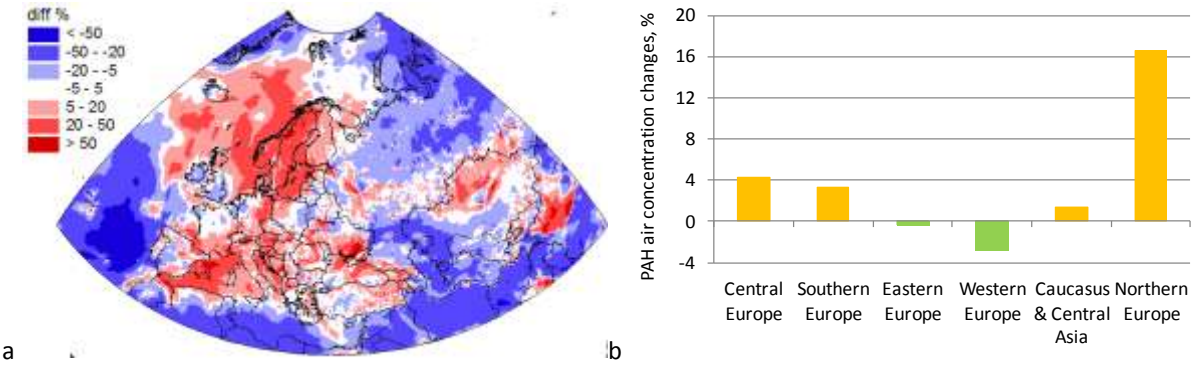

Fig. 3.34. *Spatial distribution of relative changes of sum of 4 PAH air concentration between 2018 and 2017 due to inter-annual variation of meteorological conditions (a) and relative changes of averaged air concentrations over different sub-regions of the EMEP domain (b).*

Fig. 3.35 demonstrates the changes of PAH total deposition fluxes from 2017 to 2018. The largest increase of deposition fluxes (~15%) is indicated for Western Europe (Fig. 3.35b). In countries of Northern, Southern and Central Europe deposition fluxes increased by ~7-12%. At the same time decreasing deposition fluxes can be noted for the countries of Eastern Europe, Caucasus and Central Asia. Changes of PAH pollution levels between the years 2018 and 2017 can be related to the inter-annual variations of precipitation and atmospheric circulation.

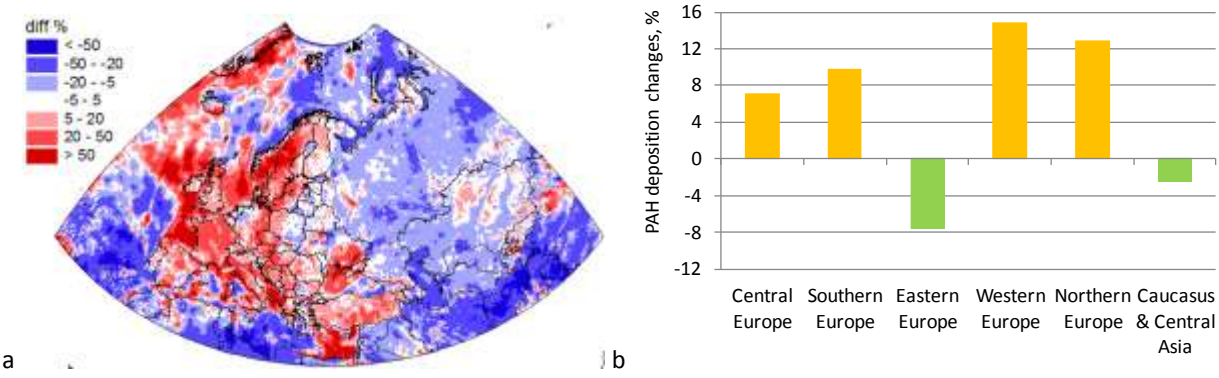

Fig. 3.35. *Spatial distribution of relative changes of sum of 4 PAH total deposition between 2018 and 2017 due to inter-annual variation of meteorological conditions (a) and relative changes of averaged total deposition in different sub-regions of the EMEP domain (b).*

Source apportionment of PAH pollution

Source apportionment of PAH pollution is carried out taking into account contributions of anthropogenic emission sources of the EMEP countries as well as contributions of emissions outside the EMEP region. Long-range transport from non-EMEP emissions is estimated using global scale modelling on the basis of inventory of global PAH emissions developed by the research group of Peking University [*Shen et al.,* 2013].

Contributions of three main groups of emission sources to annual total deposition, averaged over different parts of the EMEP region, are presented in Fig. 3.36a. The largest contributions (about 70-80%) is estimated for the EMEP anthropogenic emissions, whereas contributions of non-EMEP emissions and secondary sources are significantly lower, 20-25% and below 10%, respectively. Inter-annual variations of averaged total annual deposition of 4 PAHs from 2017 to 2018 are demonstrated in Fig. 3.36b sub-divided into different types of emission sources. It can be seen that in most of the regions changes of total deposition were mainly due to the changes of the EMEP and non-EMEP anthropogenic emissions. Different situation can be seen for the Caucasus and Central Asia region where decline of deposition was caused by comparable changes of all three types of emissions.

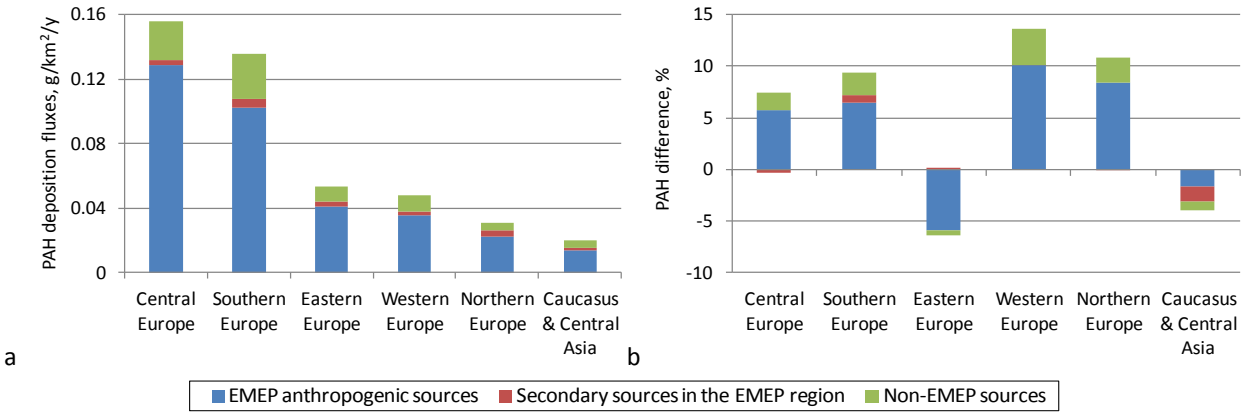

Fig. 3.36. *Deposition fluxes of sum of 4 PAHs in 2018 from EMEP anthropogenic sources, secondary sources and non-EMEP anthropogenic sources for different sub-regions of the EMEP domain (a) and relative difference in deposition fluxes between 2018 and 2017 (b).*

Transboundary transport

Model assessment of PAH distribution within the EMEP region indicates significant effect of transboundary transport on the pollution levels in the EMEP countries. The contribution of transboundary transport to deposition of PAHs exceeds 50**%** in 27 EMEP countries, and 75**%** in 7 EMEP countries. In Fig. 3.37 source apportionment of B(a)P deposition to Slovakia and Lithuania is illustrated. In particular, significant part of B(a)P deposition to Slovakia (87%) is caused by transboundary transport from Poland, Hungary, the Czech Republic and other countries, whereas national sources contributed only 13%. At the same time, in case of Lithuania contribution of national sources to the pollution of the country is accounted for 70% while atmospheric transport from other countries is less important.

Contributions of transboundary transport from countries emitters of PAHs may change considerably from year to year due to inter-annual variability of meteorological conditions and emissions. In Fig. 3.38 example of total annual deposition of B(a)P to Switzerland in 2018 is demonstrated with main contributions from other EMEP countries and their changes from 2017 to 2018. Model predictions show noticeable increase of contributions from Germany and Italy to deposition in Switzerland. In particular, contribution of Germany increased by about 22 kg/y (1.4-fold), and Italy – by 23 kg/y (1.5-fold).

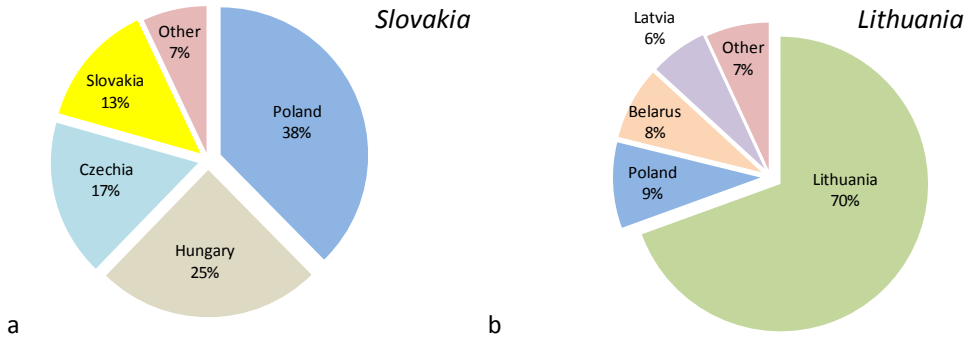

Fig. 3.37. *Contributions of the transboundary transport and national sources to B(a)P deposition in Slovakia and Lithuania.*

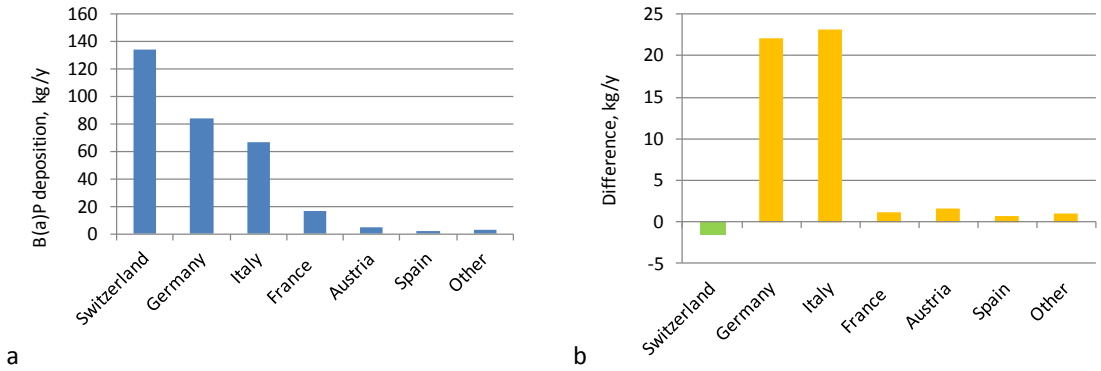

Fig. 3.38. *B(a)P deposition in Switzerland from main countries-contributors in 2018 (a) and absolute difference of B(a)P deposition between 2018 and 2017 (b).*

Transboundary transport of pollution can also be characterized using the ratio between the part of PAHs, emitted in the particular EMEP country and deposited to other EMEP countries, and total deposition of PAHs from all the sources of considered country. Modelling results for 2018 indicate that for 20 EMEP countries (about 40% of the countries) more than 50% of total deposition from national emission sources deposited to other countries. According to model estimates the largest contributions to the transboundary transport and deposition of PAHs in the EMEP region are made by the countries with relatively high emissions, namely, Ukraine, Poland, the Russian Federation, the Czech Republic, Romania, and Turkey. Detailed information on source apportionment of PAH deposition for particular EMEP countries is available in the Supplementary Data Report [*Gusev et al.*, 2019].

3.3.6. PCDD/Fs, PCBs and HCB

In this section a summary of information on PCDD/Fs, PCBs, and HCB pollution levels in 2018 within the EMEP region is presented. These pollutants are released into the environment as unintentional by-products of various anthropogenic activities. Along with anthropogenic emissions, significant contribution to the pollution by these POPs is made by the secondary emissions from the terrestrial and aquatic compartments, occurred due to direct emissions and long-term cycling of these contaminants in the environment. PCDD/Fs, PCBs, and HCB are characterized by significant persistence in the environmental media (e.g. soil, water bodies). Thus, their presence in the environment over long period of time after their release poses risk to human health and ecosystems.

Spatial patterns of PCDD/F, PCB, and HCB pollution levels in 2018

Spatial distributions of annual mean modelled air concentrations of PCDD/Fs, PCBs (PCB-153), and HCB in 2018 are presented in Fig. 3.39.

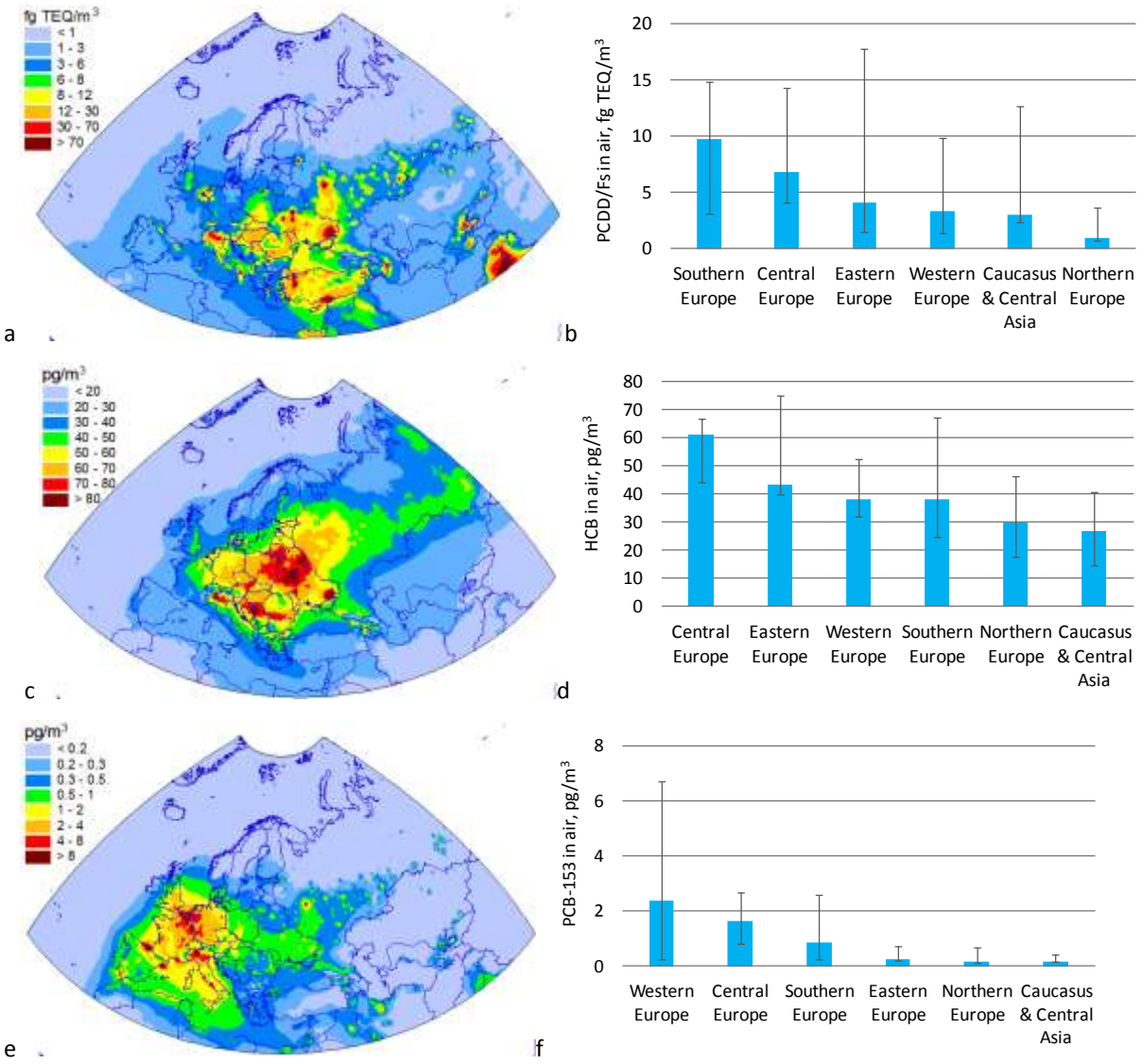

Fig. 3.39. *Spatial distribution of modelled and observed annual mean air concentrations in 2018, and annual mean air concentrations, averaged over different sub-regions of the EMEP domain, of PCDD/Fs (a,b), HCB (c,d), and PCB-153 (e,f). Whiskers indicate the range of annual mean air concentrations in the countries of particular region.*

Model predictions indicate substantial spatial gradients of PCDD/Fs and PCB-153 air concentrations in the EMEP countries, whereas for HCB spatial distribution of annual mean air concentrations is more homogeneous that can be conditioned by its relatively high persistence in the atmosphere. According to the modelling results the most significant average PCDD/F pollution levels in 2018 are characteristic of the countries of Southern Europe and Central Europe, and for HCB of the countries of Central and Eastern Europe (Fig. 3.39a,c). At the same time for PCB-153 the most significant levels of concentrations are estimated for Western Europe (Fig. 3.39e). The Central Europe is among the first two mostly polluted regions for all three considered pollutants. Maximum levels of PCDD/F and

HCB air concentrations in 2018 (Fig. 3.39b,d) are estimated for Eastern Europe, while of PCB-153 (Fig. 3.39f) for Western Europe. Differences in the geographical patterns of concentrations can be explained by different spatial distribution of emissions for the three considered pollutants.

Comparison of modelling results with available measurements of EMEP monitoring stations for PCB-153 and HCB shows reasonable agreement between measured and predicted concentrations. Namely, correlation coefficient between measurements and modelling results is about 0.75 for PCB-153 and 0.60 for HCB. Most stations are characterized by differences between modelled and observed concentrations within a factor of 2. In particular, among the 9 stations for PCB-153 the differences higher than a factor 2 is found for CZ0003R and NO0042R, and among 7 stations for HCB for IS0091R and SE0014R. Relative bias for PCB-153 is about -2%, and for HCB about -27%. Monitoring of PCDD/F air concentrations in 2018 was carried out at two EMEP stations SE0014R and SE0022R for several months, namely, for April, June, September, and December. Comparison of measured and predicted air concentrations shows systematic underestimation of observed concentrations for both stations mostly about a factor of 2.

Relative changes of spatial patterns of PCDD/F, HCB, and PCB-153 air concentrations between calculations for 2017 and 2018 are presented in Fig. 3.40. Model simulations for these two years were performed with the same set of emission data for 2017, and thus these changes can be attributed to inter-annual variations of meteorological parameters, namely, temperature, precipitation, and atmospheric circulation (Section 3.1). For PCDD/F increase of air concentrations is estimated in countries of Northern, Central, Eastern and Sothern Europe. At the same time, decreasing concentrations are characteristic of Western Europe as well as Caucasus and Central Asia. Similarly, for PCB-153 increasing pollution levels are obtained for Northern and Southern Europe, whereas for other areas decreasing concentrations are estimated. In case of HCB modelling results indicate decline of concentrations in all the regions except of Northern Europe, where levels of HCB slightly increased. It can be seen that spatial patterns of the changes of PCDD/Fs, PCB-153, and HCB air concentrations differ considerably between each other. These differences can be explained by different physical-chemical properties of these pollutants as well as different spatial distributions of their emissions.

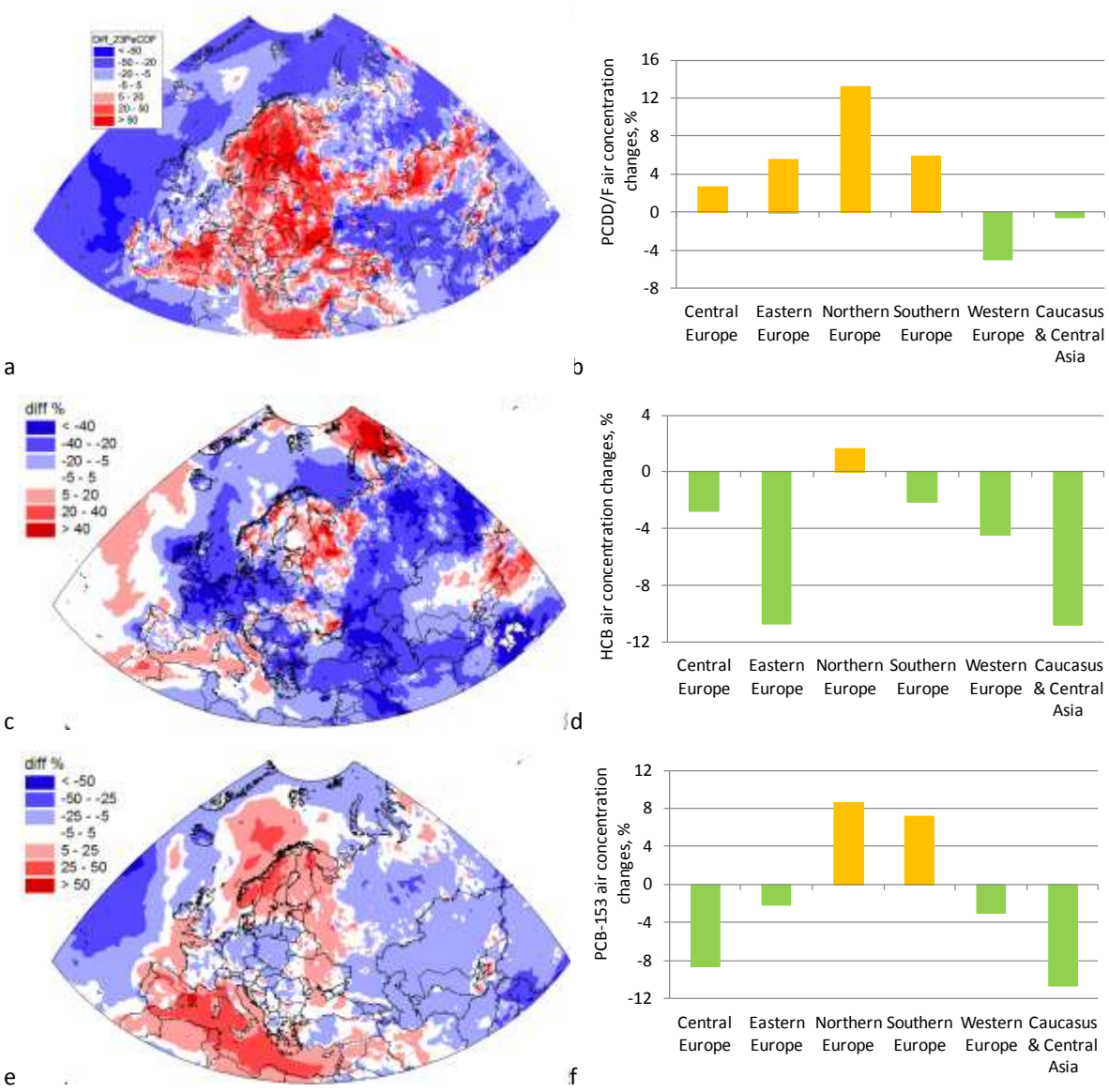

Fig. 3.40. *Spatial distribution of relative changes of air concentrations between 2018 and 2017 and relative changes of averaged air concentrations over different sub-regions of the EMEP domain for PCDD/Fs (a,b), HCB (c,d), and PCB-153 (e,f).*

Source apportionment of PCDD/Fs, PCB-153, and HCB pollution

Source apportionment of PCDD/F, PCB-153, and HCB pollution of the EMEP countries in 2018 provides information on contributions of primary anthropogenic, secondary, and non-EMEP emissions. Contribution of anthropogenic emissions in the EMEP countries is estimated for PCDD/Fs to 21-42%, for PCB-153 to 16-36%, and for HCB to 1-3% (Fig. 3.41). The largest contributions of PCDD/F anthropogenic emissions are indicated for Eastern Europe (42%), of PCB-153 for Western Europe (36%), and for HCB in Southern Europe (3%). Secondary emission sources in the EMEP countries contributed to deposition of PCDD/Fs about 60%, of PCB-153 about 70%, and of HCB about 80%. The contribution of non-EMEP emission sources is about 9% for PCDD/Fs, 4% for PCB-153, and about 18% for HCB.

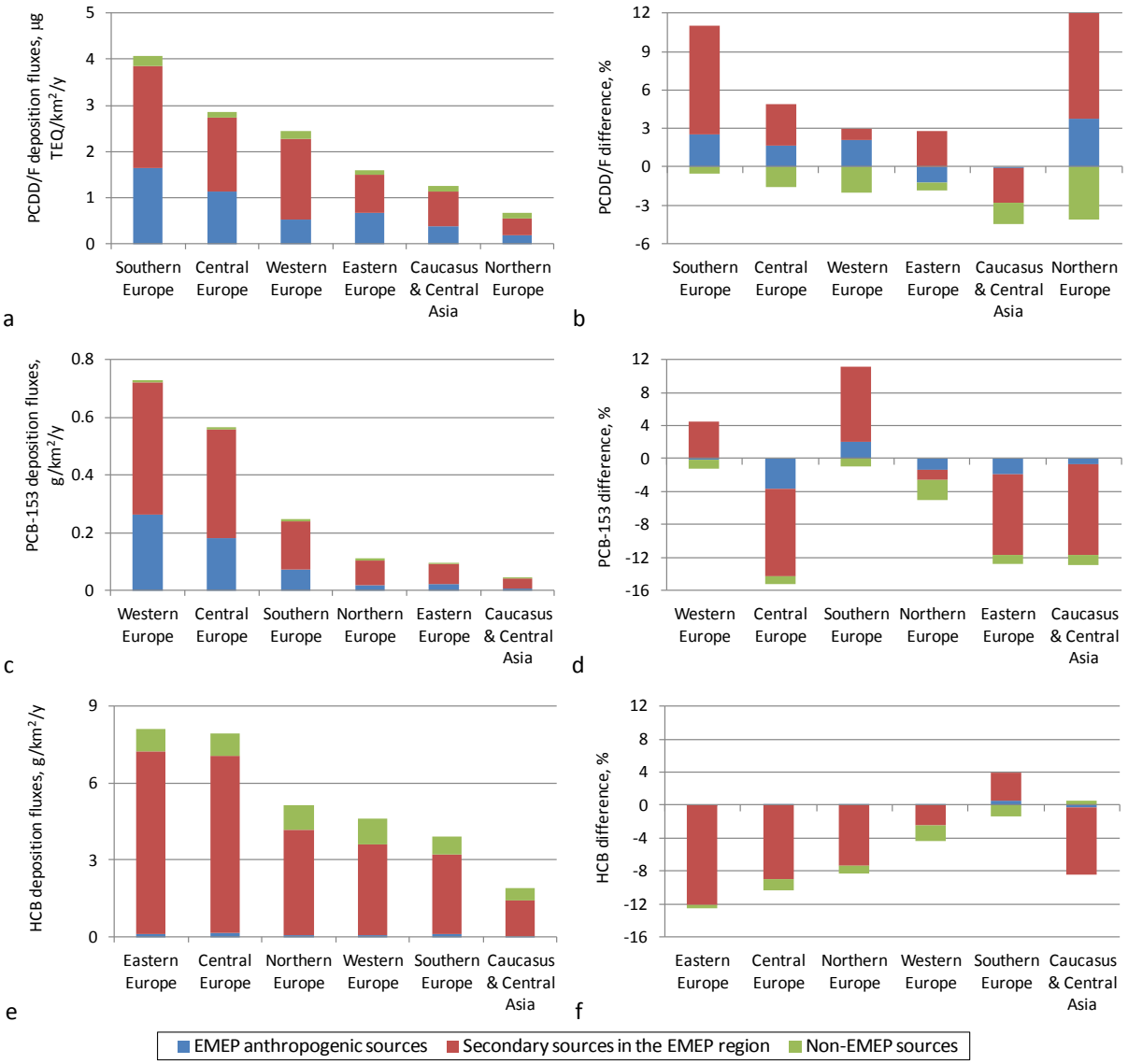

Fig. 3.41. *Deposition fluxes from EMEP anthropogenic sources, secondary sources, and non-EMEP anthropogenic sources in 2018 and relative difference in deposition fluxes between 2018 and 2017 normalized by total deposition in 2017 for different sub-regions of the EMEP domain for PCDD/Fs (a,b), PCB-153 (c,d), and HCB (e,f).*

Inter-annual differences of PCDD/F total deposition fluxes in particular sub-regions of the EMEP domain between 2017 and 2018 due to meteorological changes vary from -4% to 12% with maximum change (increase) in Northern Europe (Fig. 3.41b). For all the sub-regions the contributions of non-EMEP sources to deposition fluxes in 2018 is lower compared to 2017. At the same time, the contributions of primary anthropogenic and secondary EMEP emissions increased in 2018 leading to higher levels of pollution by PCDD/Fs.

For PCB-153 changes of total deposition fluxes range from -12% in Central Europe to 11% in Southern Europe (Fig. 3.41d). Total annual deposition fluxes of HCB in 2018 were in most of the sub-regions lower comparing to 2017 with the largest decrease about 12% in Eastern Europe (Fig. 3.41f). Similar to PCDD/Fs, contributions of non-EMEP sources to PCB-153 and HCB deposition fluxes in 2018 is lower compared to 2017, while contributions of primary anthropogenic and secondary EMEP emissions in most of sub-regions were lower in 2018 comparing to 2017.

Transboundary transport

Significance of transboundary transport for the pollution can be illustrated using proportion of contributions of national and foreign anthropogenic emission sources to deposition in the particular country. The model assessment of PCDD/F, PCB-153, and HCB long-range transport indicates considerable role of transboundary pollution between the EMEP countries. In particular, in 2018 deposition due to transboundary transport is higher than the deposition from national emissions for HCB in 39 (76%) countries. In case of PCDD/Fs and PCB-153 this situation takes place for 20 (39%) countries and 30 (59%) countries, respectively.

Emissions of POPs from the national sources of a given country undergo long-range atmospheric transport and deposition, which occurs partly over the territory of a country itself and partly over the territories of the other countries. For HCB the fraction of pollutant, deposited to other EMEP countries is higher than the fraction, deposited to the country itself, for 29 (57%) countries. For PCDD/Fs and PCB-153 these estimates are accounted for 12 (31%) and 14 (27%) countries, respectively. More detailed information on transboundary pollution for each EMEP country is available in Supplementary Data Report [*Gusev et al.*, 2020].

3.3.7. Country-specific information

The status report along with supplementary materials [*Ilyin et al.*, *Gusev et al*., 2020] contains general description of the current state of heavy metal and POP pollution in the EMEP region. More detailed information on pollution levels in each individual EMEP country is provided on the web at the MSC-E website (http://en.msceast.org/index.php/pollution-assessment/emep-countries-menu). The country-specific information includes variety of the model assessment results for each country collected in one place to facilitate access of national experts to the pollution data. In addition, the information for the EECCA countries is also available in Russian (http://www.ru.msceast.org/index.php/pollution-assessment/eecca-countries-menu).

The country-specific information includes the following elements:

- Spatial distribution of pollution levels (concentrations and deposition);
- Transboundary pollution of a country;
- Contribution of national sources to transboundary transport;
- Ecosystem-specific deposition (17 land cover categories).

The spatial distribution data include maps of heavy metal and POP air concentrations and deposition fluxes (Fig. 3.42). The information on transboundary pollution is provided in the form of pie charts with contributions of national anthropogenic emission sources and sources of other EMEP countries (Fig. 3.43a). Along with this spatial distribution maps of relative contribution of transboundary transport to deposition over the country are also given (Fig. 3.43b). The influence of the country on the pollution of the other EMEP countries is illustrated in the form of maps of total annual deposition fluxes from the country emission sources and diagrams of their distribution over the EMEP countries.

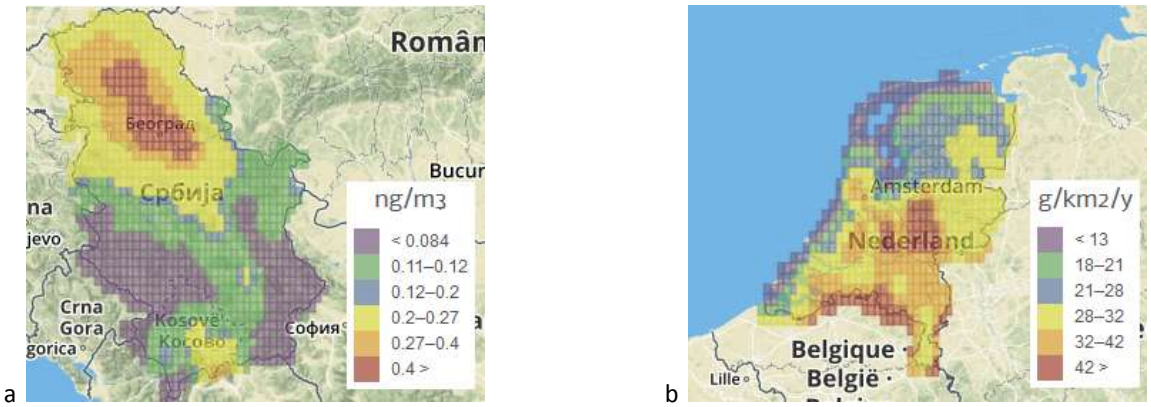

Fig. 3.42. *Annual mean air concentration of Cd in Serbia (a) and annual total deposition of B(a)P in the Netherlands (b) in 2018.*

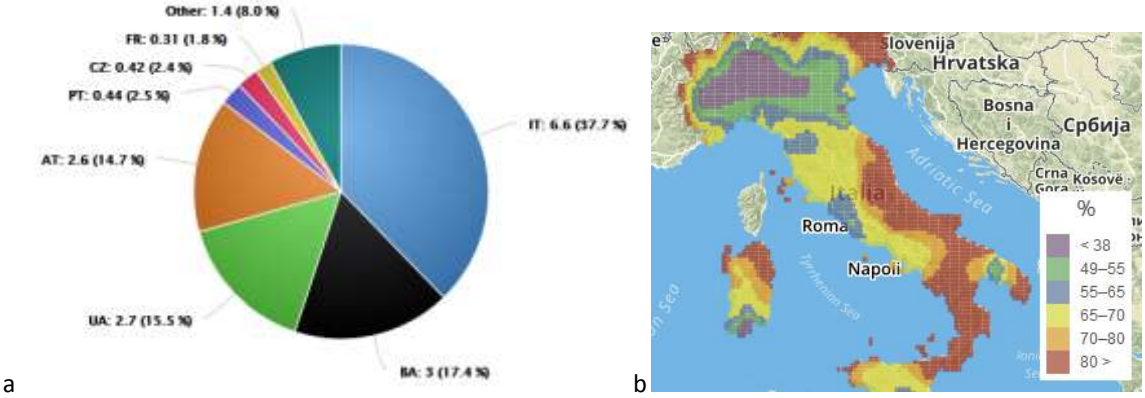

Fig. 3.43. *Transboundary pollution of HCB in Italy in 2018: (a) - contribution of own emission sources and emissions of other EMEP countries to total anthropogenic deposition; (b) – spatial pattern of relative contribution of foreign sources to anthropogenic deposition.*

Deposition to different types of ecosystems is important information for the effect community, particularly, for the assessment of harmful effects on human health and the environment. Therefore, maps of heavy metal and POP deposition to various types of land cover are also presented at the website (Fig. 3.44).

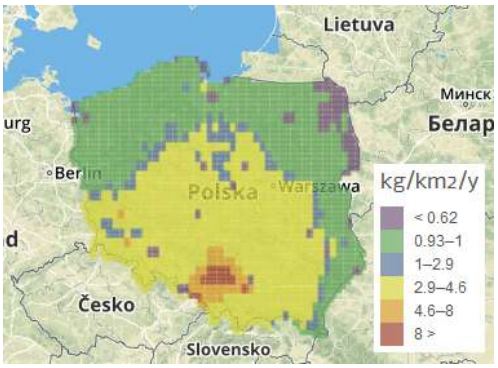

Fig. 3.44. *Annual total deposition of Pb to mixed forests in Poland in 2018.*

Detailed information on source-receptor relationships between all EMEP countries is also available in the database at the website along with other data on heavy metal and POP pollution of the EMEP domain (http://en.msceast.org/index.php/pollution-assessment/emep-domain-menu/data-hm-pop-menu). Besides, country-specific reports for individual EMEP countries are available on demand.

3.4. Information for exposure assessment

The ultimate aim of pollution assessment is evaluation of risks for human health and ecosystems associated with adverse effects of the pollution. Therefore, MSC-E continues providing the effect community with information that can be useful for the exposure assessment. In particular, information of ecosystem-specific deposition of heavy metals and POPs is provided for evaluation of the critical loads exceedances. Besides, exceedances of the PAH air quality standards are analyzed along with discussion about heavy metal and POP content in composition of particular matter that can lead to additional toxicity of atmospheric aerosol.

3.4.1. Ecosystem-specific deposition

Information on calculated deposition fluxes of heavy metals and POPs is used for evaluation of the effects of the pollutants on human health and biota. Working Group on Effects (WGE) of the Convention developed the critical loads approach in order to identify areas where the long-term adverse effects of heavy metal and POP pollution most likely occur [*de Vries et al.*, 2015a,b]. In order to support this activity of WGE, MSC-E regularly calculates deposition fluxes to various types of land cover (forests, shrubs, grasslands, crops, water bodies, etc.) within the EMEP domain. Data on the modelled Pb, Cd and Hg deposition to 17 land-cover types in 2018 is available at the MSC-E website [http://en.msceast.org/index.php/pollution-assessment/emep-domain-menu/land-use-menu] and in Supplementary Data Report [*Ilyin et al.*, 2020].

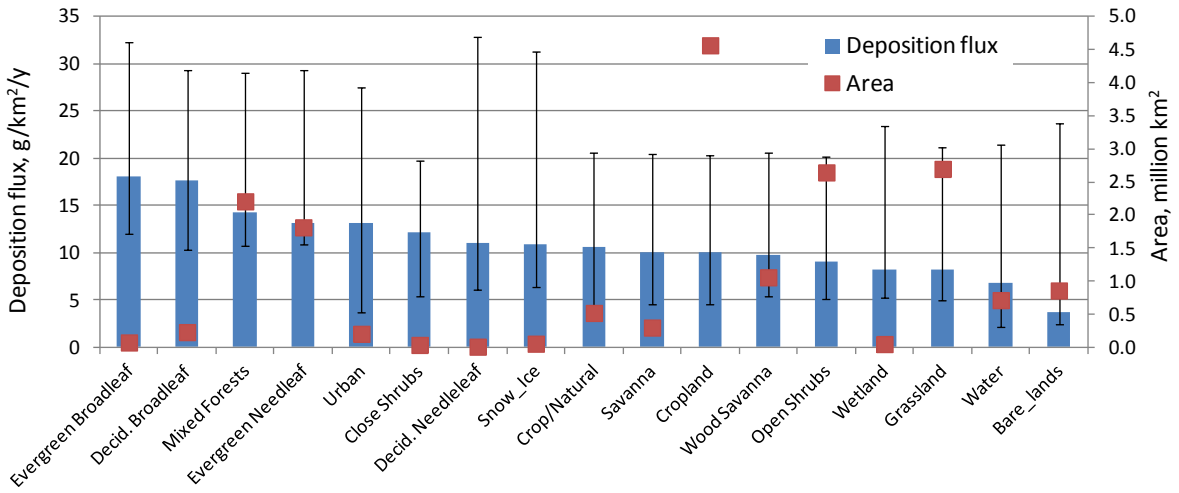

Fig.3.45. *Deposition of Hg to various ecosystem types within the EMEP domain in 2018. Bars show average value for all EMEP countries; whiskers present range deposition flux variation among the EMEP countries.*

Deposition fluxes to various land-cover types differ significantly. First of all, dry deposition depends on properties of the underlying surface, and, therefore, differs between land-cover types. For example, average deposition flux of Hg to forests is 1.5-2 fold higher than that to land-cover types with low vegetation (e.g., grasslands, arable lands, etc.) (Fig. 3.45). Another factor is proximity of areas covered with particular land-cover types to main emission sources. For example, mean Hg deposition flux to evergreen needleleaf forests is 30-40% lower than the flux to evergreen or

deciduous broadleaf forests. The reason for that is the fact that large areas covered with evergreen needleleaf forests present in the Nordic countries where pollution levels are lower compared to other parts of the EMEP domain. Maximum deposition fluxes of Hg to various types of forests are comparable. Maximum deposition flux to urban areas is also comparable with maximum deposition to forests because of location close to emission sources. High maximum deposition to the snow and ice cover type is explained by the effect of the atmospheric Hg depletion events in the Arctic.

Difference of deposition fluxes to various land-cover types is also illustrated by spatial distribution of Pb fluxes to croplands and forests. The fluxes to arable lands range from 0.2 to 1 kg/km^2/y over most of the EMEP countries (Fig. 3.46a). However, in some relatively small areas, such as the northern part of Italy, south-western Poland and the western part of Turkey Pb deposition exceeds 1.5 kg/km^2/y. The deposition flux to forests is about two-fold higher, ranging from 0.4 to 1.5 kg/km^2/y, and exceeding 3 kg/km^2/y in the most polluted areas (Fig. 3.46b). Similar peculiarities are noted for other heavy metals and also for POPs.

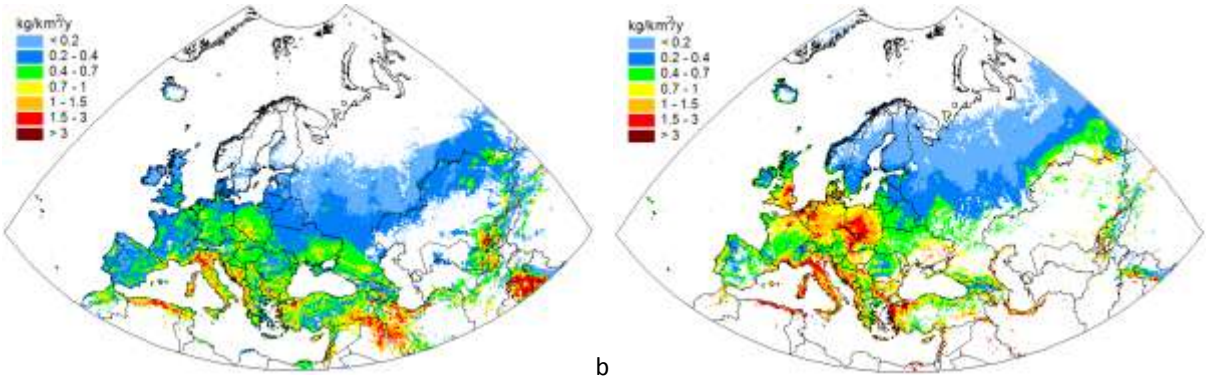

a b

Fig. 3.46. *Annual deposition flux of Pb to croplands (a) and mixed forests (b) in 2018.*

It should be noted that ***the most recent estimates of the adverse effects on human health and biota relate to 2010 and can hardly reflect present status of pollution [de Wit et al, 2015]. Therefore, more efforts of the effects community in the field of evaluation of heavy metal and POP pollution adverse impacts are needed.***

3.4.2. Exceedances of air quality standards (PAH)

PAHs are emitted to the atmosphere as a complex mixture of various PAH congeners. Many of PAHs are characterized by carcinogenic, mutagenic, and/or teratogenic properties [*Abdel-Shafy et al.*, 2016]. Taking into account possible risks for human health, the target value for B(a)P annual mean air concentrations has been set up by the European Directive 2004/107/EC equal to 1 ng/m^3 [*EU*, 2004]. Besides, upper and lower assessment thresholds for B(a)P (0.6 and 0.4 ng/m^3 respectively) are established to assess ambient air quality. Similar target level for B(a)P was also introduced as an air quality standard in a number of other countries of the EMEP domain (e.g. in the EECCA countries). In addition, the reference level of 0.12 ng/m^3 for B(a)P has been defined by World Health Organization (WHO) as a level of air concentrations corresponding to the excess lifetime cancer risk level of 10^{-5} [*WHO*, 2017].

Results of the model simulations for 2018 indicate high level of annual mean B(a)P air concentrations, exceeding the EU target value (1 ng/m^3), in Poland, Spain, Italy, Germany, the Czech Republic, Portugal, Hungary, Serbia, and Bulgaria (see Fig. 3.47a). Areas of high concentrations (above the EU target value) are also noted for some of the EECCA countries. At the same time, these estimates are subject of higher uncertainties due to incomplete emission data for this part of EMEP region (see Chapter 1).

According to modelling results, about 5% of total population of the EMEP countries in 2018 lived in areas with exceeded EU target level for annual mean B(a)P air concentrations (Fig. 3.47b). It is seen that most of these exceedances took place in urban areas. The upper assessment thresholds (UAT) and lower assessment thresholds (LAT) values were exceeded in the areas with 15% and 25% of population, respectively. In case of the WHO reference level for B(a)P only about 38% of population in the EMEP countries were in the conditions of the annual mean air concentrations below the reference level.

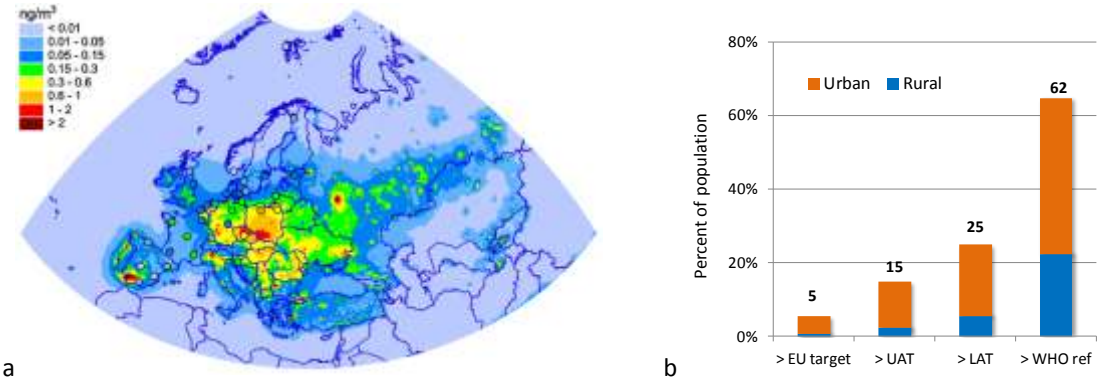

Fig. 3.47. *Spatial distribution of annual mean B(a)P air concentrations for 2018 (a) and percentage of urban and rural population of the EMEP countries in the areas with annual mean B(a)P air concentrations in 2018 exceeding the EU limit values and WHO reference level (b).*

Detailed observational data on B(a)P pollution levels are available from national monitoring in the EU countries (AIRBASE). Spatial distribution of observed annual mean B(a)P air concentrations in 2018 is presented in the Fig. 3.48a. Similar to the modelling results, the highest average B(a)P air concentrations in 2018 were observed at the monitoring stations in Central, Eastern, and Southern Europe (Fig. 3.48a).

Annual mean B(a)P air concentrations observed in 2018 in the selected European countries are illustrated in Fig. 3.48b. According to these data, B(a)P air concentrations, averaged over the monitoring sites of particular country, were above the EU target value in 6 EU countries, namely, Poland, Slovakia, Croatia, the Czech Republic, Bulgaria, and Hungary.

In addition, maximum measured B(a)P concentrations above the EU target value were also reported by some of the monitoring stations in Lithuania, Slovenia, Austria, Italy, Finland, Germany, France, Spain, and the UK. The highest concentrations were measured in the southern part of Poland (more than 10 ng/m^3). Most of exceedances of the EU target value were observed at the urban background stations.

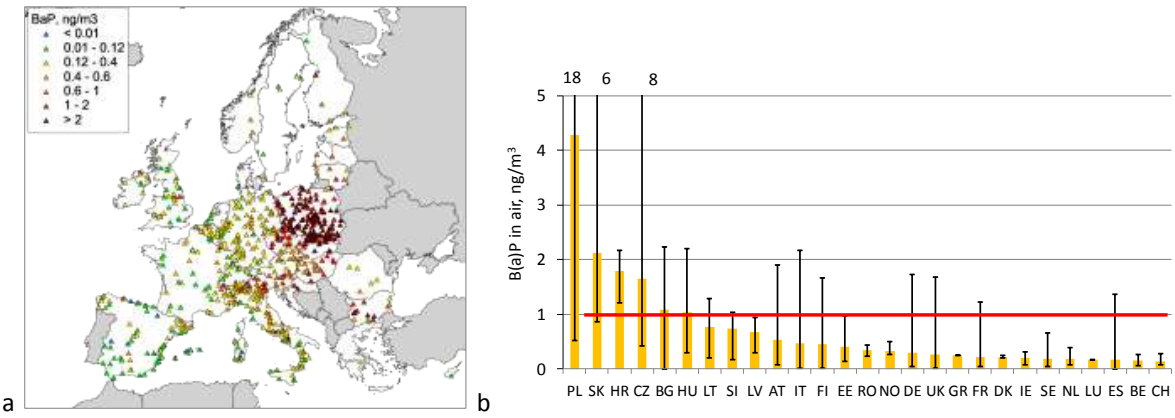

Fig. 3.48. *Spatial distribution of B(a)P air concentrations observed at AIRBASE monitoring sites in 2018 (a) and average values of measured annual mean B(a)P air concentrations in the EU countries in 2018 (b). Whiskers denote the range from minimum to maximum of measured concentrations.*

Exceedances of WHO reference level in 2018 took place in most of the countries performing regular monitoring of B(a)P pollution levels. In particular, annual mean B(a)P concentrations were higher than 0.12 ng/m^3 in 27 European countries. Thus, further measures are required to reduce elevated levels of B(a)P concentrations and their adverse effects on population.

PAHs are emitted and dispersed in the environment as mixtures of various PAH compounds. To evaluate population exposure to mixture of toxic PAHs the approach based on toxic equivalency factors can be used [*Liu et al*., 2019; *Delgado-Saborit et al*., 2011]. This approach is similar to that applied for toxic congeners of PCDD/Fs in order to estimate toxicity of a mixture of toxic PCDD/F congeners. In particular, each of the PAH compounds that contribute to the toxicity of PAH mixture has a specific toxic equivalence factor (TEF) that weights its toxicity relative to that of B(a)P [*ALS*, 2013]. The TEFs can be applied to characterize the carcinogenic potency of each considered PAH and calculate B(a)P equivalent concentration of PAH mixture.

In particular, in Fig. 3.49 spatial distribution of B(a)P equivalent concentrations of 4 PAHs (B(a)P, B(b)F, B(k)F, and IP) for 2018 is demonstrated. The map represents the sum of concentrations of individual PAHs multiplied by corresponding values of TEFs. Along with this, model estimates of B(a)P equivalent concentrations of 16 PAHs were obtained on the basis of experimental simulations (see section 4.1). The information on exceedances of the EU and WHO air quality guidelines for B(a)P as well as data on B(a)P equivalent air concentrations of PAHs can be used to support activities of the Task Force on Health and Working Group on Effects with regard to the analysis of population exposure to toxic substances and their impacts on human health.

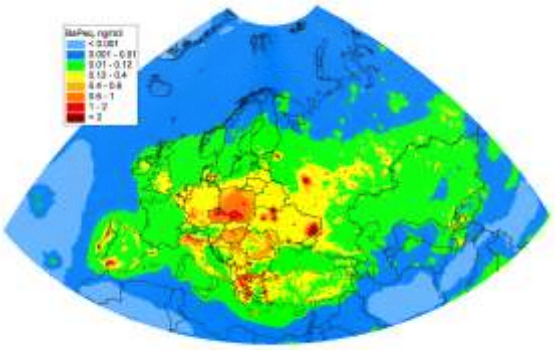

Fig. 3.49. *Spatial distribution of B(a)P equivalent concentrations of 4 PAHs (ng/m^3) in the EMEP domain based on the modelling results for 2018.*

3.4.3. Chemical composition of PM

Knowledge of the chemical composition of particulate matter allows improving determination of the possible effects on human health and the environment, and also helps in identifying the sources of PM [*Longhin*, 2012; *Rogula-Kozłowska et al*., 2016]. Adverse effects of PM include asthma, respiratory diseases, cardiovascular and cardiopulmonary diseases, heart attack, cancer of the trachea, bronchus, and lung, reproductive toxicity [*WHO*, 2013a]. According to WHO reports, hazard properties of particles may be caused by presence of heavy metals, PAHs and other organic substances [*WHO*, 2003, 2013a, 2013b]. At the same time, current air quality assessments for PM are based mainly on PM mass concentration without considering sources and chemical composition of particles.

Recently, PAHs contained in particles have been given special attention due to their adverse effects on health [*Kong et al*., 2010; *Murillo et al.,* 2016; *Zhao et al.,* 2020]. According to number of studies, most particle-bound PAHs (up to 90%) were in PM2.5. It should be noted, that the most significant PAHs emission source (>60%) is the residential combustion sector (Section 4.1), which also contributes up to 40% to PM2.5 emissions (Fig. 3.50). Thus, aerosol particles from solid fuels combustion may be enriched by the toxic PAH compounds. In some cases, despite of lack of exceedance of WHO guideline values for PM, content of PAHs in these PM is greater than established EU and WHO limits [*Siskos et al.,* 2006*; Szatyłowicz and Skoczko*, 2019].

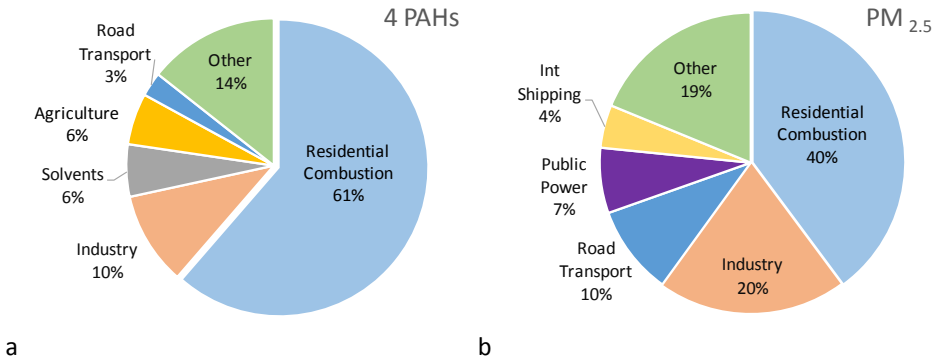

Fig. 3.50. *Sources of emission of 4 PAHs (a) and PM 2.5 (b).*

Besides, PAHs can be contained in condensable PM, which is generated from hot gaseous phase during contact with cooler ambient air. Herewith, among PAHs, compounds with 3 and 4 rings are assumed as the major part of condensable PM. In addition, a positive correlation is observed between the mass concentrations of PAHs contained in particles and concentrations of condensable PM [*Li et al*., 2017].

At the same time, particulate matter may contain Cd, Pb and other metals. In some cases, Cd associated with PM can exceed WHO guideline value (5 ng/m^3) and pose a serious health risk [*Karar et al.,* 2006; *Leili et al.,* 2008; *WHO*, 2000]. As for Pb incorporated in particles, some measurements also showed exceedance of limit values established by WHO (0.5 µg/m^3) [*Thomaidis*, 2003; *WHO*, 2000].

Thus, the impact of particulate matter (PM_{10} and $PM_{2.5}$) on human health may be more significant due to the presence of hazard constituents. Simultaneous measurements of PM and its components, such as heavy metals, PAHs and other organic pollutants (in particular, PCB and PCDD/Fs), may be useful for more precise risk assessment. The influence of chemical composition of PM on the hazard of the particles is the subject of future research.

3.5. Atmospheric loads to the marginal seas

Marine environment is protected on national and international level, in particular, by a number of regional conventions such as HELCOM, OSPAR, Barcelona Convention, Bucharest Convention, and Tehran Convention. Information on heavy metal and POP atmospheric input to marginal seas surrounding EMEP region in 2018 is prepared by MSC-E. These are the Baltic, North, Mediterranean, Black, and Caspian Seas. This section presents some examples of these results while more detailed information is available in Supplementary Data Reports [*Ilyin et al*, 2020]. Besides, information on modelled heavy metal and POP deposition to the Baltic Sea prepared for HELCOM is overviewed in Section 5.2.3.

Deposition fluxes of heavy metals and POPs to different marginal seas vary significantly depending on location of anthropogenic and secondary sources, and meteorological conditions. In case of Pb and Cd higher spatially averaged fluxes are noted for 'southern' seas, i.e., the Mediterranean, Caspian and Black, while lower fluxes are simulated for the Baltic and North Seas. For example, the highest deposition flux of Pb falls on the Mediterranean Sea, and the lowest – on the Baltic Sea (Fig. 3.51a, left). It is explained by predominant contribution of secondary sources in combination with significant impact of anthropogenic sources of heavy metals to deposition to the seas (Fig. 3.51a, right). Besides, in case of the Mediterranean Sea non-EMEP sources are also important.

Opposite situation is observed for Hg deposition. The highest Hg fluxes takes place in the North Sea, while the lowest – in the Caspian Sea (Fig. 3.51b, left). Main process driving the scavenging of mercury from the atmosphere in regions remote from anthropogenic sources is oxidation of elemental mercury with further wet removal or dry uptake of oxidized Hg. Since wet scavenging strongly depends on precipitation, higher deposition to the North Sea compared to the Caspian Sea is explained by distribution of atmospheric precipitation. The main contributor to Hg deposition is non-EMEP sources (Fig. 3.51b, right). However, it should be noted that in regional-scale calculations the contribution of Hg non-EMEP sources may be overestimated because these sources include Hg emitted by the EMEP sources which leaves the region and then returns as 'non-EMEP' Hg.

The highest deposition of POPs is noted for the Black and Baltic Sea, while the lowest – for the Caspian Sea (Fig. 3.51c, left). The exception is PCDD/Fs which deposition is the lowest to the North Sea. PCDD/Fs deposition to the Black Sea is about 3-fold higher than that to the North Sea. Relatively high deposition to the Black Sea is mainly caused by location of significant emissions in Turkey, Romania, and countries of eastern Europe. Contributions of anthropogenic (30-45%), secondary (about 40%) and non-EMEP sources (10-25%) for PCDD/Fs are comparable for the considered seas (Fig. 3.51c, right).

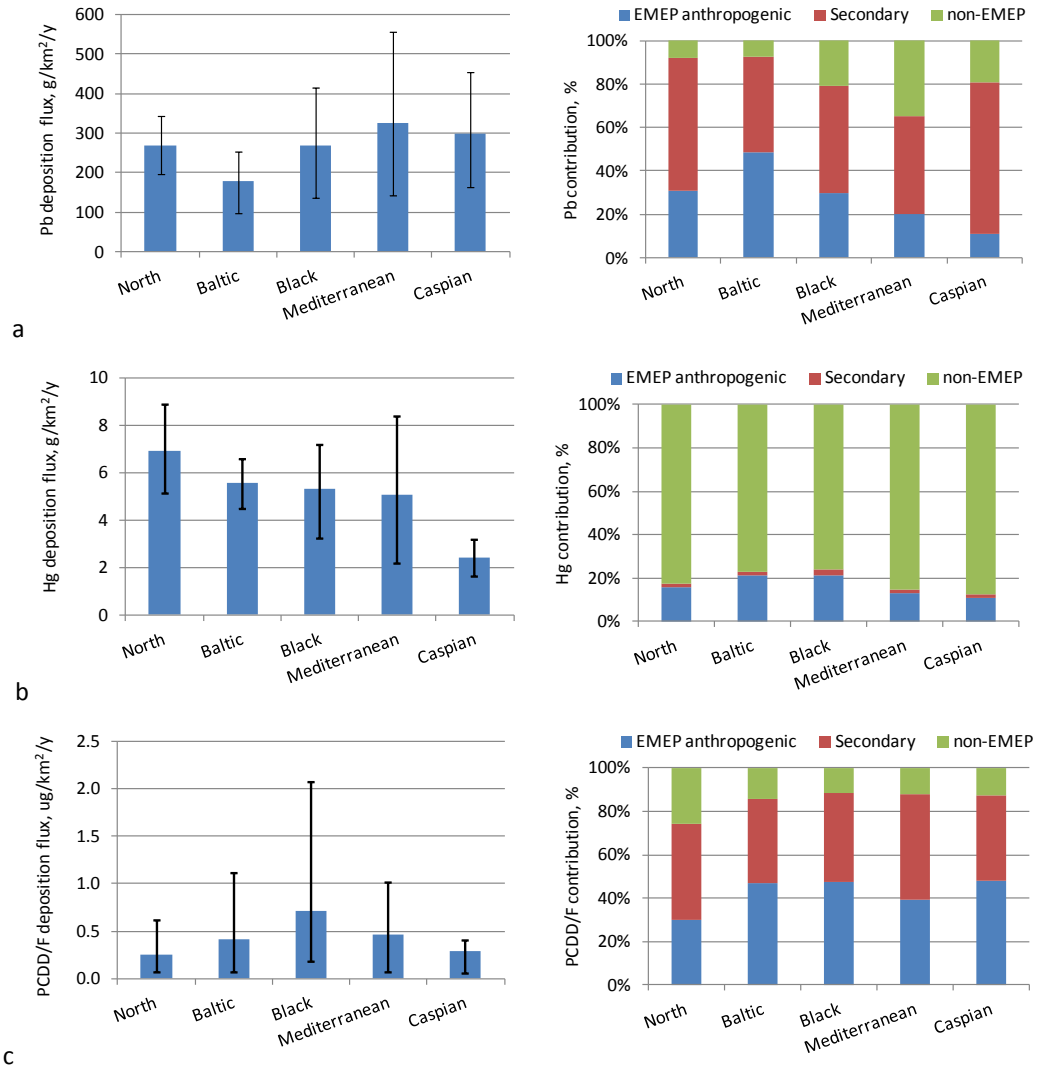

Fig. 3.51. *Mean deposition fluxes (left) and relative contribution of various source types to deposition (right) of Pb (a), Hg(b) and PCDD/Fs (c) to the marginal seas of the EMEP region in 2018. Whiskers show 10th and 90th percentiles of the deposition fluxes.*

Spatial distribution of deposition to the considered seas depends on various factors including emission distribution, meteorological conditions and properties of the pollutants. For example, deposition of B(a)P to the North Sea exhibits distinct gradient from more polluted coasts of western Europe, the United Kingdom and Scandinavia towards lower levels in the north and central parts of the sea (Fig. 3.52a). In this case the main factor is location of main emission sources on the land, while marine sources (e.g., shipping) are relatively low. Quite different character of spatial distribution of deposition takes place for Hg. Besides spatial distribution of emission sources, deposition of Hg is strongly affected by chemical transformations converting relatively inert elemental Hg to easily scavenged oxidized Hg forms. As a result, the highest deposition flux of Hg is obtained near the western coasts of Norway where high precipitation intensively washes out oxidized Hg. Spatial distribution maps for all pollutants (Pb, Cd, Hg, PAHs, PCDD/Fs, HCB and PCB-153) and other marginal seas are presented in Supplementary Data Report [*Gusev et al*., 2020].

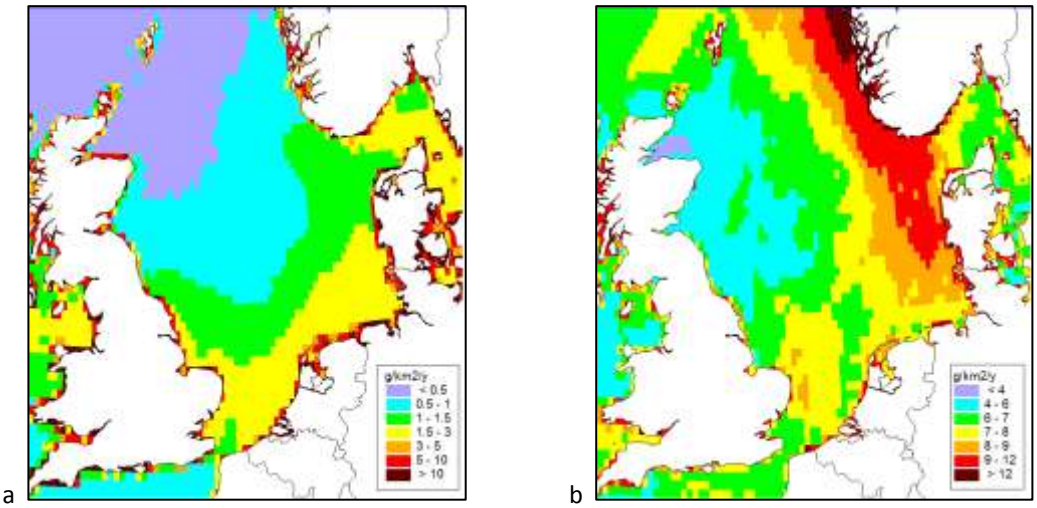

Fig. 3.52. *Total deposition of B(a)P (a) and Hg (b) over the North Sea in 2018.*

3.6. Pollution of the Arctic

Information of pollution of the Arctic by heavy metals (Pb, Cd, Hg) and POPs (PAHs, PCDD/Fs, HCB, PCBs) in 2018 is prepared by MSC-E. The information includes spatial distribution of total deposition of heavy metals and POPs and net flux for Hg, simulated for the Arctic area within the AMAP region on the base of global-scale modelling. Besides, contribution of different types of sources to the Arctic pollution and source-receptor relationships are estimated for the Arctic sector of the EMEP domain.

As a rule, deposition fluxes of heavy metals and POPs in the Arctic are lower by an order of magnitude compared to those in temperate latitudes. The reasons are remoteness of the Arctic from main emission sources of Europe, Asia or North America and relatively low precipitation amounts. For example, Pb deposition flux over most the EMEP domain exceeds 250 g/km^2/y while the flux in the Artic is 10-100 g/km^2/y (Fig. 3.53a). Similar contrast is seen for B(a)P deposition fluxes (Fig. 3.53b). The exception is hotspots of elevated B(a)P deposition fluxes in Kola Peninsula, eastern part of Russia and northern Canada, caused by significant emission sources. Smaller gradient of net deposition fluxes between Arctic and mid-latitudes is noted for Hg. It is explained by global character of Hg pollution.

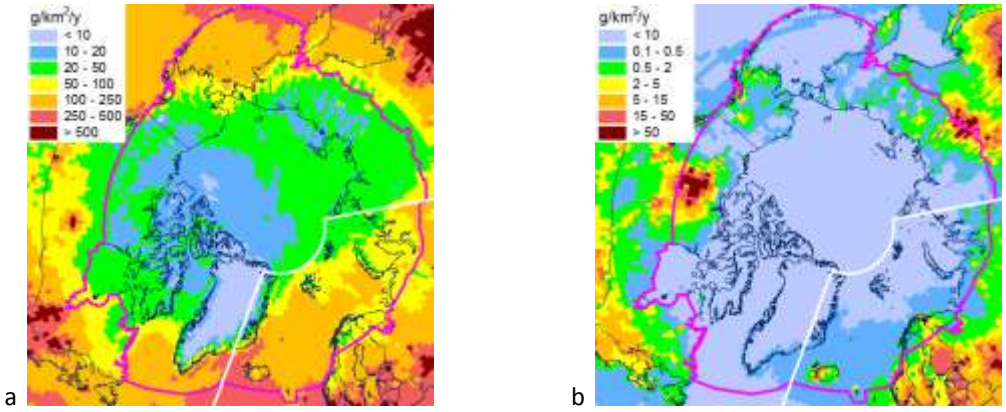

Fig. 3.53. *Total deposition fluxes of Pb (a) and B(a)P (b) to the Arctic in 2018. Purple line denotes the border of the Arctic region adopted by AMAP, and white line denotes a border of the EMEP domain.*

Three groups of sources responsible for deposition in the Arctic are singled out. These are anthropogenic emissions of the EMEP countries, secondary (historical)/natural sources and non-EMEP sources. Deposition of Pb to land areas of the Arctic within the EMEP domain is formed mostly by secondary sources, which contribution to total deposition is about 55% (Fig. 3.54). Contribution of anthropogenic sources to Pb deposition is about 2-fold lower (about 25%). The main reason of significant contribution of Pb secondary sources is re-suspension from sea surface, and low anthropogenic emissions in or close to the Arctic region. Significant contribution of secondary sources is also noted for PCDD/Fs (about 40%) and HCB (about 65%) which is explained by re-emission of historically accumulated pollutants in soils. For Cd the contribution to the Arctic deposition is made by anthropogenic sources (55%).

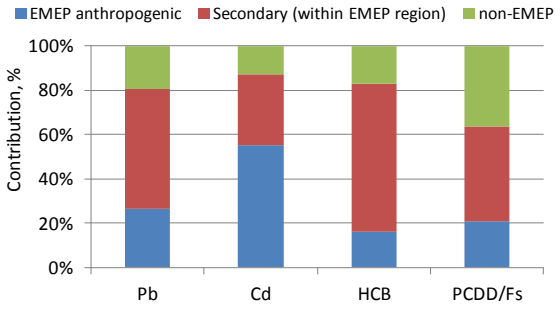

Fig. 3.54. *Relative contributions of the EMEP anthropogenic, secondary and non-EMEP sources to deposition in the Arctic (within EMEP domain) in 2018.*

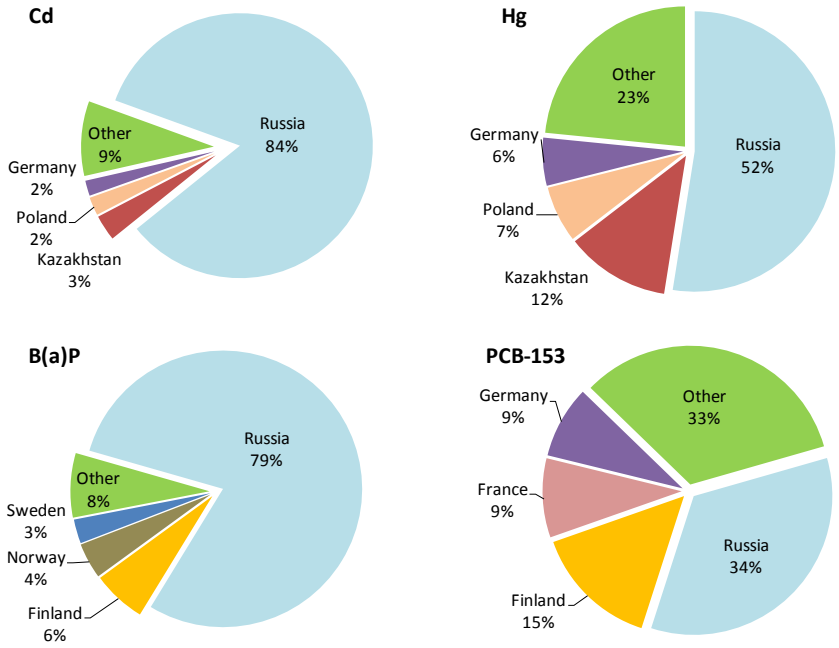

Fig. 3.55. *Source apportionment of heavy metal and POP anthropogenic deposition to the Arctic (within the EMEP domain) in 2018.*

Contribution of emission sources of different EMEP countries to deposition to land areas of the Arctic within the EMEP domain depends on a number of factors such as magnitude and remoteness of the sources from the Arctic, meteorological conditions, properties of the considered pollutants etc. For all POPs and heavy metals, the main contributor to atmospheric pollution in the Arctic is Russia (Fig. 3.55). It is not surprising because large part of the Russian territory is situated within the Arctic region. Sources of Kazakhstan take the second position in pollution of the Arctic by heavy metals. Atmospheric emissions of Pb, Cd and Hg in Kazakhstan are among the highest in the EMEP countries.

Therefore, in spite of long distance from the Arctic, the contribution of Kazakhstan sources is substantial. Similar reason could help to explain marked contribution of sources of France and Germany to deposition of PCB-153 in the Arctic. In case of B(a)P noticeable contribution is made by sources of Sweden, Norway and Finland which are located close or partly within the Arctic region. Finland is also an important contributor to atmospheric deposition of PCB-153 in the Arctic region.

3.7. Global scale pollution by heavy metals and POPs

Contamination of the EMEP countries by heavy metals and POPs is affected by long-range transport of the pollutants from emission sources located in other regions or continents. It is particular relevant for Hg and some POPs (HCB, PCDD/Fs), which are characterized by long residence time in the atmosphere. Therefore, model assessment of pollution levels in the EMEP domain is supported by global scale simulations using the GLEMOS multi-scale modelling system. Calculated concentrations are used as boundary conditions for the regional pollution modelling. In addition, global scale simulations of Hg and POP pollution levels are used for assessment of contamination of the Arctic and other regions of the globe in co-operation with other international conventions and programmes (e.g. AMAP, Stockholm Convention, Minamata Convention; see Section 5.2 for more details).

Modelled global distributions of Pb, Cd and Hg concentration in air are shown in Fig. 3.56. The highest air concentrations of Pb and Cd are estimated for Southeast Asia (above 30 ng/m^3 for Pb and 1 ng/m^3 for Cd), mainly because of large emissions in China (Figs. 3.56a and b). Elevated concentrations are also simulated in arid areas of the south-western part of Asia, Middle East and Northern Africa due to significant wind re-suspension of heavy metals in these regions. The lowest concentrations of Pb and Cd occur over the Arctic and Antarctica regions.

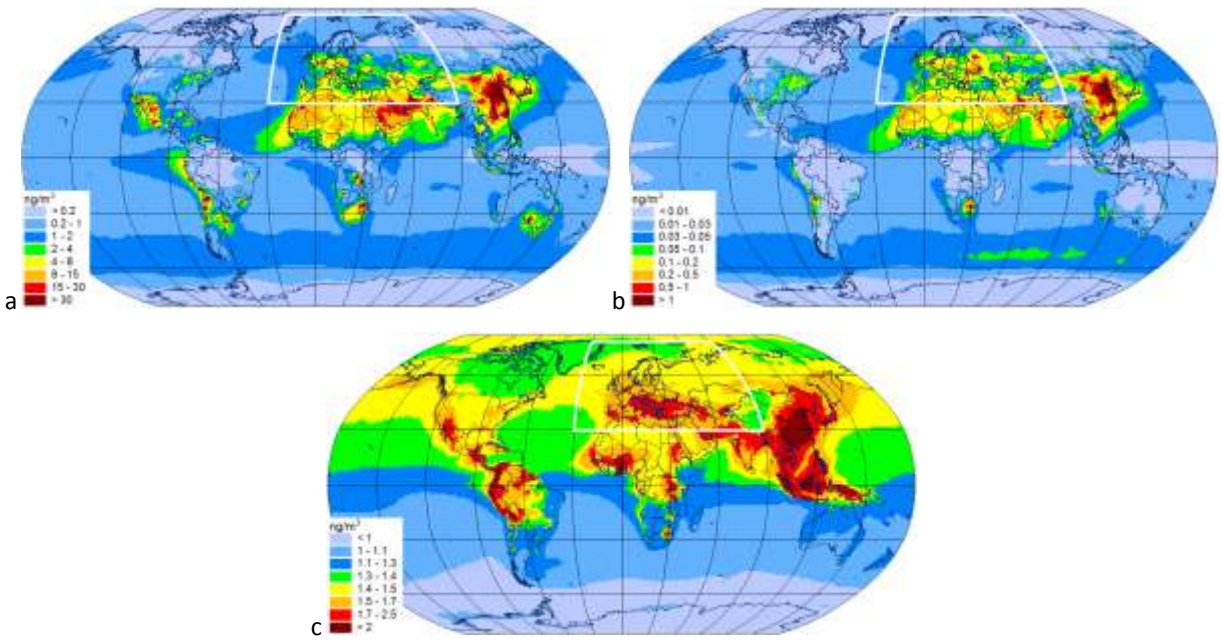

Fig. 3.56. *Global distributions of annual mean air concentration of Pb (a), Cd (b) and Hg^0 (c) in 2018. White line depicts boundary of the EMEP region.*

Air concentration of Hg^0 is more evenly distributed over the globe with lower concentrations (0.8-1.3 ng/m^3) in the Southern Hemisphere and higher concentrations (1.3-2.5 ng/m^3) in the Northern Hemisphere (Fig. 3.56c). East and Southeast Asia are characterized by the highest Hg concentrations (above 2 ng/m^3) due to large anthropogenic emissions. High concentration levels are also obtained for equatorial Africa, South America and Southeast Asia as a result of emissions from artisanal and small-scale gold mining in these regions. In addition, elevated Hg concentrations are found over Southern Europe and the western coast of North and South Americas because of natural emissions from Hg-enriched soils. The lowest concentrations are simulated over the Southern Ocean and Antarctica.

Figure 3.57 presents simulated global distributions of B(a)P, PCDD/Fs, PCB-153 and HCB air concentrations in 2018. The highest concentrations of B(a)P are estimated in East and South Asia, where B(a)P levels can exceed 2 ng/m^3 (Fig. 3.57a). High concentrations (above EU target level for B(a)P equal to 1 ng/m^3) are also predicted for some countries of Central, Eastern, and Sothern Europe. Other regions, namely, Central Africa, North and South America, and Australia are characterized by lower concentrations (0.1-0.4 ng/m^3 and below).

The highest levels of PCDD/Fs are estimated in some areas of South and Southeast Asia, and Central Africa (above 50 fg TEQ/m^3) (Fig. 3.57b). Concentrations of PCDD/Fs in Europe, North and South Americas, and Australia are considerably lower (5-25 fg TEQ/m^3). Elevated air concentrations of PCB-153 are characteristics of Europe, North America and South Asia (0.2-6 pg/m^3) (Fig. 3.57c). Levels of PCB-153 are mostly within 0.01-0.2 pg/m^3 in other regions of the Northern Hemisphere and below 0.005 pg/m^3 in the Southern Hemisphere. Spatial distribution of HCB levels in air is more homogeneous. Its concentrations largely vary within 15-70 pg/m^3 in the Northern Hemisphere and within 5-8 pg/m^3 in the Southern Hemisphere. The most significant levels (above 50 pg/m^3) are in Europe and East Asia.

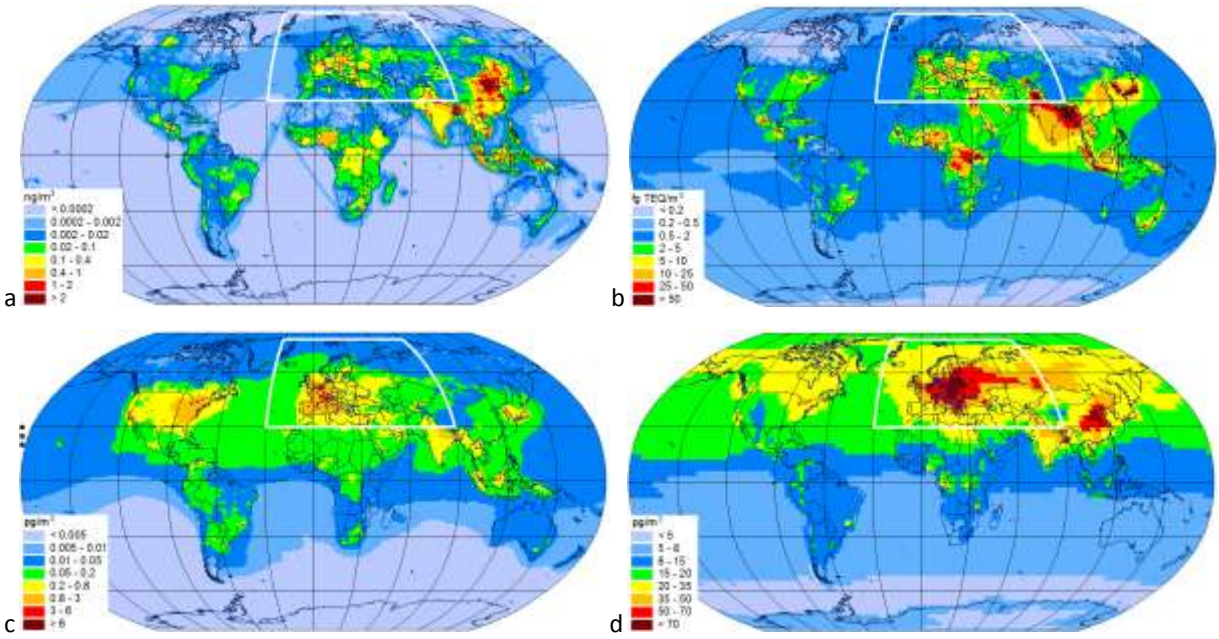

Fig. 3.57. *Global distribution of annual mean air concentration of B(a)P (a), PCDD/Fs (b), PCB-153(c), and HCB (d) in 2018. White line depicts boundary of the EMEP region.*

The global scale model simulations also allow estimating import of airborne pollution to the EMEP region and export of the pollution from the region. Figure 3.58 presents results of the assessment of import/export of Hg anthropogenic deposition to/from other regions of the globe. As seen EMEP regional sources contribute about 45% of total Hg anthropogenic deposition to the region. The major external contributors include East Asia (28%) and Africa (10%) (Fig. 3.58a). About three fourth of total Hg anthropogenic emissions of the EMEP region deposit outside the region's territory. The largest receptor of Hg deposition from the EMEP sources is the global ocean (40%) that is followed by Africa (6%), the Arctic (5%), North America (5%), and East Asia (3%).

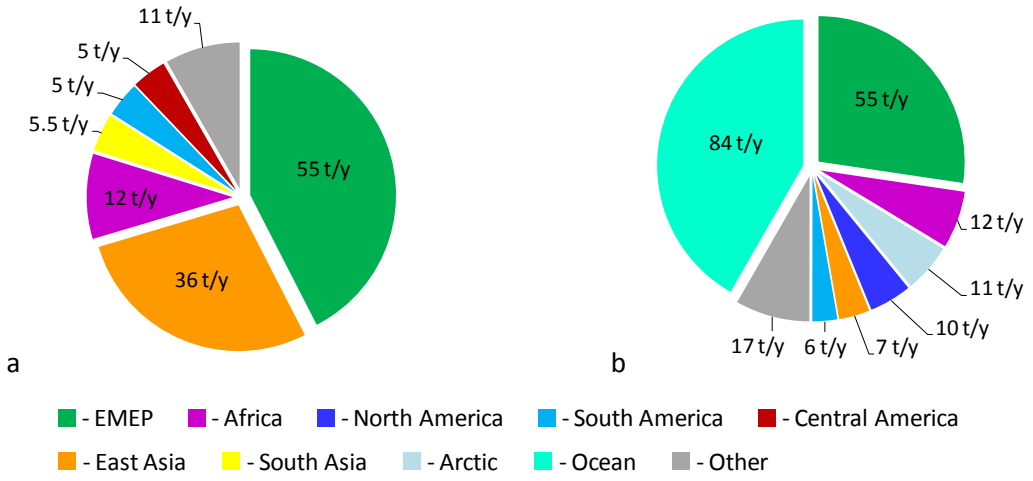

Fig. 3.58. *Mercury deposition from anthropogenic sources to the EMEP region from other regions (a) and from the EMEP region to other regions (b) in 2015.*

It should be noted that the global scale modelling of heavy metal and POP pollution requires reliable and up-to-date global emission inventories. However, no data on contemporary emissions is available for Pb, Cd, HCB and PCDD/Fs. ***Thus, improvement of the global scale assessment requires additional efforts for development of global emissions inventories for heavy metals and POPs in co-operation with other international bodies (UN Environment, Stockholm Convention, Minamata Convention).***

Chapter 4. RESEARCH ACTIVITIES

On-going research activities of MSC-E are aimed at improvement of the pollution assessment quality and further development of the modelling tools and carried out in accordance with the priorities of the long-term strategy for the Convention and the bi-annual work-plan of EMEP [ECE_EB.AIR_144_Add.2]. The main directions of the research included evaluation of PAH pollution and population exposure in the EMEP countries, downscaling of heavy metal pollution assessment for Germany, further study of Hg oxidation and reduction in the atmosphere, update of model parameterizations of gas-particle partitioning, degradation and air-surface exchange of POPs.

4.1. PAH pollution and population exposure

Polycyclic aromatic hydrocarbons (PAHs) comprise a large group of semi-volatile, hydrophobic organic compounds ubiquitous in the environment. Many of PAHs are known or suspected to have carcinogenic, mutagenic, and teratogenic properties that pose risk to human health and ecosystems. High levels and lack of decrease of PAH air concentrations in the EMEP countries during two recent decades have been indicated as an important issue in the Long-term Strategy of the Convention [ECE/EB.AIR/2018/1/Rev.1]. Specific attention in this respect is paid to the emissions from residential combustion and biomass burning as prevailing source categories of PAHs. The Strategy highlights importance of continued scientific research that can support additional efforts for the reduction of unintentional releases of PAHs in the EMEP region and especially for countries of Eastern Europe, the Caucasus and Central Asia.

To support these activities, MSC-E carries out collection and analysis of information on PAH physical-chemical properties, reported national inventories and expert estimates of emissions, and approaches to assess population exposure to PAH pollution. In addition, update of model parameterizations for most important processes governing their fate in the atmosphere, namely, gas-particle partitioning and degradation, is performed (see the section 4.4 of this report). Besides, trends in observed and modelled PAH concentrations in air are analyzed and exceedances of air quality guidelines are estimated. This study is considered as a contribution to the activities related to the analysis of POP Protocol effectiveness with regard to PAH pollution. An overview of progress in this work is presented in this section. More detailed information is presented in the Technical report [*Gusev et al*., 2020b].

Regulatory activities to control PAH emissions and pollution levels

Taking into account long-range atmospheric transport, accumulation in the environment, and adverse effects on human health, PAHs are considered as priority pollutants in the regulatory activities of many international (WHO, HELCOM, AMAP, OSPAR, etc.) and national (EU, USA, Canada, China, etc.) organizations.

Particular attention is paid to the compilation of inventories of PAH emissions, monitoring of air pollution levels, content in various products, and exceedances of guideline values as well as the assessment of population exposure and harmful effects.

In most of the cases, B(a)P is used as a marker for the assessment of PAH pollution levels and adverse effects. However, it should be noted that air quality standards for B(a)P concentrations are still not globally defined, and different limit values are established by various organizations and countries to perform assessment of exceedances. For illustration some of the air quality guideline values for B(a)P are presented in Table 4.1. Besides, different methodologies and different number of PAHs are used for the evaluation of population exposure to mixture of toxic PAHs. For instance, 4 PAHs are included in LRTAP POP Protocol, 8 PAHs in the EU REACH Regulation, and US EPA Priority list contains 16 PAHs.

Table 4.1. *Air quality guideline values for B(a)P, established by international and national regulations*

Organization or country	B(a)P guideline values, ng/m^3	Remark	Reference
World Health Organization	0.12	Corresponds to lifetime cancer risk of approximately $1 \cdot 10^{-5}$	WHO, 2017
EU	1.0	Target value	Directive 2004/107/EC
UK	0.25	Air quality objective (as annual average)	Department for Environment, Food and Rural Affairs (DEFRA), 2007
Canada, Alberta	0.30	Annual average concentration	Government of Alberta, 2019
Canada, Ontario	0.01 (annual) 0.05 (24-hour)		Government of Ontario, 2019
China	1.0 (annual) 2.5 (24-hour)	Ambient air quality standard	Ministry of Environmental Protection (MEP), China, 2012
New Zealand	0.3	Environmental standard	Ministry for the Environment (MFE), New Zealand, 2003
Russia	1.0	Maximum allowable concentrations in urban and rural areas	Ministry of Health of the Russian Federation, 2017

Selection of particular PAHs for the assessment is based on the evidence of their carcinogenic and mutagenic properties. The International Agency for Research on Cancer (IARC) has classified B(a)P as carcinogenic to humans (Group 1). Along with B(a)P, other toxic PAHs are also included in the IARC [*IARC*, 2010] and EU CLP classifications (Table 4.2). It should be noted, that according to EU CLP regulation, in some cases relevant categories are more stringent.

***Table 4.2**. IARC and ECHA classifications of 16 PAHs with regard to their carcinogenicity and genotoxicity.*

Substance	Carcinogenicity		Genotoxicity
	IARC (Groups[10])	ECHA (Categories[11])	
Benzo(a)pyrene (B(a)P)	1	1B	Genotoxic
Benzo(a)anthracene (B(a)A)	2A	1B	Genotoxic
Dibenzo(a,h)anthracene (D(a,h)A)	2A	1B	Genotoxic
Benzo(b)fluoranthene (B(b)F)	2B	1B	Genotoxic
Benzo(k)fluoranthene (B(k)F)	2B	1B	Genotoxic
Chrysene (CHRY)	2B	1B	Genotoxic
Indeno(1,2,3-cd)pyrene (IND)	2B	2	Genotoxic
Acenaphthylene (ACY)	3	1A or 1B (predicted)[12]	No enough data available
Fluoranthene (FLTH)	3	1A or 1B (predicted)	Limited evidence of genotoxicity
Pyrene (PYR)	3	No data available	Not genotoxic
Naphthalene (NAP)	3	2	Probably not genotoxic
9H-Fluorene (FLU)	3	No data available	No enough data available
Acenaphthene (ACE)	3	No data available	No enough data available
Benzo(ghi)perylene (B(ghi)P)	3	1A or 1B (predicted)	Genotoxic
Anthracene (ANTH)	3	1B or 2[13]	Not genotoxic
Phenanthrene (PHE)	3	1A or 1B (predicted)	Limited evidence of genotoxicity

IARC reported that epidemiological studies of carcinogenicity of individual PAHs are complicated by the fact that these compounds are never found in isolation in the environment but are components of complex mixtures [*IARC*, 2019]. Besides, the most of PAHs have evidence of mutagenicity and genotoxicity determined in vivo or in vitro [*SCF*, 2002]. Along with carcinogenic and mutagenic effects, the other toxicological properties also should be taken into account for B(a)P and other

[10] IARC classification groups: Group 1 - carcinogenic to humans, Group 2A - Probably carcinogenic to humans, Group 2B - Possibly carcinogenic to humans, Group 3 - Not classifiable as to its carcinogenicity to humans (Group 3 is used for substances and mixtures for which the evidence of carcinogenicity is inadequate in humans and inadequate or limited in experimental animals)

[11] ECHA Hazard categories for carcinogens:

Category 1 - May cause cancer (Category 1A - known to have carcinogenic potential for humans, classification is largely based on human evidence; Category 1B - presumed to have carcinogenic potential for humans, classification is largely based on animal evidence);

Category 2 - Suspected of causing cancer (classification on the basis of evidence obtained from human and / or animal studies, but which is not sufficiently convincing to place the substance in Category 1A or 1B)

[12] Substances predicted as likely to meet criteria for category 1A or 1B carcinogenicity, mutagenicity, or reproductive toxicity [https://echa.europa.eu/information-on-chemicals].

[13] In accordance with CLP Notification [https://www.echa.europa.eu/web/guest/information-on-chemicals/cl-inventory-database/-/discli/details/101102]

PAHs. These effects include reproductive toxicity, liver and kidney toxicity, hematological effects, pulmonary and respiratory effects, neurotoxicity, and skin irritation in case of direct contact [*Danish EPA*, 2013]. In accordance to EU CLP regulation, PAHs are classified as very toxic for aquatic environment (Category 1). Furthermore, chemical transformations of PAHs in the atmosphere can lead to the formation of other groups of toxic pollutants, such as nitrated and oxygenated PAHs, which may induce more significant toxic effects than their parental PAHs [*Keyte et al.*, 2013].

Sources of PAH emissions

PAHs are mostly released to the environment as unintentional by-products of incomplete combustion of biomass and fossil fuels [*Keyte et al.*, 2013]. Main categories of anthropogenic PAH emissions include domestic burning of wood and coal, industrial activities, road transport, and agricultural sources as well as forest fires and volcanic activities [*Balmer et al*., 2019; *Manzetti,* 2013]. Regular inventories of anthropogenic PAH emissions provide important information for monitoring of dynamics of their unintentional releases in the EMEP region.

Information on sector-specific atmospheric emissions of selected PAHs in the EMEP region indicates elevated levels of PAH emission fluxes in the in the countries of Central and Southern Europe. Time-series of total emissions of 4 PAHs in the EMEP region demonstrate almost the same emission level during the two recent decades. As an example, temporal changes of sector-specific B(a)P emissions during the period 2000-2018 are shown in Fig. 4.1a.

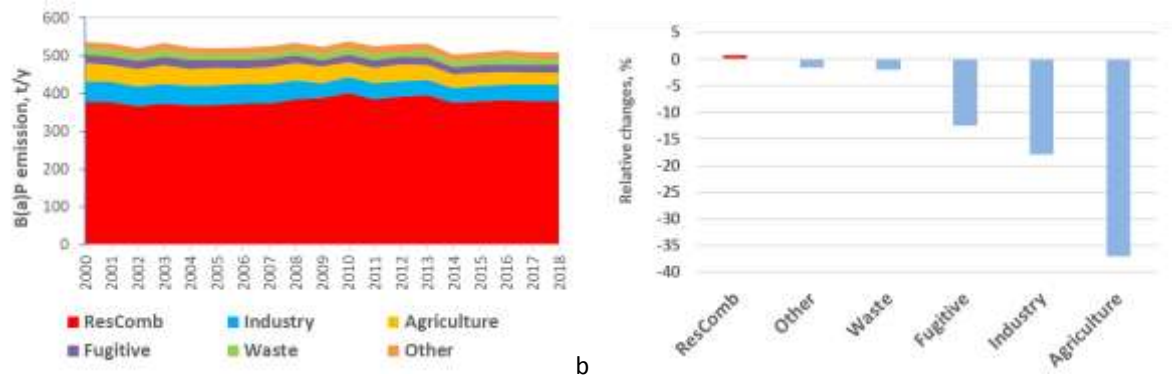

a b

Fig. 4.1. *Long-term changes of sector-specific B(a)P emissions in the EMEP countries (a) and relative changes from 2000 to 2018 (b).*

According to the reported national inventories, the largest contribution (> 60%) to total PAH emissions is made up by the Residential combustion sector (Fig. 4.1a). In the majority of countries dominating source of PAH emissions from this sector is wood combustion for domestic heating. At the same time, some of the EMEP countries are characterized by substantial contribution of coal combustion to the emissions from this sector (e.g. Poland, Ireland). Besides, significant emissions of PAHs are also reported for industrial (~10%) and agricultural (~10-15%) activities.

Along with this, a number of research-driven emission inventories are available for the evaluation of temporal and spatial trends of PAH content in the environment as well as of adverse effects. Global

scale inventory of 16 PAHs releases to the atmosphere [*Shen et al*., 2013] indicates the highest level of emissions for the countries of Eastern and Southern Asia (Fig. 4.2). The distribution of global scale PAH emissions by sectors indicates the largest contribution to total emissions of Residential and Commercial combustion (65%) similar to the EMEP emission inventories. At the same time, substantial contributions are also made by Road Transport (13%) and Deforestation and Wildfires (11%).

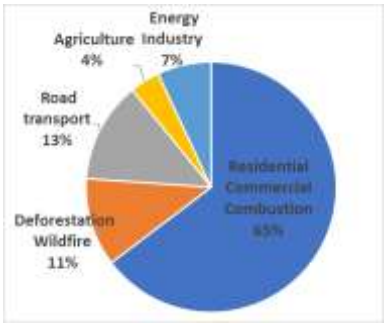

Fig. 4.2. *Contribution of major source categories to the total global emissions of 16 PAHs according to the inventory [Shen et al.,* 2013*]*

Temporal variations of PAH pollution levels

PAH long-range transport and partitioning between environmental compartments depends on their physical-chemical properties that are the basic characteristics for model parameterizations of processes, governing their fate in the environment [*Ma et al.,* 2010]. Physical-chemical properties of PAHs depend on the amount of fused aromatic rings in their chemical structure. Low molecular weight PAHs (with 2-3 rings) can present in the atmosphere predominantly in the gaseous phase, while high molecular weight PAHs (with 5-6 rings) predominantly in the particulate phase. Intermediate PAHs (with 4 rings) can present in both phases partitioning between them depending on the environmental conditions. To evaluate PAH pollution levels and their temporal variations within the EMEP region, information on physical-chemical properties of 16 PAHs was updated on the basis on available data in literature [*Gusev and Batrakova,* 2020].

Results of model assessment of temporal variations of PAH pollution levels in the EMEP countries in the period from 2000 to 2018 are shown in Fig. 4.3a on the example of B(a)P. It is shown that the period was generally characterized by small changes of annual mean concentrations in the EMEP countries.

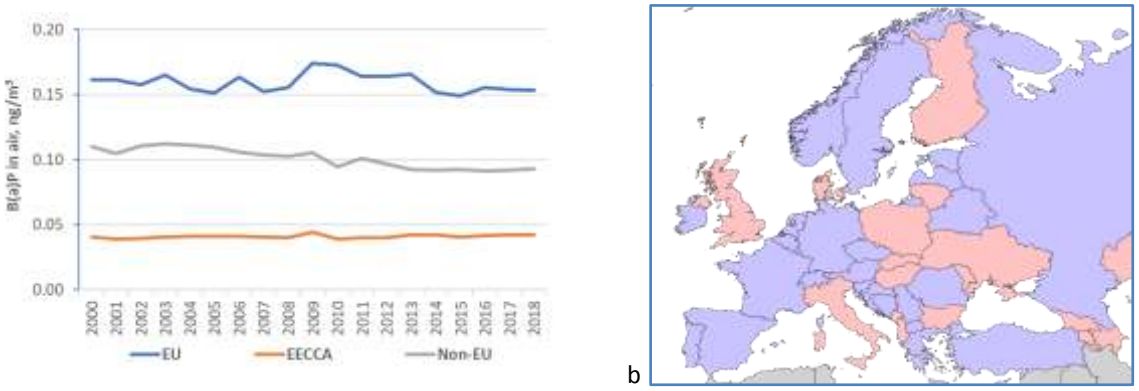

a b

Fig. 4.3. *Relative changes of average B(a)P annual mean modelled air concentrations from 2000 to 2018 in the EU, EECCA, and non-EU EMEP countries (a). Spatial distribution of changes of averaged B(a)P air concentrations in the EMEP countries for the period 2000-2018. Blue color indicates decrease and red color indicates increase of B(a)P air concentrations (b).*

In particular, according to the model predictions average levels of B(a)P concentrations in the EU and non-EU countries decreased from 2000 to 2018 by 5% and 15%, respectively, while for the EECCA countries an increase of concentrations by 3% was estimated (Fig. 4.3a). Model estimates of temporal variations of B(a)P air concentrations in the particular EMEP countries show different changes (Fig. 4.3b). For about 55% of the EMEP countries a decline of concentrations was predicted. For other EMEP countries (about 45%) increase of B(a)P concentrations was estimated for this period. In particular, increasing concentrations can be noted for some of the countries in Central and Southern Europe (e.g. Poland, Slovakia, Italy) as well as in the other parts of EMEP region (e.g. Finland, the United Kingdom).

The model estimates of temporal variations of B(a)P pollution in general correspond to long-term measurements of the EMEP monitoring sites. Comparison of annual mean and modelled B(a)P concentrations, predicted by the GLEMOS model, is illustrated on the example of selected monitoring sites in the Fig. 4.4. According to measurements and the model estimates, B(a)P pollution levels in Sweden and Spain slowly decreased in the period 2000-2018. At the same time pollution levels at background monitoring site CZ0003R in the Czech Republic was almost on the same level during this period.

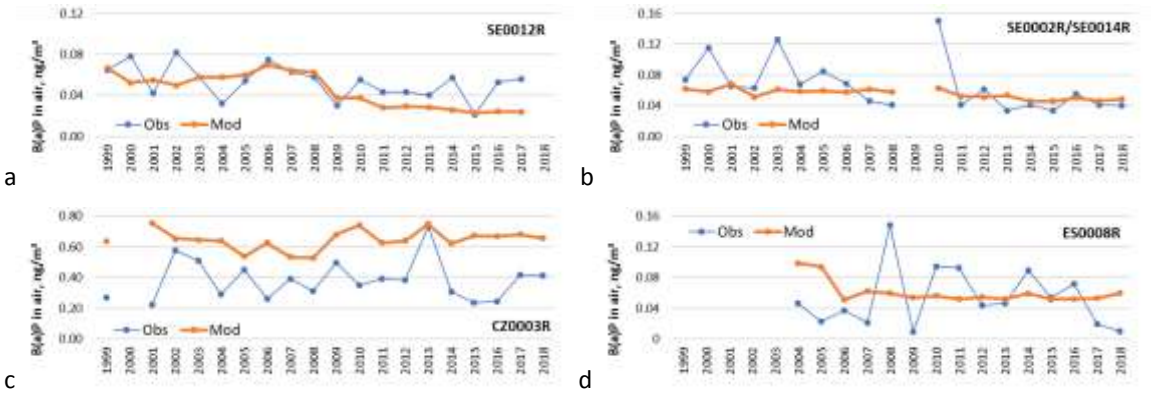

Fig. 4.4. *Comparison of annual mean modelled and observed B(a)P concentrations for the EMEP monitoring sites in Sweden (a,b), the Czech Republic (c), and Spain (d).*

At further stages of this work specific attention will be given to the analysis of statistical significance of temporal trends. Besides, model estimates of source-receptor relationships will also be taken into account in the analysis of temporal changes. In particular, contributions national and foreign emissions as well as emission sectors to PAH pollution levels will be evaluated.

Evaluation of population exposure to toxic PAHs

The information on exceedances of the EU and WHO air quality guidelines for B(a)P as well as data on B(a)P equivalent air concentrations of toxic PAHs are of importance for the analysis of population exposure to toxic substances and adverse health effects.

Annual mean B(a)P air concentrations continue to exceed EU and WHO air quality guidelines in some of the areas of the EMEP region (see section 3.4 of this report). The model simulation for 2018 shows

high levels of B(a)P concentrations for the countries of Central and Eastern Europe as well as in some areas of Spain and Turkey. Similar spatial pattern of B(a)P air concentrations was observed at the AIRBASE monitoring stations in 2018. In particular, high average annual B(a)P concentrations, above the EU target value, were observed in 2018 in 6 EU countries, namely, Poland, Slovakia, Croatia, the Czech Republic, Bulgaria, and Hungary. Most of exceedances of the EU target value were observed at the urban background stations.

Exceedances of WHO reference level in 2018 took place in most of the countries performing regular monitoring of B(a)P pollution levels. In particular, annual mean observed B(a)P concentrations were higher than 0.12 ng/m^3 in 27 European countries. Thus, further measures are required to reduce elevated levels of B(a)P concentrations and their adverse effects on population.

To evaluate population exposure to mixture of toxic PAH compounds, experimental modelling of 16 EPA PAHs was performed. Emission data for model simulations were based on the global gridded emission inventory of PKU [*Shen et al.*, 2013]. Exposure to mixture of toxic PAHs was estimated using the WHO toxicity equivalency factors defined for individual PAH compounds (TEFs) [*ALS*, 2013]. TEFs permit to characterize the carcinogenic potency of each considered PAH and calculate B(a)P equivalent concentration of mixture of 16 PAHs as the sum of the products of individual PAH compounds concentrations and their toxic equivalency factors. The spatial distribution of B(a)P equivalent concentrations of 16 PAHs is presented in Fig. 4.5a, showing the areas of high B(a)P equivalent concentrations, exceeding EU and WHO air quality guidelines in the countries of Central and Eastern Europe.

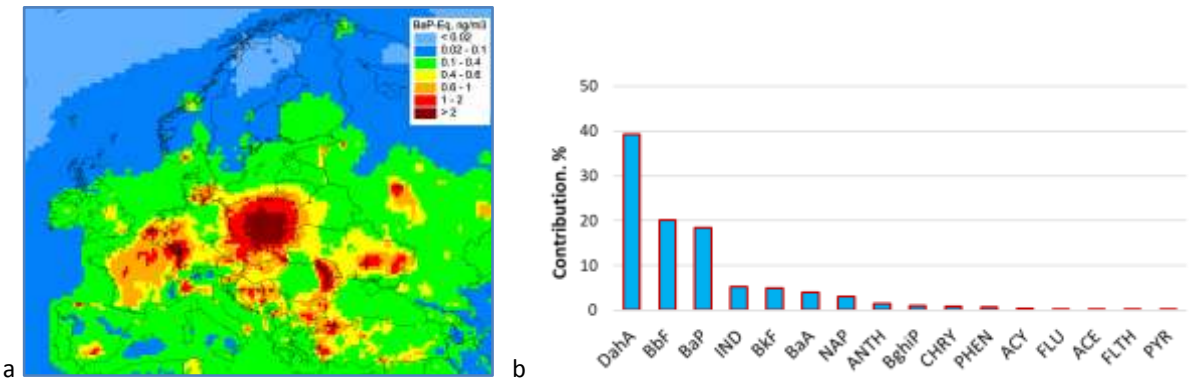

***Fig. 4.5**. Annual mean modelled B(a)P-equivalent air concentrations of 16 PAHs (a) estimated for 2018 and contributions of individual PAHs to the sum of B(a)P equivalent annual mean air concentrations of 16 PAHs.*

The modelling results make it possible to estimate the contributions of individual 16 compounds to the sum of B(a)P equivalent concentrations (Fig. 4.5b). The contribution of particular compounds depends both on the toxic equivalent factor and the magnitude of emissions. It can be seen that the largest contribution to total B(a)P equivalent concentration is made by dibenz(a,h)anthracene (DahA), followed by B(b)F and B(a)P. It can be noted that in spite of relatively high level of toxicity and significant concentrations dibenz(a,h)anthracene is not currently included in the list of PAHs considered in the POP Protocol. Thus, inclusion of additional PAH compounds into the assessment may help to characterize population exposure to toxic PAHs more accurately.

The information on exceedances of the EU and WHO air quality guidelines for B(a)P as well as data on B(a)P equivalent air concentrations of PAHs are expected to support activities of the Task Force on Health and Working Group on Effects with regard to the analysis of population exposure to toxic substances and their impacts on human health and ecosystems.

4.2. Downscaling of heavy metal pollution assessment for Germany

A case study of heavy metal pollution in Germany is performed jointly by EMEP/MSC-E and the German Environment Agency (UBA). The main objective of the study is generation of detailed information on levels and spatial distribution of air concentration and atmospheric deposition of three heavy metals – Pb, Cd, and Hg – over the country's territory for the period from 2014 to 2016. Results of the study will be used by UBA for integrative evaluation of available information about heavy metal pollution of various ecosystems (e.g. for comparison with metal concentrations in mosses) and for subsequent risk assessment. The work is funded jointly by EMEP and the country (UBA, Germany).

Variety of detailed national scale data have been prepared and provided by German national experts (UBA) for the aims of the study. Information on anthropogenic emissions of Pb, Cd and Hg in 2014, 2015 and 2016 is prepared with spatial resolution 0.1°x0.1° and vertical height level information of the model. Information on measurements from six EMEP stations located in Germany is involved in the study. Besides, measurements of air concentration and wet deposition of Pb and Cd are available from about 120 measurement stations from national monitoring networks. Information on Hg wet deposition fluxes is reported by 65 national stations. In addition to this, national data on land-cover, soil texture and concentrations of heavy metals in soils have been collected.

The model simulations of heavy metal atmospheric transport and deposition over the territory of Germany were performed with the GLEMOS model. A number of the model updates have been performed to adapt the national data and fit the model to the needs of the study. These updates are related to meteorological information, wind re-suspension of Pb and Cd and natural emissions of Hg. In order to take into account influence of national, regional and global sources on heavy metal pollution levels in Germany a multi-scale modelling approach was used.

The fine resolution modelling on national scale provides detailed patterns of heavy metal pollution in the country. The highest concentrations and deposition levels of all three metals are predicted for the western provinces because of large impact of anthropogenic emissions (Fig. 4.6). Beside the western part of the country, elevated deposition levels are also characteristics of the eastern and southern provinces. Deposition patterns of all metals are more mosaic than distribution of concentrations due to spatial variability of atmospheric precipitation and characteristics of the underlying surface. Among various ecosystems, forests and other areas covered with high vegetation are the largest receptors of heavy metal pollution.

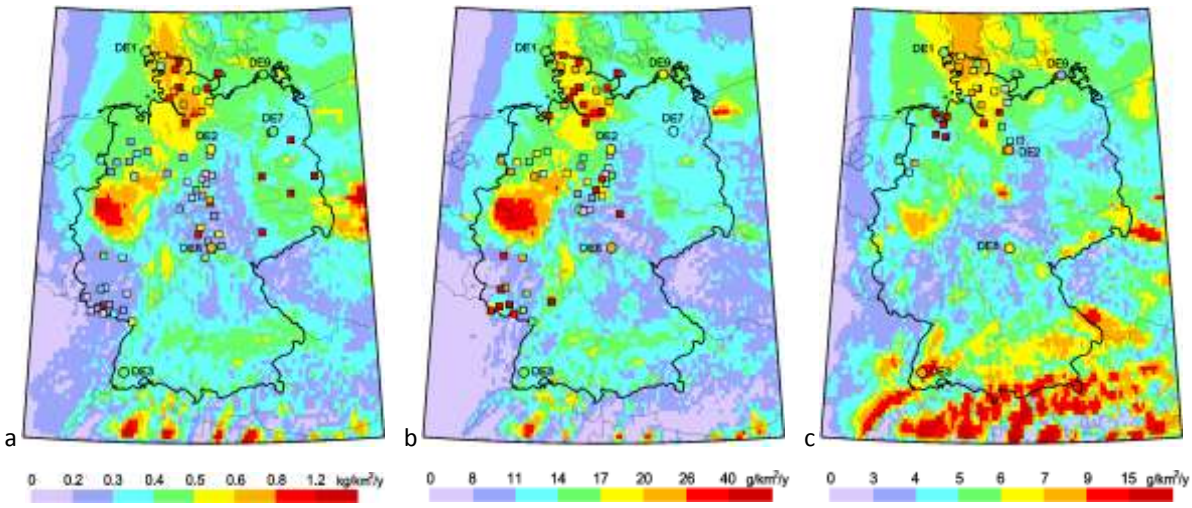

Fig. 4.6. *Spatial distribution of Pb (a), Cd (b) and Hg (c) wet deposition in 2015. Circles show the EMEP observations and squares present German national measurements in the same colour palette.*

Results of the model simulations are evaluated against measurements of heavy metals concentration in air and wet deposition at both EMEP and other national monitoring stations. Measurements from the EMEP stations are used as a base for the evaluation of the model performance. Modelled concentrations and deposition well agree with the values observed at the national EMEP stations. In particular, mean relative bias for air concentrations and wet deposition of Pb, Cd and wet deposition of Hg varies from -20% to 40%. For Hg^0 air concentrations the bias falls within ±5%. Besides, seasonal variability of the pollution levels was reproduced by the model: most peaks and minimums of monthly mean values were captured by the model (Fig. 4.7).

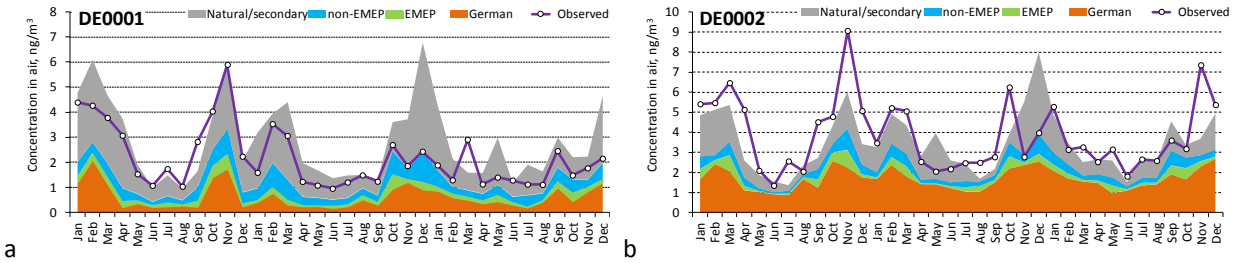

Fig. 4.7. *Comparison of simulated and observed monthly Pb concentrations in air at German EMEP stations DE0001 (Westerland, a) and DE0002 (Waldhof, b) over the period 2014-2016.*

Measurement data from national monitoring networks significantly expand the scope of the analysis. However, observations from some monitoring stations may not reflect background pollution levels (e.g. due to effect of local sources) that complicates their use for evaluation of the modelling results. Therefore, more detailed information on the methodology and sensitivity of measurements as well as on the physical conditions (such as geographical height, exposition, land cover) and pollution level/local sources in the surrounding of the monitoring stations would be needed to improve their applicability for evaluation of modelling results. Nevertheless, for most of the national stations the satisfactory agreement between modeled and observed values is found. For 65 – 75% of national stations a difference between modelled and observed air concentrations or wet deposition fluxes falls within a factor of two (Fig. 4.8).

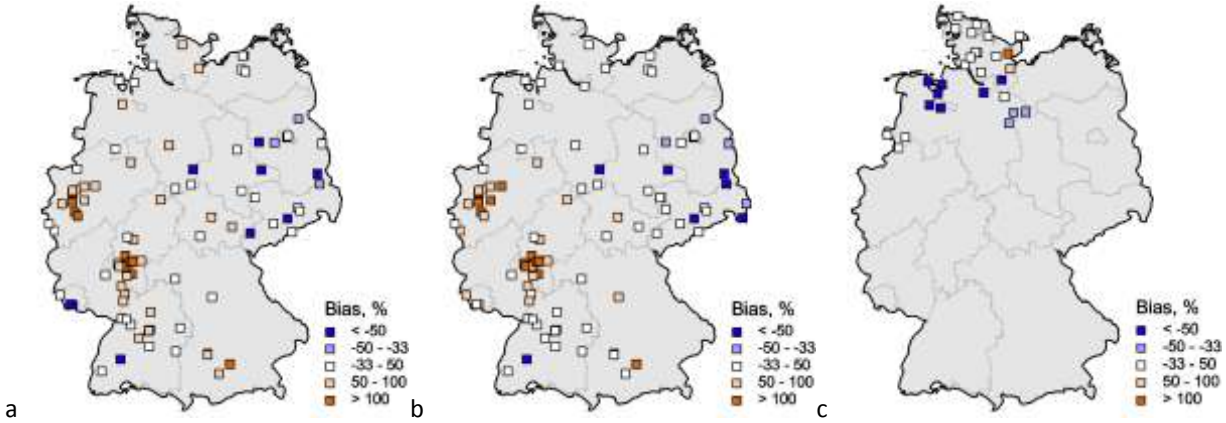

Fig. 4.8. *Relative bias of modelled Pb (a) Cd (b) air concentration and wet deposition flux of Hg (c)at German national stations for the period 2014-2016*

At a number of national stations the model also well reproduces seasonal variability of the observed levels. Modeled and measured time series are illustrated by Hg wet deposition (Fig. 4.9). Wet deposition of Hg at these sites is higher in summer and lower in winter indicating predominant role of the photooxidation chemistry. The modelling results also demonstrate relatively small contribution of national emissions to Hg deposition in comparison with long-range transport from regional, non-EMEP and secondary sources.

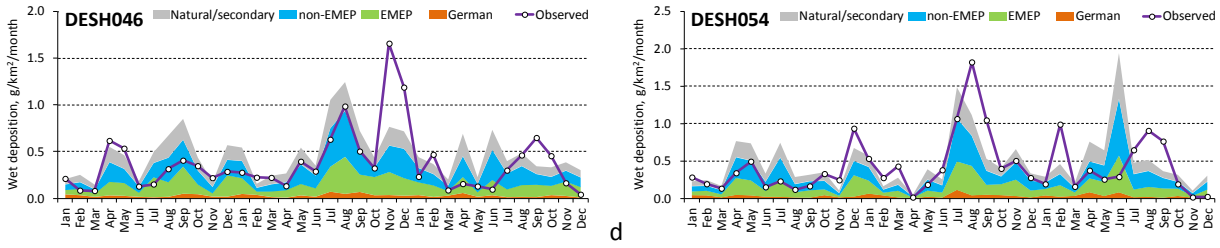

Fig. 4.9. *Comparison of simulated and observed monthly Hg wet deposition at German national stations DESH046 and DESH054 over the period 2014-2016*

Refined national emissions inventory for heavy metals and updates of other input information favour general improvement of the model assessment in comparison with previous EMEP operational modelling. Finer spatial resolution of emissions data allows more detailed evaluation of pollution patterns and leads to better agreement with observations. Even though the model performance does not change significantly over the whole territory of the country, it demonstrates considerable improvement in individual provinces or particular locations. For example, modelled Pb air concentrations based on new results are markedly improved compared to the previous operational modelling results in the Baden-Wuerttemberg province (Fig. 4.10). Besides, both spatial correlation and the relative bias of Hg wet deposition with respect to the measurements are considerably improved in the new results (Fig. 4.11).

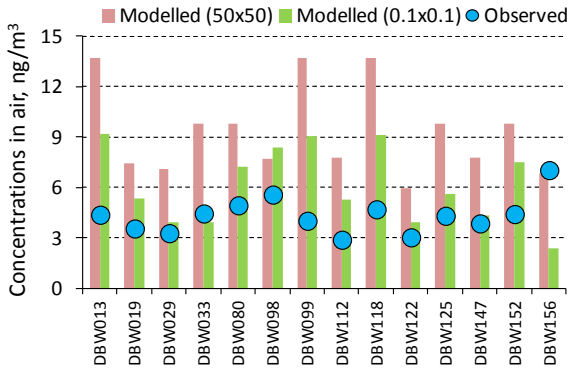

Fig. 4.10. *Modelled and observed concentrations of Pb in air at stations in Baden-Wuerttemberg province*

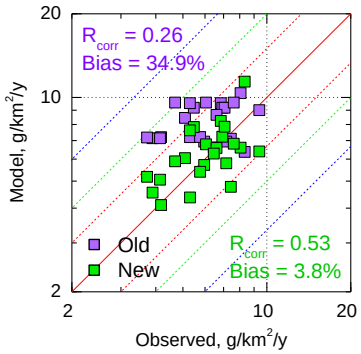

Fig. 4.11. *Comparison of old and new simulations of Hg wet deposition with observations (a) and change of relative bias*

Evaluation of the simulated country-scale patterns of heavy metal pollution against national monitoring data and measurements in moss reveals discrepancies in some locations or provinces of Germany, particularly, in the western part of the country. A number of sensitivity tests were undertaken to investigate reasons of the discrepancies between modelled and measured levels. Performed analysis showed that the differences between the modelled and measured data can result from:

- Total values and spatial distribution of anthropogenic emissions;
- Height distribution of anthropogenic emissions (especially relevant for large point sources);
- Absence of information on chemical speciation of Hg anthropogenic emissions;
- Use of measurements from monitoring stations situated close to local emission sources, which are not representative for the country-scale pollution assessment;
- Insufficient spatial resolution of the long-range model grid to resolve local scale pollution levels.

Further in-depth analysis of the revealed discrepancies requires assessment on a local scale involving national experts, collection of more detailed information on emissions (parameters of point sources, detailed structure of emission sectors, size distribution of heavy metal emissions, Hg emissions speciation), detailed measurement data (higher temporal resolution, more extensive meta data) and local scale modelling (including both EMEP and national models as well as back trajectory analysis). Results of this study are described in more detail in the Technical report [*Ilyin et al*., 2020a].

As shown, the country-scale assessment of heavy metal pollution for Germany identified a series of starting points for further in depth analysis by German experts in order to improve the knowledge about atmospheric pollution by Pb, Cd, Hg as basis for national risk assessment. Close cooperation of German experts with experts of EMEP/MSC-E is recommended to foster the overcoming of remaining discrepancies and clarification of still open questions.

4.3. Model evaluation of new mechanisms of Hg oxidation and reduction in the atmosphere

Atmospheric chemistry is critical for Hg dispersion in the atmosphere from emission sources and pollution of terrestrial and aquatic ecosystems. It determines the overall Hg residence time in the atmosphere and deposition to the ground. Despite significant improvements in measurements and modelling of Hg cycling in the environment, current knowledge on Hg oxidation and reduction mechanisms in the atmosphere remains incomplete. Gas-phase oxidation of Hg^0 by reactive halogens, in particular, by atomic bromine (Br) is considered as an important or even dominant pathway of Hg oxidation in the atmosphere [*Goodsite et al*., 2012; *Gratz et al*., 2015; *Coburn et al*., 2016; *Horowitz et al*., 2017]. The Br-initiated mechanism of Hg^0 oxidation with participation of various secondary reactants (e.g. OH, Br, BrO, NO_2, HO_2) is intensively studied by various research groups [*Dibble et al.,* 2014*; Wang et al*., 2014; *Jiao and Dibble,* 2015; 2017]. Besides, a new mechanism of Hg^{II} photo-reduction in gaseous phase was suggested by Saiz-Lopez et al. [2018], which was evaluated in detail in a previous study described in HM Status Report 2019 [*Gusev et al*., 2019].

This year we have continued evaluation of new mechanisms of Hg oxidation and reduction in the atmosphere, which were recently suggested by the scientific community. In particular, a new reaction of gas-phase photolysis of HgBr was proposed by *Saiz-Lopez et al*. [2019]. Besides, *Francés-Monerris et al.* [2019] suggested a new scheme of the photo-dissociation channels for various Hg^{II} species. And finally, a new mechanism of OH-initiated Hg oxidation in the atmosphere was developed by *Dibble et al*. [2019]. All these mechanisms were implemented into the experimental version of the GLEMOS model. The new version the model considers nine Hg chemical species in the atmosphere: Hg^0, unstable intermediates HgBr and HOHg as well as six Hg^{II} species ($HgBr_2$, HgBrOH, HgBrOOH, HgBrONO, HOHgOOH, HOHgONO). The Hg^{II} species are simulated in both gaseous and particulate state using the parameterisation of gas-particle partitioning from [*Amos et al.*, 2012]. Chemical reactions implemented in the model are given in Table 4.3. They include the two-step oxidation mechanisms initiated by Br (R1-R4) and OH (R5-R7) In addition to the oxidation reactions we also included gas-phase photo-reduction of Hg^{II} and Hg^{I} species (R8-R11) using the photolysis rates calculated with the CAM-Chem model [*Saiz-Lopez et al.,* 2018; 2019]. Six-hourly concentration fields of Br were archived from a GEOS-Chem simulation [*Parrella et al.,* 2012], Besudes, the original Br concentrations were increased by a factor of 3 above 750 hPa following *Shah et al.* [2016]. Concentrations of OH, HO_2, NO_2 and particulate matter (PM2.5) were imported from MOZART [*Emmons et al*., 2010].

The developed chemical scheme was evaluated in model simulations for the period 2007-2013 using anthropogenic emissions for 2010 [*AMAP/UNEP*, 2013]. The first 6 years of the period were used for the model spin up to achieve the steady-state Hg concentrations in the troposphere. The model results are presented as annual averages for 2013. Results of the model simulations were evaluated against a collection of ground-based measurements from various regional and global monitoring networks [*Travnikov et al*., 2017] and aircraft measurement campaigns [*Bieser et al.*, 2017; *Brooks et al.,* 2014; *Gratz et al.*, 2015; *Shah et al*., 2016].

Table 4.3. *An experimental chemical mechanism for atmospheric Hg in GLEMOS*

N	Reaction	Reference
R1	$Hg^0 + Br + M \rightarrow HgBr + M$	*Donohoue et al.* [2006]
R2	$HgBr + M \rightarrow Hg^0 + Br + M$	Dibble et al. [2012]
R3	$HgBr + Br \rightarrow Hg^0 + Br_2$	*Balabanov et al.* [2005]
R4	$HgBr + Y \overset{M}{\rightarrow} HgBrY$ $Y = Br, OH, NO_2, HO_2$	*Goodsite et al.* [2004] *Jiao and Dibble* [2017]
R5	$Hg^0 + OH + M \rightarrow HOHg + M$	*Dibble et al.* [2019]
R6	$HOHg + M \rightarrow Hg^0 + OH + M$	*Dibble et al.* [2019]
R7	$HOHg + Y \overset{M}{\rightarrow} HOHgY$ $Y = NO_2, HO_2$	*Jiao and Dibble* [2017] *Dibble et al.* [2019]
R8	$HgBrY \overset{h\nu}{\rightarrow} HgBr + products$ $Y = Br, OH, NO_2, HO_2$	*Saiz-Lopez et al.* [2018]
R9	$HgBr \overset{h\nu}{\rightarrow} Hg^0 + products$	*Saiz-Lopez et al.* [2019]
R10	$HOHgY \overset{h\nu}{\rightarrow} HOHg + products$ $Y = NO_2, HO_2$	*Dibble et al.* [2019] *Saiz-Lopez et al.* [2018]
R11	$HOHg \overset{h\nu}{\rightarrow} Hg^0 + products$	*Saiz-Lopez et al.* [2019]

Figure 4.12 shows global distribution of simulated Hg^0 surface concentration as well as evaluation of the modelling results against long-term observations. As seen the simulated spatial pattern reasonably well correlates with the observations and reproduces the inter-hemispheric gradient. However, the model overestimates measured near-surface Hg^0 levels by 40%. The overprediction can be caused by either insufficient Hg^0 oxidation in the atmosphere or too large global net emission to the atmosphere. The estimated relatively long (11.5 months) residence time of Hg in the atmosphere with respect to deposition rather indicates influence of the first factor. More certain answer to the question can be obtained from evaluation of oxidized Hg species and wet deposition.

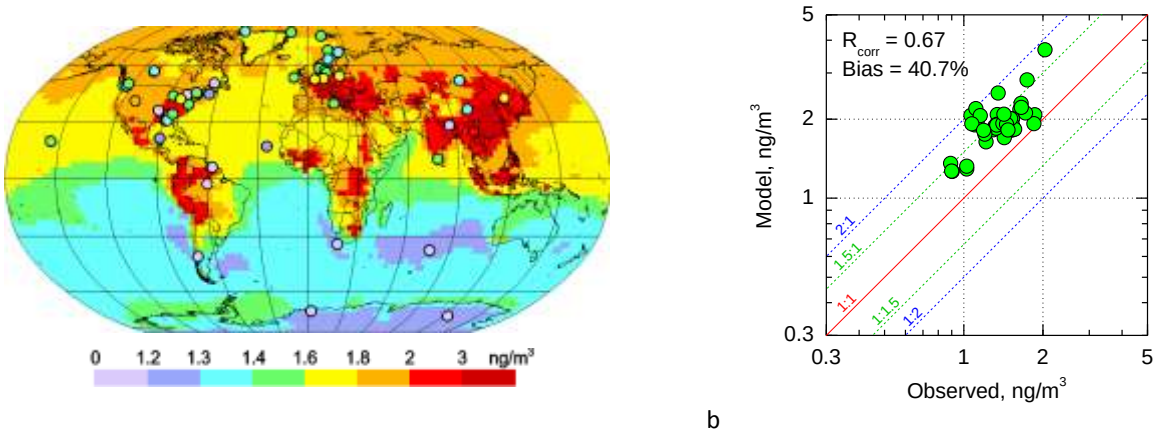

a b

Fig. 4.12. *Comparison of modelled and measured spatial patterns of Hg^0 air concentrations (a) and scatter plot of the model-to-measurement comparison at ground-based sites (b) in 2013.*

Spatial distribution of simulated Hg^{II} concentration in the surface air is sown in Fig. 4.13 along with available observations. It should be noted that currently performed measurements of Hg^{II} contains much higher uncertainties than measurements of Hg^0 [*Gustin et al.*, 2015]. Elevated Hg^{II} concentrations are predicted in industrial regions of East and South Asia, Meddle East and Europe due to direct anthropogenic emissions. Besides, relatively high concentrations also occur over Antarctica and the Southern Ocean because of intensive oxidation of Hg^0 in the atmosphere. The lowest Hg^{II} levels are in the inter-tropical convergence zone due to large-scale scavenging by precipitation. Generally, the model reproduces average Hg^{II} concentration levels observed at sea-level sites located in the northern mid-latitudes. The largest deviations characterise comparison of observed and measured concentrations in the Southern Hemisphere.

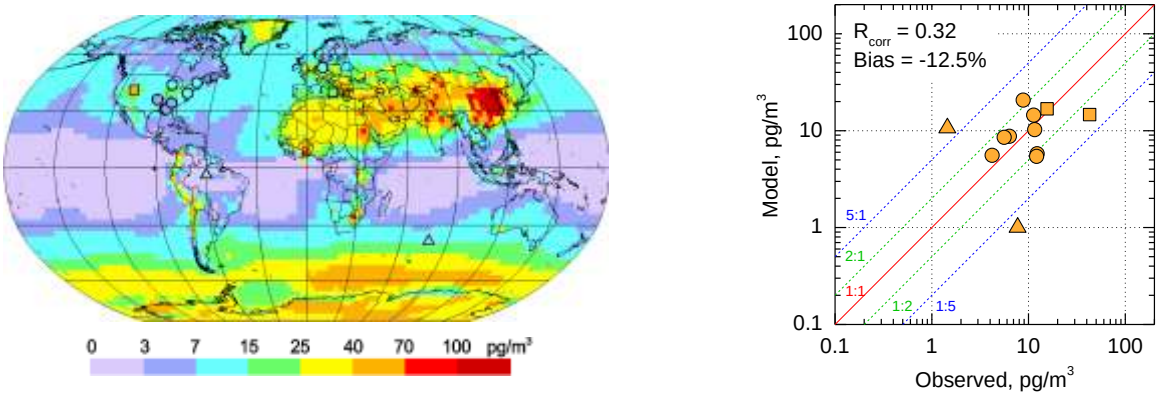

a b

Fig. 4.13. *Comparison of modelled and measured spatial patterns of Hg^{II} atmospheric concentrations (a) and scatter plot of the model-to-measurement comparison at ground-based sites (b) in 2013. Circles present sea-level sites in northern mid-latitudes; squares – high-elevation sites; triangles – sites in the southern hemisphere.*

The model also successfully reproduces seasonal variation of Hg^{II} concentration in the near-surface air measured at sea-level monitoring sites (Fig. 4.14). Both modelled and observed concentrations have maximum in late winter /early spring and minimum in late summer / early autumn. This seasonality is mostly explained by the Br-initiated chemistry and the gas-particle partitioning of oxidised Hg species [*Travnikov et al*. 2017]. However, the model tends to overpredict the measurements in the winter months. Besides, the modeling results demonstrate higher variation of Hg^{II} concentration among the sites.

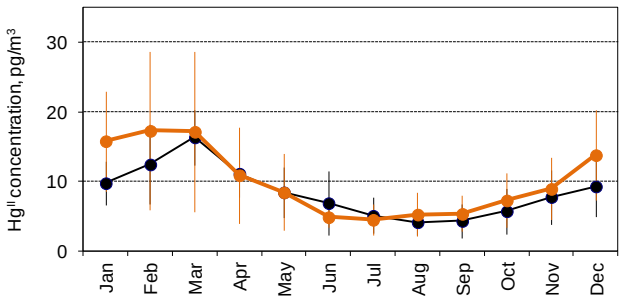

Fig. 4.14. *Comparison of modelled and measured monthly mean Hg^{II} concentration in 2013 at sea-level measurement sites located in temperate latitudes of the Northern Hemisphere. Whiskers show the standard deviation among the sites.*

More information for the analysis is provided by evaluation of simulated vertical profiles of Hg^0 and Hg^{II} in the northern mid-latitudes (Fig. 4.15). As seen the model predicts vertical distribution of Hg^0 that is comparable with aircraft observations in the free troposphere from [*Bieser et al.*, 2017] but overestimates observed Hg^0 levels near the ground (Fig. 4.15a). In contrast, the model considerably underpredicts measured Hg^{II} concentrations in the free troposphere from aircraft measurement campaigns in North America [*Brooks et al.*, 2014; *Shah et al.*, 2016; *Gratz et al.*, 2015] (4.15b). The underestimation results from insufficient Hg^{II} production in the atmosphere due to oxidation of Hg^0. It also explains the overprediction of Hg^0 near the ground. Analysis of Hg^{II} composition shows prevailing contribution of HgBrOH to oxidized Hg species in the free atmosphere (Fig. 4.15c). It differs significantly from previous estimates, where the atmospheric Hg^{II} was dominated by HgB_2 and HgBrONO [*Ilyin et al.,* 2019]. The difference is caused by application of the updated scheme of the photo-dissociation channels [*Francés-Monerris et al.*, 2019], which predicts significant proportion of HgBrONO and HgBrOOH photo-dissociated to HgBrO with further production of HgBrOH in reaction with methane.

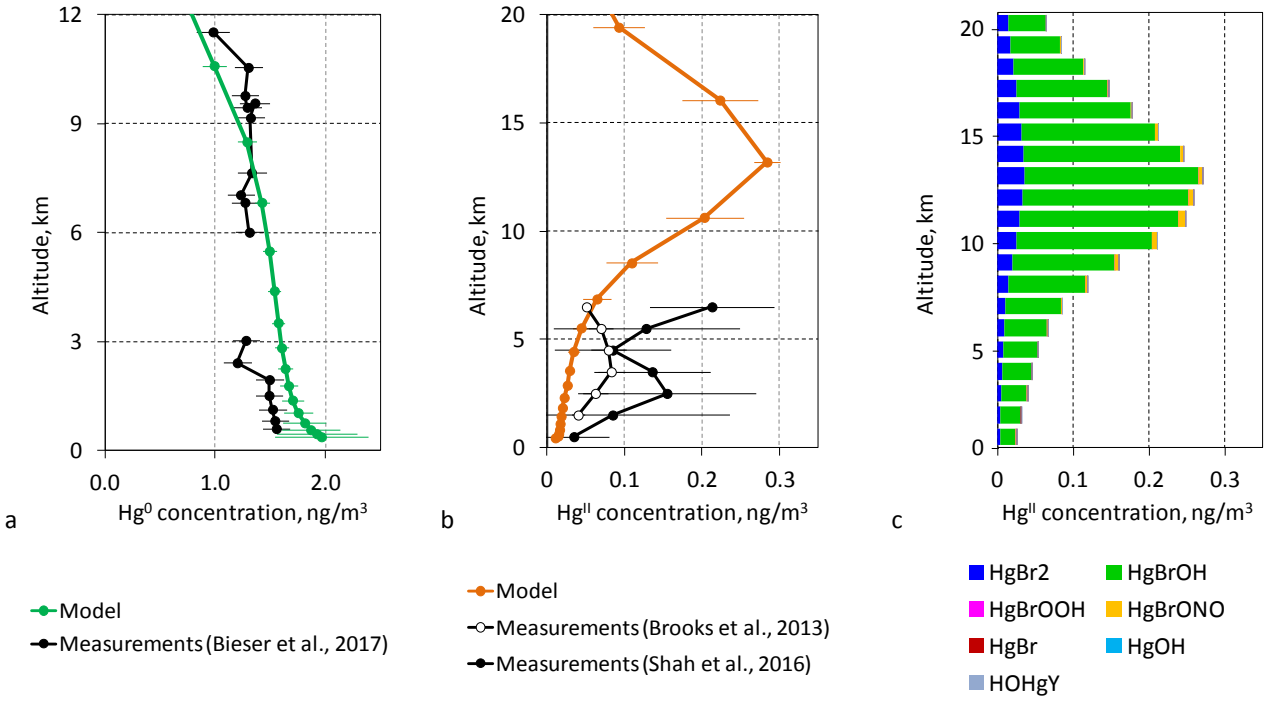

Fig. 4.15. *Modelled and measured vertical profiles of Hg^0 (a) and Hg^{II} (b) concentrations over northern mid-latitudes and contribution of various species to Hg^{II} concentration (c). Measurements of Hg^0 are form aircraft campaigns (Bieser et al., 2017); Hg^{II} measurements are from campaigns [Brooks et al., 2014 and Shah et al., 2016; Gratz et al., 2015].*

Underestimation of Hg^0 oxidation and production of Hg^{II} in the free troposphere leads to underprediction of wet deposition. Comparison of modeled and observed wet deposition fluxes shows biased low by 40% simulations at measurement sites mostly located in the northern mid-latitudes (Europe and North America) (Fig. 4.16). The underprediction is not found in the Southern Hemisphere, which is characterized by stronger chemical production of Hg^{II} (Fig. 4.16a).

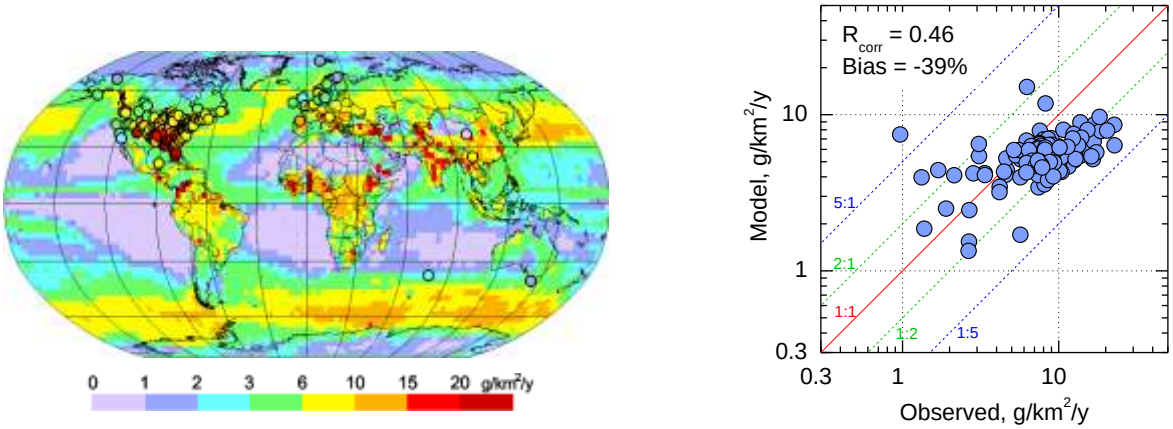

a b

Fig. 4.16. *Comparison of modelled and measured spatial patterns of Hg wet deposition (a) and and scatter plot of the model-to-measurement comparison at ground-based sites (c) in 2013.*

Thus, the model tests show that the current understanding of the Hg atmospheric redox chemistry is still incomplete. Inclusion of the newest chemical mechanisms of Hg oxidation initiated by the reactions with Br and OH and photo-reduction of oxidized Hg allows partly reproducing the observations but demonstrates insufficient Hg oxidation in the free troposphere. Further analytical studies of Hg redox mechanisms are needed along with the model evaluation to improve model assessment of Hg pollution on both global and regional scales. More detailed analysis of the considered mechanisms including their model evaluation with GLEMOS is presented in a peer-reviewed paper [*Saiz-Lopez et al.*, 2020].

4.4. Update of model parameterization of gas-particle partitioning and degradation for B(a)P

The most important processes, governing B(a)P fate in the atmosphere, include its partitioning between gaseous and particulate phases and chemical transformations (degradation) [*Lohmann and Lammel*, 2004; *Keyte et al.*, 2013]. Parameterizations of B(a)P sorption to various components of aerosol particles (organic and inorganic sub-fractions) as well as heterogeneous reactions of particle-bound B(a)P with ozone is subject of significant uncertainties [*Shrivastava et al.*, 2017]. This year the work on the improvement of model parameterization of these processes is continued. Brief overview of the progress in this work is given below.

Gas-particle partitioning

A number of model parameterizations of different complexity have been developed to describe the partitioning of semi-volatile POPs (including PAHs) between the gaseous and particulate phases. In the current version of the GLEMOS model a parameterization of gas-particle partitioning process (GPP) based on B(a)P absorption into organic matter and adsorption to black carbon (DUAL-OM_EC) [*Dachs and Eisenreich*, 2000; *Lohmann and Lammel*, 2004] is implemented. In addition, a

parameterization based on the poly-parameter linear free energy relationships (pp-LFER) [*Goss and Schwarzenbach*, 2001; *Shahpoury et al.*, 2016] is being tested. Brief description of both approaches is given below.

According to *dual organic matter (OM) absorption and black carbon (BC) adsorption parameterization,* particulate fraction φ^{ab+bc} of B(a)P is calculated from the equation:

$$\varphi^{ab+bc} = K_p^{ab+bc} \cdot TSP/(1 + K_p^{ab+bc} \cdot TSP), \quad (4.1)$$

where TSP is the concentration of suspended particulate matter, μg/m^3, and partition coefficient K_p^{ab+bc} can be calculated from:

$$K_p^{ab+bc} = 10^{-12} \cdot (0.32 \cdot f_{OM} \cdot K_{oa} + 0.55 \cdot f_{BC} \cdot K_{sa}) \quad (4.2)$$

Here f_{OM} is the fraction of OM, and f_{BC} is the fraction of BC in aerosol particles. K_{oa} and K_{sa} are octanol-air and soot-air partition coefficients. Parameterization of K_{oa} is given in [*Gusev et al.,* 2006]. For K_{sa} the parameterization suggested by [*van Noort,* 2003] is used in the current version of the model:

$$\log K_{sa} = -0.85 \cdot \log p_L^0 + \log(998/a_{soot}) + 8.94, \quad (4.3)$$

where p_L^0 is subcooled liquid pressure, and specific aerosol surface of soot a_{soot} is assumed to be 18.21 m^2/g [*Efstathiou et.al.,* 2016].

In the *pp-LFER parameterization* B(a)P absorption into the two distinct phases of organic aerosol (OA) is considered: to liquid phase, consisting of both water soluble and organic soluble OA, and to semi-solid/solid organic polymer phase. Organic soluble phase is represented by dry dimethyl sulfoxide (DMSO) and solid/semi-solid organic polymer phase is represented by the polyurethane ether (PU). In addition, adsorption on black carbon is considered. Partition coefficient between these phases and the atmospheric gas phase, m^{3}air/μg TSP is given by:

$$K_p = 10^{-6}(K_{\mathrm{BC}-air} \cdot f_{\mathrm{BC}} \cdot a_{soot}) + 10^{-12}(K_{\mathrm{DMSO}-air} \cdot f_{\mathrm{DMSO}}/\rho_{\mathrm{DMSO}} + K_{\mathrm{PU}-air} \cdot f_{\mathrm{PU}}), \quad (4.4)$$

Here, fractions f_{DMSO} and f_{PU} are assumed to be equal to 0.6 and 0.4 times OA fraction [*Shahpoury et al.,* 2016], ρ_{DMSO} is the density of DMSO, 1.1 kg/L. Partition coefficients $K_{\mathrm{BC}-air}$ and $K_{\mathrm{DMSO}-air}$ are given by:

$$\log K_{x-air} = eE + sS + aA + bB + lL + c, \quad (4.5)$$

where x can be BC or DMSO, and

$$\log K_{\mathrm{PU}-air} = sS + aA + bB + lL + c, \quad (4.6)$$

Temperature dependency of the gas-particle partitioning coefficient K_p for arbitrary ambient temperature *T* is determined using the van't Hoff relationship:

$$K_p(T) = K_{p0} \cdot \ exp\big(-K_{pT}(1/T - 1/T_{ref}\big), \qquad (4.7)$$

where reference temperature $T_{ref} = T_1$ is chosen to be 283.15°K (10° C). The coefficients in formulas (4.5 – 4.7) are given in the Technical Report [*Gusev et al.*, 2020a].

Atmospheric degradation

Degradation of B(a)P in the atmosphere can occur both in gaseous and particulate phase. In gaseous phase it can react with hydroxyl radical (OH), NO_3 and ozone. The latter two reactants are generally less effective comparing to the reactions with OH radical. However, the reactions with NO_3 can significantly contribute to the degradation of B(a)P in the atmosphere during the night-time [*Keyte et al.*, 2013].

In Table 4.4 the degradation constants of pseudo-first and second order, calculated on the basis of the values given in [*Mu et al.*, 2018], are presented. Typical average values of reactant concentrations obtained from MOZART-4 model are shown in column 2. In current version of the GLEMOS model lower value of degradation constant of 2nd order for the reaction of B(a)P with OH radical (5.0×10^{-11} cm^3/molecules/sec) is used.

Table 4.4. *Degradation constants used for B(a)P.*

Reactant	Concentrations, molecules/cm^3	2nd order degradation constant, cm^3/molecules/sec	1st order degradation constant, sec^{-1}
OH	$8 \cdot 10^5$	1.5×10^{-10}	$1.2 \cdot 10^{-4}$
NO_3	$4.43 \cdot 10^7$	5.4×10^{-11}	$2.39 \cdot 10^{-3}$
O_3	$1.25 \cdot 10^{12}$	2.6×10^{-17}	$3.26 \cdot 10^{-5}$

Calculations, presented in the Table 4.4, show that reactions with NO_3 radical can represent important pathway of B(a)P degradation in gaseous phase, whereas reactions with ozone (at ozone concentration of 50 ppb) are less important comparing to OH and NO_3 radicals. At the same time, according to the study of [*Mu et al.,* 2017] degradation of B(a)P due to reactions with NO_3 is less significant comparing to OH radical.

Another important pathway of degradation is heterogeneous reactions of B(a)P in particulate phase with ozone. The rate of degradation of B(a)P, sorbed on various components of aerosol particles, namely organic matter, black carbon, aerosol water, and mineral fraction, is different and depends also on the air temperature and humidity.

There is a number of papers describing degradation rates of particle-bound B(a)P due to heterogeneous reaction with ozone. According to experimental studies [*Kahan and Donaldson*, 2006; *Kwamena et al*., 2004, 2007], the value of degradation constant of second order for B(a)P reaction with ozone can be well described by a Langmuir–Hinshelwood mechanism. It should be noted that the values of degradation constants for this reaction, published in literature, vary in wide range (up to three orders of magnitude). In current version of the GLEMOS model the 2nd order degradation

constant for particle-bound B(a)P reaction with ozone is chosen to be $1.68 \cdot 10^{-16}$ for B(a)P fraction absorbed by organic matter [*Kwamena et al.,* 2004], and $5.3 \cdot 10^{-17}$ for B(a)P fraction adsorbed on elemental carbon [*Perraudin et al.,* 2007].

Test model simulations with updated model parameterizations

To explore sensitivity of modelling results to changes of the GPP model parameterization, model simulations with the two described above approaches were performed for 2017. Additional model runs were also carried out with modified description of B(a)P degradation in gaseous and particulate phases. In particular, for gaseous phase degradation reactions with NO_3 and ozone were included, and for particulate phase alternative values of degradation constants were used. The results of test model simulations were compared with measurements of selected EMEP monitoring stations performed in 2017. Main statistical parameters, namely correlation coefficients, relative bias, and root mean square error with respect to measurement data were estimated for these runs. Detailed description of test model simulations and evaluation of the modelling results is given in Technical Report [*Gusev et al.*, 2020a].

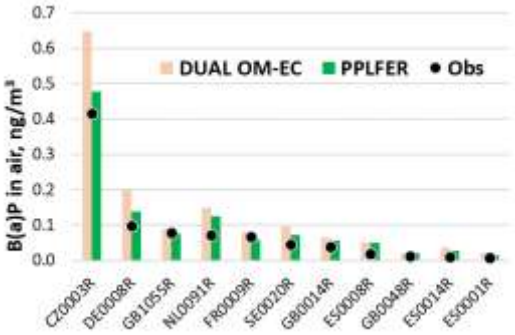

Fig. 4.17. *Comparison of test modelling results with two GPP parameterizations (DUAL-OM_EC and pp-LFER) and annual mean observed B(a)P air concentrations for 2017 for the stations where the agreement with measurements was better in case of pp-LFER parameterization.*

Evaluation of the two GPP parameterizations showed comparable results with somewhat better agreement of modelling results with measurements in case of pp-LFER approach. In particular, in both test simulations spatial correlation of model predictions and measurements is about 0.6, and relative bias is about -20% – -40%. For about a half of monitoring stations the agreement of modelling results in case of pp-LFER parameterization was better than that of DUAL-OM_EC (Fig. 4.17). However, for the other monitoring stations the use of pp-LFER parameterization resulted in lower agreement with measurements.

Along with this, relative fraction of B(a)P in particulate phase was closer to measurements in case of the use of pp-LFER parameterization. In particular, according to measurements of B(a)P concentrations in the atmosphere the fraction of B(a)P in particulate phase exceeded 80-90% [*Akyüz and Çabuk*, 2010; *Possanzini et al.*, 2004; *Cincinelli et al.*, 2007; *Esen et al.*, 2006; *Cheruyiot et al.*, 2015, etc.]. Spatial distribution of relative fraction of annual mean B(a)P air concentrations in particulate phase for the two model simulations (with DUAL-OM_EC and pp-LFER parameterizations) is shown in Fig. 4.18. In case of pp-LFER the area with relative fraction of B(a)P in particulate phase higher than 0.8 is substantially wider comparing to DUAL-OM_EC.

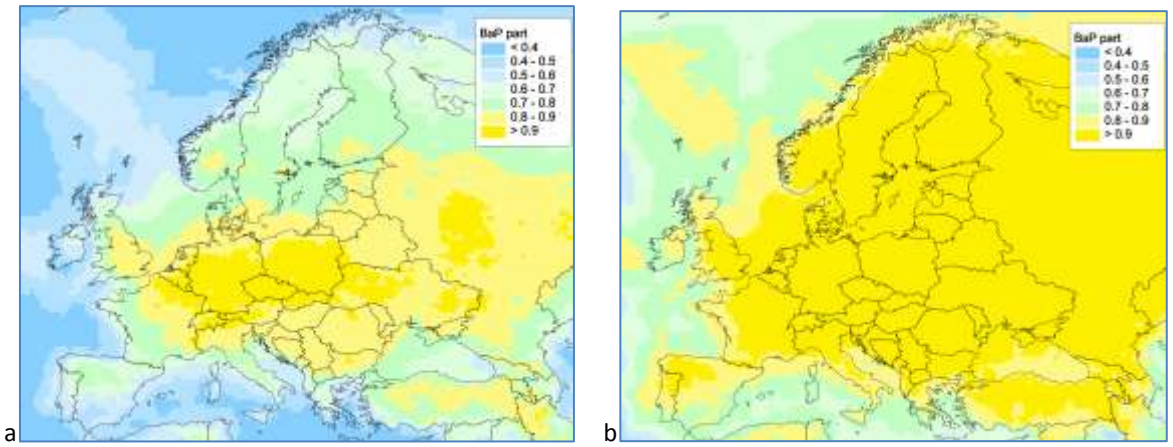

Fig. 4.18. *Spatial distribution of relative fraction of annual mean B(a)P air concentrations in particulate phase in case of DUAL-OM_EC (a) and pp-LFER (b) parameterizations.*

Besides, pp-LFER approach is more flexible with respect to the inclusion of different components of aerosol particles into the description of GPP of B(a)P. Therefore, analysis and testing of this approach will be continued at further stages in order to use pp-LFER parameterization in the operational model simulations.

Preliminary results of model simulations with the use of alternative parameterization of B(a)P degradation in gaseous and particulate phases did not show noticeable improvement of the agreement between model predictions and measurements. Inclusion of additional reactants NO_3 and ozone resulted in lower spatial correlation and in the increase of the bias between predicted and observed concentrations. Similarly, alternative values of degradation rate for B(a)P in particulate phase led to substantial decrease of the modelled concentrations and poor agreement with measurements. Thus, further analysis of model parameterization of B(a)P degradation process in the atmosphere is required.

4.5. Air-vegetation gaseous exchange of POPs and Hg: literature review and model parameterization update

Gaseous exchange of POPs and Hg between the atmosphere and vegetation is an important process that affects their distribution in the environment and can lead to human and wildlife exposure to harmful levels of their concentrations [*Barber et al.*, 2002]. There is a number of approaches that are implemented in the multi-compartment models to describe the air-vegetation exchange of POPs. The review of literature sources on these topics is presented in Technical Report [*Gusev et al.*, 2020a]. In particular, vegetation can be presented in the model as a single homogeneous compartment, for which the processes of uptake from and re-emission to the atmosphere of POPs are defined [*McLachlan,* 1999]. Another approach to the description of air-vegetation exchange considers vegetation and soil as parts of a single compartment (ecosystem) [*Sutton et al.*, 1993]. Below brief outline of main features of these two approaches is presented.

Vegetation as a single compartment

There are two main pathways for POP uptake by vegetation: root uptake from soil and leaf uptake from the atmosphere. However, a number of papers consider the root uptake for heavy PAHs to be negligible. For the uptake by leaves, it is found that for the pollutants with high molecular weight stomatal pathway is not essential [*Riederer*, 1990; *Paterson et al*., 1991; *McLachlan*, 1999; *Barber et al*., 2004].

Therefore, in this review only leaf uptake from the atmosphere through the plant cuticle is considered. The following equation is used for calculation of the flux between air and vegetation [*McLachlan and Horstmann*, 1998; *McLachlan*, 1999]:

$$F_{air-veg} = g_{tot} \cdot \left(C_{atm} - \frac{C_{veg}}{BCF}\right), \quad (4.8)$$

where C_{veg} and C_{atm} are POP concentrations in the vegetation and the atmosphere, BCF is the bioconcentration factor, and g_{tot} is total conductance (mass transfer coefficient) for POP gaseous flux to vegetation being a reciprocal to the resistance R_{tot}.

Total conductance g_{tot} of leaf uptake of POPs by leaves can be calculated from [*Barber et al.*, 2004]:

$$\frac{1}{\mathrm{g_{tot}}} = \frac{1}{\mathrm{g_a}} + \frac{1}{\mathrm{g_b}} + \frac{1}{\mathrm{g_c} + \mathrm{g_s}}, \quad (4.9)$$

where $\mathrm{g_a}$ is the aerodynamical conductance for turbulent transport,

$\mathrm{g_b}$ is the boundary layer conductance,

$\mathrm{g_c}$ is the cuticular conductance,

$\mathrm{g_s}$ is the stomatal conductance.

According to the above discussion, the parameter $\mathrm{g_s}$ (stomatal conductance) in formula (4.9) should be put to zero. Calculations of the rest parameters in formulas (4.8) and (4.9) are given in Technical Report [*Gusev et al*., 2020a].

This approach to describe air-vegetation exchange of POPs in gaseous phase is currently implemented in the current version of the GLEMOS model. Along with the exchange of POPs with the atmosphere, the vegetation compartment in the model is also connected with the soil compartment and forest litter through the parameterization of POP transfer.

Combined vegetation and soil compartments

In this approach a concept of compensation points is used [*Zhang et al.*, 2009, 2010; *Wang et al.*, 2014]. The compensation points depend on pollutant concentrations in media, and are the values of air concentrations, for which the exchange flux between the considered medium and air changes its direction. As such, compensation point of vegetation in the above model can be identified with the second term of the right-hand part of formula (4.8) above, namely C_{veg}/BCF. Combined compartment

that comprises the soil and vegetation (canopy) can be also characterized by the overall compensation point χ_{cnp}. This parameter is chosen in such a way that the flux from canopy to the air can be given by:

$$F_{tot} = \frac{\chi_{cnp} - C_{atm}}{R_a + R_b} \tag{4.10}$$

where R_a is an aerodynamic resistance, R_b is a resistance of boundary layer, and fluxes from cuticle and soil to air are given by:

$$F_{cut} = \frac{1}{R_{cut}}\left(\chi_{cut} - \chi_{cnp}\right), \qquad \chi_{cut} = \frac{C_{cut}}{BCF} \tag{4.11}$$

The term χ_{cut} is the cuticle compensation point. Thus, the flux for vegetation-covered soil is:

$$F_{soil} = \frac{1}{R_{ac} + R_{soil}}\left(\chi_{soil} - \chi_{cnp}\right) \tag{4.12}$$

where R_{ac} is the canopy aerodynamic resistance, R_{soil} is soil resistance, and χ_{soil} is soil compensation point calculated as:

$$\chi_{soil} = \frac{C_{soil}}{P_{soil-air}} \tag{4.13}$$

Here C_{soil} is the concentration of pollutant in soil, and $P_{soil-air}$ is soil-air partitioning coefficient calculated in parameterization of soil processes.

Applying the approach of [*Sutton et al.,* 1998], we can obtain the relation for χ_{cnp} by equating expression (4.10) for F_{tot} to the sum of fluxes from soil and vegetation (cuticle):

$$\chi_{cnp} = \left[\frac{C_{atm}}{R_a + R_b} + \frac{LAI \cdot \chi_{cut}}{R_{cut}} + \frac{\chi_{soil}}{R_{ac} + R_{soil}}\right] / \left[\frac{1}{R_a + R_b} + \frac{LAI}{R_{cut}} + \frac{1}{R_{ac} + R_{soil}}\right] \tag{4.14}$$

Further, assuming *LAI* = 0 and R_{ac} = 0 we obtain the relation for the flux from bare soil to the atmosphere:

$$F_{soil} = \frac{1}{R_a + R_b + R_{soil}}\left(\chi_{soil} - C_{air}\right) \tag{4.15}$$

This approach has been applied for wide range of gaseous pollutants and thus can be implemented in the GLEMOS model to describe air-vegetation gaseous exchange for POPs and Hg at further steps of model development.

4.6. Sensitivity of the GLEMOS model to different sets of chemical reactants

Modelling of atmospheric transport of POPs and Hg requires information on air concentrations of different reactants and constituents of aerosol particles that affects their chemical transformations. Currently, the GLEMOS model is adapted to use of the chemical reactants ozone (O_3), hydroxyl radical (OH), nitrogen dioxide (NO_2), nitrate radical (NO_3), hydroperoxyl radical (HO_2) as well as sulfur dioxide (SO_2), particulate matter (PM2.5) and its components - elemental (BC) and organic (OC) carbon.

Two chemistry transport models: MOZART (Model for Ozone and Related chemical Tracers, version 4) and GEOS-Chem Classic (GCC, version 12.5.0), were considered to provide gridded data on required set of atmospheric species for the GLEMOS model. Selected ouput variables from GEOS-Chem and MOZART models were processed, compared between each other, and evaluated against available measurements. Test model simulations using the output of these models on the example of B(a)P are briefly descibed in this section. More detailed description of processing and evaluation of GEOS-Chem and MOZART data including models setup is presented in the Technical Report [*Gusev et al*., 2020a].

B(a)P partitioning between the gaseous and particulate phases as well as degradation in both phases are the most important processes affecting its long-range transport in the atmosphere. The model parameterizations of these processes, applied in the GLEMOS model, require the data on atmospheric reactants (O_3, OH) and elemental and organic carbon (BC, OC) content in the aerosol particles. These data were imported from the MOZART and GEOS-Chem models and used in test model simulations to explore the effect of differences between these model outputs on GLEMOS modelling results for B(a)P.

Spatial distributions of annual mean B(a)P concentrations in 2015 modelled using the output of MOZART and GEOS-Chem models are presented in Figure 4.19a,b respectively. The absolute and relative difference between the two sets of modelling results is shown in Fig. 4.19c,d. The absolute difference was caclulated as difference between annual mean B(a)P concentrations obtained using GEOS-Chem data and annual B(a)P levels obtained using MOZART data. The relative difference was computed by dividing this absolute difference by annual B(a)P levels obtained using MOZART data and converting to percents.

Though both distributions appear to be rather similar, there is a noticeable (10-20%) differences of B(a)P concentration levels in Western Europe and in Eastern Europe. Utilizing the reactant data from GEOS-Chem instead of data from MOZART leads to reduction of absolute values of B(a)P concentrations in Germany, Portugal and the United Kingdom (Fig. 4.19c). But it should be noted that calculated concentrations of B(a)P in Germany and Portugal are generally much higher than, for example, in France or Spain, and, as seen from the relative difference field, the calculated values in all these countries decreased approximately by 5-15%.

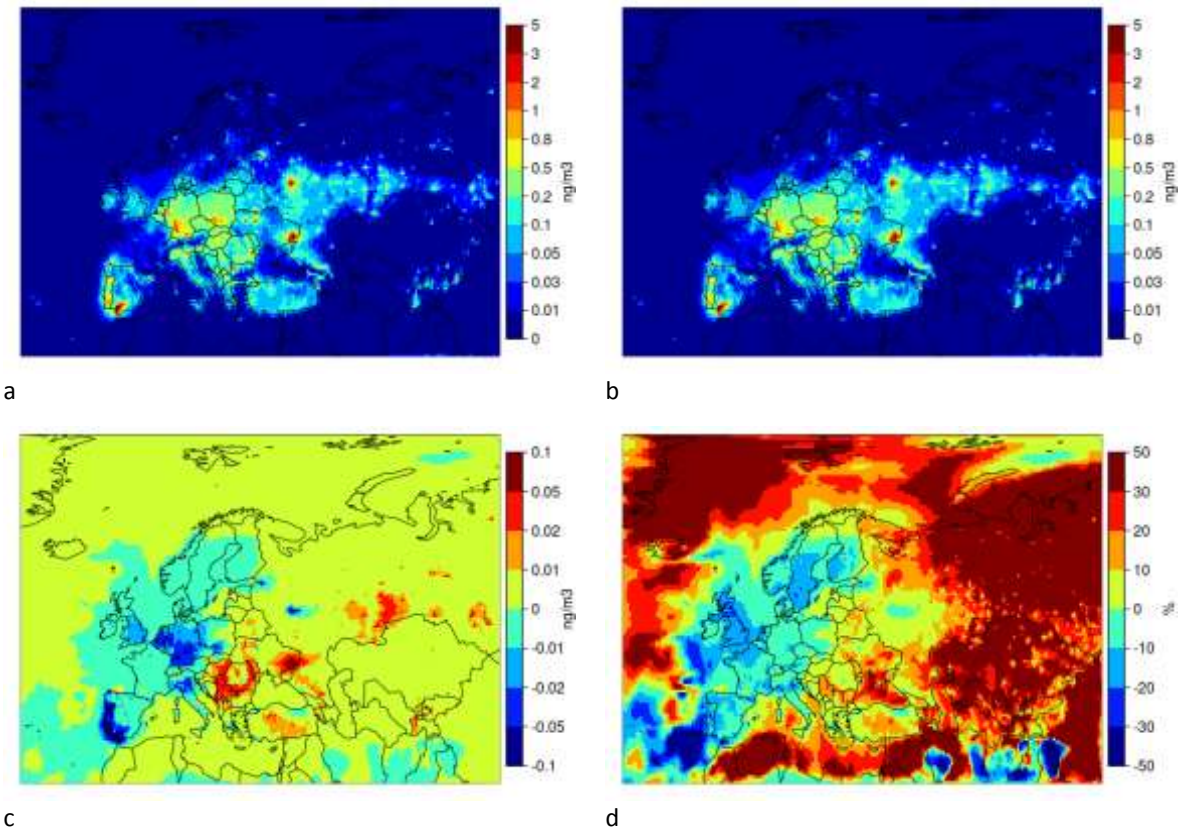

Fig. 4.19. *Spatial distributions of annual mean B(a)P air concentrations in the EMEP region for 2015, generated by the GLEMOS model based on the output from MOZART (a) and GEOS-Chem model (b) and absolute (c) and relative difference (d) between these two sets of annual mean B(a)P air concentrations.*

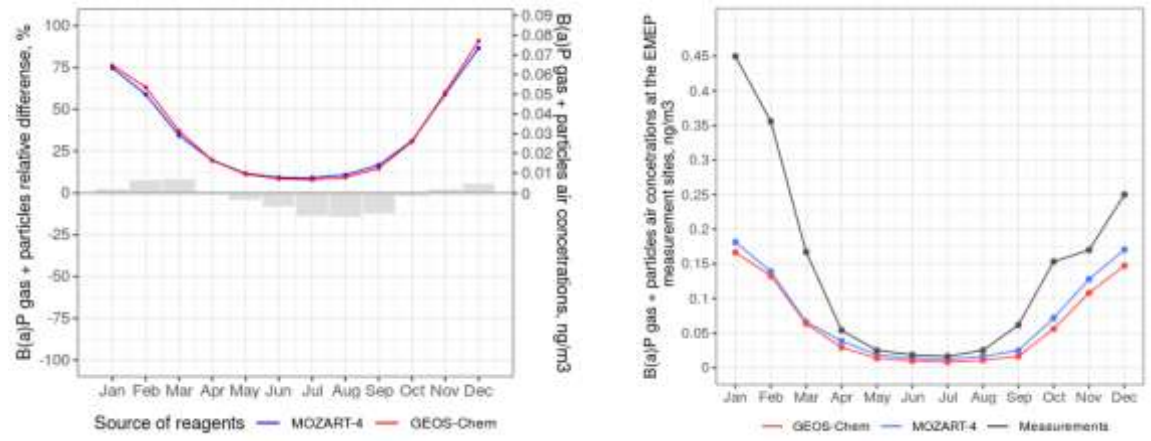

Fig 4.20. *Comparison of monthly mean B(a)P air concentrations for 2015, obtained in simulations with the two different sets of data from MOZART-4 and GEOS-Chem models. Gray bars show relative difference between the monthly mean air concentrations of B(a)P, simulated utilizing GEOS-Chem and MOZART data (a). Comparison of averaged model predictions of B(a)P air concentrations, generated using the basis of GEOS-Chem and MOZART data, and measurements of selected EMEP monitoring stations for 2015 (b).*

Application of data from GEOS-Chem leads to 5% higher total average B(a)P air concentrations in February, March and December, and 5-10% lower in period from May to September comparing to the simulation based on MOZART data (Fig. 4.20a). These differences can be explained by the different concentration levels of the reactants, imported from the GEOS-Chem and MOZART models. The winter increase in B(a)P levels can be caused by higher concentrations of both elemental and organic carbon modeled by GEOS-Chem in this period (Fig. 4.21a,b). At the same time, the concentrations of the hydroxyl radical and ozone, the substances causing B(a)P degradation, remained unchanged or decreased (Fig. 4.21c,d). Also GEOS-Chem produced 15–20% lower concentrations of ozone and elemental carbon from May to September and 1.5 times higher OH levels, comparing to MOZART, which caused a decrease in B(a)P concentration levels in the summer period.

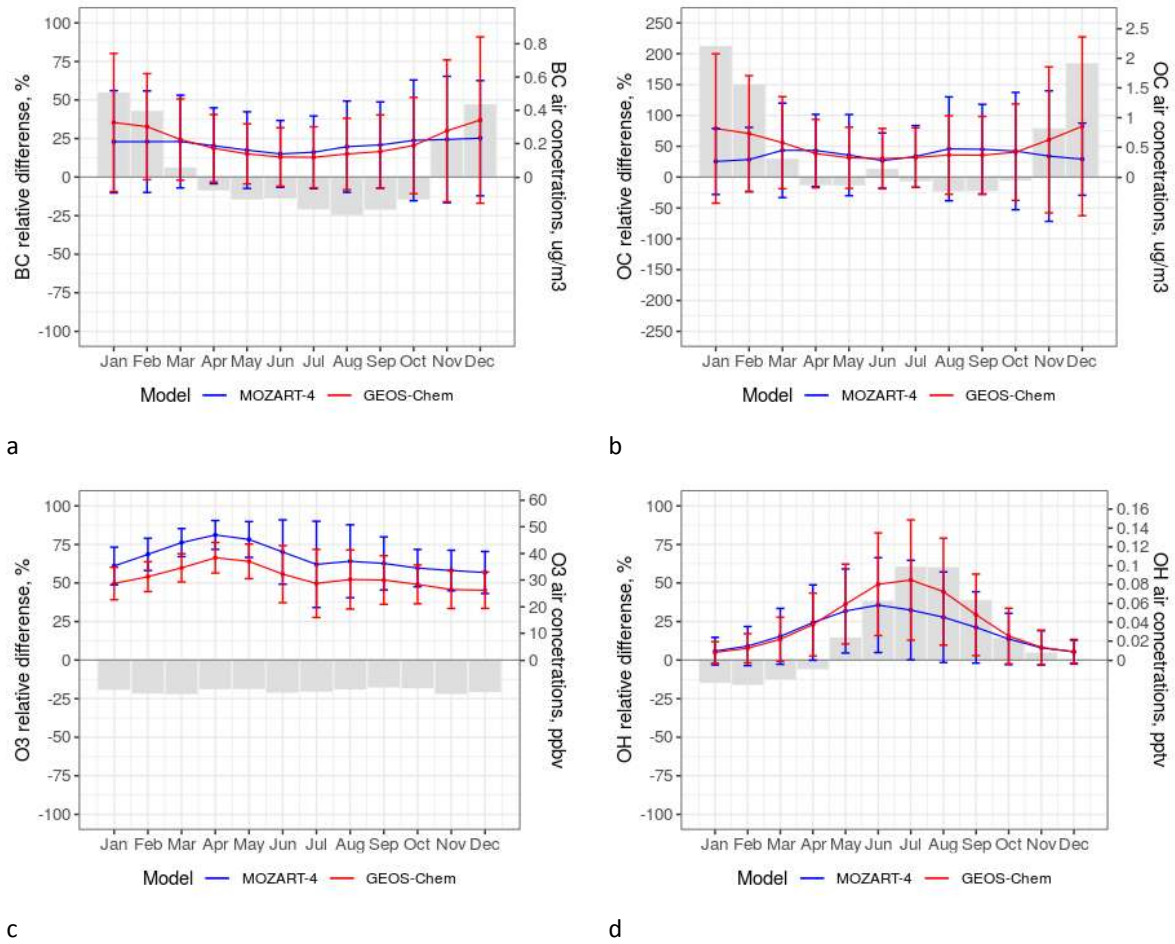

Fig. 4.21. *Comparison of monthly mean elemental carbon (a), organic carbon (b), ozone (c) and hydroxyl radical (d), concentrations obtained from MOZART and GEOS-Chem models in air in the EMEP region in 2015. Gray bars show relative difference between monthly mean concentrations of species, simulated by GEOS-Chem and MOZART models, which is calculaced as difference between GEOS-Chem data and MOZART data divided by MOZART output values and presented as percents.*

Comparison of modelling results with seasonal variations of B(a)P air concentrations, observed at the EMEP monitoring stations, is shown in Fig. 4.20b. Locaton of selected monitoring stations and c criteria of their selection are described in the Technical Report [*Gusev et al.*, 2020b]. It is seen that

the highest under-prediction of observed B(a)P concentrations is obtained for February and January. In the other months all simulated values agree with measurements within a factor of 2.

Results of comparison indicate that modelled B(a)P concentrations in case of GEOS-Chem data were slightly lower comparing to the results based on MOZART data throughout the whole year. Thus, application of GEOS-Chem data led to some decrease of the bias between the GLEMOS model results and measurements. Besides, the spatial and temporal correlations between the modelled and measured B(a)P air concentrations are slightly improved by the use of GEOS-Chem data.

Test model simulations of B(a)P with two datasets on atmospheric reactants and particulate matter showed generally better agreement with measurements in case of data from GEOS-Chem model. Comparing to the MOZART model, the GEOS-Chem model provides a wider range of simulated substances. In particular, unlike the MOZART model, it generates atomic bromine (Br) concentration data, which are required for GLEMOS simulations of mercury. Therefore, the GEOS-Chem model is planned to be preferably used as a chemical preprocessor of reactants concentrations for the GLEMOS model in future.

Chapter 5. COOPERATION

Scientific co-operation is an important part of MSC-E activities aimed at support and improvement of heavy metal and POP pollution assessment within EMEP as well as dissemination of the assessment results to wider international audience. For this purpose MSC-E collaborates with Subsidiary bodies to the Convention and other international organizations and programs.

5.1. Subsidiary bodies of the Convention

Co-operation with Subsidiary bodies of the Convention includes collaborative work with the Working Group on Effects (WGE), the Task Force on Measurements and Modelling (TFMM), the Task Force on Hemispheric Transport of Air Pollution (TF HTAP), and the Task Force on Techno-Economical Issues (TF TEI).

5.1.1. Evaluation of modelling results using data on moss surveys

In the framework of co-operation with WGE, MSC-E took part in the 33rd Task Force meeting of the International Cooperative Programme on Effects of Air Pollution on Natural Vegetation and Crops (ICP-Vegetation) held in Riga, Latvia. MSC-E presented the comparison of Pb, Cd and Hg modelled deposition in the EMEP region with concentrations of these metals in mosses observed in moss survey 2015/2016. Country-mean values of deposition and concentrations in mosses, their long-term trends and spatial distribution were analyzed. The impact of wind re-suspension on pollution levels in different parts of the EMEP region was investigated using the data on measurements in mosses.

Assessment of heavy metal pollution levels in the EMEP countries is carried out using the results of atmospheric modelling and monitoring at the EMEP network. EMEP monitoring data are aimed at reporting concentrations in air, in precipitation and deposition fluxes at daily, weekly or monthly period. However, only the north-western part of the EMEP region is covered by monitoring stations, while in the eastern Europe, Caucuses and Central Asia EMEP stations are rare or absent (Fig. 5.1).

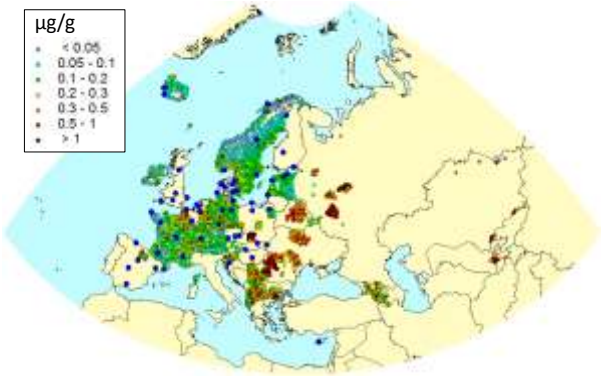

Fig. 5.1. *Location of the EMEP network stations (blue circles) and moss survey plots (dots) in 2015.*

Information about pollution levels could be derived from measurements of heavy metal concentrations in mosses, collected during regular moss surveys. Mosses do not have roots and obtain all nutrients from the atmosphere [*Dołęgowska and Migaszewski*, 2014; *Rühling and Tyler,* 1973; *Harmens et al*., 2010]. Their tissues can accumulate heavy metals from atmospheric deposition. Unlike station-based measurements, temporal resolution of data derived from moss surveys is not high. According to sampling methods, concentrations in mosses characterize amount of heavy metals

accumulated for three-year period [*Harmens et al*., 2010; *ICP-Vegetation*, 2015; *Schröder et al*., 2013]. Besides, concentration in mosses is affected not only by atmospheric deposition, but also by other factors (moss growth rate, sea-spray aerosols etc.) [*Dołęgowska and Migaszewski*, 2014; *Holy et al*., 2009, *Nickel and Schröder*, 2019]. Therefore, interpretation of measurements in mosses could be challenging task. Nevertheless, measurements in mosses can be useful supplementary information for characterization of heavy metal pollution levels.

Country-mean values

One of parameters used in the evaluation of the modelling results is averaged over county's territory concentrations in mosses and deposition flux. For comparability of spatially distributed concentrations and deposition fluxes normalization was carried out: each parameter was divided by its median value. After the normalization, dimensionless deposition fluxes and concentrations in mosses become comparable.

In most of the countries involved in moss survey in 2015/2016, relatively high averaged deposition values agree with relatively high average concentrations in mosses, and vice versa (Fig. 5.2). However, in some countries averaged normalized deposition and concentrations differ markedly. Mosses in the Czech Republic were sampled in the north-eastern part of the country, which is known for the high levels of heavy metal pollution levels compared to other parts of the country [*CHMI*, 2015]. Therefore, high concentrations of Cd and Hg in mosses in the Czech Republic do not characterize the country as a whole. Relatively high levels of Cd and Pb in some countries of south-eastern Europe, Caucasus and Central Asia may be caused by contribution of re-suspended dust affecting sampling in mosses [*Frontasyeva et al*., 2020].

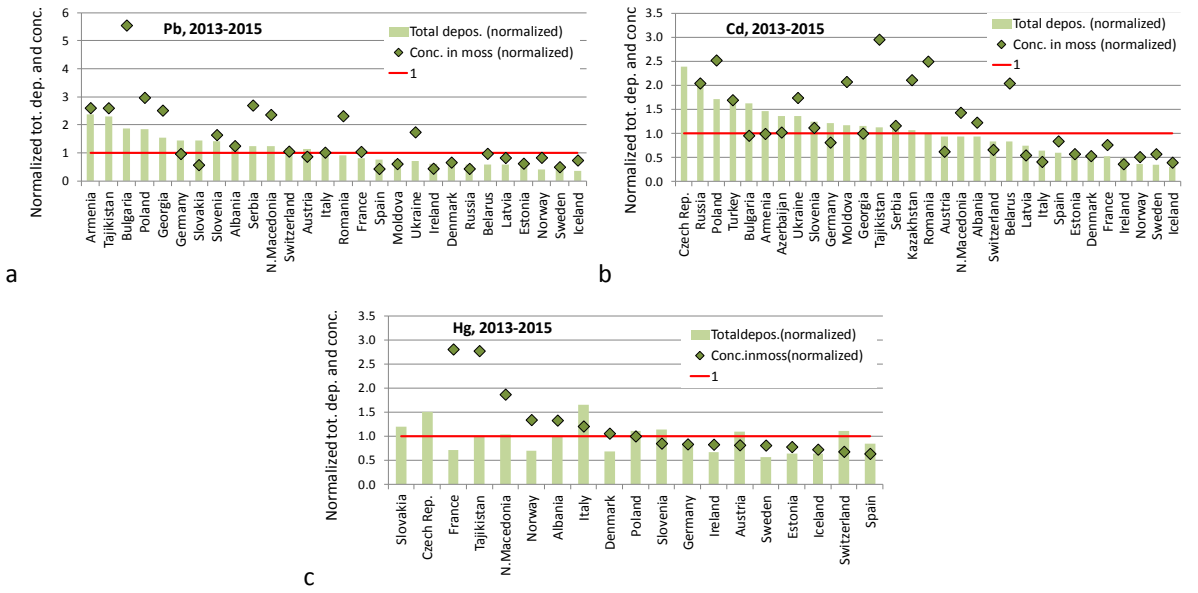

Fig. 5.2. *Average over country's territories normalized deposition fluxes of Pb(a), Cd(b) and Hg(c) in 2013-2015 and concentrations in mosses surveyed in 2015.*

Long-term changes

Another application of moss measurement data is analysis of long-term changes of pollution levels. Pan-European moss surveys have been carried out once in every five years starting from 1990. For the comparison of modeled pollution levels with the observed concentrations in mosses deposition for 1990-2010, calculated in the old EMEP grid were used [*de Wit et al.*, 2015]. For the comparison with the moss data obtained in the 2015/2016 survey, the deposition for 2013-2015 simulated on the new latitude-longitude grid were used. Therefore, the modelled time series are not uniform, and the comparison of long-term changes of concentration in mosses and deposition should be considered as preliminary.

Analysis of the long-term changes of Pb and Cd levels was undertaken for nine countries where measurements in mosses were available for 1990-2015. For this period overall reduction of deposition and concentrations in mosses made up 80 – 90% for Pb (Fig. 5.3) and 35 – 80% for Cd. For Hg less information on measurements in mosses was available, and thus only two countries were found for analysis of changes between 1995 and 2015. The reduction of concentrations in mosses and total deposition ranged from 2 to 40%.

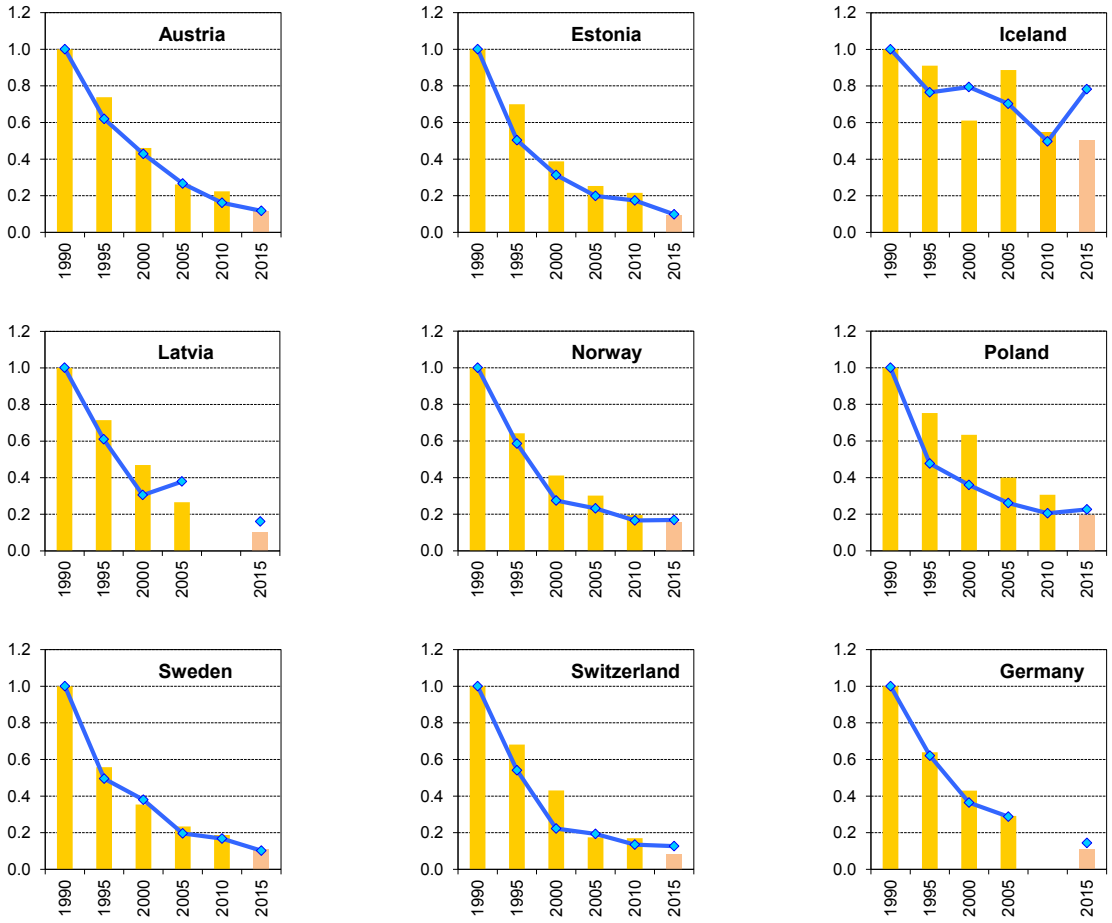

Fig. 5.3. *Long-term changes of Pb normalized concentrations in mosses and deposition fluxes averaged over country's territories in 1990 – 2015.*

Spatial distributions

Since mosses obtain their nutrients from the atmosphere, it is reasonable to assume proportionality of concentrations in mosses and atmospheric total deposition. Therefore, dense spatial coverage of moss measurements could be used for the analysis of spatial distribution of depositions. Spearmen correlation coefficient is used as a measure of similarity of the modelled deposition fields and concentrations in mosses.

The correlation coefficients were calculated between total deposition fluxes averaged over 2013-2015 and the concentrations in mosses in countries participated in the survey for 2015. Relatively high correlation coefficients (0.5 – 0.7) for Pb and Cd were obtained for countries with high spatial gradients of pollution levels, e.g., for Poland, Norway or Sweden (Fig. 5.4). In most of countries the correlation coefficient for Pb, Cd and Hg is low (below 0.4).

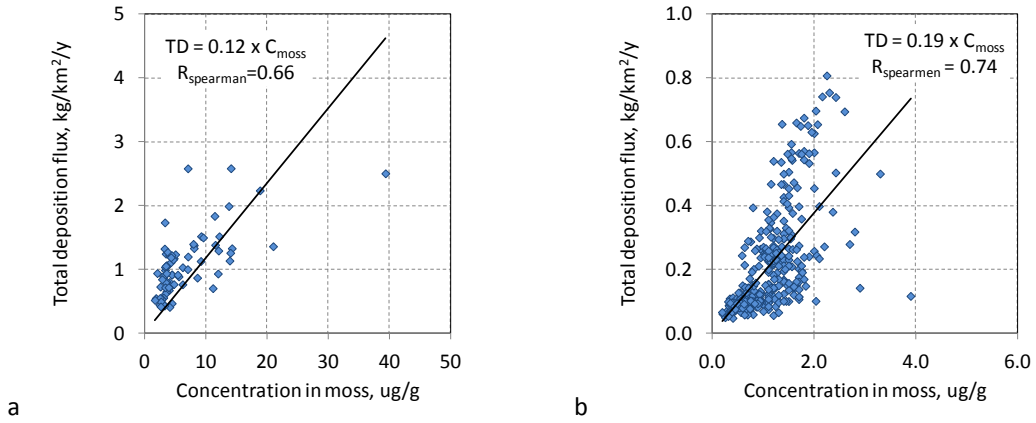

Fig. 5.4. *Comparison of spatial distribution of total deposition fluxes and concentrations in mosses in Poland (a) and Sweden (b)*

Relatively low correlation can be explained by the influence of factors other than deposition. Concentration of heavy metals in mosses can depend on moss species, rate of moss growth, effects of sea-salt aerosols on ionic exchange between moss tissues and ambient air, etc. Joint efforts of modelers and moss monitoring community are needed to investigate these effects and to improve interpretation of heavy metal concentrations in mosses.

Besides, the effect of the modelling factors such as spatial resolution and separation of total deposition into wet and dry components on the correlation were analyzed. It was shown that the change of modelling spatial resolution from 0.4°x0.4° to 0.2°x0.2° favoured some increase of the correlation between deposition fluxes and concentrations in mosses in some countries, e.g., in Slovenia, Switzerland, Russia (Fig. 5.5).

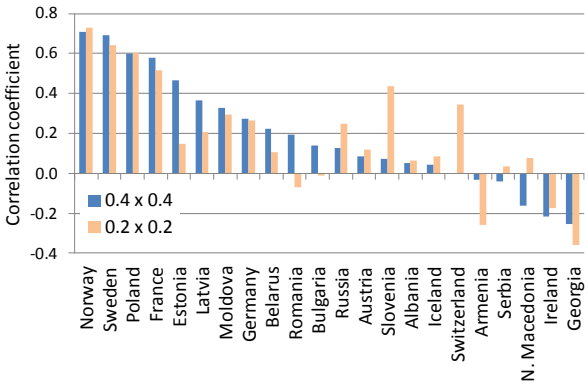

Fig. 5.5. *Spearmen correlation coefficients between Pb concentrations in mosses and total deposition fluxes calculated with resolution 0.4°x0.4° to 0.2°x0.2°.*

Nevertheless, the correlation coefficient remained almost the same in countries where is was relatively high (> 0.5), e.g., in Norway, Sweden, Poland or France. Besides, in some countries, e.g., in Estonia, Romania and Belarus, some decline of the correlation took place. In general, the increase of spatial resolution does not lead to principle improvements of the correlation.

Correlation coefficients between concentrations in mosses and total deposition fluxes were compared with the correlations with wet and dry deposition fluxes. On one hand, correlation coefficients calculated for wet and dry fluxes remain below 0.5 – 0.6 for most of countries (Fig. 5.6). On the other hand, marked differences in the correlation coefficients are noted for some countries. For example, Rc in Switzerland for total deposition of Cd flux is 0.45. However, for wet deposition flux the Rc is around zero, while for the dry flux is 0.58. Similar increase of Rc for dry deposition flux and decline for wet deposition flux is observed for Latvia, Albania, North Macedonia, Georgia. It can be supposed that dry deposition is better predictor for concentrations in mosses than total or wet deposition. However, more research is needed to test this assumption. Dry deposition flux strongly depends on type of the underlying surface. As a rule, dry deposition velocity is higher in forests compared to low vegetation environments because of larger surface area for taking up pollutants. *Nickel S. and Schröder W.* [2019] demonstrated that leaf area index can be even stronger predictor that total deposition flux for interpretation of spatial distribution of concentrations of Pb and Cd in mosses in Germany. Therefore, in further work on comparison of deposition fluxes and concentrations in mosses it will likely be important to take into account land-cover type where the mosses are sampled.

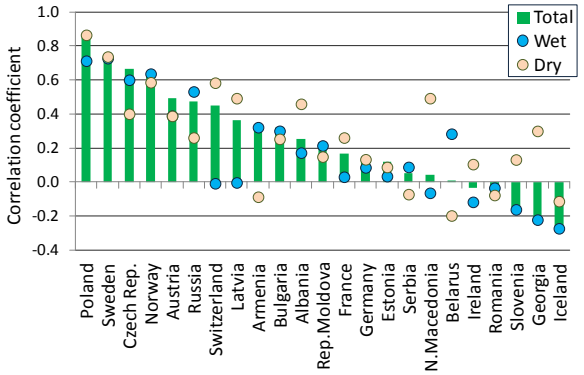

Fig. 5.6. *Spearmen correlation coefficients between Cd concentrations in mosses and total, wet and dry deposition fluxes.*

Modelled information about source attribution of pollution levels can be important for interpretation of measured levels of heavy metals in mosses. Levels of heavy metals in mosses sampled in Central Asia and the south-eastern part of Europe are substantially higher than those in the north-western part of the EMEP region. These high levels are partly caused by anthropogenic emissions and by re-suspension of dust containing heavy metals, especially by contribution of re-suspension from bare lands (deserts). This contribution varies from 15% to 70% (Fig. 5.7).

Results of the atmospheric modelling and biomonitoring were used to evaluate the role of wind re-suspension in the south-eastern part of the EMEP region. Biomonitoring data contain information on aluminium (Al) and iron (Fe). These elements are abundant in soils and rocks [*Kabata-Pendias*, 2010] and are often used as reference elements for investigation of enrichment of pollution relative to background levels [e.g., *Paripurnanda et al.*, 2013]. Similar to Cd and Pb, concentrations in mosses of these crustal elements is much higher in the south-eastern part of the EMEP region (Central Asia, Caucasus, south-eastern Europe) compared to north-western part (Central, Western Europe, Scandinavia) (Fig. 5.8).

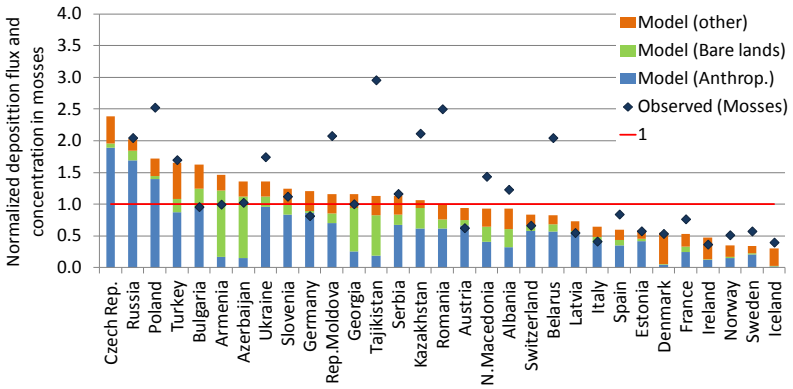

Fig. 5.7. *Normalized country-averaged deposition fluxes of Cd caused by different emission sources in 2013-2015 and concentrations in mosses surveyed in 2015.*

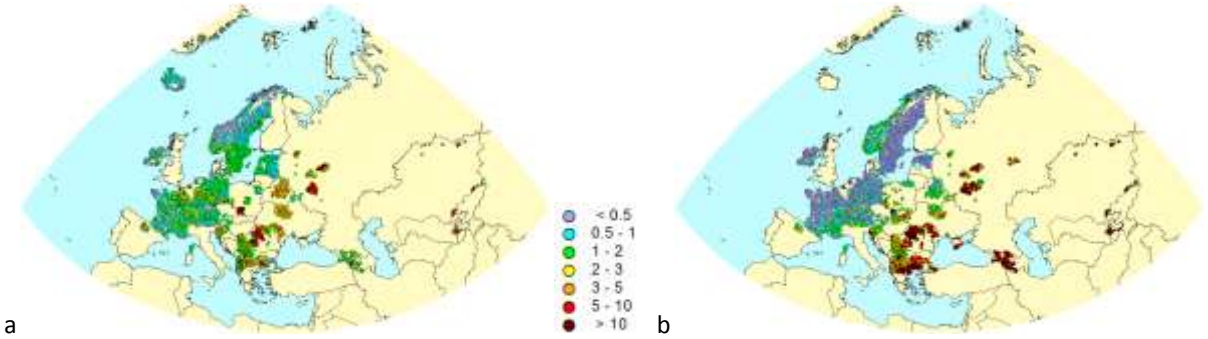

a b

Fig. 5.8. *Normalized concentrations of Cd (a) and Al (b) in mosses surveyed in 2015*

In order to characterize a potential role of wind re-suspension from bare lands, the ratios of observed normalized concentrations of Al and Fe to Cd and Pb measured in mosses was introduced. To identify the role of re-suspension from bare land a ratio of modeled deposition from secondary (bare lands) and anthropogenic sources was used. These modelled and observed ratios for Cd and Pb are depicted in Fig. 5.9. Relatively high modeled and observed ratios are noted for countries in Caucasus (Armenia, Azerbaijan, Georgia) and Central Asia (Tajikistan). It means that both the model and measurements reflect high contribution of wind re-suspension compared to other EMEP countries. The ratios in the western part of the EMEP region are low. It means that contribution of wind re-suspension from bare lands to deposition is much smaller than the contribution from the anthropogenic sources.

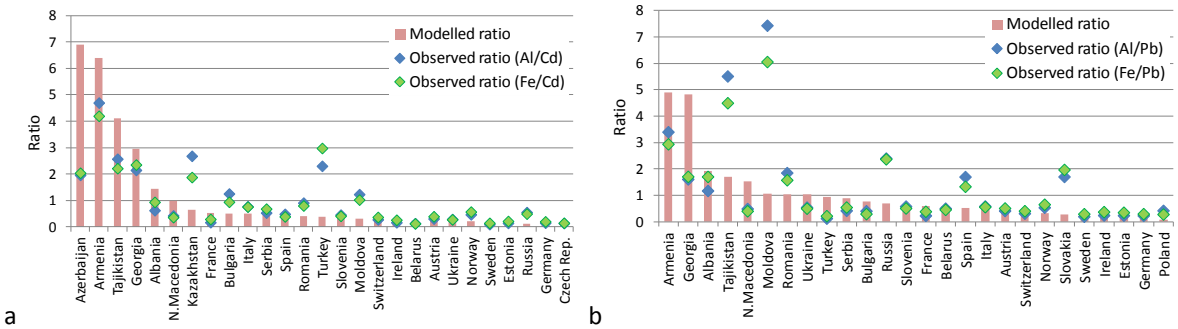

a b

Fig. 5.9. *Ratios of modelled deposition re-suspension from bare lands and from anthropogenic sources (modelled ratio) and ratios of normalized concentrations of Al and Fe to Cd and Pb measured in mosses (observed ratio) for Cd (a) and Pb (b)*

For some countries the difference between modeled and observed ratios is significant. For example, the observed high ratios for Cd are noted in Kazakhstan and Turkey, and for Pb – in Tajikistan and Republic of Moldova. These discrepancies can be caused by uncertainties of anthropogenic emissions or modeled wind re-suspension of heavy metals in these regions or peculiarities of moss sampling.

The results presented in this section demonstrate that the biomonitoring results can be successfully used for the verification of modelled deposition fluxes averaged over country's territory and their long-term changes. Besides, the use of moss measurements favoured evaluation of secondary sources in the southern regions of the EMEP. For the analysis of spatial distribution of heavy metals various factors have to be taken into account. Cooperation between the modelling community and experts from WGE/ICP-Vegetation is needed to facilitate progress in the interpretation of moss measurement results and analysis of heavy metal pollution in the EMEP region.

5.1.2. Task Force on Measurements and Modelling

The outcome of MSC-E activities related to the model assessment of heavy metal and POP pollution in the EMEP region was discussed at the recent online TFMM meeting held this year in May.

In particular, results of a national-scale case study of heavy metal pollution in Germany were presented. They included modelled levels of Pb, Cd and Hg in Germany in 2014-2016 and their evaluation against EMEP and national measurement data. Possible reasons of the identified discrepancies between modelled and observed levels were analyzed. It was shown that fine resolution modelling on a country scale provided detailed patterns of heavy metal pollution and reasonably reproduces background EMEP measurements. The inclusion of measurement data from national monitoring networks significantly increased the potential of the modelling results verification. More detailed description of this work is presented in section 4.2.

The progress in the assessment of POP pollution in the EMEP region was outlined with focus on the pollution by toxic PAHs. Main emphasis in this work was given to the evaluation of contemporary PAH pollution levels and their trends during the two recent decades. It was shown that observed and modelled air concentrations of the 4 PAHs, defined in the POP Protocol, were still high and continued to exceed air quality guidelines. To improve assessment of B(a)P long-range transport and seasonal variability, research activities in framework of B(a)P case study for Poland and multi-model analysis of B(a)P pollution within the EMEP EuroDelta-Carb inter-comparison were initiated. Along with this, importance of consideration of wider list of toxic PAHs was emphasized and experimental model simulations were carried out to estimate population exposure to mixture of 16 toxic PAHs. Specific attention was also paid to the interaction of PAHs and PM in the atmosphere, and contribution of toxic PAHs to the adverse effects of aerosol particles. Finally, it was stressed that this work was considered as the contribution to the analysis of the effectiveness of POP Protocol in line with the Long-term Strategy of the Convention.

A number of research issues and initiatives related to air pollution modelling were discussed at the TFMM meeting. Some of them could be further applied for the analysis of heavy metal and POP pollution levels. In particular, joint EMEP initiative on evaluation of COVID-19 lockdown effect on pollution levels was considered as future TFMM activity.

5.1.3. Task Force on Hemispheric Transport of Air Pollution

Long-term trends of heavy metal and POP pollution within the EMEP region have been recently analyzed as a part of the CLRTAP assessment [*Maas and Grennfelt*, 2016; *Colette et al.*, 2016]. However, a number of questions with regard to reasons of the long-term changes of pollution levels remain unanswered. It particularly relates to pollutants, which are characterised by global dispersion in the atmosphere and accumulation in other environmental media, such as Hg and some POPs.

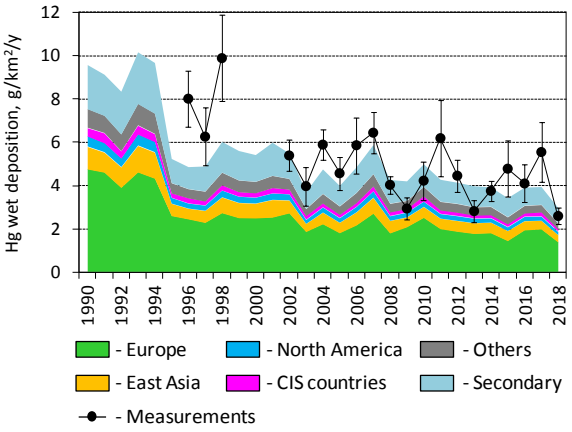

Fig. 5.10. *Long-term changes of annual Hg wet deposition at measurement site DE9 (Zingst, Germany)*

To answer the questions MSC-E is initializing (in accordance with the EMEP bi-annual workplan) the work on model retrospective analysis of the key factors affecting long-term changes of Hg and POP levels in the EMEP and other regions (Fig. 5.10). The study will be performed in collaboration with the POP and Hg scientific communities within the framework of the Task Force on Hemispheric Transport of Air Pollution (TF HTAP). Preliminary program of the study includes:

1. Review of available global Hg and POP emissions inventories;
2. Collection of long-term measurements from the EMEP and other monitoring networks;
3. Model assessment of long-term trends of Hg and POP pollution in the EMEP and other regions;
4. Analysis of key drivers of long-term pollution changes including
    - Anthropogenic emissions (EMEP vs. non-EMEP);
    - Secondary emissions from land and sea surfaces;
    - Meteorological conditions (climate change);
    - Surface conditions (land use, ice cover etc.)

Formation of the expert communities and discussion of the research program are planned at a series of virtual meetings to be organized in October-November 2020 under support and guidance of TF HTAP.

5.1.4. Task Force on Techno-Economical Issues

Further reduction of PAH pollution levels in the EMEP countries is an important direction of work emphasized in the Long-term Strategy of the Convention. Specific attention in this respect is paid to the reduction of emissions from residential combustion and biomass burning as prevailing source categories for PAHs. Important contribution to this activity is the preparation of the Code of good practice for wood-burning and small combustion installations, carried out by TF TEI

[ECE/EB.AIR/2019/5, 2019]. This document is aimed to provide recommendations on good practices and best available techniques for domestic wood heating installations that would lead to the reduction of PAH emissions.

In line with the workplan, MSC-E continues analysis of information on trends in PAH pollution levels as well as on the exceedances of air quality guidelines in the EMEP region. In particular, information on PAH emissions in the reported national inventories for the 4 PAHs of the POP Protocol is analyzed. Besides, collection and analysis of physical-chemical properties and expert estimates of emissions for wider list of PAHs is carried out. Long-term changes of PAH pollution levels are evaluated on the basis of the monitoring data and modelling results. An overview of progress in this work is presented in Section 4.1 of this report. More detailed information can be found in the Technical report [*Gusev et al.*, 2020b].

5.2. International organizations

The Centre actively participates in cooperation with other international organizations and programmes to facilitate information exchange and improve quality of the pollution assessment both in the EMEP region and on wider scales. This year international co-operation was focused on scientific collaboration with the Arctic Monitoring and Assessment Programme, the Stockholm and Minamata Conventions and the Helsinki Commission.

5.2.1. Arctic Monitoring and Assessment Programme

EMEP continues long-term co-operation with the Arctic Monitoring and Assessment Programme (AMAP). Currently, MSC-E participates in the on-going AMAP Assessment of the Arctic pollution by Hg providing the results of model simulations and contributing to preparation of the report. In particular, the Centre processes and illustrates multi-model simulations of Hg pollution levels in the Arctic based on both previous [*AMAP/UN Environment*, 2019] and new simulation results. Four chemistry transport models for Hg take part in the study – GLEMOS (EMEP/MSC-E), GEOS-Chem (Massachusetts Institute of Technology, USA), GEM-MACH-Hg (Environment and Climate Change Canada, Canada), DEHM (Institute of Atmospheric Pollution Research, Denmark). The modelling results are evaluated against measurements of Hg^0 air concentration and wet deposition in the Arctic and adjacent areas.

Figure 5.11 shows simulated spatial distribution of annual Hg^0 air concentration and Hg wet deposition in the Arctic. The air concentration gradually decreases from 1.45 ng/m^3 in the European sector of the Arctic to 1.3 ng/m^3 over the Canadian Archipelago (Fig. 5.11a). Surface air concentrations of Hg^0 in the high Arctic vary seasonally decreasing in spring because of the atmospheric Hg depletion events (AMDEs) and increasing in summer due to intensive re-emission from snow. The modelled Hg^0 air concentrations in the Arctic well agree with available observations. The largest Hg wet deposition fluxes (above 7 μg/m^2/y) are predicted over the Northern Atlantic and

the Norwegian Sea, whereas the lowest fluxes (below 3 μg/m^2/y) are over Greenland, the Canadian Archipelago and Eastern Siberia (Fig. 5.11b). The models tend to somewhat overestimate observed wet deposition in the high Arctic due to peculiarities of Hg scavenging from the atmosphere by precipitation at low temperatures.

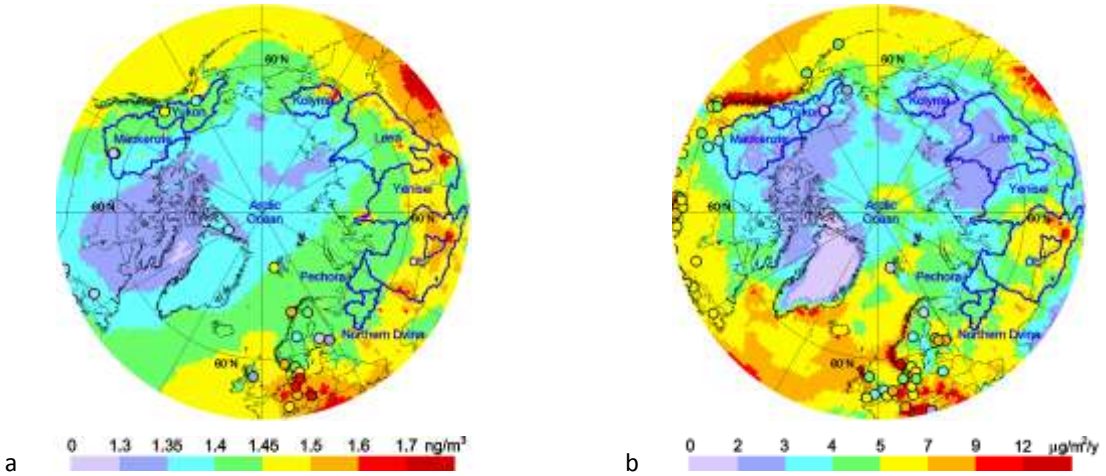

Fig. 5.11. *Model ensemble median Hg^0 concentration in surface air (a) and Hg wet deposition flux (b) in 2015. Circles show observations in the same color scale.*

Spatial pattern of total Hg deposition reflects spatial variations of both wet and dry deposition fluxes. The highest Hg deposition occurs over terrestrial areas of Northern Europe, the Northern Atlantic and the Greenland Sea (Fig. 5.12a). Larger Hg deposition is also simulated in the sub-Arctic regions of Europe, Siberia and Canada. It is particularly important when considering deposition to watersheds of large Arctic rivers, which accumulate and bring Hg to the Arctic Ocean. The rivers run-off is considered among the largest sources of Hg in the Arctic Ocean [*Sonke et al.*, 2018]. Simulated average Hg deposition fluxes to watersheds of the largest Arctic rivers are shown in Fig. 5.12b. The largest deposition fluxes are characteristics of the watershed of Northern Dvina and Ob (12 μg/m^2/y), whereas the lowest occur over the Kolyma catchment (7 μg/m^2/y).

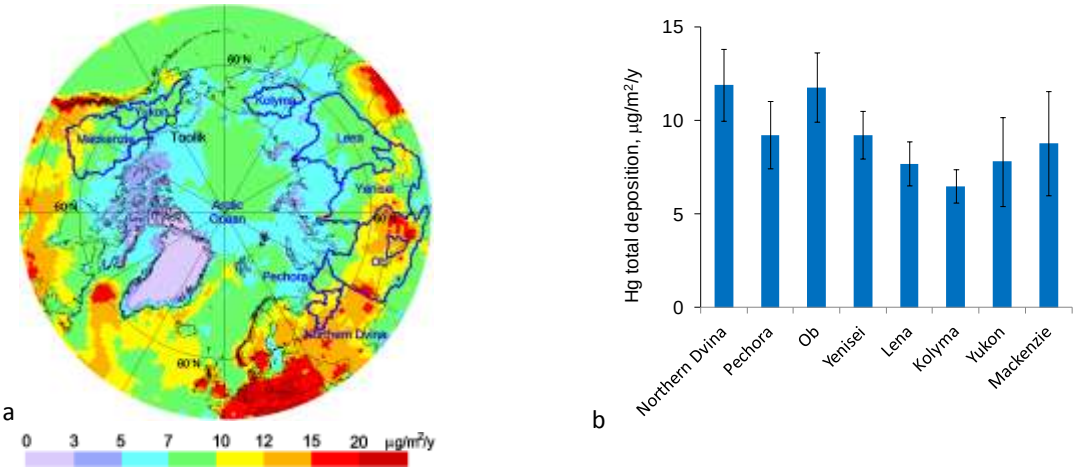

Fig. 5.12. *Model ensemble median Hg deposition in the Arctic (a) and average deposition flux to watersheds of the largest Arctic rivers (b) in 2015.*

Total atmospheric deposition of Hg to the Arctic varies significantly along the year. The largest atmospheric load of Hg to the terrestrial part of the Arctic (north 60°N) is 26 tonnes/month in summer due to increased Hg^0 photo-oxidation in the atmosphere and enhanced dry deposition to vegetation. The lowest deposition is in winter (2 tonnes/month). In contrast, the largest atmospheric input of Hg to the aquatic part of the Arctic takes place in spring (22 tonnes/month) due to effect of AMDEs. Mercury deposition to the Arctic is largely affected by contribution of natural and secondary sources (63-74%). Deposition from contemporary emission sources is dominated by contribution of East Asia (10%), which is followed by Africa (4%), Europe (3%) and the CIS countries (3%).

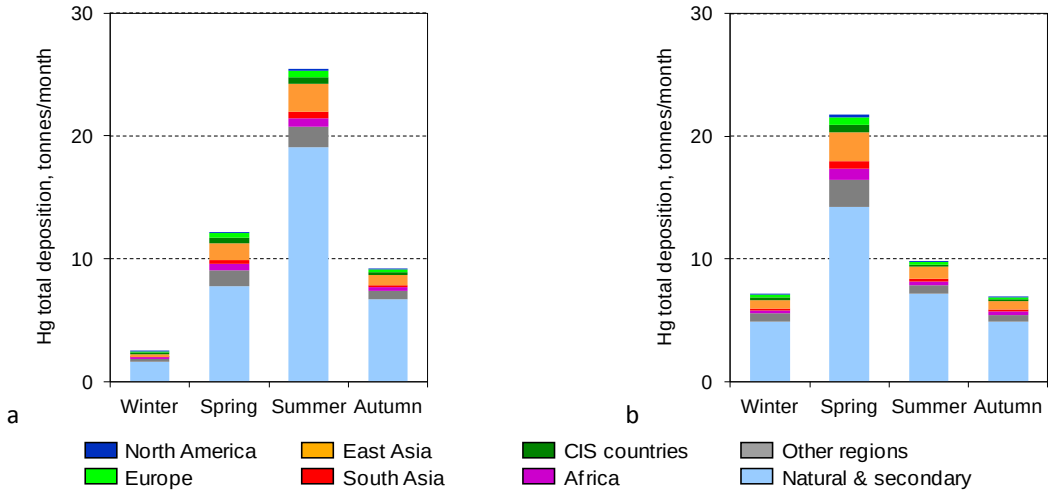

Fig. 5.13. *Source apportionment of Hg deposition to terrestrial (a) and aquatic (b) areas of the Arctic (north 60°N) in different seasons of 2015.*

Co-operation with the Arctic Monitoring and Assessment Programme on assessment of heavy metal and POP pollution is strategic direction of the EMEP activities that leads to mutual outreach, information-sharing and, ultimately, improvement of the pollution assessment.

5.2.2. Stockholm and Minamata Conventions

This year MSC-E continued co-operation with experts of the Stockholm Convention on POPs. There is a process of the preparation of the third global and regional monitoring reports (GMP-3) under the Stockholm Convention, initiated in 2019. In framework of this activity, updating of monitoring data on POPs, collected in the Global Monitoring Plan Data Warehouse (GMP DWH), is carried out. New monitoring data are being included into the GMP DWH database and harmonized with previous content. MSC-E took part in the webinar organized by RECETOX to present information on the updating of GMP DWH database, and on the outputs of POP data harmonization and visualization tools. During this meeting various aspects related to the usage of data in the analysis of POP pollution levels were discussed.

In addition, MSC-E continues following the activities of the scientific and policy making communities aimed at support and development of the Minamata Convention on Mercury. In particular, the Centre presented the new research results and participated in discussion of the topical issues related

to Hg pollution on a global scale at the 14th International Conference on Mercury as a Global Pollutant held in Krakow, Poland in September 2019. Besides, various aspects of Hg pollution on both hemispheric and global scales are a subject of discussion within the Task Force on Hemispheric Transport of Air Pollutants (TF HTAP) (Section 5.1.3). Closer integration of the relevant activities within TF HTAP and the Minamata Convention could facilitate resolving the Hg pollution problem both in the EMEP region and on a global scale.

5.2.3. Helsinki Commission

In accordance with the Memorandum of Understanding between the Baltic Marine Environment Protection Commission (HELCOM) and the United Nations Economic Commission for Europe (UN ECE) MSC-E continued cooperation with HELCOM and carried out evaluation of airborne pollution load of heavy metals and POPs to the Baltic Sea. This work is performed on the basis of the long-term contract between EMEP and HELCOM.

This year long-term variations of Pb, Cd, Hg, and PCDD/Fs deposition fluxes to the Baltic Sea were estimated for the period 1990-2017. Along with this, source apportionment of annual deposition was carried out for 2017. Results of the assessment were summarized in the Joint report of the EMEP Centres for HELCOM [*Gauss et al*., 2019] and presented in the indicator fact sheets, published on the HELCOM website (*http://www.helcom.fi*).

Anthropogenic emissions of Pb, Cd, Hg, and PCDD/Fs in the HELCOM countries declined from 1990 to 2017 by 89%, 36%, 48%, and 35%, respectively. Russia, Poland, and Germany were the main contributors to the emissions among the HELCOM countries in 2017. Their share in total emission of the HELCOM countries exceeded 90% for these pollutants. The most noticeable drop of Pb, Cd, Hg, and PCDD/F emissions took place in the beginning of 1990s, while during the subsequent period of time the changes were less significant and were almost levelled off for some pollutants (Fig. 5.14a).

Model assessment of long-term variations of pollution indicated considerable decrease of atmospheric deposition of Pb (by 81%), Cd (by 59%), and PCDD/Fs (by 72%) to the Baltic Sea in the period 1990-2017, whereas Hg deposition declined within this period by only 29% (Fig. 5.14b). It is seen that deposition of selected pollutants are subject of noticeable inter-annual variations that reflects the influence of changes of meteorological conditions from year to year (e.g. changes of atmospheric transport pathways, precipitation amount). The decrease of deposition varies substantially among different sub-basins of the Baltic Sea. In particular, the largest decrease of Cd and Pb deposition took place in the Bothnian Bay sub-basin (by 76% and 89%, respectively), Hg deposition in the Sound sub-basin (by 52%), PCDD/F deposition in the Gulf of Riga sub-basin (by 60%).Anthropogenic emission sources of the HELCOM countries contributed to annual Pb, Cd, Hg, and PCDD/Fs deposition to the Baltic Sea in 2017 about 30%, 36%, 14%, and 47%, respectively. Russia, Poland, and Germany were the main contributors of anthropogenic Pb, Cd, Hg, and PCDD/Fs deposition to the Baltic Sea. Along with anthropogenic emissions significant contribution (more than 50%) to deposition of considered pollutants to the Baltic Sea was made by secondary emission sources (e.g. re-emission from soil and sea water compartments) as well as by the long-range transport from the emission sources located outside the HELCOM countries.

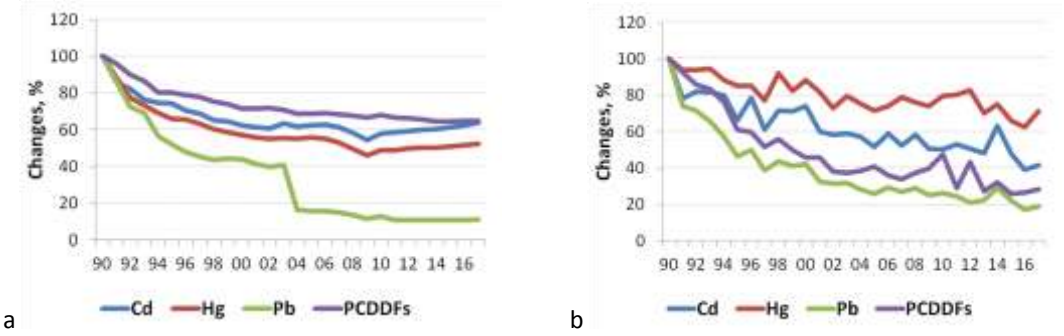

Fig. 5.14. *Relative changes of annual total emissions of HELCOM countries (a) and annual atmospheric Pb, Cd, Hg, and PCDD/F deposition to the Baltic Sea in the period 1990-2017 (b)*

The information on airborne input of Pb, Cd, Hg, and PCDD/Fs to the Baltic Sea was presented and discussed during the 11th Meeting of the Working Group on Reduction of Pressures from the Baltic Sea Catchment Area (HELCOM PRESSURE 11-2019) held in Brussels, Belgium, in October 2019.

6. MAIN CHALLENGES AND DIRECTIONS OF FUTURE RESEARCH

The Status Report summarizes EMEP activities in the field of heavy metal and POP pollution assessment in 2020. It contains information on heavy metal and POP pollution levels, transboundary transport between the EMEP countries, ecosystem-specific deposition etc. It also describes research and development activities aimed at improvement of the modelling tools as well as cooperation with national experts of the EMEP countries, CLRTAP Subsidiary Bodies, and international organizations. Main challenges of heavy metal and POP pollution assessment and directions of future research are outlined below.

- High levels and slow decrease of PAH air concentrations in the EMEP countries are recognized as an important issue by the Long-term Strategy of the Convention that highlights the need of scientific research to support the efforts for reduction of PAH emissions and pollution levels. Detailed assessment of trends in observed and modelled PAH concentrations, contributions of the key emission sources, and exceedances of the EU and WHO target levels will be further performed to support activities of TF Health and WGE as well as to contribute to the analysis of the effectiveness of the POP Protocol in co-operation with TFTEI.

- Model parameterizations of B(a)P sorption to various components of aerosol particles, and heterogeneous reactions of particle-bound B(a)P with ozone are subject of significant uncertainties. The work on improvement of the model parameterizations of these processes will be continued. A multi-model analysis for B(a)P pollution is planned for further improvement of the quality of B(a)P modelling in the framework of the EMEP EuroDelta-Carb intercomparison exercise in co-operation with TFMM and national experts. Besides, detailed assessment of PAH pollution in Poland will be carried out with emphasis on evaluation of air quality guidelines exceedances and testing national emissions data.

- Mercury pollution remains to be a topic issue addressed in both the Convention and other international bodies. However, the knowledge on Hg cycling and accumulation in the environment is still incomplete. In particular, chemical transformations of Hg in the atmosphere are poorly understood as well as the air-surface exchange processes. Therefore, testing the newly discovered Hg oxidation and photo-reduction mechanisms will be continued in co-operation with other research groups. Besides, additional attention will be paid to Hg exchange processes between the atmosphere and other environmental media (water bodies, vegetation etc.) for evaluation of long-term Hg accumulation and ecosystems exposure.

- Mercury and some POPs are characterized by long residence time and transport potential in the atmosphere as well as by cycling and accumulation in various environmental media. Therefore, assessment of Hg and POP pollution in the EMEP countries should take into account contribution of direct anthropogenic and secondary emissions from both regional and global sources. Besides, relative importance of these source types can change in time due to reduction of anthropogenic emissions. A retrospective analysis of long-term changes of Hg and POP pollution will be performed in co-operation with TF HTAP to identify the key drives of the pollution changes.

- Detailed assessment of heavy metal and POP pollution on a national scale is performed within a framework of country-specific studies in co-operation with national experts and involving variety of national data. A recent study for Germany provided a lot of useful information on heavy metal pollution levels in the country but also revealed a number of issues connected with national emissions, monitoring and model estimates. The discovered issues will be further examined in order to improve assessment of heavy metal pollution on both national and regional scales.

- Heavy metals and POPs occur in the atmosphere being partly or fully bound to aerosol particles. Besides, toxicity of these pollutants can contribute to the adverse effects caused by particulate matter on human health and biota. In order to reach further progress in the assessment of heavy metal and POP pollution, more attention has to be paid to particle-related processes occurred with heavy metals and POPs in the atmosphere.

- Evaluation of adverse effects of heavy metal and POP pollution on human health and ecosystems is of high importance. MSC-E will continue long-term co-operation with WGE focusing on joint analysis of heavy metal measurements in moss in co-operation with ICP Vegetation, support of ICP Integrated Monitoring, ICP Forests and ICP Waters with information on Hg deposition to various ecosystems as well as data exchange with TF Health on B(a)P pollution levels and exceedances of air quality guidelines.

REFERENCES

Aas W., Breivik K., Nizzetto P.B., Pfaffhuber K.A. [2020] Heavy metals and POP measurements 2020 EMEP/CCC-Report 3/2020.

Abdel-Shafy, H. I., & Mansour, M. S. M. [2016]. A review on polycyclic aromatic hydrocarbons: Source, environmental impact, effect on human health and remediation. Egyptian Journal of Petroleum, 25(1), 107–123. doi:10.1016/j.ejpe.2015.03.011.

Akyüz M., H. Çabuk [2010] Gas–particle partitioning and seasonal variation of polycyclic aromatic hydrocarbons in the atmosphere of Zonguldak, Turkey, Science of the Total Environment 408 (2010) 5550–5558.

ALS [2013] Benzo(a)pyrene toxic equivalence quotient (TEQ) and aggregate organochlorine pesticides parameters, *EnviroMail* No. 59 Re-Release, July, 2013.

AMAP/UN Environment [2019] Technical Background Report for the Global Mercury Assessment 2018. Arctic Monitoring and Assessment Programme, Oslo, Norway/UN Environment Programme, Chemicals and Health Branch, Geneva, Switzerland. viii + 426 pp including E-Annexes.

AMAP/UNEP [2013] Technical Background Report for the Global Mercury Assessment 2013a. Arctic Monitoring and Assessment Programme, Oslo, Norway / UNEP Chemicals Branch, Geneva, Switzerland, vi + 263 pp., available at: http://www.amap.no/documents/download/1265 (last access: 10 April 2018).

Amos, H. M., Jacob, D. J., Holmes, C. D., Fisher, J. A., Wang, Q., Yantosca, R. M., Corbitt, E. S., Galarneau, E., Rutter, A. P., Gustin, M. S., Steffen, A., Schauer, J. J., Graydon, J. A., Louis, V. L. St., Talbot, R. W., Edgerton, E. S., Zhang, Y., and Sunderland, E. M. [2012] Gas-particle partitioning of atmospheric Hg(II) and its effect on global mercury deposition, Atmos. Chem. Phys., 12, 591–603, doi:10.5194/acp-12-591-2012.

Balabanov N., Shepler B., Peterson K. [2005] Accurate global potential energy surface and reaction dynamics for the ground state of HgBr2, J. Phys. Chem. A, 109, 8765—8773.

Balmer J.E., Hung H., Yu Y., Letcher R.J., & Muir D.C.G. [2019]. Sources and environmental fate of pyrogenic polycyclic aromatic hydrocarbons (PAHs) in the Arctic. Emerging Contaminants, 5, 128–142. doi:10.1016/j.emcon.2019.04.002.

Barber J.L, G.O. Thomas, G. Kerstiens, K.C. Jones [2004] Current issues and uncertainties in the measurement and modelling of air–vegetation exchange and within-plant processing of POPs, Environmental Pollution 128 (2004) 99–138.

Barber J.L., P.B. Kurt, G.O. Thomas, G. Kerstenes, K. Jones [2002] Investigation into the Importance of the Stomatal Pathway in the Exchange of PCBs between Air and Plants, Environ. Sci. Technol. 2002, 36, 4282-4287.

Beyer A., Wania F., Gouin T., Mackay D., & Matthies M. [2003] Temperature dependence of the characteristic travel distance. *Environmental Science & Technology, 37*, 766-771.

Bieser J., Slemr F., Ambrose J., Brenninkmeijer C., Brooks S., Dastoor A., DeSimone F., Ebinghaus R., Gencarelli C.N., Geyer B., Gratz L.E., Hedgecock I.M., Jaffe D., Kelley P., Lin C.-J., Jaegle L., Matthias V., Ryjkov A., Selin N.E., Song S., Travnikov O., Weigelt A., Luke W., Ren X., Zahn A., Yang X., Zhu Y., and Pirrone N. [2017] Multi-model study of mercury dispersion in the atmosphere: vertical and interhemispheric distribution of mercury species, Atmos. Chem. Phys., 17, 6925-6955, doi: 10.5194/acp-17-6925-2017.

Blunden, J. and D. S. Arndt, Eds., [2019]. State of the Climate in 2018. *Bull. Amer. Meteor. Soc.*, **100** (9), Si–S305, doi:10.1175/2019BAMSStateoftheClimate.1.

Bogdal C., Müller C.E., Buser A.M., Quante M., Wang Z., Scheringer M., Gerecke A.C., Schmid P., Zennegg M., MacLeod M. and K.Hungerbühler [2014] Emissions of Polychlorinated Biphenyls, Polychlorinated Dibenzo-p-dioxins, and Polychlorinated Dibenzofurans during 2010 and 2011 in Zurich, Switzerland. *Environ. Sci. Technol.,* 48, 482−490.

Breivik K., Alcock R., Li Y.-F., Bailey R.E., Fiedler H. and J.M.Pacyna [2004] Primary sources of selected POPs: regional and global scale emission inventories. *Environmental Pollution,* 128, 3–16.

Breivik K., Sweetman A., Pacyna J.M. and K.C.Jones [2007] Towards a global historical emission inventory for selected PCB congeners - A mass balance approach-3. An update. *Science of the Total Environment*, 377, 296-307.

Brooks, S., Xinrong, R., Cohen, M., Luke, W. T., Kelley, P., Artz, R., Hynes, A., Landing, W., and Martos, B. [2014] Airborne Vertical Profiling of Mercury Speciation near Tullahoma, TN, USA, Atmosphere, 5, 557–574, https://doi.org/10.3390/atmos5030557, 2014.

Brubaker, W.W., & Hites, R.A. [1998]. OH reaction kinetics of polycyclic aromatic hydrocarbons and polychlorinated dibenzo-p-dioxins and dibenzofurans. Journal of Physical Chemistry A, 102, 915-921.

Cheruyiot N.K., W.-J. Lee, J.K. Mwangi , L.-C. Wang, N.-H. Lin, Y.-C. Lin, J. Cao, R. Zhang , G.-P. Chang-Chien [2015] An Overview: Polycyclic Aromatic Hydrocarbon Emissions from the Stationary and Mobile Sources and in the Ambient Air, Aerosol and Air Quality Research, 15: 2730–2762.

CHMI [2015]. Air pollution in the Czech Republic. Graphic Yearbook, 2015. Czech Hydrometeorological Institute. http://portal.chmi.cz/historicka-data/ovzdusi?l=en. Visited 12.02.2020.

Cincinelli A., M. Del Bubba, T. Martellini, A. Gambaro, L. Lepri [2007] Gas-particle concentration and distribution of n-alkanes and polycyclic aromatic hydrocarbons in the atmosphere of Prato (Italy), Chemosphere 68 (2007) 472–478.

Coburn S., B. Dix, E. Edgerton, C. D Holmes, D. Kinnison, Q. Liang, A. Ter Schure, S. Wang, and R. Volkamer [2016] Mercury oxidation from bromine chemistry in the free troposphere over the southeastern US, Atmospheric Chemistry and Physics, 16(6), 3743–3760, doi:10.5194/acp-16-3743-2016.

Colette A. et al. [2016] Air pollution trends in the EMEP region between 1990 and 2012. EMEP: CCC-Report 1/2016, Kjeller, Norway.

Dachs J. and Eisenreich S.J. [2000] Adsorption onto aerosol soot carbon dominates gas-particle partitioning of polycyclic aromatic hydrocarbons, Environ. Sci. Technol., 34, 3690–3697, doi:10.1021/es991201.

Danish EPA [2013] Polyaromatic Hydrocarbons (PAH). Evaluation of health hazards and estimation of a quality criterion in soil, Environmental Project No. 1523, 2013; ISBN no. 978-87-93026-78-0 https://www2.mst.dk/Udgiv/publications/2013/12/978-87-93026-78-0.pdf.

De Vries W, Groenenberg J.E. and Posch M. [2015b] Mass balance approaches to assess critical loads and target loads of metals for terrestrial and aquatic ecosystems. pp. 207-222. In: Critical loads and dynamic risk assessments. Nitrogen, acidity in terrestrial and aquatic ecosystems. Edited by W. de Vries, J-P. Hettelingh and M. Posch. *Envitornmental pollution* 25, Springer.

De Vries W., Posch M., Sverdrup H.U., Larssen T., de Wet H.A., Bobbink R. and Hettelingh J-P. [2015a] Geochemical indicators for use in the computation of critical loads and dynamic risk assessment. pp 15-58. In: Critical loads and dynamic risk assessments. Nitrogen, acidity in terrestrial and aquatic ecosystems. Edited by W. de Vries, J-P. Hettelingh and M. Posch. *Envitornmental pollution* 25, Springer.

De Wit H.A., Hettelingh J-P., and Harmens H. [2015] Trends in ecosystem and health responses to long-range transported atmospheric pollutants. Norwegian Institute for Water Research, 92p.

Defra [2007] The Air Quality Strategy for England, Scotland, Wales and Northern Ireland, 1. (https://assets.publishing.service.gov.uk/government/uploads/system/uploads/attachment_data/file/69336/pb12654-air-quality-strategy-vol1-070712.pdf).

Delgado-Saborit J.M., C. Stark, R.M. Harrison [2011] Carcinogenic potential, levels and sources of polycyclic aromatic hydrocarbon mixtures in indoor and outdoor environments and their implications for air quality standards. *Environment International* 37 (2011), 383–392.

Dibble T., Tetu H.L., Lam K.T., Thackray C.P., Jacob D.J. [2019] Modeling the OH-Initiated Oxidation of Mercury in the Global Atmosphere Without Violating Physical Laws. Chemistry Faculty Scholarship.

Dibble, T.S., M.J. Zelie and H. Mao [2012] Thermodynamics of reactions of ClHg and BrHg radicals with atmospherically abundant free radicals. Atmospheric Chemistry and Physics, 12:10271-10279.

Dibble, T.S., M.J. Zelie and Y. Jiao [2014] Quantum chemistry guide to PTRMS studies of as yet undetected products of the bromine atom initiated oxidation of gaseous elemental mercury. Journal of Physical Chemistry A, 118:7847-7854.

Dołęgowska S. and M. Migaszewski Z. [2014]. Terrestrial mosses as trace element bioindicators: a review. Pp 25 – 69. In: Moss. Classification, development and growth and functional role in ecosystems. Ed. by: Mohamed J. ISBN: 978-1-63117-396-7, Nova Science Publishers, Inc.

Donohoue D., Bauer, D., Cossairt B., and Hynes A. [2006] Temperature and pressure dependent rate coefficients for the reaction of Hg with Br and the reaction of Br with Br: A pulsed laser photolysispulsed laser induced fluorescence study, J. Phys. Chem. A, 110, 6623–6632, doi:10.1021/jp054688j.

ECHA [2019] https://echa.europa.eu/-/echa-starts-work-on-persistent-organic-pollutants.

Efstathiou C.I., J. Matejovicová, J. Bieser, and G. Lammel [2016] Evaluation of gas-particle partitioning in a regional air quality model for organic pollutants. *Atmos. Chem. Phys*., 16, 15327–15345.

EMEP/EEA Guidebook [2013] EMEP/EEA air pollutant emission inventory guidebook – 2013. EEA Technical report No 12/2013. Available at: https://www.eea.europa.eu/publications/emep-eea-guidebook-2013.

EMEP/EEA Guidebook [2016] EMEP/EEA air pollutant emission inventory guidebook – 2016. EEA Technical report No 21/2016. Available at: https://www.eea.europa.eu/publications/emep-eea-guidebook-2016.

Emmons, L. K., Walters, S., Hess, P. G., Lamarque, J.-F., Pfister, G. G., Fillmore, D., Granier, C., Guenther, A., Kinnison, D., Laepple, T., Orlando, J., Tie, X., Tyndall, G., Wiedinmyer, C., Baughcum, S. L., and Kloster, S. [2010] Description and evaluation of the Model for Ozone and Related chemical Tracers, version 4 (MOZART-4), Geosci. Model Dev., 3, 43–67, doi:10.5194/gmd-3-43-2010.

Esen F., S. S. Cindoruk, and Y. Tasdemir [2006] Ambient Concentrations and Gas/Particle Partitioning of Polycyclic Aromatic Hydrocarbons in an Urban Site in Turkey, Environmental Forensics, 7:303–312.

European Commission [2001] Ambient air pollution by polycyclic aromatic hydrocarbons (PAH). Position Paper. Annexes. Prepared by the Working group on polycyclic aromatic hydrocarbons (July 27th 2001) (https://ec.europa.eu/environment/archives/air/pdf/annex_pah.pdf).

Fernandez P., Grimalt J.O., and Vilanova R.M. [2002] Atmospheric gas-particle partitioning of polycyclic aromatic hydrocarbons in high mountain regions of Europe, *Environ. Sci. Technol*., 36, 1162–1168, doi:10.1021/es010190t, 2002.

Fiedler H. [2007] National PCDD/PCDF release inventories under the Stockholm Convention on Persistent Organic Pollutants, *Chemosphere,* 67, 96–108.

Finizio A., Mackay D., Bidleman T., & Harner T. [1997] Octanol-air partition coefficient as a predictor of partitioning of semi-volatile organic chemicals to aerosols. *Atmospheric Environment, 31*, 2289-2296.

Francés-Monerris A., et al. [2019] Photodissociation mechanisms of major Hg(II) species in the atmospheric chemical cycle of mercury. Angewandte Chemie. DOI: 10.1002/anie.201915656.

Frontasyeva M., Harmens H., Uzhinskiy A., Chaligava O. and participants of the moss survey. Mosses as biomonitors of air pollution: 2015/2016 survey on heavy metals, nitrogen and POPs in Europe and beyond. — Dubna: JINR, 2020. — 136 p.

Gauss M., J. Bartnicki, A. Gusev, W. Aas, H. Klein [2019] Atmospheric Supply of Nitrogen, Cadmium, Lead, Mercury, and PCDD/Fs to the Baltic Sea in 2017. MSC-W Technical Report 1/2019. https://emep.int/publ/helcom/2019/index.html.

Goodsite M.E., Plane J.M.C. and Skov H. [2004] A Theoretical Study of the Oxidation of Hg0 to HgBr2 in the Troposphere, Environ. Sci. Technol., 38, 1772–1776.

Goodsite, M. E., Plane, J. M. C., and Skov, H. [2012] Correction to A Theoretical Study of the Oxidation of Hg0 to HgBr2 in the Troposphere, Environ. Sci. Technol., 46, 5262, doi:10.1021/es301201c.

Goss K.-U. and R. P. Schwarzenbach [2001] Linear free energy relationships used to evaluate equilibrium partitioning of organic compounds. *Environ. Sci. Technol.*, 35, 1–9, doi:10.1021/es000996d.

Government of Alberta [2019] Alberta Ambient Air Quality Objectives and Guidelines Summary. AEP, Air Policy, 2016, No. 2. (https://open.alberta.ca/dataset/0d2ad470-117e-410f-ba4f-aa352cb02d4d/resource/4ddd8097-6787-43f3-bb4a-908e20f5e8f1/download/aaqo-summary-jan2019.pdf)

Government of Ontario [2019] Ontario's Ambient Air Quality Criteria (https://www.ontario.ca/page/ontarios-ambient-air-quality-criteria-sorted-contaminant-name).

Gratz L.E., Ambrose J.L., Jaffe D.A., Shah V., Jaegle L., Stutz J., Festa J., Spolaor M., Tsai C., Selin N.E., Song S., Zhou X., Weinheimer A.J., Knapp D.J., Montzka D.D., Flocke F.M., Campos T.L., Apel E., Hornbrook R., Blake N.J., Hall S., Tyndall G.S., Reeves M., Stechman D., and Stell M. [2015] Oxidation of mercury by bromine in the subtropical Pacific free troposphere, Geophysical Research Letters, 42, 10.1002/2015gl066645.

Gusev A, Kleimenov M., V. Shatalov [2020a] Assessment of transboundary pollution by toxic substances: Heavy metals and POPs. PART III. Further development of GLEMOS modelling system. MSC-E Technical Report 3/2020.

Gusev A. and N. Batrakova [2020] Assessment of PAH pollution levels, key sources and trends: contribution to analysis of the effectiveness of the POPs Protocol. Progress Report. MSC-E Technical Report 2/2020.

Gusev A., I. Ilyin, V. Shatalov, O. Travnikov, N. Batrakova, O. Rozovskaya, I. Strijkina, K.Brevik, Nizzetto P.B., W. Aas, K. Mareckova, S. Poupa, C. Sosa, M. Tista, R. Wankmueller, F. Couvidat [2019] Assessment of transboundary pollution by toxic substances: Heavy metals and POPs. EMEP Status Report 2/2019.

Gusev A., Ilyin I., Mantseva L., Rozovskaya O., Shatalov V. and Travnikov O. [2006]. Progress in further development of MSCE-HM and MSCE-POP models (implementation of the model review recommendations). EMEP/MSC-E Technical Report 4/2006.

Gusev A., O.Rozovskaya, Shatalov V., I.Strijkina [2020] Assessment of transboundary pollution by toxic substances: Heavy metals and POPs. Part I. Supplementary materials for POPs. MSC-E Data Report 2/2020.

Gusev A., O.Rozovskaya, V. Shatalov [2007] Modelling POP long-range transport and contamination levels by MSCE-POP model. EMEP/MSC-E Technical Report 1/2007 .

Gusev A., Rozovskaya O., Shatalov V., Vulykh N., Aas W., Breivik K., Couvidat F. and M.G.Vivanco [2018] Persistent Organic Pollutants: assessment of transboundary pollution on global, regional, and national scales. EMEP Status Report 3/2018.

Gusev A., Shatalov V. and O.Rozovskaya [2014] Pilot Modelling of PCDD/F Transport and Fate on Global Scale and within the European Region. *Organohalogen Compounds*. Vol. 76, 958-961.

Gustin M.S., H.M. Amos, J. Huang, M.B. Miller, and K. Heidecorn [2015] Measuring and modelling mercury in the atmosphere: a critical review, Atmospheric Chemistry and Physics, 15(10), 5697–5713, doi:10.5194/acp-15-5697-2015.

Harmens H., Norris D.A., Steinnes E., Kubin E., Piispanen J., Alber R., Aleksiayenak Y., Blum O., Cos¸kun M., Damh M., De Temmerman L., Fernández J.A., Frolova M., Frontasyeva M., González-Miqueom L., Grodzinska K., Jeran Z., Korzekwa S., Krmar M., Kvietkus K., Leblond S., Liiv S., Magnússon S.H., Mankovská B., Pesch R., Rühling Å., Santamaria J.M., Schröder W., Spiric Z., Suchara I., Thöni L., Urumov V., Yurukova L., Zechmeister H.G. [2010]. Mosses as biomonitors of atmospheric heavy metal deposition: Spatial patterns and temporal trends in Europe. Environmental Pollution 158 (2010) 3144 -3156.

HMCR [2020]. Hydrometeorological Centre of Russia. The main peculiarities of atmospheric circulation and weather in the northern hemisphere. https://meteoinfo.ru/circulation-review. Accessed on June 5, 2018.

Holy, M., Pesch, R., Schröder, W., Harmens, H., Ilyin, I., Alber, R., Aleksiayenak, Y., Blum, O., Coskun, M., Dam, M., De Temmerman, L., Fedorets, N., Figueira, R., Frolova, M., Frontasyeva, M., Goltsova, N., Miqueo, L.G., Grodzinska, K., Jeran, Z., Korzekwa, S., Krmar, M., Kubin, E., Kvietkus, K., Larsen, M., Leblond, S., Liiv, S., Magnusson, S., Mankovska, B., Mocanu, R., Piispanen, J., Rühling, A., Santamaria, J., Steinnes, E., Suchara, I., Thöni, L., Turcsanyi, G., Urumov, V. , Wolterbeek, B., Yurukova, L., Zechmeister, H.G., [2009]. First thorough identification of factors associated with Cd, Hg and Pb concentrations in mosses sampled in the European surveys 1990, 1995, 2000 and 2005. Journal of Atmospheric Chemistry 63, 109–124.

Horowitz, H.M., D.J. Jacob, Y. Zhang, T.S. Dibble, F. Slemr, H.M. Amos, J.A. Schmidt, E.S. Corbitt, E.A. Marais and E.M. Sunderland [2017] A new mechanism for atmospheric mercury redox chemistry: Implications for the global mercury budget. Atmospheric Chemistry and Physics Discussions, 1-33, 10.5194/acp-2016-1165.

Hung, H., Katsoyiannis, A.A., Brorström-Lunden, E., Olafsdottir, K., Aas, W., Breivik, K., Bohlin-Nizzetto, P., Sigurdsson, A., Hakola, H., Bossi, R., Skov, H., Sverko, E., Barresi, E., Fellin, P., Wilson, S. [2016] Temporal trends of persistent organic pollutants (POPs) in arctic air: 20 ears of monitoring under the Arctic Monitoring and Assessment Programme (AMAP). *Environmental Pollution*, 217, 52-61.

IARC [2010] Some non-heterocyclic polycyclic aromatic hydrocarbons and some related exposures. IARC Monogr. Eval. Carcinog. Risks Hum., 92: 1–853. Available at: http://monographs.iarc.fr/ENG/Monographs/vol92/mono92- 6.pdf.

IARC [2019] Tumour Site Concordance and Mechanisms of Carcinogenesis. Edited by Baan RA, Stewart BW, Straif K. IARC Scientific Publication No. 165. (https://publications.iarc.fr/Book-And-Report-Series/Iarc-Scientific-Publications/Tumour-Site-Concordance-And-Mechanisms-Of-Carcinogenesis-2019).

ICP Vegetation, [2015]. Heavy metals, nitrogen and POPs in European mosses: 2015 survey. Monitoring manual. ICP Vegetation Programme Coordination Centre, CEH. Bangor, UK. http://icpvegetation.ceh.ac.uk.

Ilyin I. , O. Travnikov, G. Schütze, S. Feigenspan and K. Uhse [2020a] Country-scale assessment of heavy metal pollution: A case study for Germany. Joint Report of MSC-E and German Environment Agency. MSC-E Technical Report 1/2020.

Ilyin I., Rozovskaya O., O.Travnikov, I.Strijkina [2020] Assessment of transboundary pollution by toxic substances: Heavy metals and POPs. Part I. Supplementary materials for heavy metals. MSC-E Data Report 1/2020.

Ilyin I., Rozovskaya O., Travnikov O., Aas W. and K.A.Pfaffhuber [2018] Assessment of heavy metal transboundary pollution on global, regional and national scales. EMEP Status Report 2/2018.

Jiao, Y. and Dibble T.S., 2015. Quality structures, vibrational frequencies, and thermochemistry of the products of reaction of BrHg• with NO2, HO2, ClO, BrO, and IO. Journal of Physical Chemistry A, 119:10502-10510.

Jiao, Y. and Dibble, T. S. (2017) First kinetic study of the atmospherically important reactions BrHg + NO2 and BrHg + HOO, Phys. Chem. Chem. Phys., 19, 1826–1838, doi:10.1039/c6cp06276h.

Kabata-Pendias, A. [2010]. Trace Elements in Soils and Plants. 4th Edition, CRC Press, 548 Pages.

Kahan, T. F., Kwamena, N.-O. A., & Donaldson, D. J. [2006] Heterogeneous ozonation kinetics of polycyclic aromatic hydrocarbons on organic films. Atmospheric Environment, 40(19), 3448–3459. doi:10.1016/j.atmosenv.2006.02.004.

Karar, K., Gupta, A. K., Kumar, A., & Biswas, A. K. [2006] Characterization and Identification of the Sources of Chromium, Zinc, Lead, Cadmium, Nickel, Manganese and Iron in Pm10 Particulates at the Two Sites of Kolkata, India. Environmental Monitoring and Assessment, 120(1-3), 347–360. doi:10.1007/s10661-005-9067-7.

Karimi, P., Peters, K. O., Bidad, K., & Strickland, P. T. [2015] Polycyclic aromatic hydrocarbons and childhood asthma. European Journal of Epidemiology, 30(2), 91–101.doi:10.1007/s10654-015-9988-6.

Keyte I.J., Harrison R.M., Lammel G. [2013] Chemical reactivity and long-range transport potential of polycyclic aromatic hydrocarbons – a review, The Royal Society of Chemistry, DOI: 10.1039/c3cs60147a.

Kong S., Ding X., Bai Z., Han B., Chen L., Shi J., Li Z. [2010] A seasonal study of polycyclic aromatic hydrocarbons in PM2.5 and PM2.5−10 in five typical cities of Liaoning Province, China. J. Hazard. Mater. 2010, 183 (1−3), 70−80.

Kwamena, N.-O. A., Clarke, J. P., Kahan, T. F., Diamond, M. L., & Donaldson, D. J. [2007. Assessing the importance of heterogeneous reactions of polycyclic aromatic hydrocarbons in the urban atmosphere using the Multimedia Urban Model. Atmospheric Environment, 41(1), 37–50. doi:10.1016/j.atmosenv.2006.08.016

Kwamena, N.-O. A., Thornton, J. A., & Abbatt, J. P. D. [2004] Kinetics of Surface-Bound Benzo[a]pyrene and Ozone on Solid Organic and Salt Aerosols. The Journal of Physical Chemistry A, 108(52), 11626–11634. doi:10.1021/jp046161x

Lammel, G., Sehili, A.M., Bond, T.C., Feichter, J., & Grassl, H. [2009] Gas/particle partitioning and global distribution of polycyclic aromatic hydrocarbons - A modelling approach. *Chemosphere, 76*, 98-106

Larssen S., Sluyter R. and Helmis C. [1999]. Criteria for EUROAIRNET. The EEA Air Quality Monitoring and Information network. Technical Report no. 12. EEA, Copenhagen, 43 p.

Leili, M., Naddafi, K., Nabizadeh, R., Yunesian, M., & Mesdaghinia, A. [2008] The study of TSP and PM10 concentration and their heavy metal content in central area of Tehran, Iran. Air Quality, Atmosphere & Health, 1(3), 159–166. doi:10.1007/s11869-008-0021-z.

Li, J., Li, X., Zhou, C., Li, M., Lu, S., Yan, J., … Shou, C. [2017] Correlation between Polycyclic Aromatic Hydrocarbon Concentration and Particulate Matter during the Removal Process of a Low-Low Temperature Electrostatic Precipitator. Energy & Fuels, 31(7), 7256–7262. doi:10.1021/acs.energyfuels.7b00145.

Li, Jingwei, Xiaodong Li, Chenyang Zhou, Min Li, Shengyong Lu, Jianhua Yan, Zhifu Qi, and Chunhui Shou [2017] Correlation between Polycyclic Aromatic Hydrocarbon Concentration and Particulate Matter during the Removal Process of a Low-Low Temperature Electrostatic Precipitator; Energy & Fuels; 2017 31 (7), 7256-7262; DOI: 10.1021/acs.energyfuels.7b00145.

Liu X., H. Zhang, W. Pan, Q. Xue, J. Fu, G. Liu, M. Zheng, A. Zhang [2019] A novel computational solution to the health risk assessment of air pollution via joint toxicity prediction: A case study on selected PAH binary mixtures in particulate matters. *Ecotoxicology and Environmental Safety* 170 (2019), 427–435.

Liu, H., Xu, C., Jiang, Z.-Y., & Gu, A. [2016]. Association of polycyclic aromatic hydrocarbons and asthma among children 6–19 years: NHANES 2001–2008 and NHANES 2011–2012. Respiratory Medicine, 110, 20–27.doi:10.1016/j.rmed.2015.11.003.

Lohmann, R., & Lammel, G. [2004]. Adsorptive and Absorptive Contributions to the Gas-Particle Partitioning of Polycyclic Aromatic Hydrocarbons: State of Knowledge and Recommended Parametrization for Modelling. Environmental Science & Technology, 38(14), 3793–3803. doi:10.1021/es035337q.

Longhin, E. [2012] Particulate matter toxicity and health effects: in vitro assessment of the mechanisms of action. University of Milano-Bicocca Department Of Environmental Sciences.

Ma. Y.-G., Lei, Y. D., Xiao, H., Wania, F., & Wang, W.-H. [2010] Critical Review and Recommended Values for the Physical-Chemical Property Data of 15 Polycyclic Aromatic Hydrocarbons at 25 °C. Journal of Chemical & Engineering Data, 55(2), 819–825. doi:10.1021/je900477x.

Maas R. and Grennfelt P. (eds) [2016] Towards Cleaner Air. Scientific Assessment Report 2016. EMEP Steering Body and Working Group on Effects of the Convention on Long-Range Transboundary Air Pollution, Oslo. xx+50pp.

Mackay D, Shiu WY, Ma K-C, Lee CS [2006]Handbook of Physical-chemical Properties and Environmental Fate for Organic Chemicals, 2nd edition, CRC Press.

Manzetti S. [2013] Polycyclic Aromatic Hydrocarbons in the Environment: Environmental Fate and Transformation. Polycyclic Aromatic Compounds, 33(4), 311–330. doi:10.1080/10406638.2013.781042

McLachlan M.S. and M. Horstmann [1998] Forest as filters of airborne organic pollutants. A model, Environ. Sci. Technol. 1998, 32, 413-420.

MEP (Ministry of Environmental Protection, China) [2012] National Standard GB 3095-2012, (http://english.mee.gov.cn/Resources/standards/Air_Environment/quality_standard1/201605/W020160511506615956495.pdf

Meyer T., Wania F., & Breivik K. [2005] Illustrating sensitivity and uncertainty in environmental fate models using partitioning maps. *Environmental Science & Technology, 39*, 3186-3196.

MFE (Ministry for the Environment, New Zealand) [2003] Health effects of CO, NO2, SO2, ozone, benzene and benzo(a)pyrene in New Zealand, Air quality technical report, 43, Wellington.

MHRF (Ministry of Health of the Russian Federation) [2017] GN 2.1.6.3492-17. Maximum allowable concentrations (MACs) of pollutants in the air of urban and rural areas (http://docs.cntd.ru/document/556185926).

Michael S. McLachlan [1999] Framework for the Interpretation of Measurements of SOCs in Plants, Environ. Sci. Technol. 33, 1799-1804.

Miura, K., Shimada, K., Sugiyama, T., Sato, K., Takami, A., Chan, C.K., Kim, I.S., Kim, Y.P., Lin, N.-H., & Hatakeyama, S. [2019] Seasonal and annual changes in PAH concentrations in a remote site in the Pacific Ocean. *Scientific Reports, 9*, 12591.

Mu Q., M. Shiraiwa, M. Octaviani, N. Ma, A. Ding, H. Su, G. Lammel, U. Pöschl, and Y. Cheng [2018] Temperature effect on phase state and reactivity controls atmospheric multiphase chemistry and transport of PAHs. Sci. Adv., 4: eaap7314, 1-8.

Mu Qing, Gerhard Lammel, Christian N. Gencarelli, Ian M. Hedgecock, Ying Chen, Petra Pribylová, Monique Teich, Yuxuan Zhang, Guangjie Zheng, Dominik van Pinxteren, Qiang Zhang, Hartmut Herrmann, Manabu Shiraiwa, Peter Spichtinger, Hang Su, Ulrich Pöschl, and Yafang Cheng, Regional modelling of polycyclic aromatic hydrocarbons [2017] WRF-Chem-PAH model development and East Asia case studies, Atmos. Chem. Phys., 17, 12253–12267, 2017 https://doi.org/10.5194/acp-17-12253-2017

Murillo, J.H. et al. [2016] Polycyclic aromatic hydrocarbons in PM2.5 and PM10 atmospheric particles in the Metropolitan Area of Costa Rica: Sources, temporal and spatial variations, Atmospheric Pollution Research (2016), http://dx.doi.org/10.1016/ j.apr.2016.10.002.

Nickel S. and Schröder W. [2019]. Correlating elements content in mosses collected in 2015 across Germany with spatially associated characteristics of sampling sites and their surroundings. Environ Sci Eur (2019) 31:80.

Paripurnanda L., Saravanamuthu V. and Jaya K. [2013]: Road-Deposited Sediment Pollutants: A Critical Review of their Characteristics, Source Apportionment, and Management, Critical Reviews in Environmental Science and Technology, 43:13, pp. 1315-1348.

Parrella, J. P., Jacob, D. J., Liang, Q., Zhang, Y., Mickley, L. J., Miller, B., Evans, M. J., Yang, X., Pyle, J. A., Theys, N., and Van Roozendael, M. [2012] Tropospheric bromine chemistry: implications for present and pre-industrial ozone and mercury, Atmos. Chem. Phys., 12, 6723–6740, doi:10.5194/acp-12-6723-2012.

Paterson S., Mackay D., Bacci E., Calamari D. [1991] Correlation of the equilibrium and kinetics of leaf-air exchange of hydrophobic organic chemicals. Environmental Science and Technology 25,866 – 871.

Perraudin E., H. Budzinski, E. Villenave [2007] Kinetic Study of the Reactions of Ozone with Polycyclic Aromatic Hydrocarbons Adsorbed on Atmospheric Model Particles, J Atmos Chem (2007) 56:57–82 DOI 10.1007/s10874-006-9042-x .

Pinterits M, K.Mareckova, B. Ullrich, R.Wankmueller, M.Anys [2020] Inventory Review 2020. Review of emission data reported under the LRTAP Convention and NEC Directive, Stage 1 and 2 and review, Status of gridded and LPS data. CEIP Inventory Review Report 2020. Technical Report CEIP 4/2020. In preparation.

Possanzini M, Palo VD, Gigliucci P, Sciano MCT, Cecinato A. [2004] Determination of phasedistributed PAH in Rome ambient air by denuder/GC-MS method. Atmos Environ 2004; 38: 1727–34.

Prevedouros, K., Brorstrom-Lunden, E., Halsall, C.J., Jones, K.C., Lee, R.G.M., & Sweetman, A.J. [2004] Seasonal and long-term trends in atmospheric PAH concentrations: Evidence and implications. *Environmental Pollution, 128*, 17-27.

Pulles T., Kok H. and U.Quass [2006] Application of the emission inventory model TEAM: Uncertainties in dioxin emission estimates for central Europe. *Atmospheric Environment,* 40, 2321–2332.

Pulles T., Kok H., Quass U., Juery C. and J.Matejovicova [2005] Dioxin emissions in candidate countries. TNO Report R&I-A R 2005/054. Available at:http://ec.europa.eu/environment/archives/dioxin/pdf/rapport_2005.pdf.

Riederer M. [1990] Estimating partitioning and transport of organic chemicals in the foliage/atmosphere system: discussion of a fugacity based model. Environmental Science and Technology 24,829– 837.

Rogula-Kozłowska, W., Majewski, G., Błaszczak, B., Klejnowski, K., & Rogula-Kopiec, P. (2016). Origin-Oriented Elemental Profile of Fine Ambient Particulate Matter in Central European Suburban Conditions. International Journal of Environmental Research and Public Health, 13(7), 715. doi:10.3390/ijerph13070715

Rühling Å and Tyler G. [1973]. Heavy metal deposition in Scandinavia. Water, Air and Soil Pollution 2, pp 445-455.

Saiz-Lopez A., Acuña A.U., Trabelsi T., Carmona-García J., Dávalos J.Z., Rivero D., Cuevas C.A., Kinnison D.E., Sitkiewicz S.P., Roca-Sanjuán D., and Francisco J.S. [2019] Gas-Phase Photolysis of Hg(I) Radical Species: A New Atmospheric Mercury Reduction Process. Journal of the American Chemical Society 141(22):8698-8702.

Saiz-Lopez A., Sitkiewicz S.P., Roca-Sanjuaįn D., Oliva-Enrich J.M. , Daįvalos J.Z. , Notario R., Jiskra M., Xu Y., Wang F., Thackray C.P. , Sunderland E.M. , Jacob D.J. , Travnikov O., Cuevas C.A. , Acuana A.U., Rivero D., Plane J.M.C. , Kinnison D.E. , Sonke J.E. [2018] Photoreduction of gaseous oxidized mercury changes global atmospheric mercury speciation, transport and deposition. Nature Comm. 9, 4796, doi: 10.1038/s41467-018-07075-3.

Saiz-Lopez A., Travnikov O., Sonke J.E., Thackray C.P., Jacob D.J., Carmona-García J., Francés-Monerris A., Roca-Sanjuán D., Acuña A.U., Dávalos J.Z., Cuevas C.A., Jiskra M., Wang F., Bieser J., Plane J.M.C., and Francisco J.S. [2020] New photochemistry of oxidized Hg(I) and Hg(II) species reveals missing mercury oxidation in the troposphere. PNAS, under review.

Schröder W., Pesch R., Hertel A., Schonrock S., Harmens H., Mills G. and Ilyin I. [2013]. Correlation between atmospheric deposition of Cd, Hg and Pb and their concentrations in mosses specified for ecological land classes covering Europe. Atmospheric Pollution Research,4, (2013), 267-274.

Scientific Committee on Food (SCF) [2002] Opinion of the Scientific Committee on Food on the risks to human health of Polycyclic Aromatic Hydrocarbons in food. Expressed on 4 December 2002 (https://ec.europa.eu/food/sites/food/files/safety/docs/sci-com_scf_out153_en.pdf).

Shah, V., Jaeglé, L., Gratz, L. E., Ambrose, J. L., Jaffe, D. A., Selin, N. E., Song, S., Campos, T. L., Flocke, F. M., Reeves, M., Stechman, D., Stell, M., Festa, J., Stutz, J., Weinheimer, A. J., Knapp, D. J., Montzka, D. D., Tyndall, G. S., Apel, E. C., Hornbrook, R. S., Hills, A. J., Riemer, D. D., Blake, N. J., Cantrell, C. A., and Mauldin III, R. L. [2016] Origin of oxidized mercury in the summertime free troposphere over the southeastern US, Atmos. Chem. Phys., 16, 1511–1530, https://doi.org/10.5194/acp-16-1511-2016, 2016.

Shahpoury P., G. Lammel, A. Albinet, A. Sofuoglu, Y. Dumanoglu, S. C. Sofuoglu, Z. Wagner, and V. Zdimal [2016] Evaluation of a conceptual model for gas-particle partitioning of polycyclic aromatic hydrocarbons using poly-parameter linear free energy relationships. *Environ. Sci. Technol.*, 50, 22, 12312-12319.

Shatalov V., Gusev A., Dutchak S., Rozovskaya O., Sokovykh V. and N.Vulykh [2010] Persistent Organic Pollutants in the Environment. EMEP Status Report 3/2010.

Shatalov V., Ilyin I., Gusev A., Rozovskaya O. and O.Travnikov [2014] Heavy Metals and Persistent Organic Pollutants: Model Assessment of Pollution and Research Activities. EMEP/MSC-E Technical report 4/2014.

Shen H., Huang Y., Wang R., Zhu D., Li W., Shen G., Wang B., Zhang Y., Chen Y., Lu Y., Chen H., Li T., Sun K., Li B., Liu W., Liu J. and S.Tao [2013] Global atmospheric emissions of polycyclic aromatic hydrocarbons from 1960 to 2008 and future predictions, *Environ. Sci. Technol*., 47, 6415–6424.

Shrivastava M., Lou S., Zelenyuk A., Easter R.C., Corley R.A., Thrall B.D., … Tao S. [2017] Global long-range transport and lung cancer risk from polycyclic aromatic hydrocarbons shielded by coatings of organic aerosol. Proceedings of the National Academy of Sciences, 114(6), 1246–1251. doi:10.1073/pnas.1618475114.

Siskos P.A., Bakeas E.B., Thomaidis N.S. [2006] Chemical Characterization of airborne particles in Greece. In Trends in Environmental Research (edited by Davis E.B.) ISBN 1-59454-485-9.

Skamarock W.C., Klemp J.B., Dudhia J., Gill D.O., Barker D.M., Duda M.G., Huang X-Y., Wang W. and Powers J.G. [2008]. A Description of the Advanced Research WRF Version 3. NCAR/TN–475+STR NCAR TECHNICAL NOTE.

Sonke J.E., Teisseren R., Heimbürger-Boavida L.-R., Petrova M., Marusczaka N., Le Dantec T., Chupakov A.V., Lia C., Thackray C.P., Sunderland E.M., Tananaev N., Pokrovsky O.S. [2018] Eurasian river spring flood observations support net Arctic Ocean mercury export to the atmosphere and Atlantic Ocean, PNAS 115 (50), doi: 10.1073/pnas.1811957115.

Sutton M.A., D. Fowler, B. Moncrieff [1993] The exchange of atmospheric ammonia with vegetated surfaces. I: Unfertilized vegetation, Q. J. R. Meteorol. Sac., 119, pp. 1023-1045 .

Sutton M.A., J.K. Burkhardt, D. Guerin, E. Nemitz, D. Fowler [1998] Development of resistance models to describe measurements of bi-directional ammonia surface-atmosphere exchange, Atmospheric Environment Vol. 32, No. 3, pp. 473Ð480.

Szatyłowicz, E., & Skoczko, I. [2019] Evaluation of the PAH Content in Soot from Solid Fuels Combustion in Low Power Boilers. Energies, 12(22), 4254. doi:10.3390/en12224254.

Theakston F. [2000] Air quality guidelines for Europe. Second edition. WHO Regional Publications, European Series, No. 91, ISBN 92 890 1358 3.

Thomaidis, N. S., Bakeas, E. B., & Siskos, P. A. [2003] Characterization of lead, cadmium, arsenic and nickel in PM2.5 particles in the Athens atmosphere, Greece. Chemosphere, 52(6), 959–966. doi:10.1016/s0045-6535(03)00295-9.

Tista M. and R.Wankmueller [2019b] Methodologies applied to the CEIP GNFR gap-filling 2019. Part III: Persistent organic pollutants (Benzo(a)pyrene, Benzo(b)fluoranthene, Benzo(k)fluoranthene, Indeno(1,2,3-cd)pyrene, Total polycyclic aromatic hydrocarbons, Dioxin and Furan, Hexachlorobenzene, Polychlorinated biphenyls) of the year 2017. Technical report CEIP 3/2019.

Tista M., Matthews B. and R.Wankmueller [2019a] Methodologies applied to the CEIP GNFR gap-filling 2019. Part II: Heavy Metals (Pb, Cd, Hg) of the year 2017. Technical report CEIP 2/2019.

Travnikov O., Angot H., Artaxo P., Bencardino M., Bieser J., D'Amore F., Dastoor A., De Simone F., Diéguez M. D. C., Dommergue A., Ebinghaus R., Feng X. B., Gencarelli C. N., Hedgecock I. M., Magand O., Martin L., Matthias V., Mashyanov N., Pirrone N., Ramachandran R., Read K. A., Ryjkov A., Selin N. E., Sena F., Song S., Sprovieri F., Wip D., Wängberg I., and Yang X. [2017] Multi-model study of mercury dispersion in the atmosphere: atmospheric processes and model evaluation, Atmos. Chem. Phys., 17, 5271-5295, doi:10.5194/acp-17-5271-2017.

UNECE [1979] The 1979 Geneva Convention on Long-range Transboundary Air Pollution. United Nations Economic Commission for Europe.http://www.unece.org/env/lrtap/welcome.html.

UNECE [2014] Guidelines for reporting emission data under the Convention on Long-range Transboundary Air Pollution (ECE/EB.AIR/130). Available at: http://www.ceip.at/fileadmin/inhalte/emep/2014_Guidelines/ece.eb.air.125_ADVANCE_VERSION_reporting_guidelines_2013.pdf.

UNECE [2019] Monitoring strategy for the Cooperative Programme for Monitoring and Evaluation of the Long-range Transmission of Air Pollutants in Europe for the period 2020–2029. EB Decision 2019/1, ECE/EB.AIR/144/Add.1. URL: http://www.unece.org/fileadmin/DAM/env/documents/2019/AIR/EB_Decisions/Decision_2019_1.pdf.

van Noort, P. [2003] A thermodynamics-based estimation model for adsorption of organic compounds by carbonaceous materials in environmental sorbents, Environ. Toxicol. Chem., 22, 1179–1188, doi:10.1002/etc.5620220601.

Vione, D., Barra, S., de Gennaro, G., de Rienzo, M., Gilardoni, S., Perrone, M. G., & Pozzoli, L. [2004] Polycyclic Aromatic Hydrocarbons in the Atmosphere: Monitoring, Sources, Sinks and Fate. II: Sinks and Fate. Annali Di Chimica, 94(4), 257–268. doi:10.1002/adic.200490031.

Wang X., C.-J. Lin, X. Feng [2014] Sensitivity analysis of an updated bidirectional air–surface exchange model for elemental mercury vapor, Atmos. Chem. Phys., 14, 6273–6287.

Wang, F. Saiz-Lopez A., Mahajan A.S., Gómez Martín J.C., Armstrong D., Lemes M., Hay T., and Prados-Roman C. [2014] Enhanced production of oxidised mercury over the tropical Pacific Ocean: A key missing oxidation pathway. Atmos. Chem. Phys. 14, 1323–1335.

WHO [2000] Air quality guidelines for Europe, World Health Organization, Regional Office for Europe, Copenhagen (http://www.euro.who.int/__data/assets/pdf_file/0005/74732/E71922.pdf).

WHO [2003] Health aspects of air pollution with particulate matter, ozone and nitrogen dioxide. Report on a WHO working group. EUR/03/5042688 WHO, Bonn.

WHO [2013a] Health effects of particulate matter Policy implications for countries in eastern Europe, Caucasus and central Asia. ISBN 978 92 890 0001 7 (http://www.euro.who.int/__data/assets/pdf_file/0006/189051/Health-effects-of-particulate-matter-final-Eng.pdf).

WHO [2017] Evolution of WHO air quality guidelines: past, present and future. Copenhagen. WHO Regional Office for Europe. (http://www.euro.who.int/__data/assets/pdf_file/0019/331660/Evolution-air-quality.pdf).

WHO Technical report [2013b] Review of Evidence on Health Aspects of Air Pollution. REVIHAAP Project. (https://www.euro.who.int/__data/assets/pdf_file/0004/193108/REVIHAAP-Final-technical-report-final-version.pdf)

WMO [2019] Annual Bulletin on the Climate in WMO Region VI - Europe and Middle East - 2017 . Ed. by Deutscher Wetterdienst. Responsible Mächel H. https://www.dwd.de/DE/leistungen/ravibulletinjahr/bulletin_2017.pdf,jsessionid=FB49DAFE415EAE6932E5A46DC080353.live11051?__blob=publicationFile&v=3. Accessed on April 30, 2018.

WWF [2005] WWF, Stockholm Convention “New POPs”, Screening Additional POP Candidates, April 2005. http://assets.panda.org/DOWnloads/newpopsfinal.pdf

Yang, X., Cox, R., Warwick, N., Pyle, J., Carver, G., O’Connor,F., and Savage, N. [2005] Tropospheric bromine chemistry and its impacts on ozone: A model study, *J. Geophys. Res.,* 110, D23311, doi:10.1029/2005JD006244.

Yang, X., Pyle, J. A., Cox, R. A., Theys, N., and Van Roozendael, M. [2010] Snow-sourced bromine and its implications for polar tropospheric ozone, *Atmos. Chem. Phys*., 10, 7763–7773, doi:10.5194/acp-10-7763-2010.

Yong Y., Katsoyiannis A., Bohlin-Nizzetto P., Brorstrom-Lunden E., Ma J.M., Zhao Y., Wu Z., Tych W., Mindham D., Sverko E.[2019] Polycyclic aromatic hydrocarbons not declining in Arctic air despite global emission reduction. *Environmental Science & Technology*, 53, 2375-2382.

Zhang L., L. P. Wright, P. Blanchard [2009] A review of current knowledge concerning dry deposition of atmospheric mercury, Atmospheric Environment 43, 5853–5864.

Zhang L., L.P. Wright, and W.A.H. Asman [2010] Bi-directional air-surface exchange of atmospheric ammonia: A review of measurements and a development of a big-leaf model for applications in regional-scale air-quality models, J. Geophys. Res. 2010, 115, D20310, doi:10.1029/2009JD013589.

Zhao, Tong, Lingxiao Yang, Qi Huang, Yan Zhang, Shujun Bie, Jingshu Li, Wan Zhang, Shengfei Duan, Hongliang Gao, Wenxing Wang [2020] PM2.5-bound polycyclic aromatic hydrocarbons (PAHs) and their derivatives (nitrated-PAHs and oxygenated-PAHs) in a road tunnel located in Qingdao, China: Characteristics, sources and emission factors. Science of The Total Environment 2020, 720 , 137521. https://doi.org/10.1016/j.scitotenv.2020.137521.

Annex A

UPDATE OF THE ASSESSMENT RESULTS WITH THE NEW EMISSIONS REPORTING DATA

Model assessment of heavy metal and POP pollution levels for 2018, presented in Chapter 3, is based on the gridded emissions data for the previous year 2017 and meteorological data for 2018. Air concentrations and deposition described here were simulated using both emission and meteorological data for 2018. Therefore, the difference between the results presented below and those described in other parts of the report is caused entirely by changes of the emission data used in modelling. Relative difference between these two modelling results is calculated as follows:

$$\Delta_{emis} = \frac{(Y_{2018} - Y_{2017})}{Y_{2017}} \cdot 100\% ,$$

where Y_{2018} and Y_{2017} are pollution levels (air concentrations or deposition) based on meteorological data for 2018 and emissions for 2018 and 2017, respectively. Major changes of the emissions in the EMEP countries between these two years are described in Annex B.

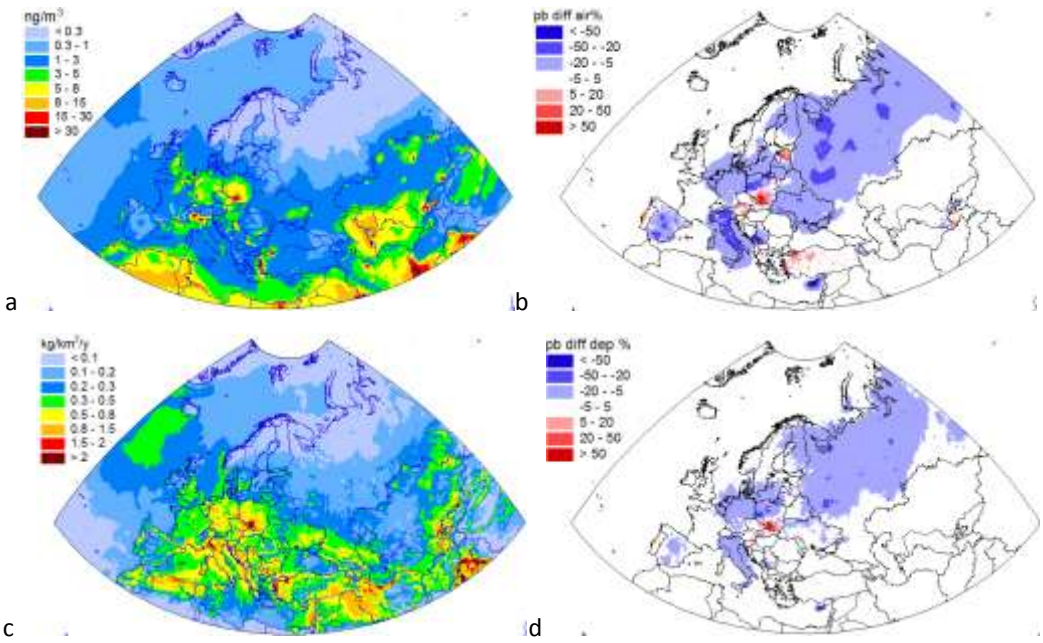

Fig. A.1. *Annual mean air concentrations (a) and total deposition fluxes (c) of Pb based on the emissions data for 2018 and their relative changes (b and d) from the results based on the emissions data for 2017.*

Air concentrations and total deposition of Pb decreased in Germany, Spain, Italy, Cyprus, in a number of countries in the eastern part of the EMEP region and in the northern part of Poland. The most significant decrease of air concentrations (20-30% or higher) occurred in Italy and Cyprus (Fig. A.1). It corresponds to the reported emission decrease in these countries. Increase of air concentrations is noted for the southern part of Poland, Estonia, Turkey, Austria, and in some regions of other

countries. As a rule, magnitude of concentration or deposition change in particular countries is smaller than the reported change of the emissions. It is explained by contribution of other sources to overall pollution levels such as non-EMEP emissions and wind re-suspension. Besides, the response of deposition fluxes to the changes of emissions are commonly weaker compared to the response of air concentrations.

The most marked decrease of Cd concentrations and deposition fluxes took place in Portugal, Italy, north of Poland, Lithuania, Russia and Armenia. Over large part of these countries the decline of air concentrations and deposition is within 5-30% (Fig. A.2). The change of total emissions used in modelling in these countries was – 29% - -94%. The special case is Poland, where Cd emission change was -24%. However, due to the change in spatial distribution, the stronger decline of emissions and, hence, the modelled levels occurred in the northern part, and the increase – in the southern part of the country. Other countries/regions where marked increase of pollution levels took place were the Netherlands, Spain, Turkey, Greece, Slovakia, the Czech Republic, North Macedonia and Norway. Some increase of Cd pollution levels in the southern parts of Serbia and Bosnia and Herzegovina was likely caused by increased transboundary transport from other countries, first of all, from Greece and North Macedonia.

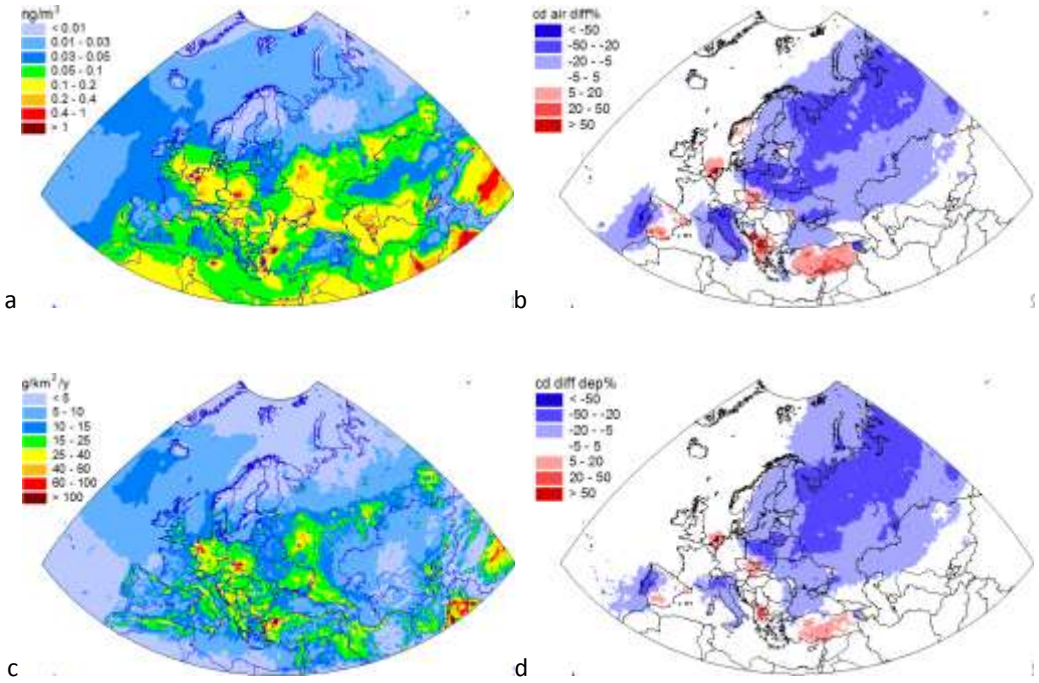

Fig.A.2. *Annual mean air concentrations (a) and total deposition fluxes (c) of Cd based on the emissions data for 2018 and their relative changes (b and d) from the results based on the emissions data for 2017.*

The major contribution to Hg air concentrations in the EMEP region is made by non-EMEP sources. Therefore, the response of modelled air concentrations to the changes of anthropogenic emissions in the EMEP countries is relatively weak. Only in Armenia, where the increase of emissions was bigger than 4800%, air concentrations of Hg increased by 20-30% (Fig. A.3). Unlike Pb and Cd, the response of Hg deposition to changes of the emissions is stronger than the response of air concentrations.

Mercury air concentrations are mostly presented by long-lived and globally spreading elemental mercury (Hg^0), whereas the Hg deposition is largely formed by easily scavenged oxidized Hg forms with shorter lifetime. Besides, anthropogenic emissions are partly consist of oxidised Hg. Mercury deposition fluxes decreased by 5-20% in Italy, north-western Poland, some regions of Germany, Russia and Turkey due to emission changes between 2017 and 2018. The most significant increase of Hg deposition took place in Armenia and neighbouring countries and in the north-eastern part of Kazakhstan.

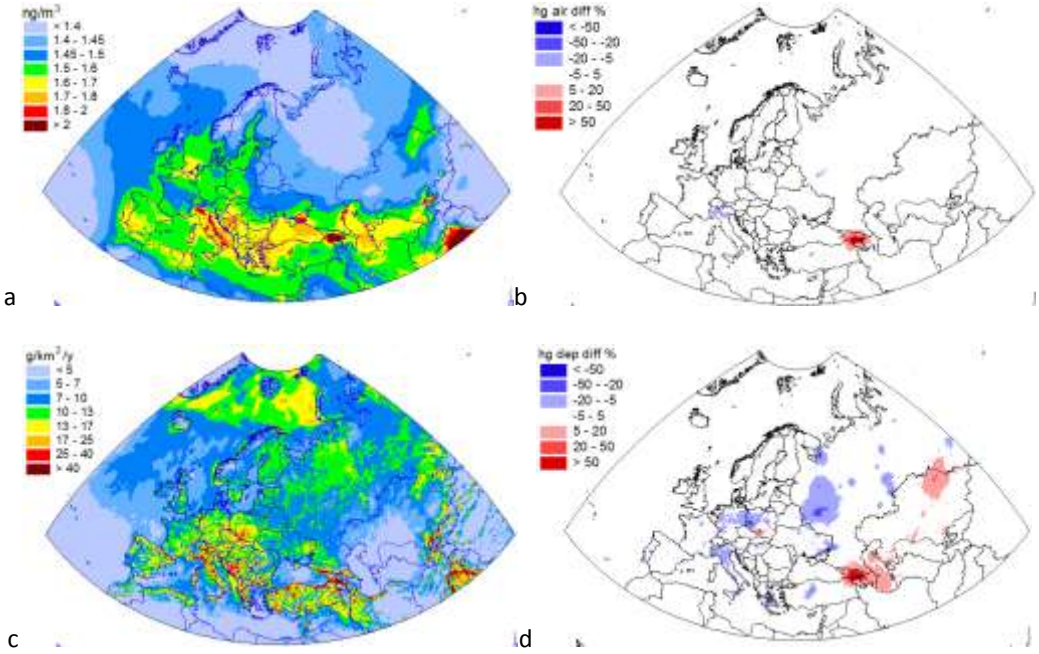

Fig. A.3. *Annual mean air concentrations (a) and total deposition fluxes (c) of Hg based on the emissions data for 2018 and their relative changes (b and d) from the results based on the emissions data for 2017.*

Model predictions of air concentrations and total deposition fluxes of PCDD/Fs on the basis of emission data for 2018 show increase of pollution levels by 5-20% in most countries of Central and Eastern Europe as well as in Spain and Portugal due to increased emissions in Denmark, The Netherlands, Poland, Austria, Russia, and Portugal (Fig. A.4). At the same time decline of PCDD/F pollution levels is noted for the Caucasus and Central Asia due to decrease of emissions in Armenia and Azerbaijan, and in Southern Europe due to decline of PCDD/F emissions in Romania, Slovakia, and Greece.

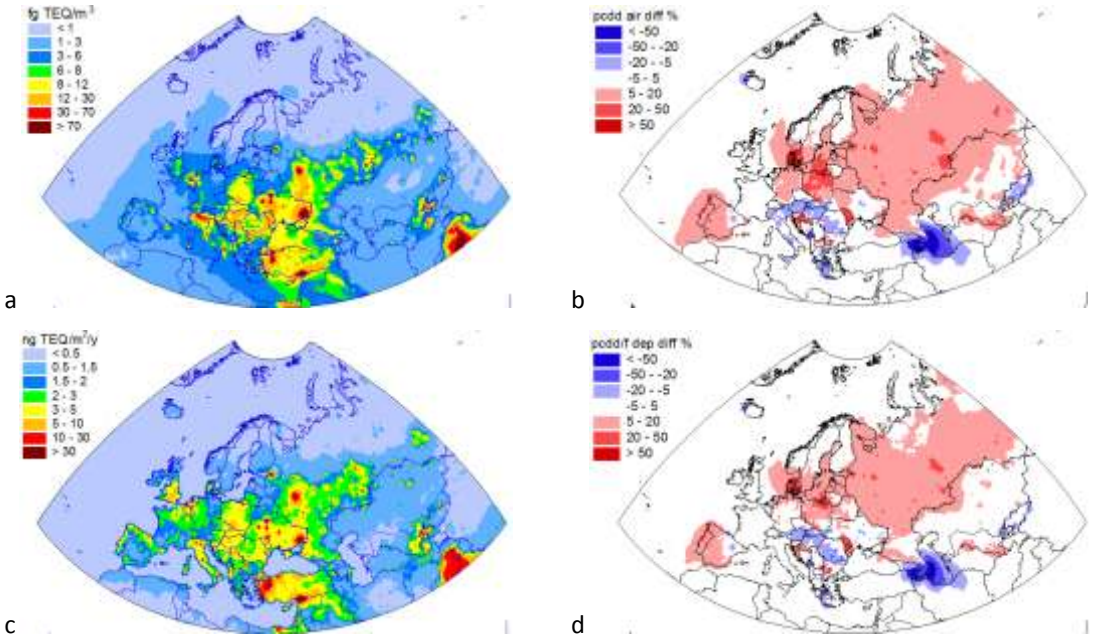

Fig. A4. *Annual mean air concentrations (a) and total deposition fluxes (c) of PCDD/Fs based on the emissions data for 2018 and their relative changes (b and d) from the results based on the emissions data for 2017.*

Significant contribution to air concentrations and deposition of HCB in the EMEP region was made by secondary and non-EMEP emission sources. Thus, the effect of changes of the HCB anthropogenic emissions from 2017 to 2018 on the inter-annual variations of modelled air concentrations and deposition fluxes of HCB was relatively small (Fig. A.5).

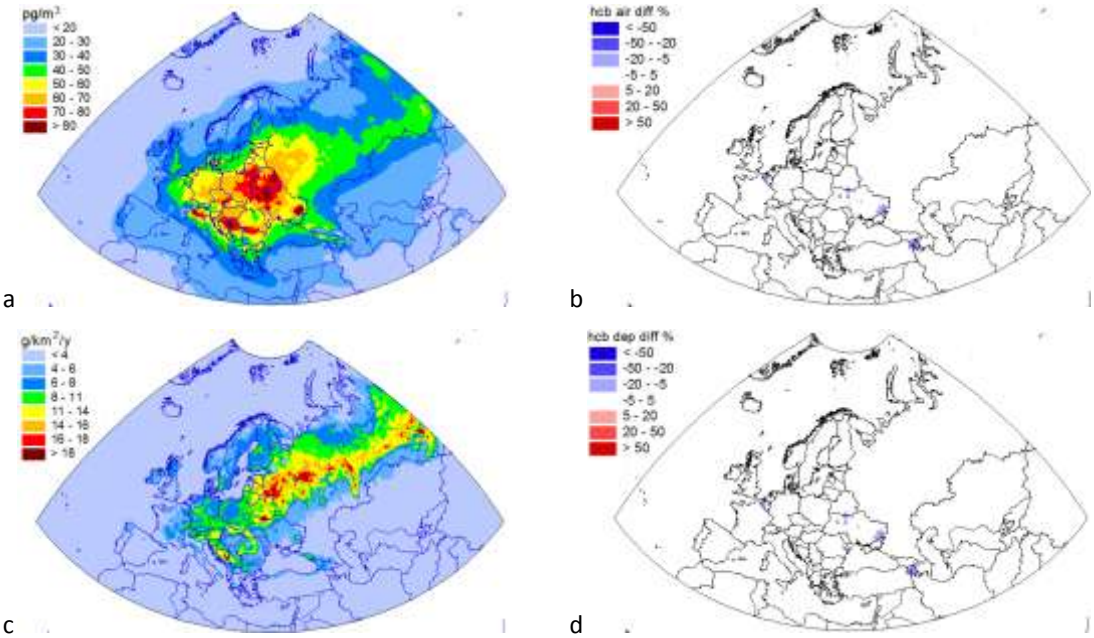

Fig. A.5. *Annual mean air concentrations (a) and total deposition fluxes (c) of HCB based on the emissions data for 2018 and their relative changes (b and d) from the results based on the emissions data for 2017.*

Model simulations of 4 PAHs based on the 2018 emission data indicate increased levels of air concentrations and total deposition fluxes in the countries in Central and Eastern Europe as well as the Caucasus and Central Asia in comparison with the results based on 2017 emission data (Fig. A.6). These changes demonstrate the effect of increased PAH emissions in Poland, Slovakia, and Russia. Declining levels of pollution due to the changes of emissions are estimated for Kirgizstan, Armenia, and Portugal.

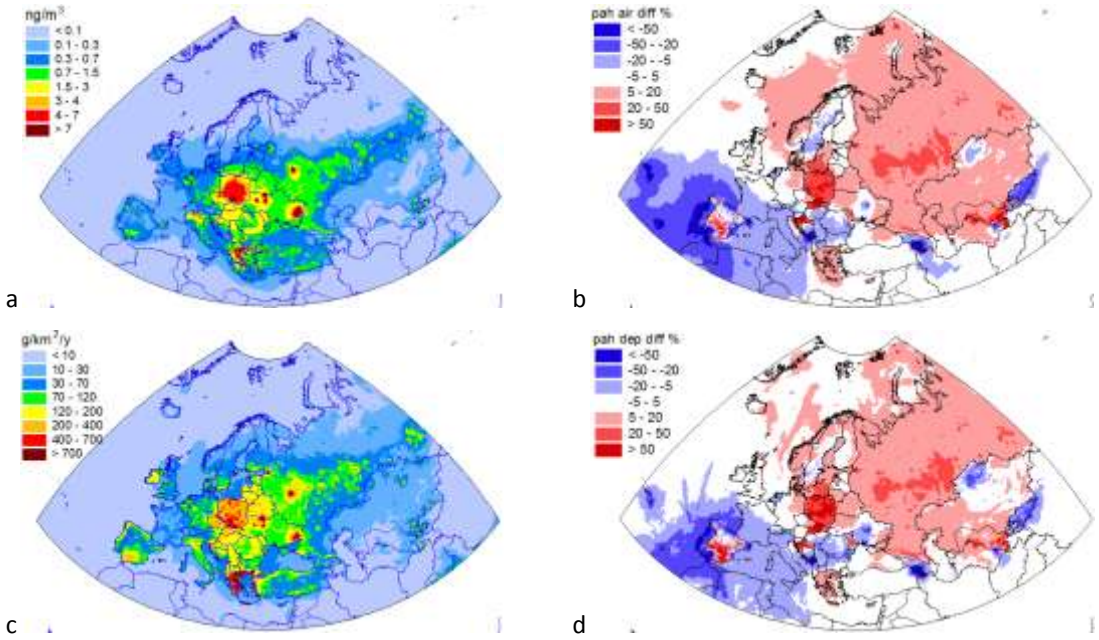

Fig. A.6. *Annual mean air concentrations (a) and total deposition fluxes (c) of the sum of 4 PAHs based on the emissions data for 2018 and their relative changes (b and d) from the results based on the emissions data for 2017.*

The updated information on heavy metal and POP pollution in 2018 in the EMEP region and individual EMEP countries is available at the EMEP website [http://en.msceast.org/index.php/pollution-assessment/emep-domain-menu].

Annex B1

REPORTING OF MAIN HMs AND POPs IN EMEP EAST REGION

Table B1. *Reporting of main heavy metals (Pb, Cd, Hg) in EMEP-East region since 2015*

	2015	2016	2017	2018	2019	2020
Armenia	2008 - 2013 (only Pb, only a few sectors)	2014		2016	2017	
Azerbaijan	1990 - 2013 (only Hg, only a few sectors)	1990-2014 (Pb, Cd: 1995-2014)	1990 - 2015 (Pb, Cd: 1995-2015)	1990 - 2016 (Pb, Cd: 1995-2016)	1995-2017 (Hg1990-2017)	
Belarus	2013			2014-2016	2017	2018
Georgia	2007 - 2013 (no Hg)	2007-2014 (Cd, Hg: 2013-2014)	2007 - 2015	2007-2016	2007-2017	
Kazakhstan		2013-2014	1990, 2000, 2005, 2010 - 2015	1990 - 2016		1990 - 2018
Kyrgyzstan		2014 (only Hg)	2015 (only Hg)		2017	2018
Republic of Moldova	2013	1990-2014 (no emissions calculated for the waste sector)	1990 - 2015			1990 - 2017
Russian Federation						
Ukraine	2013	2014	2015	2016		2016, 2017, 2018
Turkey					1990 - 2017 *(just for very few IPPU categories)*	1990 - 2018 *(just for very few IPPU categories)*

Table B2. *Reporting of POPs (PCDD/Fs, PAHs, HCB, PCBs) in EMEP East region since 2015*

	2015	2016	2017	2018	2019	2020
Armenia		2014		2016 (only PCDD/Fs)	2017 (No HCB, no PCBs)	
Azerbaijan	1995-2013	1995-2014 (no HCB, no PCBs)	1995-2015	1995-2016	1995 -2017 (HCB, PCBS no data for 2000)	
Belarus	2013			2014-2016	2017	2018
Georgia	2007-2013 (no HCB)	2007-2014 (PCDD/Fs) 2013-2014 (PAHs, HCB, PCBs)	2007-2015	2007-2016 (HCB only 2013-2016)	2007-2017	
Kazakhstan		2013-2014	1990, 2000, 2005, 2010-2015	1990-2016		1990 -2018
Kyrgyzstan					2017	2018
Republic of Moldova	2013	1990-2014 (no emissions calculated for the waste sector)	1990-2015			1990-2017
Russian Federation						
Ukraine	2013 (no PCDD/Fs)				2017	2017, 2018
Turkey						

EMISSION CHANGES BETWEEN 2018 (REPORTED IN 2020) AND 2017 DATA (REPORTED IN 2019) OVER±15 % (DATA SETS USED FOR GRIDDING)

Data values represent the 'total national totals'. The column 'data sources' in the table below indicates the following four cases:

- *"reported"*: both 2017 and 2018 data are reported by country.
- *"gapfilled":* both 2017 and 2018 data are gap-filled by expert estimates
- *"new gapfilled":* 2017 data was reported by country and 2018 data had to be gap-filled by expert estimates (because it was not reported by country)
- *"new reported":* 2017 data was gap-filled, 2018 data is as reported by country

The indicator *"new"* in column *"% change"* indicates that the value has been either reported or gap-filled for the first time.

Component	Country	Data sources	Unit	2018 value	2017 value	% change	Value change
Cd	AM	new reported	t	0.013	0.209	-94%	-0.196
Cd	MD	gapfilled	t	0.368	0.224	65%	0.144
Cd	RU	gapfilled	t	43.434	63.070	-31%	-19.636
Cd	RUE	gapfilled	t	22.375	32.491	-31%	-10.115
Cd	FR	reported	t	2.636	3.168	-17%	-0.532
Cd	CY	reported	t	0.036	0.053	-32%	-0.017
Cd	CZ	reported	t	1.399	1.167	20%	0.232
Cd	ES	reported	t	4.904	4.221	16%	0.683
Cd	GR	new reported	t	1.938	1.398	39%	0.540
Cd	IS	reported	t	0.006	0.047	-88%	-0.041
Cd	IT	reported	t	5.331	7.461	-29%	-2.130
Cd	LT	reported	t	0.195	0.396	-51%	-0.201
Cd	MC	new gapfilled	t	0.000	0.000	26%	0.000
Cd	ME	new reported	t	0.188	0.072	159%	0.115
Cd	MK	reported	t	0.603	0.126	378%	0.476
Cd	MT	reported	t	0.005	0.001	413%	0.004
Cd	NL	reported	t	2.324	0.765	204%	1.559
Cd	NO	reported	t	0.508	0.430	18%	0.078
Cd	PL	reported	t	9.451	12.365	-24%	-2.914
Cd	PT	reported	t	2.037	4.602	-56%	-2.564
Cd	SK	reported	t	1.682	1.215	38%	0.466
Hg	AM	new reported	t	16.625	0.338	4812%	16.286

Hg	KZT	gapfilled	t	24.554	18.666	32%	5.888
Hg	MD	gapfilled	t	0.102	0.156	-34%	-0.053
Hg	RU	gapfilled	t	8.051	18.280	-56%	-10.229
Hg	RUE	gapfilled	t	4.148	9.417	-56%	-5.269
Hg	FR	reported	t	3.188	3.795	-16%	-0.606
Hg	BE	reported	t	1.370	1.050	31%	0.320
Hg	CY	reported	t	0.036	0.100	-64%	-0.064
Hg	FI	reported	t	0.677	0.579	17%	0.098
Hg	GR	new reported	t	1.132	1.647	-31%	-0.515
Hg	HU	reported	t	1.025	1.342	-24%	-0.317
Hg	IS	reported	t	0.015	0.062	-76%	-0.047
Hg	IT	reported	t	6.998	9.160	-24%	-2.162
Hg	ME	new reported	t	0.049	0.095	-48%	-0.046
Hg	MT	reported	t	0.031	0.026	18%	0.005
Hg	PT	reported	t	1.425	2.090	-32%	-0.665
Pb	AM	new reported	t	1.723	3.710	-54%	-1.988
Pb	MD	gapfilled	t	1.477	3.194	-54%	-1.717
Pb	RU	gapfilled	t	139.857	222.208	-37%	-82.351
Pb	RUE	gapfilled	t	72.048	114.471	-37%	-42.423
Pb	AT	reported	t	19.257	15.662	23%	3.596
Pb	BE	reported	t	13.606	25.144	-46%	-11.538
Pb	CY	reported	t	0.388	18.454	-98%	-18.067
Pb	GR	new reported	t	10.595	8.202	29%	2.393
Pb	IS	reported	t	0.769	1.958	-61%	-1.189
Pb	IT	reported	t	214.034	274.781	-22%	-60.746
Pb	ME	new reported	t	0.454	3.623	-87%	-3.169
Pb	MK	reported	t	2.590	2.212	17%	0.378
Pb	NL	reported	t	5.042	8.618	-41%	-3.576
Pb	SK	reported	t	31.145	43.684	-29%	-12.539
B(a)P	AM	new reported	t	0.087	2.550	-97%	-2.463
B(a)P	KG	gapfilled	t	4.112	5.727	-28%	-1.615
B(a)P	MD	gapfilled	t	3.247	2.011	61%	1.236
B(a)P	RU	gapfilled	t	86.900	68.651	27%	18.249
B(a)P	RUE	gapfilled	t	23.100	18.249	27%	4.851
B(a)P	ES	new reported	t	27.824	41.518	-33%	-13.694
B(a)P	HR	reported	t	4.793	1.920	150%	2.874
B(a)P	HU	reported	t	8.036	9.849	-18%	-1.813
B(a)P	IT	gapfilled	t	20.113	24.249	-17%	-4.136
B(a)P	MC	new gapfilled	t	0.000	0.000	97%	0.000
B(a)P	ME	new reported	t	0.002	3.546	-100%	-3.544
B(a)P	MT	reported	t	0.006	0.008	-17%	-0.001
B(a)P	NL	reported	t	1.565	1.949	-20%	-0.384

B(a)P	PL	reported	t	73.148	42.935	70%	30.213
B(a)P	PT	new reported	t	4.603	10.800	-57%	-6.197
B(a)P	RO	new reported	t	17.436	22.220	-22%	-4.784
B(a)P	RS	new reported	t	6.635	7.874	-16%	-1.239
B(a)P	SE	reported	t	2.265	3.523	-36%	-1.258
B(a)P	SK	reported	t	6.197	1.150	439%	5.047
B(b)F	AM	new reported	t	0.084	3.336	-97%	-3.252
B(b)F	KG	gapfilled	t	5.860	8.175	-28%	-2.315
B(b)F	MD	gapfilled	t	3.496	2.143	63%	1.353
B(b)F	RU	gapfilled	t	97.927	74.589	31%	23.338
B(b)F	RUE	gapfilled	t	26.031	19.828	31%	6.204
B(b)F	BG	reported	t	4.961	5.909	-16%	-0.949
B(b)F	ES	new reported	t	35.904	45.109	-20%	-9.206
B(b)F	HR	reported	t	4.581	2.131	115%	2.450
B(b)F	HU	reported	t	8.351	10.116	-17%	-1.764
B(b)F	MC	new gapfilled	t	0.000	0.000	62%	0.000
B(b)F	ME	new reported	t	0.008	4.439	-100%	-4.431
B(b)F	MK	reported	t	1.319	2.069	-36%	-0.750
B(b)F	MT	reported	t	0.069	0.028	147%	0.041
B(b)F	NL	reported	t	1.513	1.882	-20%	-0.370
B(b)F	PL	reported	t	81.704	46.704	75%	35.000
B(b)F	PT	new reported	t	4.000	8.640	-54%	-4.640
B(b)F	RO	new reported	t	17.403	20.552	-15%	-3.149
B(b)F	RS	new reported	t	7.324	8.699	-16%	-1.374
B(b)F	SE	reported	t	2.365	3.583	-34%	-1.218
B(b)F	SK	reported	t	6.046	1.207	401%	4.839
B(k)F	AM	new reported	t	0.032	1.138	-97%	-1.106
B(k)F	KG	gapfilled	t	2.310	3.222	-28%	-0.912
B(k)F	MD	gapfilled	t	1.702	0.829	105%	0.873
B(k)F	RU	gapfilled	t	43.907	29.924	47%	13.983
B(k)F	RUE	gapfilled	t	11.671	7.954	47%	3.717
B(k)F	BG	reported	t	1.919	2.361	-19%	-0.442
B(k)F	DK	reported	t	1.433	0.988	45%	0.444
B(k)F	ES	new reported	t	49.054	18.097	171%	30.957
B(k)F	HR	reported	t	1.749	0.795	120%	0.954
B(k)F	HU	reported	t	3.393	4.061	-16%	-0.668
B(k)F	IS	reported	t	0.021	0.026	-17%	-0.004
B(k)F	LU	reported	t	0.113	0.090	25%	0.023
B(k)F	MC	new gapfilled	t	0.000	0.000	62%	0.000

B(k)F	ME	new reported	t	0.007	4.154	-100%	-4.146
B(k)F	MK	reported	t	0.501	1.145	-56%	-0.644
B(k)F	MT	reported	t	0.013	0.008	74%	0.006
B(k)F	NL	reported	t	0.795	1.007	-21%	-0.212
B(k)F	PL	reported	t	37.007	14.347	158%	22.661
B(k)F	PT	new reported	t	1.969	11.782	-83%	-9.813
B(k)F	RO	new reported	t	7.159	8.750	-18%	-1.590
B(k)F	RS	new reported	t	2.862	3.431	-17%	-0.569
B(k)F	SE	reported	t	0.826	1.281	-36%	-0.455
B(k)F	SK	reported	t	3.636	1.062	242%	2.575
IP	AM	new reported	t	0.048	1.801	-97%	-1.753
IP	KG	gapfilled	t	1.944	2.716	-28%	-0.772
IP	MD	gapfilled	t	1.722	1.118	54%	0.604
IP	AT	gapfilled	t	1.309	1.838	-29%	-0.528
IP	BA	gapfilled	t	0.957	1.185	-19%	-0.229
IP	BG	reported	t	2.680	3.226	-17%	-0.545
IP	ES	new reported	t	9.302	32.125	-71%	-22.823
IP	FI	gapfilled	t	1.831	2.382	-23%	-0.551
IP	HR	reported	t	2.803	1.068	162%	1.735
IP	HU	reported	t	4.656	5.604	-17%	-0.947
IP	IT	gapfilled	t	12.819	18.763	-32%	-5.944
IP	MC	new gapfilled	t	0.000	0.000	99%	0.000
IP	ME	new reported	t	0.037	0.569	-94%	-0.533
IP	MK	reported	t	0.698	1.205	-42%	-0.508
IP	MT	reported	t	0.012	0.007	70%	0.005
IP	NL	reported	t	0.741	0.944	-22%	-0.203
IP	PL	reported	t	30.598	47.583	-36%	-16.985
IP	PT	new reported	t	2.621	3.633	-28%	-1.012
IP	RO	new reported	t	9.753	12.775	-24%	-3.022
IP	RS	new reported	t	3.639	4.605	-21%	-0.965
IP	SE	reported	t	1.242	1.625	-24%	-0.383
IP	SK	reported	t	2.558	0.667	284%	1.892
PAH	AM	new reported	t	0.249	8.826	-97%	-8.577
PAH	KG	gapfilled	t	14.226	19.840	-28%	-5.614
PAH	MD	gapfilled	t	10.168	6.102	67%	4.067
PAH	RU	gapfilled	t	283.315	226.283	25%	57.032
PAH	RUE	gapfilled	t	75.312	60.151	25%	15.160
PAH	HR	reported	t	13.991	5.930	136%	8.061
PAH	HU	reported	t	24.437	29.629	-18%	-5.193
PAH	IT	reported	t	66.781	79.928	-16%	-13.147

PAH	MC	new gapfilled	t	0.001	0.000	76%	0.000
PAH	ME	new reported	t	0.052	12.707	-100%	-12.656
PAH	MK	new gapfilled	t	4.605	6.367	-28%	-1.762
PAH	MT	reported	t	0.101	0.051	100%	0.051
PAH	NL	reported	t	4.614	5.783	-20%	-1.169
PAH	PL	new gapfilled	t	222.458	151.575	47%	70.883
PAH	PT	gapfilled	t	13.194	34.856	-62%	-21.663
PAH	RO	new gapfilled	t	51.751	64.298	-20%	-12.548
PAH	RS	new gapfilled	t	20.460	24.608	-17%	-4.148
PAH	SE	reported	t	7.042	10.286	-32%	-3.245
PAH	SK	new gapfilled	t	18.438	4.059	354%	14.378
PCDD/F	AM	new reported	g I-TEQ	0.556	49.951	-99%	-49.395
PCDD/F	AZ	gapfilled	g I-TEQ	5.176	112.553	-95%	-107.377
PCDD/F	KG	gapfilled	g I-TEQ	14.595	20.234	-28%	-5.639
PCDD/F	MD	gapfilled	g I-TEQ	44.441	12.962	243%	31.479
PCDD/F	RU	gapfilled	g I-TEQ	1 409.676	1 113.644	27%	296.032
PCDD/F	RUE	gapfilled	g I-TEQ	374.724	296.032	27%	78.692
PCDD/F	AT	reported	g I-TEQ	34.410	40.726	-16%	-6.316
PCDD/F	BG	reported	g I-TEQ	54.923	42.009	31%	12.914
PCDD/F	DK	reported	g I-TEQ	35.719	21.572	66%	14.148
PCDD/F	GR	new reported	g I-TEQ	29.301	39.522	-26%	-10.221
PCDD/F	HR	reported	g I-TEQ	28.172	16.226	74%	11.946
PCDD/F	IS	reported	g I-TEQ	0.369	1.938	-81%	-1.569
PCDD/F	LU	reported	g I-TEQ	1.374	2.017	-32%	-0.643
PCDD/F	MC	new gapfilled	g I-TEQ	0.005	0.006	-16%	-0.001
PCDD/F	ME	new reported	g I-TEQ	0.136	3.319	-96%	-3.183
PCDD/F	NL	reported	g I-TEQ	34.932	23.027	52%	11.905
PCDD/F	PL	reported	g I-TEQ	316.072	259.017	22%	57.055
PCDD/F	PT	reported	g I-TEQ	55.438	44.117	26%	11.321
PCDD/F	RO	reported	g I-TEQ	153.027	189.764	-19%	-36.737
PCDD/F	SK	reported	g I-TEQ	47.026	75.162	-37%	-28.136
HCB	AM	new reported	kg	0.003	28.000	-100%	-27.997
HCB	MD	gapfilled	kg	0.199	0.115	73%	0.084
HCB	RUE	gapfilled	kg	0.455	1.668	-73%	-1.214
HCB	FR	reported	kg	23.888	6.504	267%	17.384
HCB	BE	reported	kg	4.832	35.094	-86%	-30.263
HCB	BG	reported	kg	1.578	0.218	624%	1.360
HCB	CY	reported	kg	0.028	0.009	206%	0.019
HCB	DE	reported	kg	11.892	15.067	-21%	-3.175
HCB	ES	reported	kg	12.745	1.929	561%	10.816

HCB	GR	new reported	kg	3.324	2.544	31%	0.780
HCB	HR	reported	kg	0.564	0.284	99%	0.281
HCB	HU	reported	kg	2.257	1.436	57%	0.821
HCB	IE	reported	kg	2.556	2.000	28%	0.557
HCB	IS	reported	kg	0.069	0.091	-24%	-0.022
HCB	LV	reported	kg	0.515	0.306	69%	0.209
HCB	MC	new gapfilled	kg	0.012	0.000	29130%	0.012
HCB	ME	new reported	kg	0.112	1.628	-93%	-1.516
HCB	MK	reported	kg	1.657	6.669	-75%	-5.012
HCB	NO	reported	kg	1.335	1.608	-17%	-0.272
PCB	AM	new reported	kg	0.009	12.268	-100%	-12.259
PCB	KG	gapfilled	kg	3.912	5.146	-24%	-1.234
PCB	MD	gapfilled	kg	1.604	405.338	-100%	-403.734
PCB	AT	reported	kg	32.090	38.157	-16%	-6.067
PCB	BE	reported	kg	5.477	2.822	94%	2.655
PCB	CH	new reported	kg	480.481	-	NEW	480.481
PCB	DK	reported	kg	0.528	43.294	-99%	-42.766
PCB	IE	reported	kg	7.936	11.422	-31%	-3.486
PCB	IS	reported	kg	0.035	0.095	-63%	-0.060
PCB	IT	reported	kg	116.030	189.164	-39%	-73.134
PCB	LT	reported	kg	1.499	1.809	-17%	-0.310
PCB	LU	reported	kg	2.094	3.642	-43%	-1.548
PCB	MC	new gapfilled	kg	0.023	0.000	60955%	0.023
PCB	ME	new reported	kg	0.038	0.763	-95%	-0.725
PCB	MK	reported	kg	29.024	25.123	16%	3.900
PCB	NL	reported	kg	0.233	0.000	224690%	0.233
PCB	PL	reported	kg	178.131	578.365	-69%	-400.234

Annex B3

OVERVIEW OF GAP-FILLING IN 2020

	Cd	Hg	Pb
Albania	X	X	X
Armenia	X	X	X
Aral Lake	-	-	-
Asian Areas	X	X	X
Austria	X	X	X
Atlantic Ocean	-	-	-
Azerbaijan	X	X	X
Bosnia and Herzegovina	X	X	X
Baltic Sea	-	-	-
Belgium	X	X	X
Bulgaria	X	X	X
Black Sea	-	-	-
Belarus	X	X	X
Caspian Sea	-	-	-
Switzerland	X	X	X
Cyprus	X	X	X
Czechia	X	X	X
Germany	X	X	X
Denmark	X	X	X
Estonia	X	X	X
Spain	X	X	X
Finland	X	X	X
France	X	X	X
United Kingdom	X	X	X
Georgia	X	X	X
Greece	X	X	X
Croatia	X	X	X
Hungary	X	X	X
Ireland	X	X	X
Iceland	X	X	X

	Cd	Hg	Pb
Italy	X	X	X
Kyrgyzstan	X	X	X
Kazakhstan	X	X	X
Liechtenstein	X	X	X
Luxembourg	X	X	X
Latvia	X	X	X
Monaco	X	X	X
Republic of Moldova	X	X	X
Montenegro	X	X	X
Mediterranean Sea	-	-	-
North Macedonia	X	X	X
Malta	X	X	X
Netherlands	X	X	X
Norway	X	X	X
North Africa	X	X	X
North Sea	-	-	-
Poland	X	X	X
Portugal	X	X	X
Romania	X	X	X
Serbia	X	X	X
Russian Federation	X	X	X
Russian Federation in the extended EMEP domain	X	X	X
Sweden	X	X	X
Slovenia	X	X	X
Slovakia	X	X	X
Tajikistan	X	X	X
Turkmenistan	X	X	X
Turkey	X	X	X
Ukraine	X	X	X
Uzbekistan	X	X	X

	B(a)P	B(b)F	B(k)F	PCDD/F	HCB	IP	PAH	PCB
Albania	X	X	X	X	X	X	X	X
Armenia	X	X	X	X	X	X	X	X
Aral Lake	-	-	-	-	-	-	-	-
Asian Areas	-	-	-	-	-	-	-	-
Austria	X	X	X	X	X	X	X	X
Atlantic Ocean	-	-	-	-	-	-	-	-
Azerbaijan	X	X	X	X	X	X	X	X
Bosnia and Herzegovina	X	X	X	X	X	X	X	-
Baltic Sea	-	-	-	-	-	-	-	-
Belgium	X	X	X	X	X	X	X	X
Bulgaria	X	X	X	X	X	X	X	X
Black Sea	-	-	-	-	-	-	-	-
Belarus	X	X	X	X	X	X	X	X
Caspian Sea	-	-	-	-	-	-	-	-
Switzerland	X	X	X	X	X	X	X	-
Cyprus	X	X	X	X	X	X	X	X
Czechia	X	X	X	X	X	X	X	X
Germany	X	X	X	X	X	X	X	X
Denmark	X	X	X	X	X	X	X	X
Estonia	X	X	X	X	X	X	X	X
Spain	X	X	X	X	X	X	X	X
Finland	X	X	X	X	X	X	X	X
France	X	X	X	X	X	X	X	X
United Kingdom	X	X	X	X	X	X	X	X
Georgia	X	X	X	X	X	X	X	X
Greece	X	X	X	X	X	X	X	X
Croatia	X	X	X	X	X	X	X	X
Hungary	X	X	X	X	X	X	X	X
Ireland	X	X	X	X	X	X	X	X
Iceland	X	X	X	X	X	X	X	X
Italy	X	X	X	X	X	X	X	X
Kyrgyzstan	X	X	X	X	X	X	X	X
Kazakhstan	X	X	X	X	X	X	X	X
Liechtenstein	X	X	X	X	X	X	X	-
Lithuania	X	X	X	X	X	X	X	X
Luxembourg	X	X	X	X	X	X	X	X
Latvia	X	X	X	X	X	X	X	X
Monaco	X	X	X	X	X	X	X	X
Republic of Moldova	X	X	X	X	X	X	X	X
Montenegro	X	X	X	X	X	X	X	X
Mediterranean Sea	-	-	-	-	-	-	-	-
North Macedonia	X	X	X	X	X	X	X	X
Malta	X	X	X	X	X	X	X	X
Netherlands	X	X	X	X	X	X	X	X
Norway	X	X	X	X	X	X	X	X

	B(a)P	B(b)F	B(k)F	PCDD/F	HCB	IP	PAH	PCB
North Africa	-	-	-	-	-	-	-	-
North Sea	-	-	-	-	-	-	-	-
Poland	X	X	X	X	X	X	X	X
Portugal	X	X	X	X	X	X	X	X
Romania	X	X	X	X	X	X	X	X
Serbia	X	X	X	X	X	X	X	X
Russian Federation	X	X	X	X	X	X	X	-
Russian Federation in the extended EMEP domain	X	X	X	X	X	X	X	-
Sweden	X	X	X	X	X	X	X	X
Slovenia	X	X	X	X	X	X	X	X
Slovakia	X	X	X	X	X	X	X	X
Tajikistan	X	X	X	X	X	X	X	-
Turkmenistan	X	X	X	X	X	X	X	-
Turkey	X	X	X	X	X	X	X	-
Ukraine	X	X	X	X	X	X	X	X
Uzbekistan	X	X	X	X	X	X	X	-

X *Reported (also in previous years!)*

X *Partly replaced*

X *Replaced*

X *Partly expert estimates/reported data*

X *Expert estimates only*